To the Graduate Council:

I am submitting herewith a dissertation written by Ismail A. Tag entitled "A Finite Element Approach to the Problem of Sound Propagation and Attenuations in Jet Engine Air Intakes." I recommend that it be accepted in partial fulfillment of the requirements for the degree of Doctor of Philosophy, with a major in Mechanical Engineering.

Edward Lumsdaine, Major Professor

We have read this dissertation
and recommend its acceptance:

Accepted for the Council:

Vice Chancellor
Graduate Studies and Research

Thesis
T86
T333
cop. 2

A FINITE ELEMENT APPROACH TO THE PROBLEM OF SOUND PROPAGATION AND ATTENUATION IN JET ENGINE AIR INTAKES

A Dissertation

Presented for the

Doctor of Philosophy

Degree

The University of Tennessee, Knoxville

Ismail A. Tag

June 1978

1361936

ACKNOWLEDGEMENT

The author is very much indebted to Dr. Edward Lumsdaine, the major professor and the research advisor for his initiation of the project, guidance and counselling without which the present work could not have been successfully achieved.

Thanks are due to Dr. M. Milligan, Head of the Mechanical and Aerospace Engineering Department at the University of Tennessee and the doctoral committee members Drs. Hodgson, Serbin and Wilkerson for their encouragement and assistance. Thanks also go to Dr. E. Akin of the Department of Engineering Science and Mechanics for his computer programming assistance.

The author wishes to gratefully acknowledge the financial support provided by the Mechanical and Aerospace Engineering Department and the National Aeronautics and Space Administration under Grant NGR1081 and the National Science Foundation under Grant NSF OIP 74-21450.

ABSTRACT

The general non-linear three-dimensional equation for the acoustic velocity potential is derived by using a perturbation technique.

The non-linear three-dimensional equation is then linearized and solved using a finite element algorithm based on Galerkin formulation for a harmonic time dependence. The solution is carried out in complex number notation for the acoustic velocity potential.

Sound pressure levels and acoustic velocities are calculated from post element solutions. Plane wave source or higher order mode excitation is applied at one end of a variable area duct, while a reflection boundary condition based on experimental predictions is applied at the free end of the duct.

A finite element computer program has been developed from a series of building blocks which are machine-independent. The program utilizes the minimum storage, and the resulting global matrix is stored in banded form.

Exact solutions are compared with the finite element predictions for constant area duct geometries to assess the accuracy of the numerical technique.

Finally the finite element predictions are compared with experimental values for variable area ducts carrying high subsonic Mach number flows and subjected to plane waves and high order mode excitation.

All the checks demonstrated the adequacy of the finite element model for predicting the acoustic properties of jet engine air intakes.

TABLE OF CONTENTS

CHAPTER			PAGE
I.	INTRODUCTION		1
	I.1	Overview	1
	I.2	Statement of the Problem	2
	I.3	Importance of the Study	5
	I.4	Scope and Organization of the Text	7
II.	LITERATURE SURVEY		8
	II.1	Introduction	8
	II.2	Finite Difference Method	8
	II.3	Integral and Weighted Residual Methods	9
	II.4	Finite Element Method	11
	II.5	Experimental Studies	13
III.	FINITE ELEMENT FORMULATION OF THE TWO-DIMENSIONAL WAVE EQUATION		15
	III.1	Introduction	15
	III.2	Mathematical Model	16
	III.3	Integral Formulation for the No Flow Case M = 0	17
	III.4	Finite Element Model	17
	III.5	The Two-Dimensional No Flow Case .	22
	III.6	Numerical Results for the One-Dimensional and Two-Dimensional Cases	23

CHAPTER PAGE

III.7 A Comparison with Existing Results 27

III.8 The One-Dimensional Wave Equation with Flow 34

III.9 Galerkin's Method 36

III.10 Numerical Results for the One-Dimensional Case with Mean Flow . 39

IV. DERIVATION OF THE NON-LINEAR AXISYMMETRIC ACOUSTIC EQUATION 43

IV.1 Introduction 43

IV.2 Mathematical Model 43

IV.3 The Linear Problem 46

IV.4 Boundary Conditions 47

V. A FINITE ELEMENT ALGORITHM FOR THE AXISYMMETRIC WAVE EQUATIONS 53

V.1 Introduction 53

V.2 Finite Element Formulation 53

V.3 Finite Element Methodology and Computer Implementation 55

V.4 Input Specified Flux Components on Boundary Segments 62

V.5 Element Square Matrix 63

V.6 Assembly of Element Equations into System Equations 64

V.7 Application of Nodal Parameter Boundary Conditions 65

CHAPTER PAGE

V.8 Equation Solving Technique 67
V.9 Isoparametric Elements and Numerical Quadrature 68
VI. EXPERIMENTAL INVESTIGATION OF THE INFLUENCE OF HIGH-SPEED FLOW ON SOUND PROPAGATION . . 74
VI.1 Introduction 74
VI.2 Description of Inlets and Test Facility 75
VII. DISCUSSION OF RESULTS, CONCLUSION AND RECOMMENDATIONS 88
VII.1 No Flow Results 88
VII.2 Flow Cases 134
VII.3 Conclusion 156
VII.4 Recommendations for Future Work . . 158
REFERENCES 159
APPENDIXES 164
A. THE TWO-DIMENSIONAL WAVE EQUATION . 165
B. SOME ASPECTS OF THE CALCULUS OF VARIATION 171
C. SOME RESULTS FOR RIGHT ANGLE AND CIRCULAR BENDS OF RECTANGULAR CROSS SECTIONS 174
D. DERIVATION OF THE POTENTIAL EQUATION IN A DUCT 178

CHAPTER PAGE

E. INSTRUCTIONS FOR USING THE FINITE ELEMENT COMPUTER PROGRAM AND A PROGRAM LISTING 183

F. NON-LINEAR EFFECTS ON SOUND PROPAGATION IN A VARIABLE AREA DUCT CARRYING HIGH SUBSONIC MACH NUMBER FLOWS 205

VITA 218

LIST OF FIGURES

FIGURE		PAGE
I.1	Cross-Section in a Variable Area Duct Showing Coordinate System	3
I.2	Schematic of Experimental Setup in NASA-Langley Research Center	4
III.1	One-Dimensional Exact and Finite Element Solutions	24
III.2	Pressure Distribution Along the Center-line of a Constant Area Soft Wall Duct	25
III.3	Pressure Distribution Along the Soft Wall of a Constant Area Duct	26
III.4	Pressure Distribution at the Entrance and the Exit of a Hard Wall Variable Area Duct	28
III.5	Pressure Distribution Along the Center-line for a Variable Area Duct	29
III.6	Pressure Distribution Along the Wall for a Variable Area Duct	30
III.7	Pressure Distribution Along the Center-line of a Soft Wall Variable Area Duct	31
III.8	Pressure Distribution Along the Soft Wall of a Variable Area Duct	32

FIGURE PAGE

III.9 Pressure Distribution at the Entrance and the Exit of a Soft Wall Variable Area Duct 33

III.10 Attenuation in a Two-Dimensional Soft Wall Duct 35

III.11 Finite Element and Exact Acoustic Pressure Distribution in a Hard Wall Duct Carrying Mean Flow (M=+0.5) 40

III.12 Finite Element and Exact Acoustic Pressure Distribution in a Hard Wall Duct Carrying Mean Flow (M=-0.5) 42

V.1 Flow Chart for the Finite Element Computer Program 56

V.2 Isoparametric Quadrilateral Element . . . 70

VI.1 Mach Number Distribution for 18 lbm_m/sec 76

VI.2 Experimental Setup to Determine the Influence of High-Speed Flow on Noise Attenuation 77

VI.3 Schematic of Experimental Apparatus Showing Two Inlets with Aerodynamic Instrumentation 79

VI.4 Schematic of Test Section Showing the Microphone and Sound Driver Positions 80

VI.5 Monitoring System for Acoustic Drivers . 82

FIGURE PAGE

VI.6 Variation of Phase Angle with Microphone Position (1,0) Mode 85

VI.7 Variation of Phase Angle with Microphone Position (2,0) Mode 86

VI.8 Influence of Choking on the Signal-to-Noise Ratio of Eight Acoustic Drivers 87

VII.1 Exact and Finite Element Solutions for Wave Propagation in a Constant Area Duct 89

VII.2 Pressure Distribution Along Duct Wall (Duct 2,Mach Num=0.0 Mode=(0,0),Freq=1.37) 90

VII.3 Pressure Distribution Along Duct Wall (Duct 3,Mach Num=0.0,Mode=(0,0),Freq=1.37) 91

VII.4 Pressure Distribution Along Duct Wall (Duct 4,Mach Num=0.0,Mode=(0,0),Freq=1.37) 92

VII.5 Far-Field Sound Pressure Level Under Static Conditions (Mode(0,0),Freq=500 Hz) 94

VII.6 Pressure Distribution Along Duct Wall (Duct 3,Mach Num=0.0,Mode=(0,0),Freq=2.68) 95

VII.7 Pressure Distribution Along Duct Wall (Duct 4,Mach Num=0.0,Mode=(0,0),Freq=2.68) 96

VII.8 Far-Field Sound Pressure Level Under Static Conditions(Mode(0,0),Freq=1000 Hz) 97

VII.9 Acoustic Velocity Potential (Real Part) Along Duct Wall (Duct 3,Mach Num=0.0,Mode=(0,0), Freq=2.68) 98

FIGURE PAGE

VII.10 Acoustic Velocity Potential (Real Part) Along Duct Wall (Duct 4,Mach Num=0.0,Mode=(0,0), Freq=2.68) 99

VII.11 Pressure Distribution Along Duct Wall (Duct 2,Mach Num=0.0,Mode=(1,0),Freq=2.108) 100

VII.12 Pressure Distribution Along Duct Wall (Duct 3,Mach Num=0.0,Mode=(1,0),Freq=2.108) 101

VII.13 Pressure Distribution Along Duct Wall (Duct 4,Mach Num=0.0,Mode=(1,0),Freq=2.108) 102

VII.14 Far-Field Sound Pressure Level Under Static Conditions (Mode=(1,0),Freq=765 Hz) 104

VII.15 Pressure Distribution Along Duct Wall (Duct 2,Mach Num=0.0,Mode=(1,0),Freq=2.76) 105

VII.16 Pressure Distribution Along Duct Wall (Duct 3,Mach Num=0.0,Mode=(1,0),Freq=2.76) 106

VII.17 Pressure Distribution Along Duct Wall (Duct 4,Mach Num=0.0,Mode=(1,0),Freq=2.76) 107

VII.18 Far-Field Sound Pressure Level Under Static Conditions (Mode=(1,0),Freq=1000 Hz) 108

VII.19 Pressure Distribution Along Duct Wall (Duct 2,Mach Num=0.0,Mode=(1,0),Freq=4.2) 109

VII.20 Pressure Distribution Along Duct Wall (Duct 3,Mach Num=0.0,Mode=(1,0),Freq=4.2) 110

VII.21 Pressure Distribution Along Duct Wall (Duct 4,Mach Num=0.0,Mode=(1,0),Freq=4.2) 111

FIGURE PAGE

VII.22 Far-Field Sound Pressure Level Under Static Conditions (Mode=(1,0),Freq=1600 Hz) 112
VII.23 Acoustic Velocity Potential (Real Part) Along Duct Wall(Duct 2,Mach Num=0.0,Mode=(1,0),Freq=4.2) 113
VII.24 Acoustic Velocity Potential (Real Part) Along Duct Wall(Duct 3,Mach Num=0.0,Mode=(1,0),Freq=4.2) 114
VII.25 Acoustic Velocity Potential (Real Part) Along Duct Wall(Duct 4,Mach Num=0.0,Mode=(1 0),Freq=4.2) 115
VII.26 Pressure Distribution Along Duct Wall (Duct 2,Mach Num=0.0,Mode=(1,0),Freq=5.36) 117
VII.27 Pressure Distribution Along Duct Wall (Duct 3,Mach Num=0.0,Mode=(1,0),Freq=5.36) 118
VII.28 Pressure Distribution Along Duct Wall (Duct 4,Mach Num=0.0,Mode=(1,0),Freq=5.36) 119
VII.29 Acoustic Velocity Potential (Real Part) Along Duct Wall(Duct 2,Mach Num=0.0,Mode=(1,0),Freq=5.36) 120
VII.30 Acoustic Velocity Potential (Real Part) Along Duct Wall(Duct 3,Mach Num=0.0,Mode=(1,0),Freq=5.36) 121
VII.31 Acoustic Velocity Potential (Real Part) Along Duct Wall(Duct 4,Mach Num=0.0,Mode=(1,0),Freq=5.36) 122
VII.32 Pressure Distribution Along Duct Wall (Duct 2,Mach Num=0.0,Mode=(2,0),Freq=3.375) 123
VII.33 Pressure Distribution Along Duct Wall (Duct 3,Mach Num=0.0,Mode=(2,0),Freq=3.375) 124

FIGURE PAGE

VII.34 Pressure Distribution Along Duct Wall (Duct 4,Mach Num=0.0,Mode=(2,0),Freq=3.375) 125

VII.35 Far-Field Sound Pressure Under Static Conditions (Mode=(2,0),Freq=1223 Hz) 126

VII.36 Pressure Distribution Along Duct Wall (Duct 2,Mach Num=0.0,Mode=(2,0),Freq=6.56) 127

VII.37 Pressure Distribution Along Duct Wall (Duct 3,Mach Num=0.0,Mode=(2,0),Freq=6.56) 128

VII.38 Pressure Distribution Along Duct Wall (Duct 4,Mach Num=0.0,Mode=(2,0),Freq=6.56) 129

VII.39 Far-Field Sound Pressure Level Under Static Conditions (Mode=(2,0),Freq=2000 Hz) 130

VII.40 Acoustic Velocity Potential (Real Part) Along Duct Wall(Duct 2,Mach Num=0.0,Mode=(2,0),Freq=6.56) 131

VII.41 Acoustic Velocity Potenial (Real Part) Along Duct Wall(Duct 3,Mach Num=0.0,Mode=(2,0),Freq=6.56) 132

VII.42 Acoustic Velocity Potential (Real Part) Along Duct Wall(Duct 4,Mach Num=0.0,Mode=(2,0),Freq=6.56) 133

VII.43 Pressure Distribution Along Duct Wall (Duct 2,Mach Num=0.0,Mode=(2,0),Freq=8.58) 135

VII.44 Pressure Distribution Along Duct Wall (Duct 3,Mach Num=0.0,Mode=(2,0),Freq=8.58) 136

VII.45 Pressure Distribution Along Duct Wall (Duct 4,Mach Num=0.0,Mode=(2,0),Freq=8.58) 137

FIGURE PAGE

VII.46 Acoustic Velocity Potential (Real Part) Along Duct Wall(Duct 2,Mach Num=0.0,Mode=(2,0),Freq=8.58) 138

VII.47 Acoustic Velocity Potential (Real Part) Along Duct Wall(Duct 3,Mach Num=0.0,Mode=(2,0),Freq=8.58) 139

VII.48 Acoustic Velocity Potential (Real Part) Along Duct Wall(Duct 4,Mach Num=0.0,Mode=(2,0),Freq=8.58) 140

VII.49 Pressure Distribution Along Duct Wall (Duct 2,Mach Num=0.68,Mode=(0,0),Freq=1.37) 141

VII.50 Pressure Distribution Along Duct Wall (Duct 2,Mach Num=0.95,Mode=(0,0),Freq=1.37) 142

VII.51 Pressure Distribution Along Duct Wall (Duct 3,Mach Num=0.68,Mode=(0,0),Freq=1.37) 144

VII.52 Pressure Distribution Along Duct Wall (Duct 3,Mach Num=0.95,Mode=(0,0),Freq=1.37) 145

VII.53 Pressure Distribution Along Duct Wall (Duct 4,Mach Num=0.68,Mode=(0,0),Freq=1.37) 146

VII.54 Pressure Distribution Along Duct Wall (Duct 4,Mach Num=0.95,Mode=(0,0),Freq=1.37) 147

VII.55 Pressure Distribution Along Duct Wall (Duct 3,Mach Num=0.68,Mode=(1,0),Freq=2.76) 148

VII.56 Pressure Distribution Along Duct Wall (Duct 3,Mach Num=0.95,Mode=(1,0),Freq=2.76) 149

VII.57 Pressure Distribution Along Duct Wall (Duct 4,Mach Num=0.68,Mode=(1,0),Freq=2.76) 150

FIGURE PAGE

VII.58 Pressure Distribution Along Duct Wall (Duct 4,Mach Num=0.95,Mode=(1,0),Freq=2.76) 151

VII.59 Pressure Distribution Along Duct Wall (Duct 3,Mach Num=0.68,Mode=(2,0),Freq=3.375) 152

VII.60 Pressure Distribution Along Duct Wall (Duct 3,Mach Num=0.95,Mode=(2,0),Freq=3.375) 153

VII.61 Pressure Distribution Along Duct Wall (Duct 4,Mach Num=0.68,Mode=(2,0),Freq=3.375) 154

VII.62 Pressure Distribution Along Duct Wall (Duct 4,Mach Num=0.95,Mode=(2,0),Freq=3.375) 155

VII.63 Comparison of Sound Attenuation Due to Flow for Three Inlets 157

A.1 Two-Dimensional Duct with Lining 166

C.1 Circular and Rectangular Bends with and without Lining 175

C.2 Acoustic Pressure Distribution (Real Part) in a Rectangular Bend 176

C.3 Acoustic Pressure Distribution (Real Part) in a Circular Bend 177

F.1 Exact, Runge-Kutta and Finite Difference Solution (Frequency = 5.0) 213

F.2 Exact, Runge-Kutta and Finite Difference Solutions (Frequency = 2.0) 214

F.3 Linear and Non-Linear Solutions (M = 0.0) 215

FIGURE PAGE

F.4 Linear and Non-Linear Solutions
(M = 0.5) 216

F.5 Linear and Non-Linear Solutions
(M = 0.8) 217

NOMENCLATURE

A	Area
b	Boundary
$[B^e]$	Book Keeping Matrix
{C}	Column Vector
C	Speed of Sound
e	Element
E	Number of Elements
f'	Derivative with respect to x
f	A Constant
H	Duct Height
H_i	Basic Function
$[H^e(x)]$	Interpolation Functions
i	$\sqrt{-1}$
I	Variational Statement
k	Wave Number
L	Differential Operator, Duct Length
M	Mach Number
m	Spinning Mode Number
N	Number of Nodal Points
n	Normal, Constant Exponent
$\{P^e\}$	Nodal Values of Pressure
p	Dimensionless Acoustic Pressure
$\bar{p}$	Approximate Solution
Q	Number of Quadrature Points
R	Local Coordinate, Function in r

R_p	Pressure Reflection Ratio
R_ϕ	Velocity Potential Reflection Ratio
r	Cylindrical Coordinate
S	Area
[S]	Global Matrix
$[S^e]$	Element Square Matrix
T	Matrix Transpose
t	Dimensionless Time
U	Mach Number in the Axial Direction
u	Acoustic Velocity
V	Mach Number in the Radial Direction
v	Volume
$\bar{V}$	Steady State Velocity Vector
W_i	Weight Function for Numerical Integration
x,X	Cartesian Coordinate
y,Y	Cartesian Coordinate
z,Z	Cartesian and Cylindrical Coordinate
Z	Function in z, Impedance Ratio

Greek Symbols

η	Dimensionless Frequency
ω	Exciting Frequency
β	i, j, ... k, ...
ζ	Diminsionless Density
γ	A Constant, Specific Heat Ratio
ε	Residual Error

Θ	Cylindrical Coordinate
Φ	Non-Dimensional Velocity Potential
$\tilde{\phi}$	Steady Component
$\bar{\phi}$	Unsteady Acoustical Component
∇	Gradient
ψ	Function in Radial Direction

CHAPTER I

INTRODUCTION

I.1 Overview

There has been a great interest in studying the influence of high subsonic Mach number flows on the propagation and attenuation of sound along aircraft engine ducts. Such a study enables one to optimize the existing designs of the ducts in order to reduce noise without the excessive penalties incurred when implementing the choked inlets (a device which accelerates inlet air to sonic velocities to reduce inlet noise). The need for more flexible suppressor design techniques which can handle acoustic flow field complications stimulated this research work both numerically and experimentally. There is to date no analytical method which can account for all design variables encountered in the flow field such as variable area duct and the subsequent velocity gradients of the compressible flows, the complexity of noise sources, presence of lining material and the reflection boundary condition at the duct termination. In order to handle the complexity of the problem at hand, researchers have embarked upon numerical techniques such as the finite difference method or semi-numerical techniques such as the integral methods. Implementation of finite element techniques has been favorable in many types of engineering

problems; however, the use of the method in solving the wave equation has not been seriously considered. The mathematical model as shown in Figure I.1 is an axisymmetric variable area duct with its centerline located on the Z-axis; the noise source (compressor fan) is located at one end of the duct (Z = 0) and the other end is directed towards the radiation field. The experimental investigation of the influence of high subsonic Mach number flows on the propagation of sound along the duct needs a special facility in order to obtain a clean noise source at the high Mach number flows. The complexity of the noise field generated by the compressor fan is one of the difficulties in conducting a reliable test program and therefore a spinning mode synthesizer to produce a spinning-mode sound of a given frequency and sufficient intensity is required. In addition, in order to suppress the compressor fan noise, a choked inlet is to be introduced downstream of the test section and the spinning-mode synthesizer.

Finally, to obtain a high subsonic Mach number flow under these circumstances, a transonic compressor is used. Figure I.2 shows the relative location of the components used for the experimental investigation.

I.2 Statement of the Problem

The purpose of the research work reported here is to:

1. Efficiently implement a finite element technique to solve the problem of sound propagation in

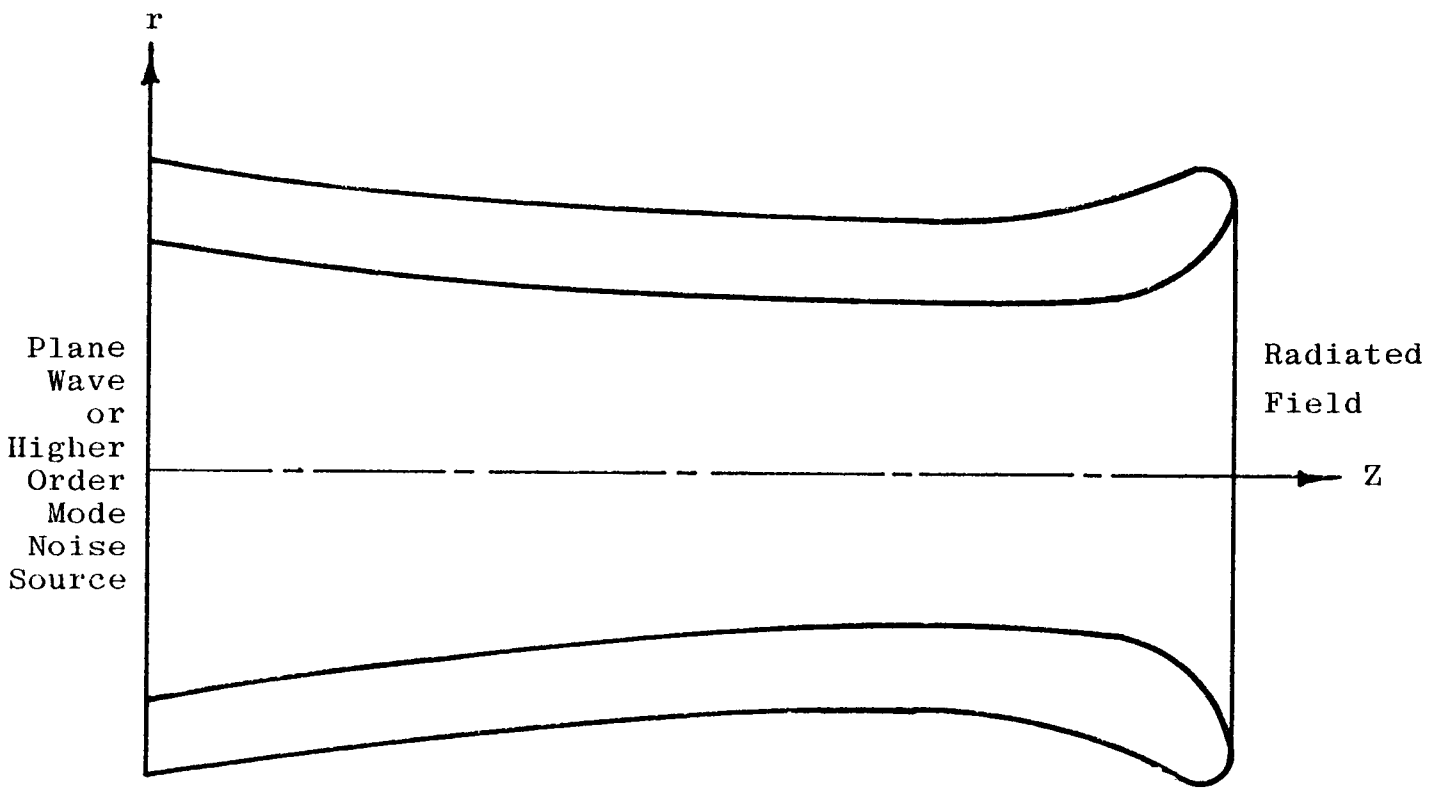


Figure I.1 Cross-Section in a Variable Area Duct
Showing Coordinate System

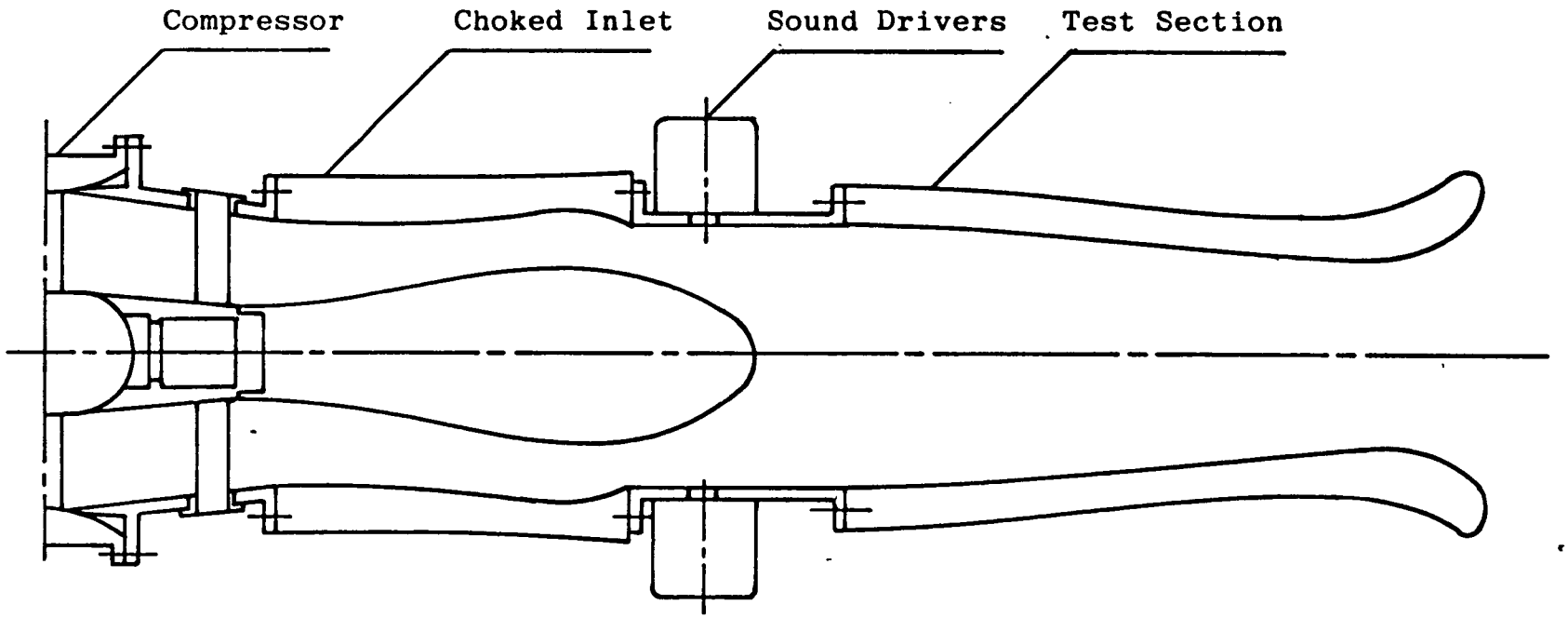


Figure I.2 Schematic of Experimental Set-up
in NASA-Langley Research Center

axisymmetric hard wall variable area ducts carrying high subsonic Mach number flows and compare the finite element solution with the exact one for the two-dimensional constant area cases with or without mean flow.

2. Experimentally, investigate the influence of high subsonic Mach number flows on sound propagation and attenuation in simulated aircraft inlet ducts.

I.3 Importance of the Study

An efficient finite element technique for solving the linear wave equation in its general form is highly needed; therefore, a general purpose finite element program has been developed for the problems of a complex number nature with the following considerations:

1. The computer program is written using complex number notation unlike most of the existing finite element programs which deal with real numbers only.
2. A dynamic storage is required to allow using the program on different size machines (machine-independent program).
3. In-core storage for the resulting system of equations is accomplished in non-symmetric banded form to minimize computer storage.
4. The resulting system of equations is solved

in complex number fashion using matrix triangularization and back substitution which is proven to be highly efficient technique in matrix algebra.

5. Post element solution on an element-by-element basis is required to generate the acoustic properties of the duct under consideration.
6. Extending the program to the three-dimensional cases can be done in a straightforward manner.

As for the experimental analysis, the test was conducted in the anechoic chamber transonic compressor facility of the NASA-Langley Research Center.

The experiment facility encompasses the following unique features:

1. A spinning-mode synthesizer is capable of generating the plane wave and two circumferential modes [(0,0), (1,0), (2,0)].
2. A translating centerbody choked inlet is used to suppress the noise generated by the compressor fan and thus provides a quiet high subsonic Mach number flow through the test section.

Experiments using such a facility can be extended to study the effect of high Mach number flows in the presence of lining material.

I.4 Scope and Organization of the Text

Following this introductory chapter, a literature survey is presented in Chapter II. A finite element model for the two-dimensional wave equation in terms of the acoustic pressure along with example problems is presented in Chapter III. In Chapter IV, the general non-linear axisymmetric acoustic equation for the velocity potential is derived. Boundary conditions are presented for the linearized equation.

A finite element algorithm for the axisymmetric wave equation using Galerkin's formulation is presented in Chapter V. In addition, the highlights of the finite element methodology and computer implementation are sketched out. Chapter VI summarizes the experimental investigation of the influence of high subsonic Mach number flows on sound propagation. In this chapter, a description of the test facility and test sections (inlets) is discussed along with the instrumentation and test procedure. Chapter VII is devoted to the presentation of finite element predictions and test results. Discussion, conclusion and recommendations are also presented in Chapter VII.

The main text is followed by appendixes which contain basic, detailed information pertinent to the continuation and/or completion of the presented material.

CHAPTER II

LITERATURE SURVEY

II.1 Introduction

A review is given of current numerical and integral methods for calculating the propagation of sound along aircraft engine inlets. The review includes finite difference, integral and weighted residual methods and finally, the finite element method. Emphasis is focused on the numerical approaches using finite element methods. A survey of recent experimental work is also presented.

II.2 Finite Difference Method

The finite difference approach for numerically analyzing the problem of sound propagation has been widely considered in recent years. An extensive survey of the acoustics of aircraft inlets has been presented by Nayfeh et al.[1], in which they summarized some of the finite difference techniques implemented in duct acoustics such as central-difference methods.

Alfredson[2] used the finite difference method for predicting steady state sound fields. In his analysis, he presented the one-dimensional case, axisymmetric case and finally solved the problem of predicting sound fields in a right angle bend in a rectangular duct. He concluded that the finite difference approach is of particular value for calculating the sound fields in irregular shapes with non-

uniform boundary conditions and that it may be the only mathematical method available for predicting the results in these circumstances.

Baumeister and Bittner[3] solved the problem of sound propagation in one-dimensional straight hard-wall duct and in a two-dimensional straight soft-wall duct without steady flow using a finite difference algorithm and decomposing the governing equations into their real and imaginary parts.

Baumeister and Rice[4] presented a difference theory for noise propagation in an acoustically-lined duct with mean flow by extending the work of Baumeister and Bittner to include uniform mean flow. They solved the one-dimensional hard-wall duct with mean flow and the two-dimensional soft-wall duct with no mean flow.

In a recent study Baumeister[5] presented an analysis of sound propagation in ducts using the wave envelope concept. In his analysis, Baumeister transformed the governing equations to a form with a non-oscillatory solution along the duct length and then applied a finite difference algorithm.

Quinn[6] applied a finite difference algorithm for computing sound propagation in non-uniform ducts.

II.3 Integral and Weighted Residual Methods

Bell et al.[7] used the integral equation method for determining the resonant frequencies and natural modes

of arbritrarily shaped ducts.

More recently Quinn[8] used this approach to solve the reduced wave equation in ducts containing no flow or uniform flow. In his analysis Quinn solved the problem of sound propagation in variable cross sectional ducts and ducts with axially varying wall linings.

The method of weighted residual has been very popular when calculating eigenvalues and mode shapes. Several researchers have embarked upon implementing the technique for handling problems with smoothly varying axial impedances and cross section for no flow cases. The presence of non-uniform flow complicates the selection of the basis functions for rapid convergence and consequently limits the applicability of the technique.

Unruh and Eversman[9] applied the weighted residual method of Galerkin to solve the acoustic transmission problem in an attenuating duct.

Beckemeyer and Eversman[10] presented the variational statement and used Ritz expansion for studying the propagation of acoustic waves in non-uniform wave guides.

Eversman et al.[11] used the method of weighted residuals to solve the problem of sound transmission in non-uniform ducts without flow. More recently Eversman[12] extended the technique to include the cases of non-uniform two-dimensional ducts with flow.

II.4 Finite Element Method

The application of the finite element methods to acoustic-related problems as pointed out by Watson and Lansing[13] has been very limited. In addition, the implementation of the technique in the determination of the acoustic properties of jet engine air intakes has not been seriously considered.

In acoustic-related fields, Watson and Lansing gave a summary of some of the leading works.

Gladwell[14] was the first to apply a finite element method to calculate the natural frequencies of the one- and two-dimensional Helmholtz equation.

Mason[15] applied the finite element technique to the acoustic damping problem. Herting and Joseph[16] used the technique to analyze the acoustic problem of solid rocket motor cavities.

Craggs[17, 18, 19] has done an extensive work on applying the finite element technique for determining the natural modes and frequencies of complex shaped enclosures, studying the boundary flexibility and sound transmission between irregular enclosures and presenting some practical applications of acoustic finite elements.

Shuku and Ishihara[20] have analyzed the acoustic field in irregularly shaped rooms using the finite element method based on a variational formulation.

Davies[21] has presented an excellent comparison of the relative advantage of the various numerical methods for solving the hollow-wave guide problem. In the analysis, Davies studied the finite difference and the finite element approaches along with some other methods which result in a standard form of the matrix-eigenvalue problem.

The problem of determining the acoustic properties of turbofan inlets using finite element techniques was first considered in a recent study by Sigman et al.[22]. They applied the technique in combination with Galerkin's method to solve the linerarized axisymmetric velocity potential equation by decomposing the governing equation and the boundary conditions to their real and imaginary parts, then solving the problem in a real number fashion. In their analysis, they used triangular elements. More recently, the problem was reconsidered by Abrahamson[23] who applied a finite element algorithm for sound propagation in axisymmetric ducts containing compressible mean flow. Abrahmanson carried out his solution in complex number notation for four degrees of freedom per node, acoustic pressure and the three acoustic velocity components.

Decomposition of the governing equations as was done by Sigman and his co-workers resulted in doubling the number of unknowns and destroying the structure of the global matrix, hence lowering the efficiency of the solution. Although Abrahamson's solution was carried out

in its complex number form, the number of degrees of freedom per node was unnecessarily increased and thus lowered the efficiency of his solution. The study by Abrahamson was published while this present research work has been in its final phases and showed itself to be the most efficient one to date.

Eversman et al.[24] have done a recent study on a comparative evaluation of finite element and weighted residuals computational schemes for the problem of acoustic wave transmission in non-uniform ducts. They pointed out that their finite element results can be improved if the same number of elements is used across the duct with a non-uniform distribution, in other words, by positioning smaller elements near the outer boundary and larger ones near the centerline, a measure which has been accounted for already in this research work presented herein.

II.5 Experimental Studies

Lumsdaine[25] found that sizeable attenuation of a plane wave is possible by changing the velocity gradients in the diffusion section of a variable area duct carrying high subsonic Mach number flows.

Plumblee and Dean[26] made some measurements of the acoustic field inside and outside constant area ducts subjected to plane wave or higher order mode excitation in the presence of low Mach number flows.

A search in the literature failed to uncover any experimental work on variable area ducts tested under high-order mode excitation generated by a spinning-mode synthesizer in the presence of high subsonic Mach number flows.

CHAPTER III

FINITE ELEMENT FORMULATION OF THE TWO-DIMENSIONAL WAVE EQUATION

III.1 Introduction

The application of a finite element technique in solving the two-dimensional wave equation in hard and soft wall ducts with and without mean flow is presented in this chapter. A variational statement for the no flow case exists. For the case when mean flow is present, a Galerkin formulation is implemented. For the one-dimensional case, element matrices can be formed and integrated in a closed form representation. The global matrix is formed through the application of an assembly algorithm over all the elements. After applying the forced boundary condition to the system equation the resulting tridiagonal system is solved using the Thomas algorithm in a complex number notation. Whereas for the two-dimensional case, the assembly algorithm results in a banded global matrix with a bandwidth dependent upon the numbering scheme of the element nodes, after applying the forced boundary condition at one end of the duct and the non-reflection boundary condition at the other end, the system of equations is triangularized using Gauss elimination and then solved using back substitution in a complex number formulation.

The one-dimensional finite element solution is compared with the exact one for hard-wall duct with or

without flow and the agreement seems to be excellent for the no flow case when ten elements were considered. For the flow case thirty elements were considered in the axial direction when the flow is in the direction of wave propagation or opposite to it.

III.2 Mathematical Model

The steady non-dimensional two-dimensional wave equation for the acoustic pressure in a uniform duct carrying low Mach number flow can be written as (see Appendix A),

$$(1-M^2)\left(\frac{\partial^2 p}{\partial x^2}\right) + \left(\frac{\partial^2 p}{\partial y^2}\right) - 2i(2\pi\eta)M\frac{\partial p}{\partial x} + (2\pi\eta)^2 p = 0 \qquad \text{(III.2.1)}$$

One end of the duct is subjected to a forced boundary condition where the noise source is located. A non-reflection boundary is imposed at the other end and yields a gradient boundary condition. For a hard-wall duct a zero pressure gradient is imposed at the boundary or mathematically,

$$p(0,y) = 1 \qquad \text{at the source} \qquad \text{(III.2.2)}$$

$$\frac{\partial p}{\partial x} = \frac{-i(2\pi\eta)}{1+M}p \qquad \text{at the free end} \qquad \text{(III.2.3)}$$

$$\frac{\partial p}{\partial n} = 0 \qquad \text{for hard walls.} \qquad \text{(III.2.4)}$$

For no flow cases the wall boundary condition takes the form:

$$\frac{\partial p}{\partial n} = -\frac{i(2\pi\eta)}{Z}p \qquad \text{(III.2.5)}$$

where Z is the impedance ratio of the soft-wall duct.

For the one-dimensional cases, Equations (III.2.1)-(III.2.4) reduce to

$$(1-M^2)\frac{d^2p}{dx^2} - 2i(2\pi\eta)M\frac{dp}{dx} + (2\pi\eta)^2p = 0 \qquad \text{(III.2.6)}$$

$$p(0) = 1 \qquad \text{(III.2.7)}$$

$$\frac{dp}{dx} = -\frac{i(2\pi\eta)}{1+M}p \qquad \text{(III.2.8)}$$

III.3 Integral Formulation for the No Flow Case M=0

The finite element model of the problem is based on an integral formulation. From calculus of variation, it can be shown that the solution of the problem at hand is detained by minimizing the functional (see Appendix B),

$$I = \frac{1}{2}\int_0^L [(\frac{dp}{dx})^2 - (2\pi\eta)^2p^2]dx + \frac{1}{2}\, i(2\pi\eta)p^2 \Big|_{\text{free end}} \qquad \text{(III.3.1)}$$

Mathematically,

$$\frac{\partial I}{\partial p} = 0 \qquad \text{must be satisfied.} \qquad \text{(III.3.2)}$$

III.4 Finite Element Model

A. Element Behavior and Geometry

Introducing a set of N nodal points in the region from x=0 to x=L, let this set of nodes divide the region into a total of E one-dimensional elements. Assume each element has two nodes say i,j with coordinates x_i and x_j, respectively. Also, let the degrees of freedom at the

nodes i,j be p_i and p_j. The acoustic pressure variation is assumed linear along the element ij, that is

$$p^e(x) = \alpha_1 + \alpha_2 x \qquad \text{(III.4.1)}$$

In a matrix representation,

$$p^e(x) = [1 \quad x] \begin{Bmatrix} \alpha_1 \\ \alpha_2 \end{Bmatrix} \qquad \text{(III.4.2)}$$

Symbolically

$$p^e(x) = [N(x)] \{\alpha^e\} \qquad \text{(III.4.3)}$$

This expression, of course, is valid throughout the element, including the nodal points. At the nodes,

$$\begin{Bmatrix} p_i \\ p_j \end{Bmatrix} = \begin{bmatrix} 1 & x_i \\ 1 & x_j \end{bmatrix} \begin{Bmatrix} \alpha_1 \\ \alpha_2 \end{Bmatrix}$$

or

$$\{P^e\} = [C^e] \{\alpha^e\} \qquad \text{(III.4.4)}$$

where $\{P^e\}$ represents the unknown nodal values of acoustic pressure. To solve for $\{\alpha^e\}$,

$$\{\alpha^e\} = [C^e]^{-1} \{P^e\} \equiv [CI^e] \{P^e\} \qquad \text{(III.4.5)}$$

where

$$[CI^e] = \frac{1}{(x_j - x_i)} \begin{bmatrix} x_j & -x_i \\ -1 & 1 \end{bmatrix} \qquad \text{(III.4.6)}$$

Now $\{p^e(x)\}$ can be rewritten as

$$p^e(x) = [N(x)][CI^e] \{P^e\}$$

or

$$p^e(x) = [H^e(x)] \{P^e\} \qquad \text{(III.4.7)}$$

where

$$[H^e(x)] = [N(x)][CI^e]$$

In this simple case $[H^e]$ can be obtained in a closed form and is given by

$$H^e(x) = [(\frac{x_j - x}{x_j - x_i})(\frac{x - x_i}{x_j - x_i})]$$

$$= [H_i(x) \quad H_j(x)] \qquad \text{(III.4.8)}$$

In a local coordinate system, this can be expressed as

$$[H^e(R)] = [H_1(R) \quad H_2(R)]$$

where $H_1(R) = 1-R$ and $H_2(R) = R$

and in general $\sum_{i=1}^{N} H_i = 1$

B. Expression for the Derivative

From above, it was shown that

$$\{p^e\} = [H^e]\{P^e\} \equiv \{P^e\}^T [H^e]^T$$

where T stands for maxtix transpose. The first derivative with respect to the x direction can now be written as

$$\frac{dp^e}{dx} = [\frac{dH^e}{dx}]\{P^e\} = \{P^e\}^T [\frac{dH^e}{dx}]^T \qquad \text{(III.4.9)}$$

C. System Equations

To get the system of algebriac equations resulting from dividing the domain into elements, the functional I will be considered to be composed of two elements

$$I = \sum_{e=1}^{E} I^e + I^b \qquad \text{(III.4.10)}$$

where

$$I^e = \frac{1}{2} \int_{x_i}^{x_j} [(\frac{dp}{dx})^2 - (2\pi\eta)^2 p^2] dx \qquad \text{(III.4.11)}$$

and

$$I^b = \frac{1}{2} i(2\pi\eta)p^2 \qquad \text{(III.4.12)}$$

and where I^e denotes the contribution of each element in the domain and I^b is the contribution resulted from the gradient boundary condition at the free end.

The governing system of equation results from

$$\frac{\partial I}{\partial \{P\}} = \{0\} \qquad \text{(III.4.13)}$$

where

$$\{P\}^T = \{p_1 \; p_2 \; \cdots \; p_N\} \qquad \text{(III.4.14)}$$

$$\sum_{e=1}^{E} \frac{\partial I^e}{\partial \{P\}} + \frac{\partial I^b}{\partial \{P\}} = \{0\} \qquad \text{(III.4.15)}$$

Equation (III.4.15) gives a set of algebraic equations in the unknown vector $\{P\}^T$.

Generalizing the shape function concept, we have

$$I^e = \frac{1}{2} \int_{x_i}^{x_j} \{P^e\}^T ([\frac{\partial H^e}{\partial x}]^T [\frac{\partial H^e}{\partial x}] \{P^e\} - (2\pi\eta)^2 [H^e]^T [H^e] \{P^e\}) dx \qquad \text{(III.4.16)}$$

Since $\{P^e\}$ are unknown constants

$$I^e = \frac{1}{2}\{P^e\}^T\left[\int_{x_i}^{x_j}\left(\left[\frac{\partial H^e}{\partial x}\right]^T\left[\frac{H^e}{x}\right]\right.\right.$$

$$\left.\left. - (2\pi n)^2[H^e]^T[H^e]\right)dx\right]\{P^e\} \qquad \text{(III.4.17)}$$

or symbolically,

$$I^e = \frac{1}{2}\{P^e\}^T[S^e]\{P^e\} \qquad \text{(III.4.18)}$$

To evaluate $\sum_E \frac{\partial I^e}{\partial\{P\}} = 0$, we must express I^e as a function of all the nodal values $\{P\}$; this can be done by introducing a matrix $[B]$ such that $\{P^e\} = [B^e]\{P\}$. Now, I^e can be written in the form

$$I^e = \frac{1}{2}\{P\}^T\left[[B^e][S^e][B^e]\right]\{P\} \qquad \text{(III.4.19)}$$

Differentiating with respect to $\{P\}$ we get

$$\frac{\partial I^e}{\partial\{P\}} = [B^e][S^e][B^e]\{P\} \qquad \text{(III.4.20)}$$

Similarly for the boundary we have,

$$P = \{P^b\} = [B^b]\{P\} \qquad \text{(III.4.21)}$$

and

$$\frac{\partial I^b}{\partial\{P\}} = [B^b][S^b][B^b]\{P\} \qquad \text{(III.4.22)}$$

Thus,

$$\left(\sum_{e=1}^{E}[B^e]^T[S^e][B^e]\right)\{P\} + \left([B^b]^T[S^b][B^b]\right)\{P\} = \{0\}$$

Symbolically,

$$([S^e] + [S^b])\{P\} = \{0\}$$

or

$$[S]\{P\} = \{0\} \qquad \text{(III.4.23)}$$

which is the governing system of equations to be solved for the unknown nodal parameters {P}. Since the element matrix $[S^e]$ is symmetric [S] is also symmetric. Upon applying the forced boundary condition, the above system of equations takes the form

$$[S]\{P\} = \{C\}, \qquad \text{(III.4.24)}$$

A computer program has been developed to assemble the element matrices, apply boundary conditions and then solve the resulting system of equations. For the one-dimensional problem, the system is tridiagonal and the Thomas algorithm is implemented in a complex number version to obtain the solution

III.5 The Two-Dimensional No Flow Case

In the foregoing analysis the finite element methodology has been illustrated for the one-dimensional no-flow wave equation. This section extends the analysis to the two-dimensional case. Although a variational statement does exist for the problem, a numerical quadrature is introduced to integrate the expressions:

$$[S^e] = \int_A \int ([\frac{\partial H^e}{\partial x}]^T [\frac{\partial H^e}{\partial x}] + [\frac{\partial H^e}{\partial Y}]^T [\frac{\partial H^e}{\partial Y}]$$

$$- (2\pi\eta)^2 [H^e]^T [H^e]) dA \qquad \text{(III.5.1)}$$

Numerically,

$$[S^e] = \sum_{i=1}^{Q} W_i ([\frac{\partial H^e}{\partial x}]_i^T [\frac{\partial H^e}{\partial x}]_i + [\frac{\partial H^e}{\partial Y}]_i^T [\frac{\partial H^e}{\partial Y}]_i$$

$$- (2\pi\eta)^2 [H^e]_i^T [H^e]_i) \qquad \text{(III.5.2)}$$

where Q is the number of quadrature points, W_i is the tabulated weight function. Here again, the element square matrix is symmetric and hence the global matrix [S] which facilitates the solution of the resulting system of equations. Generally speaking, the matrix [S] is a banded one with a bandwidth dependent on the node numbering scheme.

III.6 Numerical Results for the One-Dimensional and Two-Two-Dimensional Case

In order to assess the accuracy of the finite element technique, the one-dimensional problem is solved using 10 and 20 elements, and the solution is compared with the exact one for $\eta = 1.0$. Figure III.1 shows the real and the imaginary parts of the non-dimensionalized acoustic pressure. For the 20-element case, agreement seems to be excellent, while the solution is not as accurate at the termination for the 10-element case. Figures III.2 and III.3 present the shape of the wave along a two-

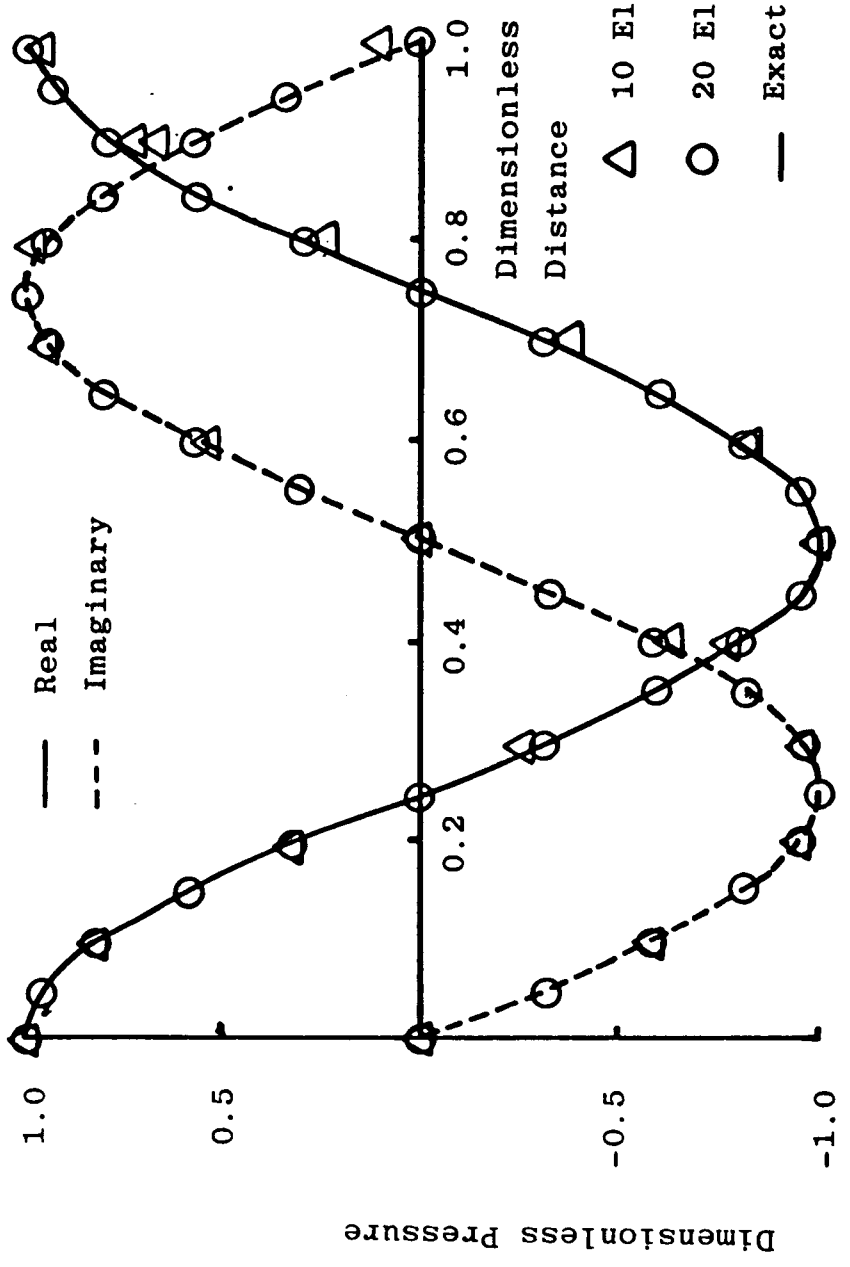


Figure III.1 One-Dimensional Exact and Finite Element Solutions

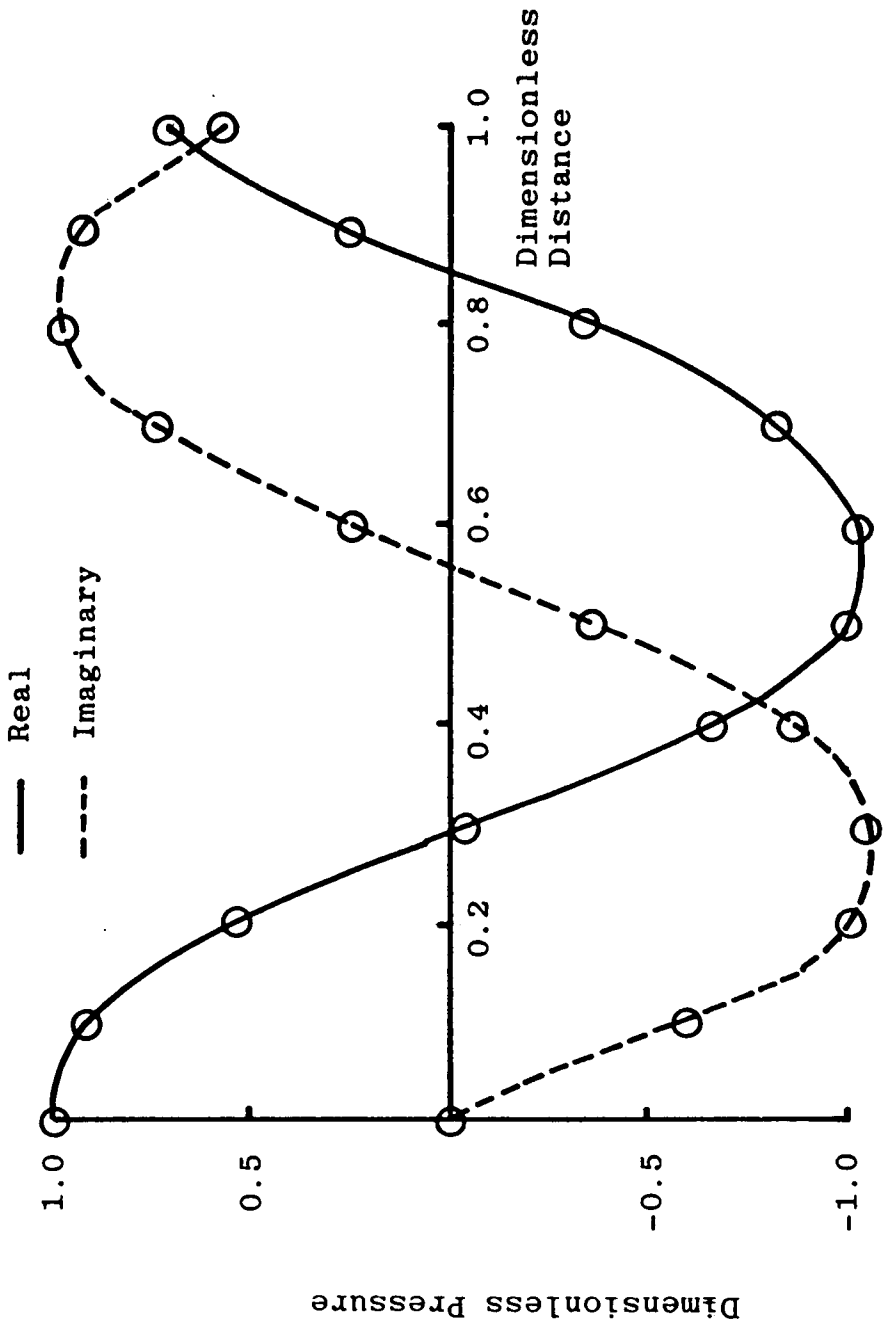


Figure III.2 Pressure Distribution Along the Centerline of a Constant Area Soft Wall Duct

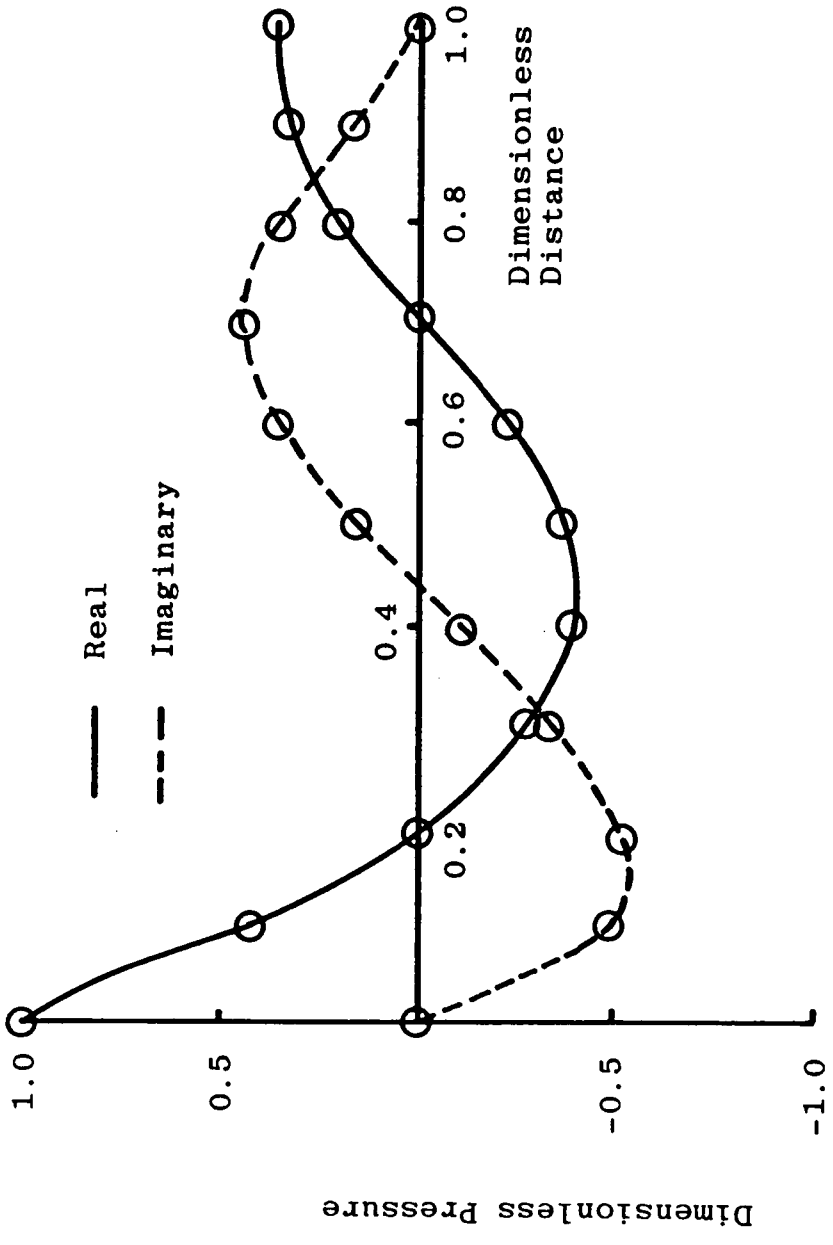


Figure III.3 Pressure Distribution Along the Soft Wall of a Constant Area Duct

dimensional soft-wall duct of length to height ratio L/H = 1.0 and wall specific impedance of (0.388-0.846i); the acoustic wave is distorted and greatly attenuated near the wall.

For a two-dimensional hard-wall duct [y = 0.5 cosh (1.25 x)] Figure III.4 shows that the distortion of the wave resembles that for the straight soft-wall duct. Figures III.5 and III.6 show the shape of the wave along the centerline and the wall. If the walls are treated with lining of specific impedance (0.388-0.844i) the effect is more appreciable along the wall than at the centerline as indicated in Figures III.7, III.8 and III.9. Later in this study (see Appendix C) the two-dimensional wave propagation in rectangular cross section will be solved to illustrate the versatility of the finite element technique in solving the wave equation when the geometry of the sound field and/or the boundary conditions are irregular. Such an application is highly needed to study the problem of noise propagation and attenuation in industrial ducts to optimize the existing designs by alleviating noise and reducing pressure loss.

III.7 A Comparison with Existing Results

The problem of sound attenuation in a two-dimensional lined duct considered by Quinn[8] and solved by the integral equation is reconsidered in this study and solved using the finite-element algorithm. In his analysis,

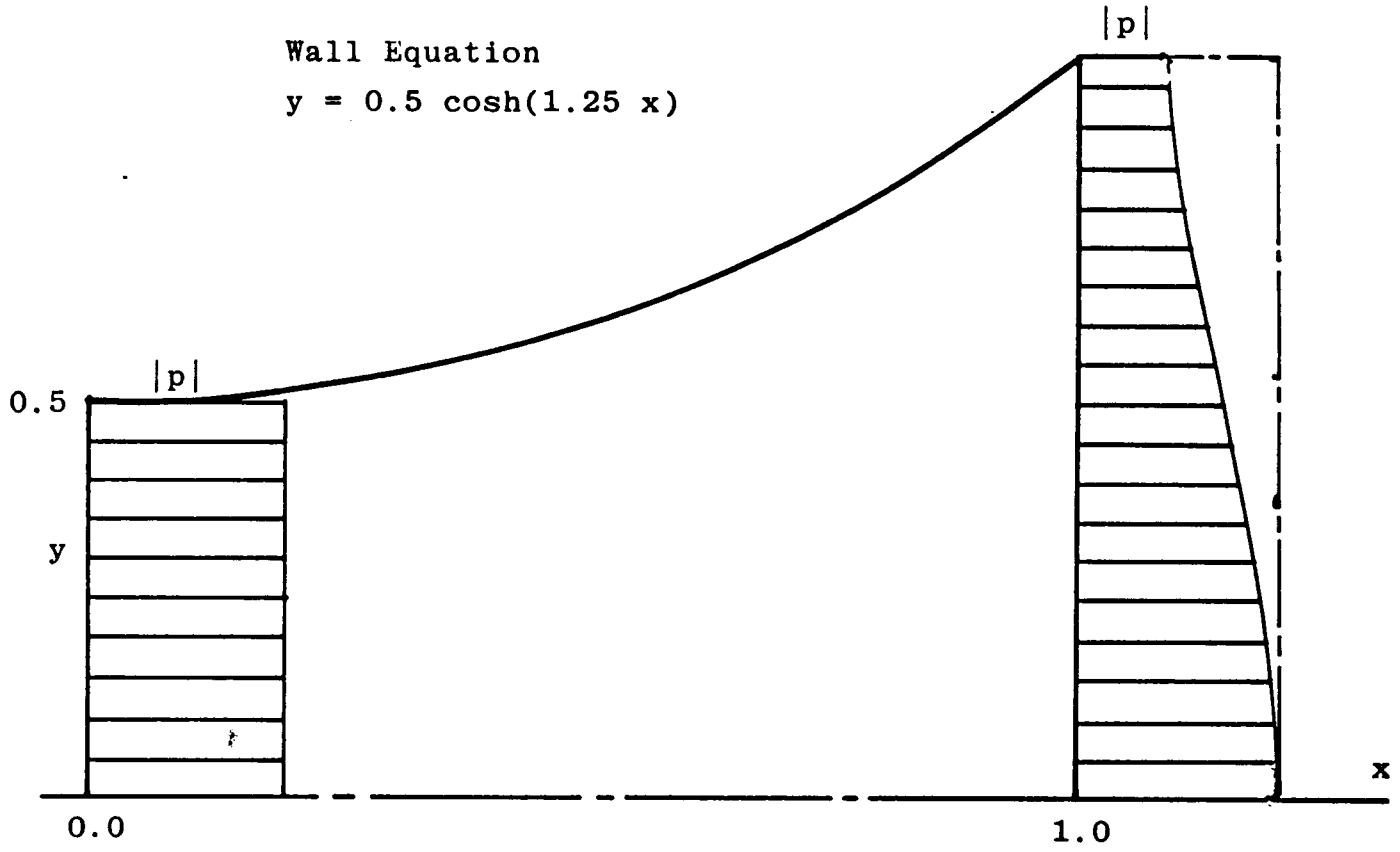


Figure III.4 Pressure Distribution at the Entrance and the Exit of a Hard Wall Variable Area Duct

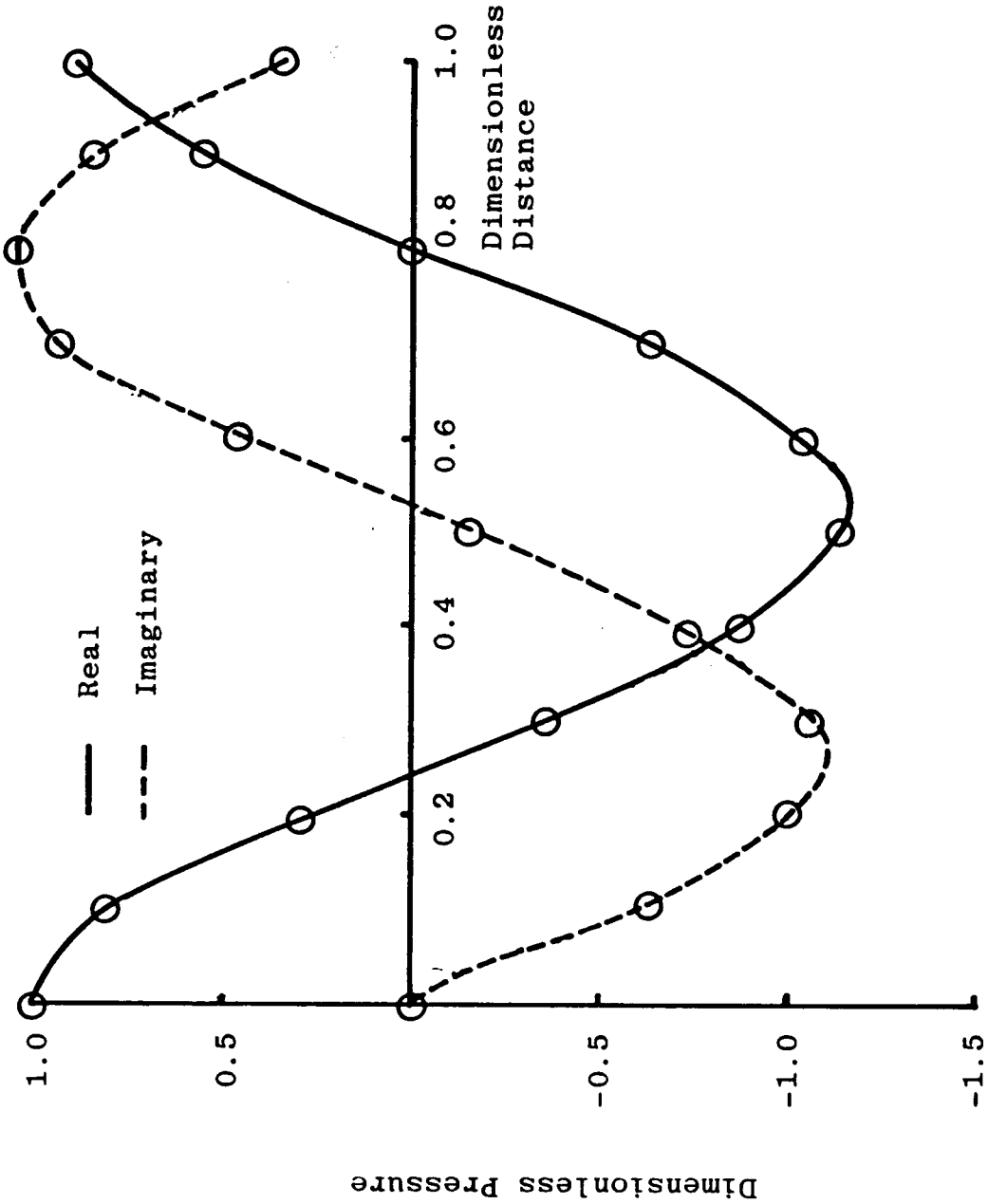


Figure III.5 Pressure Distribution Along the Centerline for a Variable Area Duct

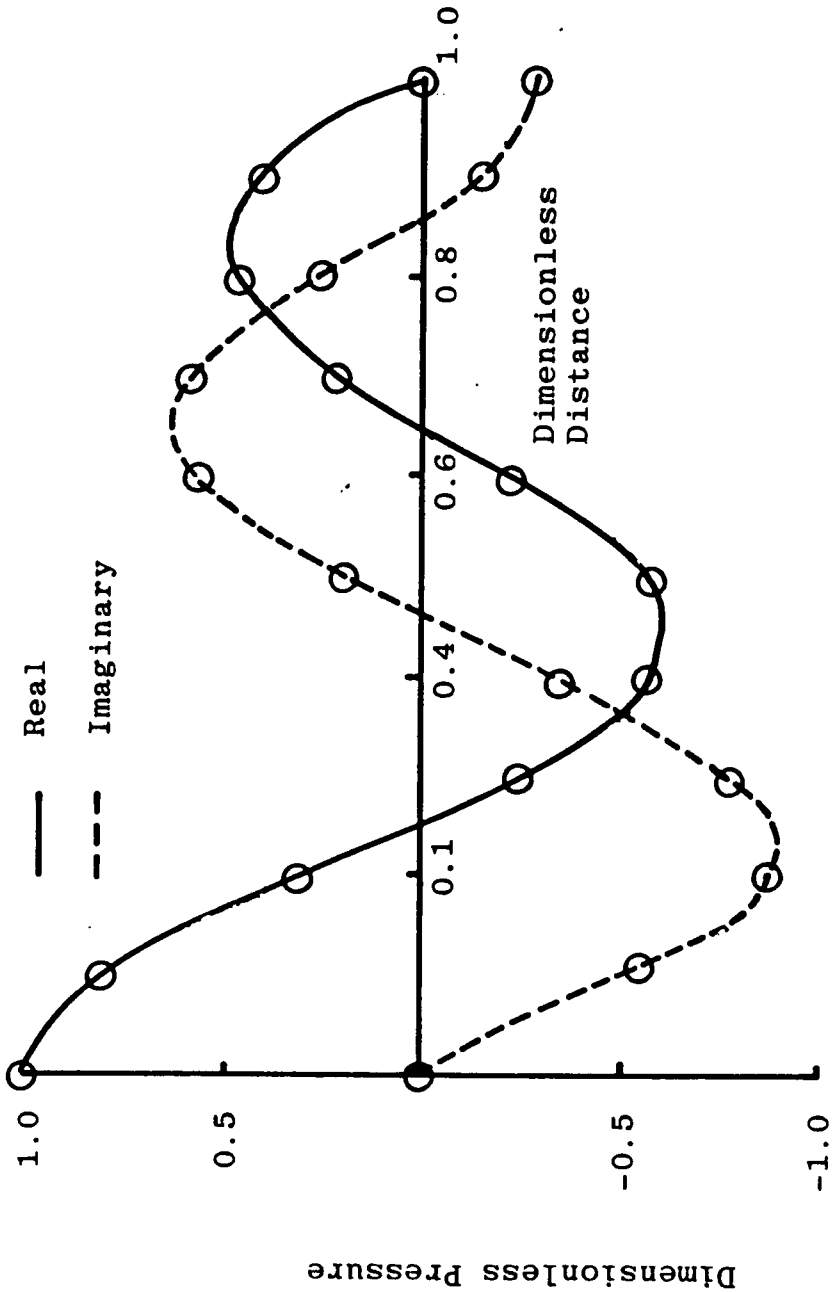


Figure III.6 Pressure Distribution Along the Wall for a Variable Area Duct

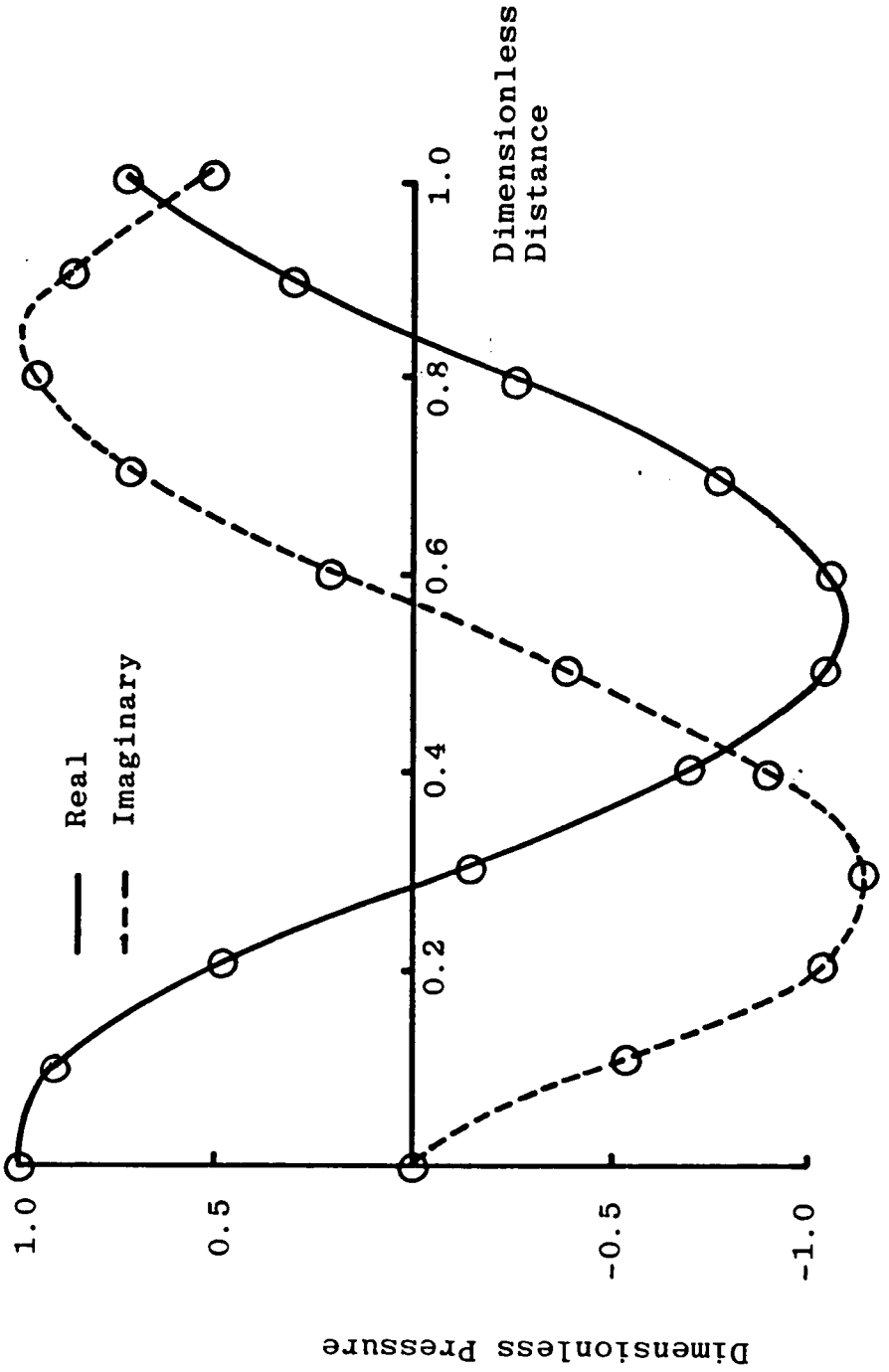


Figure III.7 Pressure Distribution Along the Centerline of a Soft Wall Variable Area Duct

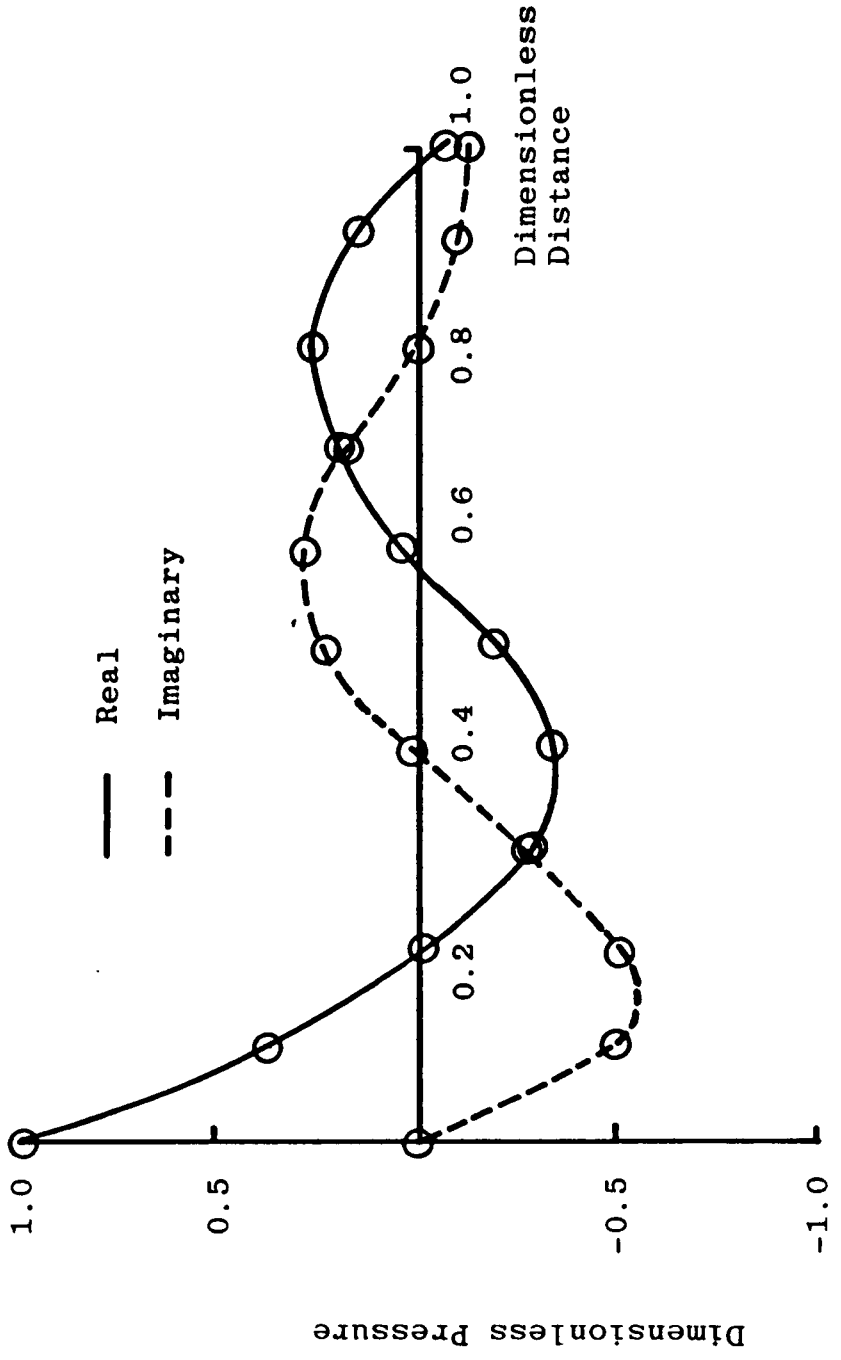


Figure III.8 Pressure Distribution Along the Soft Wall of a Variable Area Duct

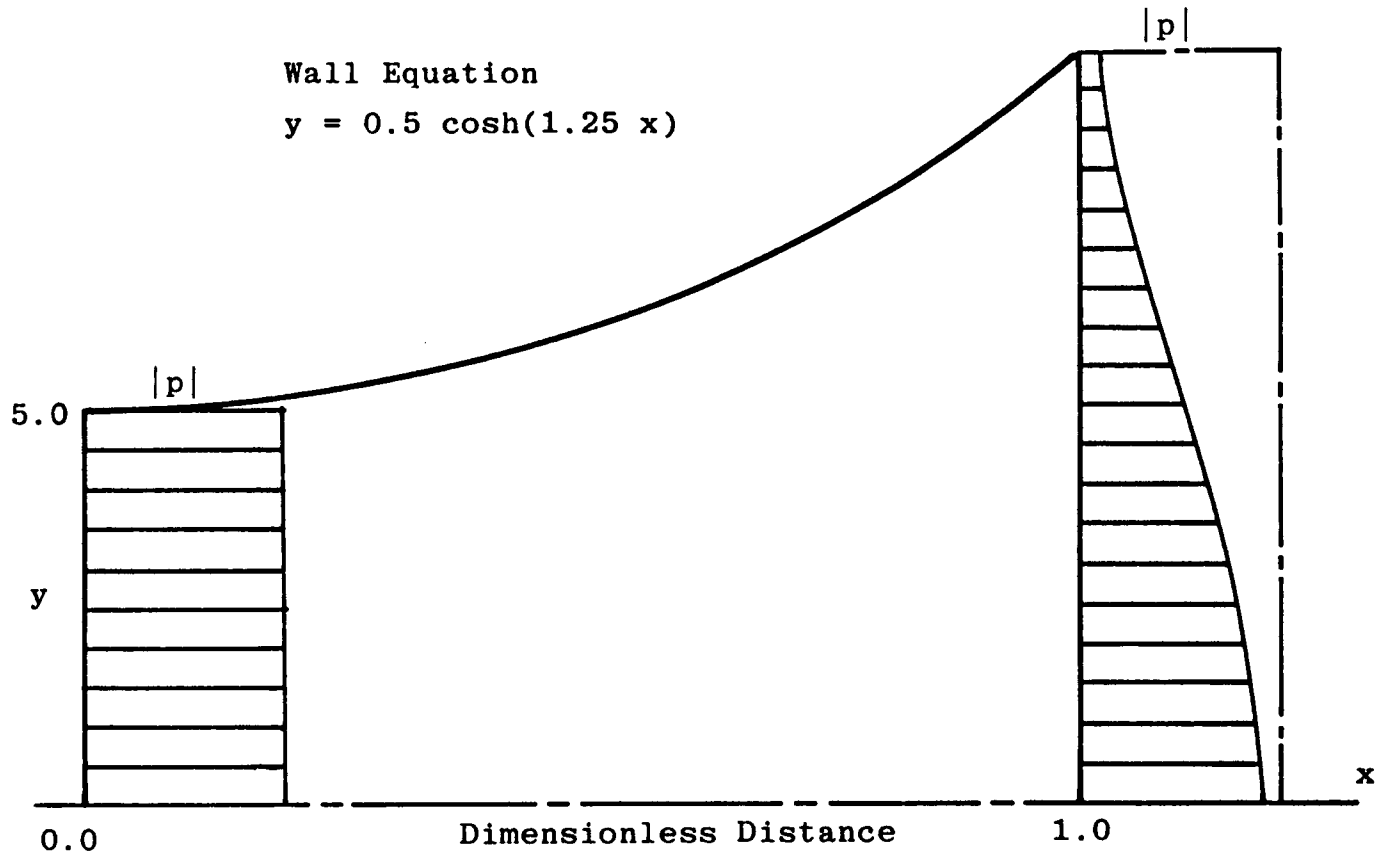


Figure III.9 Pressure Distribution at the Entrance and the Exit of a Soft Wall Variable Area Duct

Quinn compared the finite difference results with the integral solution for different mesh points along the x and y directions for dimensionless frequency $\eta = 1.0$ and specific wall impedance of (0.388-0.846i) of a uniform duct with L/H = 0.5. Finite difference results gave a sound attenuation of (-2.8 dB) for a 10 x 10 mesh, while the integral equation gave (-3.51 dB) for the same number of mesh points. Figure III.10 gives the attenuation along the duct using the finite element technique and the total attenuation is (-2.92 dB) for the same number of mesh points.

The conclusion that can be drawn from this analysis is that the finite element method can give comparable accuracy with both the finite-difference and the integral equation techniques.

III.8 The One-Dimensional Wave Equation with Flow

The steady non-dimensional one-dimensional wave equation is

$$(1-M^2)\frac{d^2p}{dx^2} - 2i(2\pi\eta)M\frac{dp}{dx} + (2\pi\eta)^2p = 0 \qquad \text{(III.8.1)}$$

with boundary conditions

$$p(0) = 1 \qquad \text{at the source} \qquad \text{(III.8.2)}$$

$$\frac{dp}{dx} = -\frac{i(2\pi\eta)}{1+M}p \qquad \text{at the free end.} \qquad \text{(III.8.3)}$$

Since the problem at hand has no variational statement due to the presence of flow, a Galerkin formulation is implemented which leads to non-symmetrical element square

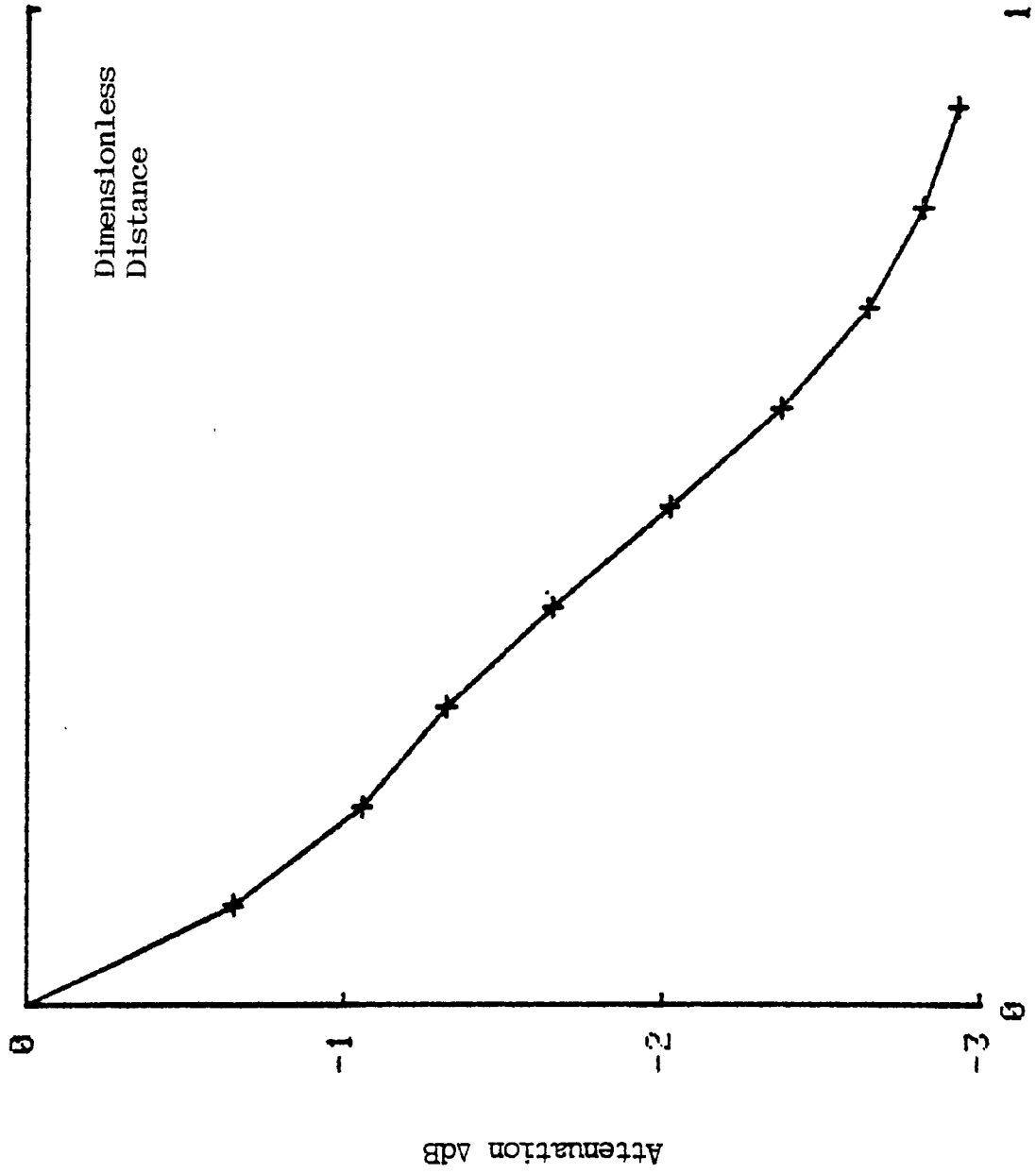


Figure III.10 Attenuation in a Two-Dimensional Soft Wall Duct

matrices. In general, the resulting global matrix is non-positive definite and non-hermitian. A special technique based on a modified Gauss elimination trangularization is employed along with back substitution to obtain the acoustic pressure at the nodes. For this particular problem, forming the element square matrix is accomplished using a closed form integration.

III.9 Galerkin's Method

In Galerkin's formulation, the solution of the differential equation is an approximate one and the condition is that the error between this solution and the exact one be orthogonal to the approximating functions. Consider the differential equation

$$Lp - f = 0 \qquad \text{(III.9.1)}$$

where L is a differential operator. Then, for an approximate solution $\bar{p} = \sum_i H_i P_i$ we get

$$L\bar{p} - f = \varepsilon \qquad \text{(III.9.2)}$$

where ε is a non-zero residual error in the original equation. Now, it is required that the weighted residual ε be minimized. One way to accomplish this is to require that $\int_A H_i \varepsilon dA = 0$ for each of the basis functions H_i. Mathematically, the basis function must be orthogonal to the error over the domain A. The application of Galerkin's method with the finite element methods yields the equation

$$\int_A H_\beta (L(\bar{p})-f)dA = 0 \qquad \text{(III.9.3)}$$

where $\beta = i, j, k, \ldots$ and p is the unknown parameter and is approximated by $p = [H_i, H_j, H_k, \ldots]\{P\}$. Applying this analysis to the problem at hand gives

$$L(p) = (1-M^2)\frac{\partial^2 p}{\partial x^2} - 2i(2\pi\eta)M\frac{\partial p}{\partial x} + (2\pi\eta)^2 p = 0 \qquad \text{(III.9.4)}$$

then,

$$\int_0^L H_\beta[(1-M^2)\frac{\partial^2 p}{\partial x^2} - 2i(2\pi\eta)M\frac{\partial p}{\partial x} + (2\pi\eta)^2 p]dx = 0 \qquad \text{(III.9.5)}$$

There is no limit on the order of the highest derivative in L(p). The highest-order derivative that is allowed in Galerkin's formulation stated above is one greater than the order of continuity in the interpolation equation. Since this study deals with linear interpolation functions which are of zero continuity, derivatives greater than the first are not allowed. In the problem under investigation this can be accomplished by integrating by parts to reduce the order of the differential operator.

Rewriting the equation for E elements we get

$$\sum_{e=1}^{E} \int_{L^e} [H^e]^T[(1-M^2)\frac{\partial^2 p}{\partial x^2} - 2i(2\pi\eta)M\frac{\partial p}{\partial x}$$

$$+ (2\pi\eta)^2 p]dx = 0 \qquad \text{(III.9.6)}$$

Upon integrating the first integral by parts,

$$\int_{L^e} [H^e]^T [(1-M^2)\frac{d^2p}{dx^2}]dx = [H^e]^T [1-M^2](\frac{dp}{dx})_{x_i}^{x_j}$$

$$- \int_{L^e} (1-M^2)(\frac{d[H^e]}{dx})^T(\frac{dp}{dx})dx \qquad \text{(III.9.7)}$$

Substitution of Equation (III.9.7) into Equation (III.9.6) yields,

$$\sum_{e=1}^{E} (\int_{L^e} [(1-M^2)(\frac{d[H^e]}{dx})^T(\frac{dp}{dx}) + 2i(2\pi\eta)M[H^e]^T\frac{dp}{dx}$$

$$- (2\pi\eta)^2[H^e]^T p]dx - (1-M^2)[H^e]^T(\frac{dp}{dx})_{x_i}^{x_j}) \qquad \text{(III.9.8)}$$

Now, if we let

$$\{p^e\} = [H^e]\{P^e\} \text{ and } \{p^b\} = [H^b]\{P^b\}$$

then

$$\sum_{e=1}^{E} (\int_{L^e} [(1-M^2)(\frac{d[H^e]}{dx})^T\frac{d[H^e]}{dx} + 2i(2\pi\eta)M[H^e]^T\frac{d[H^e]}{dx}$$

$$- (2\pi\eta)^2[H^e]^T[H^e])dx)\{P^e\}$$

$$+ (i(1-M)(2\pi\eta)[H^b]^T[H^b])\{P^b\} = \{0\} \qquad \text{(III.9.9)}$$

The first part in Equation (III.9.9) represents the assembly of element contribution which reduces to a square matrix, while the second part is the boundary contribution which is again a square matrix. The global matrix is in general a

tridiagonal one. The system of equations can be written as $[S]\{P\} = \{C\}$ after applying the forced boundary condition at one end. To illustrate, let us assume a linear interpolating function and substitute in the foregoing equation; the element contribution can be represented as (for a constant Mach number)

$$[S^e] = (1-M^2)\frac{1}{L_e}\begin{bmatrix} 1 & -1 \\ -1 & 1 \end{bmatrix} - \frac{(2\pi\eta)^2 L_e}{6}\begin{bmatrix} 2 & 1 \\ 1 & 2 \end{bmatrix}$$

$$+ i(2\pi\eta)M\begin{bmatrix} -1 & 0 \\ 0 & 1 \end{bmatrix} \qquad \text{(III.9.10)}$$

As for the boundary contribution:

$$[S^b] = i(1-M)(2\pi\eta)\begin{bmatrix} 1 & 0 \\ 0 & 0 \end{bmatrix} \qquad \text{(III.9.11)}$$

It is clear from Equation (III.9.10), that the element square matrix is no longer symmetric due to the presence of mean flow of Mach number M. Consequently, the global matrix is non-hermitian.

III.10 Numerical Results for the One-Dimensional Case with Mean Flow

Figure III.11 shows the finite element solution and the exact one for the dimensionless acoustic pressure along a one-dimensional hard-wall duct carrying steady mean flow of Mach number M in the direction of the wave propagation. The following numerical values are used:

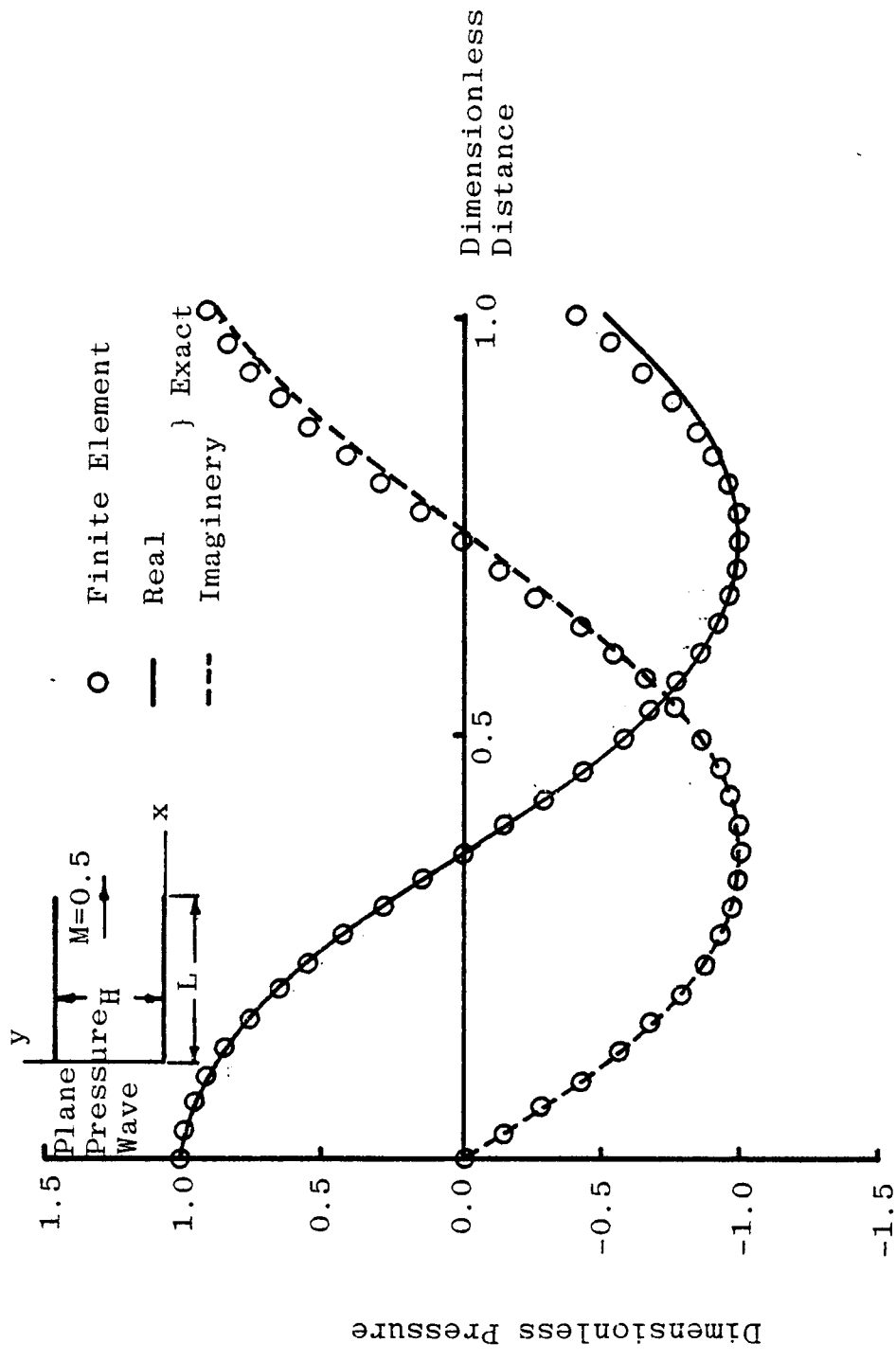


Figure III.11 Finite Element and Exact Acoustic Pressure Distribution in a Hard Wall Duct Carrying Mean Flow (M = +0.5)

Mach number = 0.5

Dimensionless frequency $\eta = 1.0$

The exact solution for the complex acoustic pressure can be written as

$$p = \cos(\frac{4}{3}\pi x) - i \sin(\frac{4}{3}\pi x) \qquad 0 \leq x \leq 1$$

The agreement between the exact solution and the finite element solution is excellent when 30 elements were used.

When the direction of flow is opposite to that of the acoustic wave, the exact solution for M = 0.5 can be written as

$$p = \cos(4\pi x) - i \sin(4\pi x) \qquad 0 \leq x \leq 1$$

For this particular case of M = 0.5 and $\eta = 1$, (Figure III.12) 30 elements resulted in reliable and accurate acoustic pressure predictions. If the Mach number and/or the dimensionless frequency is increased, a finer mesh is to be introduced for accurate results.

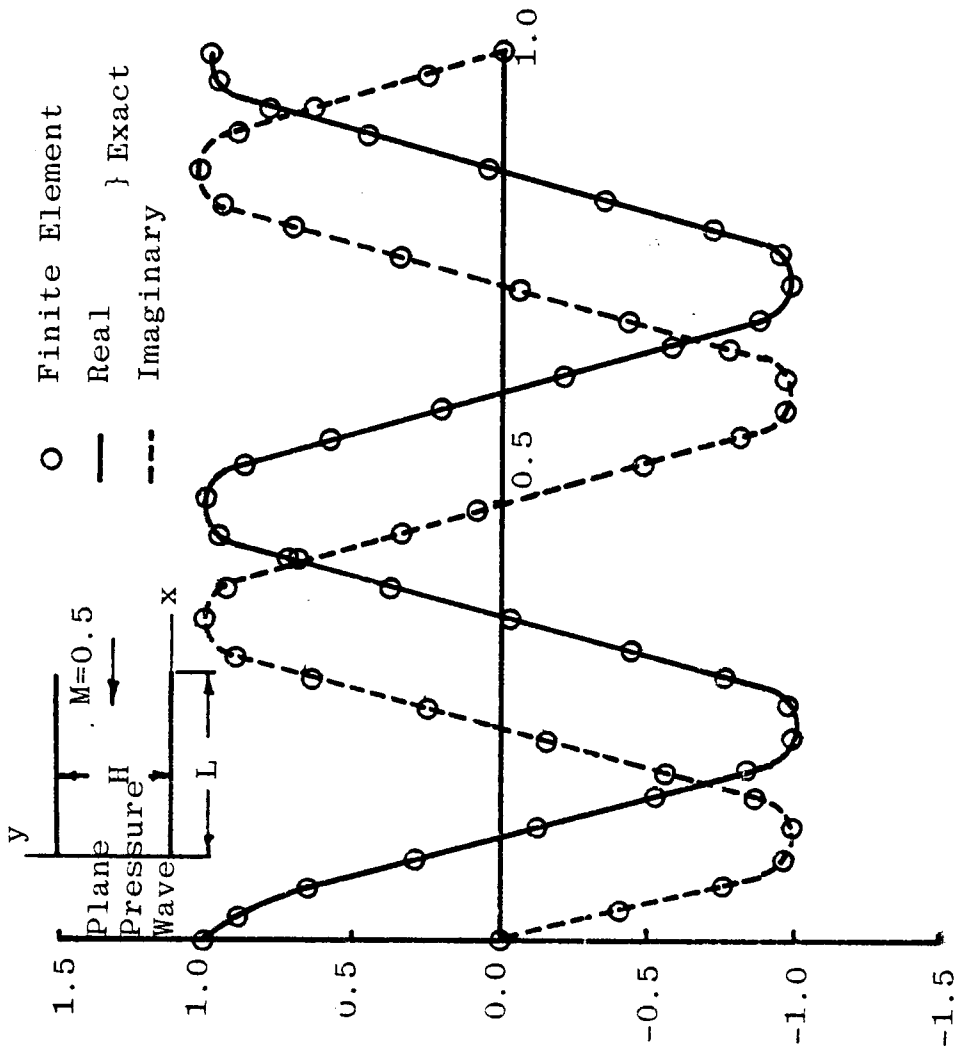


Figure III.12 Finite Element and Exact Acoustic Pressure Distribution in a Hard Wall Duct Carrying Mean Flow (M = -0.5)

CHAPTER IV

DERIVATION OF THE NON-LINEAR AXISYMMETRIC ACOUSTIC EQUATION

IV.1 Introduction

In this chapter, the general non-linear three-dimensional acoustic equation is derived by using a perturbation technique. The non-linear three-dimensional equation is then linearized and reduced to the axisymmetric one for a harmonic time dependence. Boundary conditions are then presented describing the presence of an acoustic source of higher order modes at one end and a reflection boundary condition at the other end of the duct. Duct walls are considered rigid. The acoustic equation is written in terms of the acoustic velocity potential. The flow in the variable area duct is inviscid, non-heat conducting, irrotational and one-dimensional.

IV.2 Mathematical Model

The non-linear equation for the velocity potential governing unsteady isentropic three-dimensional gas flow (see Appendix D) is

$$\nabla^2\Phi - \Phi_{tt} = 2\nabla\Phi \cdot \nabla\Phi_t + \frac{1}{2}(\gamma-1)\nabla^2\Phi(\nabla\Phi \cdot \nabla\Phi)$$

$$+ (\gamma-1)\nabla^2\Phi\Phi_t + \frac{1}{2}\nabla\Phi \cdot \nabla(\nabla\Phi \cdot \nabla\Phi) \qquad \text{(IV.2.1)}$$

where Φ is the velocity potential and γ is the ratio of specific heats. The flow parameter is composed of two parts, steady component and unsteady acoustical component. Hence, the velocity potential can be written as

$$\Phi = \tilde{\phi} + \bar{\phi} \tag{IV.2.2}$$

where $\tilde{\phi}$ is the velocity potential of the steady flow which satisfies the steady form of Equation (IV.2.1)

$$\text{(i.e)} \quad \nabla^2\tilde{\phi} = \frac{1}{2}(\gamma-1)\nabla^2\tilde{\phi}(\nabla\tilde{\phi} \cdot \nabla\tilde{\phi}) + \frac{1}{2}\nabla\tilde{\phi} \cdot \nabla(\nabla\tilde{\phi} \cdot \nabla\tilde{\phi}) \tag{IV.2.3}$$

$\bar{\phi}$ is a perturbation quantity due to the presence of the sound waves and is assumed to be small as compared to the steady component $\tilde{\phi}$.

Substituting Equation (IV.2.2) in Equation (IV.2.1) with the use of Equation (IV.2.3), we get after some algebraic manipulation:

$$\begin{aligned}(1 - \tfrac{\gamma-1}{2}\,\bar{V} \cdot \bar{V})\nabla^2\bar{\phi} - \bar{\phi}_{tt} &= 2\bar{V} \cdot [\nabla\bar{\phi}_t + \tfrac{1}{2}\nabla(\bar{V} \cdot \nabla\bar{\phi})] \\ &+ (\gamma-1)(\nabla \cdot \bar{V})(\bar{\phi}_t + \bar{V} \cdot \nabla\bar{\phi}) + \tfrac{1}{2}\nabla(\bar{V} \cdot \bar{V}) \cdot \nabla\bar{\phi} \\ &+ 2\nabla\bar{\phi} \cdot [\tfrac{1}{2}\nabla(\bar{V} \cdot \nabla\bar{\phi}) + \nabla\bar{\phi}_t] + \tfrac{1}{2}\,\bar{V} \cdot \nabla(\nabla\bar{\phi} \cdot \nabla\bar{\phi}) \\ &- (\gamma-1)\nabla^2\bar{\phi}(\bar{\phi}_t + \bar{V} \cdot \nabla\bar{\phi}) + (\tfrac{\gamma-1}{2})(\nabla \cdot \bar{V})(\nabla\bar{\phi} \cdot \nabla\bar{\phi}) \\ &+ (\tfrac{\gamma-1}{2})\nabla^2\bar{\phi}(\nabla\bar{\phi} \cdot \nabla\bar{\phi}) + \tfrac{1}{2}\nabla\bar{\phi} \cdot \nabla(\nabla\bar{\phi} \cdot \nabla\bar{\phi})\end{aligned} \tag{IV.2.4}$$

where $\bar{V}$ is the steady state velocity vector.
Equation (IV.2.4) is highly non-linear. In rewriting Equation (IV.2.4) the third order non-linear terms will

be dropped out.

Introducing the cylindrical coordinate system (r,θ,z)

$$\nabla\bar{\phi} = \bar{\phi}_r i_r + \frac{1}{r}\bar{\phi}_\theta i_\theta + \bar{\phi}_z i_z \tag{IV.2.5}$$

$$\nabla^2\bar{\phi} = \frac{1}{r}(r\bar{\phi}_r)_r + \frac{1}{r^2}\bar{\phi}_{\theta\theta} + \bar{\phi}_{zz} \tag{IV.2.6}$$

$$\nabla\bar{\phi}\cdot\nabla\bar{\phi} = \bar{\phi}_r^2 + \frac{1}{r^2}\bar{\phi}_\theta^2 + \bar{\phi}_z^2 \tag{IV.2.7}$$

Substitution of Equations (IV.2.5) - (IV.2.7) in Equation (IV.2.4) gives,

$$(1-V^2)\bar{\phi}_{rr} + (1-U^2)\bar{\phi}_{zz} - 2UV\bar{\phi}_{zr} + (\frac{1}{r}\bar{\phi}_r + \frac{1}{r^2}\bar{\phi}_{\theta\theta}) - \frac{1}{C^2}\bar{\phi}_{tt}$$

$$= [(\gamma+1)UU_z + 2VV_z + \frac{(\gamma-1)}{r}UV + (\gamma-1)V_rU]\bar{\phi}_z$$

$$+ \frac{2}{C}V\bar{\phi}_{rt} + \frac{2}{C}U\bar{\phi}_{zt} + \frac{(\gamma-1)}{C}[V_r\bar{\phi}_t + \frac{1}{r}V\bar{\phi}_t + U_z\bar{\phi}_t]$$

$$+ [(\gamma+1)VV_r + 2UU_r + \frac{\gamma-1}{r}V^2 + (\gamma-1)U_zV]\bar{\phi}_r$$

$$+ \frac{2}{C^2}[\bar{\phi}_r\bar{\phi}_{rt} + \frac{1}{r^2}\bar{\phi}_\theta\bar{\phi}_{\theta t} + \bar{\phi}_z\bar{\phi}_{zt}]$$

$$+ (\frac{\gamma-1}{C^2})[\bar{\phi}_t\bar{\phi}_{rr} + \frac{1}{r}\bar{\phi}_t\bar{\phi}_r + \frac{1}{r^2}\bar{\phi}_t\bar{\phi}_{\theta\theta} + \bar{\phi}_t\bar{\phi}_{zz}]$$

$$+ \frac{1}{C}[V_r + \frac{\gamma-1}{r}V + \frac{\gamma-1}{2}(V_r + \frac{1}{r}V + U_z)]\bar{\phi}_r^2$$

$$+ \frac{1}{C}[U_z + \frac{\gamma-1}{2}(V_r + \frac{1}{r}V + U_z)]\bar{\phi}_z^2$$

$$+ \frac{1}{C}[2V_z + \frac{\gamma-1}{r}U]\bar{\phi}_r\bar{\phi}_z$$

$$+\frac{1}{C}[(\gamma+1)V\bar{\phi}_r\bar{\phi}_{rr} + (\gamma+1)U\bar{\phi}_z\bar{\phi}_{zz} + 2U\bar{\phi}_r\bar{\phi}_{zr} + 2V\bar{\phi}_z\bar{\phi}_{zr}$$

$$+ (\gamma-1)V\bar{\phi}_r\bar{\phi}_{zz} + (\gamma-1)U\bar{\phi}_z\bar{\phi}_{rr}]$$

$$+\frac{1}{C}\frac{1}{r^2}[\frac{\gamma-1}{2}(V_r + \frac{1}{r}V + U_z) - \frac{1}{r}V]\bar{\phi}_\theta^2$$

$$+\frac{1}{C}\frac{1}{r^2}[(V + U)\bar{\phi}_\theta\bar{\phi}_{\theta r} + (\gamma-1)V\bar{\phi}_r\bar{\phi}_{\theta\theta} + (\gamma-1)U\bar{\phi}_z\bar{\phi}_{\theta\theta}] \qquad \text{(IV.2.8)}$$

where U and V are the mean flow Mach number components in the axial and radial directions, respectively.

C is the non-dimensional speed of sound defined by $C = \sqrt{1 - \frac{\gamma-1}{2}(\bar{V} \cdot \bar{V})}$

Equation (IV.2.8) is the non-linear acoustic equation in cylindrical coordinates when no-swirl flow is present

IV.3 The Linear Problem

Linearizing Equation (IV.2.8), assuming harmonic variation with time and considering axisymmetric wave propagation (i.e) one seeks a solution of the form

$$\bar{\phi}(r,\theta,z,t) = \phi(r,z)e^{-i(\omega t - \theta m)} \qquad \text{(IV.3.1)}$$

where ω is the exciting frequency

m is the spinning mode number.

Thus, Equation (IV.2.8) is written as,

$$(1-V^2)\phi_{rr} + (1-U^2)\phi_{zz} - 2UV\phi_{rz} + \frac{1}{r}\phi_r - \frac{1}{C^2}\frac{m^2}{r^2}\phi$$

$$+\frac{\omega^2}{C^2}\phi = -2\frac{i\omega}{C}V\phi_r - 2\frac{i\omega}{C}U\phi_z$$

$$- \frac{i\omega}{C} (\gamma-1)[V_r + \frac{1}{r} V + U_z]\phi$$

$$+ [(\gamma+1)VV_r + 2UU_r + \frac{\gamma-1}{r} V^2 + (\gamma-1)U_z V]\phi_r$$

$$+ [(\gamma+1)UU_z + 2VV_z + \frac{\gamma-1}{r}UV + (\gamma-1)V_r U]\phi_z \qquad \text{(IV.3.2)}$$

where $i = \sqrt{-1}$.

Equation (IV.3.2) is the steady state acoustic equation in the complex acoustic velocity potential ϕ. The solution of Equation (IV.3.2) requires boundary conditions on the independent variables r and z. Since Equation (IV.3.2) is a second order partial differential equation, two boundary conditions are needed for each independent variable.

IV.4 Boundary Conditions

A. In the Radial Direction

Since the centerline of the duct is a symmetry line we can write,

$$\phi_r = 0 \qquad \text{(IV.4.1)}$$

And for the duct boundaries, since they are considered to be hard walls, the appropriate boundary condition at the wall is

$$\phi_n = 0 \qquad \text{(IV.4.2)}$$

where n stands for the normal.

B. In the Axial Direction

Specifying a termination boundary condition requires

a study of the radiated field. Most of the researchers neglect the termination effect and assume semi-infinite duct with no reflected waves which is far from realistic. In this study, however, the effect of reflection is taken into consideration using an empirical formula based on experimental study by Lumsdaine[36] for the pressure reflection ratio.

Knowing the pressure reflection ratio, mode number, flow Mach number and the exciting frequency, the termination impedance can be easily calculated. The analysis presents the impedance ratio $\bar{Z}/Z_o$ in terms of the forementioned variables.

The three-dimensional linear acoustic equation with steady mean flow is

$$\nabla^2\phi - \frac{1}{C^2}\left(\frac{\partial}{\partial t} + UC\,\frac{\partial}{\partial z}\right)^2\phi = 0 \qquad \text{(IV.4.3)}$$

Using the separation of variables technique, the solution for the above equation in the cylindrical coordinate system can be written as

$$\phi = R(r)\,Z(z)e^{-i(\omega t - m\Theta)} \qquad \text{(IV.4.4)}$$

Substitution in the acoustic equation gives

$$-\left(\frac{R''}{R} + \frac{1}{r}\frac{R'}{R} - \frac{m^2}{r^2}\right) = (1-M^2)\,\frac{Z''}{Z} + \frac{2U}{C}\,i\omega\,\frac{Z'}{Z}$$

$$+ \frac{\omega^2}{C^2} = \chi_{mn}^2 \qquad \text{(IV.4.5)}$$

and

$$R'' + \frac{1}{r} R' + (\chi^2_{mn} - \frac{m^2}{r^2})R = 0 \qquad \text{(IV.4.6)}$$

which has a solution in the form

$$R(r) = J_m(\chi_{mn} r) \qquad \text{(IV.4.7)}$$

where χ_{mn} are the solutions of $J'_m(\chi) = 0$.

In the axial direction

$$Z'' + i \frac{2U}{1-U^2} \frac{\omega}{C} Z' + (\frac{\omega^2}{C^2} \frac{1}{1-U^2} - \frac{\chi^2_{mn}}{1-U^2})Z = 0 \qquad \text{(IV.4.8)}$$

If we let

$$k = \frac{\omega}{C} \quad ,$$

then

$$Z'' + i \frac{2Uk}{1-U^2} Z' + (\frac{k^2 - \chi^2_{mn}}{1-U^2})Z = 0 \qquad \text{(IV.4.9)}$$

hence,

$$Z(z) = A_{mn} e^{\lambda_1 z} + B_{mn} e^{\lambda_2 z} \qquad \text{(IV.4.10)}$$

where

$$\lambda_1 = -ik \frac{\alpha+U}{1-U^2}$$

$$\lambda_2 = ik \frac{\alpha-U}{1-U^2}$$

$$\alpha = \sqrt{1 - \frac{\chi^2_{mn}}{k^2} (1-U^2)}$$

$$\phi_{mn} = J_m(\chi_{mn}r)[A_{mn}e^{\lambda_1 z} + B_{mn}e^{\lambda_2 z}]e^{-i(\omega t - m\theta)} \qquad \text{(IV.4.11)}$$

with incident and reflected velocity potential amplitudes A_{mn} and B_{mn}, respectively.

$$\phi_i(\text{incident}) = A_{mn}e^{\lambda_1 z} \qquad \text{(IV.4.12)}$$

$$\phi_r(\text{reflected}) = B_{mn}e^{\lambda_2 z} \qquad \text{(IV.4.13)}$$

Let R_ϕ be the velocity potential reflection ratio

$$= \frac{\phi_r}{\phi_i}$$

and writing the expression for the acoustic pressure

$$p = -\zeta\left(\frac{\partial\phi}{\partial t} + UC\,\frac{\partial\phi}{\partial z}\right)$$

$$p_i(\text{incident}) = -\zeta\left(\frac{\partial\phi_i}{\partial t} + UC\,\frac{\partial\phi_i}{\partial z}\right)$$

$$= -\zeta(-i\omega + UC\lambda_1)_i$$

$$= i\omega\zeta\left[\frac{1 + U\alpha}{1-U^2}\right]\phi_i \qquad \text{(IV.4.14)}$$

Similarly,

$$p_r = i\omega\zeta\left[\frac{1 - U\alpha}{1-U^2}\right]\phi_r \qquad \text{(IV.4.15)}$$

Hence, the pressure reflection ratio using Equations (IV.4.14) and (IV.4.15) can be written as

$$R_p = \frac{p_r}{p_i} = \left[\frac{1 - U\alpha}{1 + U\alpha}\right]R_\phi \qquad \text{(IV.4.16)}$$

Also, since,

$$p = - \zeta(\frac{\partial}{\partial t} + UC \frac{\partial}{\partial z})\phi \qquad \text{(IV.4.17)}$$

and

$$u = - \frac{\partial \phi}{\partial z} \qquad \text{(IV.4.18)}$$

and from the definition of acoustic impedance ratio

$$Z = \frac{\bar{Z}}{Z_o} = \frac{p}{\zeta C u} \qquad \text{(IV.4.19)}$$

Combining Equations (IV.4.10), (IV.4.17), (IV.4.18) and (IV.4.19) yields,

$$Z = U + \frac{ik\phi}{u}$$

$$= U - \frac{ik[A_{mn}e^{\lambda_1 Z} + B_{mn}e^{\lambda_2 Z}]}{A_{mn}\lambda_1 e^{\lambda_1 Z} + B_{mn}\lambda_2 e^{\lambda_2 Z}} \qquad \text{(IV.4.20)}$$

Substituting for the values of λ_1 and λ_2 and considering the origin to be located at duct termination (Z=0), Equation (IV.4.20) takes the form

$$Z = U - \frac{1 + \frac{1 + U\alpha}{1 - U\alpha} R_p}{-\frac{\alpha + U}{1 - U^2} + \frac{(\alpha - U)}{1 - U^2}(\frac{1 + U\alpha}{1 - U\alpha})R_p} \qquad \text{(IV.4.21)}$$

Or

$$Z = U + \frac{1 - U^2}{U + \alpha[\frac{1-q}{1+q}]} \qquad \text{(IV.4.22)}$$

where

$$q = \frac{1 + U\alpha}{1 - U\alpha} R_p$$

Equation (IV.4.22) reduces to the one given by Sigman et al[22] when no reflection is considered (i.e.) $P_r = 0$; in this case

$$Z = \frac{1 + \alpha U}{U + \alpha}$$

Moreover, for the case of a plane wave without reflection Z=1, which is the well-known condition of ζC termination. An empirical formula for the pressure reflection ratio is written in the form

$$R_p(kR,U) = R_p(kR,O)\left(\frac{1-U}{1+U}\right)^n \qquad \text{(IV.4.23)}$$

$$n = 1.33$$

where $R_p(kR,O)$ is the pressure reflection ratio at zero velocity for any mode Reference (36).

The above analysis presents the axial boundary condition at the termination. At the other end, however, a noise source which is the fan compressor noise exists and it can be expressed mathematically in the form

$$\phi = \psi(r)e^{-i(\omega t - m\Theta)} \qquad \text{(IV.4.24)}$$

where $\psi(r)$ is a radial function in the acoustic potential velocity at the fan face.

CHAPTER V

A FINITE ELEMENT ALGORITHM FOR THE AXISYMMETRIC WAVE EQUATION

V.1 Introduction

In Chapter IV, the axisymmetric linear differential equation describing the acoustic velocity potential in a variable area duct carrying high subsonic Mach number flow was derived along with the boundary conditions. In this chapter, a finite element algorithm is implemented using Galerkin's formulation. In applying a finite element algorithm, a nonuniform distribution of elements is considered across the duct section, allowing smaller elements near the outer wall and larger ones closer to the centerline of the axisymmetric duct to provide a more accurate solution in the radial direction. Moreover, the variation in radius is taken to be linear over the elements. Within the element itself, properties are considered to vary linearly.

V.2 Finite Element Formulations

Stifness matrix can br written in the form

$$\left(\sum_{e=1}^{E} \int_{V} \{ r(1-V^2)\left[\frac{\partial H^e}{\partial r}\right]^T \left[\frac{\partial H^e}{\partial r}\right] + r(1-U^2)\left[\frac{\partial H^e}{\partial z}\right]^T \left[\frac{\partial H^e}{\partial z}\right] - 2rUV\left[\frac{\partial H^e}{\partial z}\right]^T \left[\frac{\partial H^e}{\partial r}\right]$$

$$+ r\left(-\frac{2i\omega}{C} V + (\gamma+1)VV_r + 2UU_r + \frac{\gamma-1}{r} V^2 + (\gamma-1)U_z V\right)$$

$$\left[\frac{\partial H^e}{\partial r}\right]^T [H^e]$$

$$+ r\left(-\frac{2i\omega}{C} U + (\gamma+1)UU_z + 2VV_z + \frac{\gamma-1}{r} UV + (\gamma-1)V_r U\right)$$

$$\left[\frac{\partial H^e}{\partial z}\right]^T [H^e]$$

$$+ r\left(\frac{1}{C^2}\frac{m^2}{r^2} - \frac{\omega^2}{C^2} - \frac{i\omega}{C}(\gamma-1)\left[V_r + \frac{1}{r} V + U_z\right]\right.$$

$$\left.[H^e]^T [H^e]\right\} dV\Big)$$

$$+ \left(\sum_{b=1}^{B} \int_S -r(1-U^2)\frac{ik}{(U-Z)} [H^b]^T [H^b] dS\right) \qquad \text{(V.2.1)}$$

where

Z is the impedance ratio

B is the number of boundary elements

dV is the elemental volume

dS is the elemental surface area.

A finite element program has been developed to perform the above assembly algorithm Equation(V.2.1) subjected to a forced boundary condition at the fan face Equation (IV.4.24).

Assembly algorithm is well known in the finite

element techniques. In contrast to usual technique, assembly algorithm has resulted in a banded matrix form with non-hermitian elements along the bands. After applying the forced boundary conditions, the resulting system is triangularized using Gauss' elimination technique; then a back substitution is implemented to reach a final solution for the acoustic velocity potential at the nodes. Post solution is accomplished on an element-by-element basis to obtain sound pressure and acoustic velocities at the points of numerical quadrature ,(Figure V.1).

V.3 Finite Element Methodology and Computer Implementation

In this section, the finite element programming is discussed along with a brief description of the different subroutines and their function. It was intended to write this program in building blocks, so it could be used in solving several other engineering problems with machines of different storage capacity. The program handles complex number quantities and can very well handle problems of a real number nature. This program can take any number of nodes, elements and degrees of freedom per node. The program in its written version solves the one-dimensional, two-dimensional and the axisymmetric cases. Extension to the three-dimensional case is straightforward. Four node or eight node isoparametric quadrilateral elements are optional in the program. The global matrix formulated from

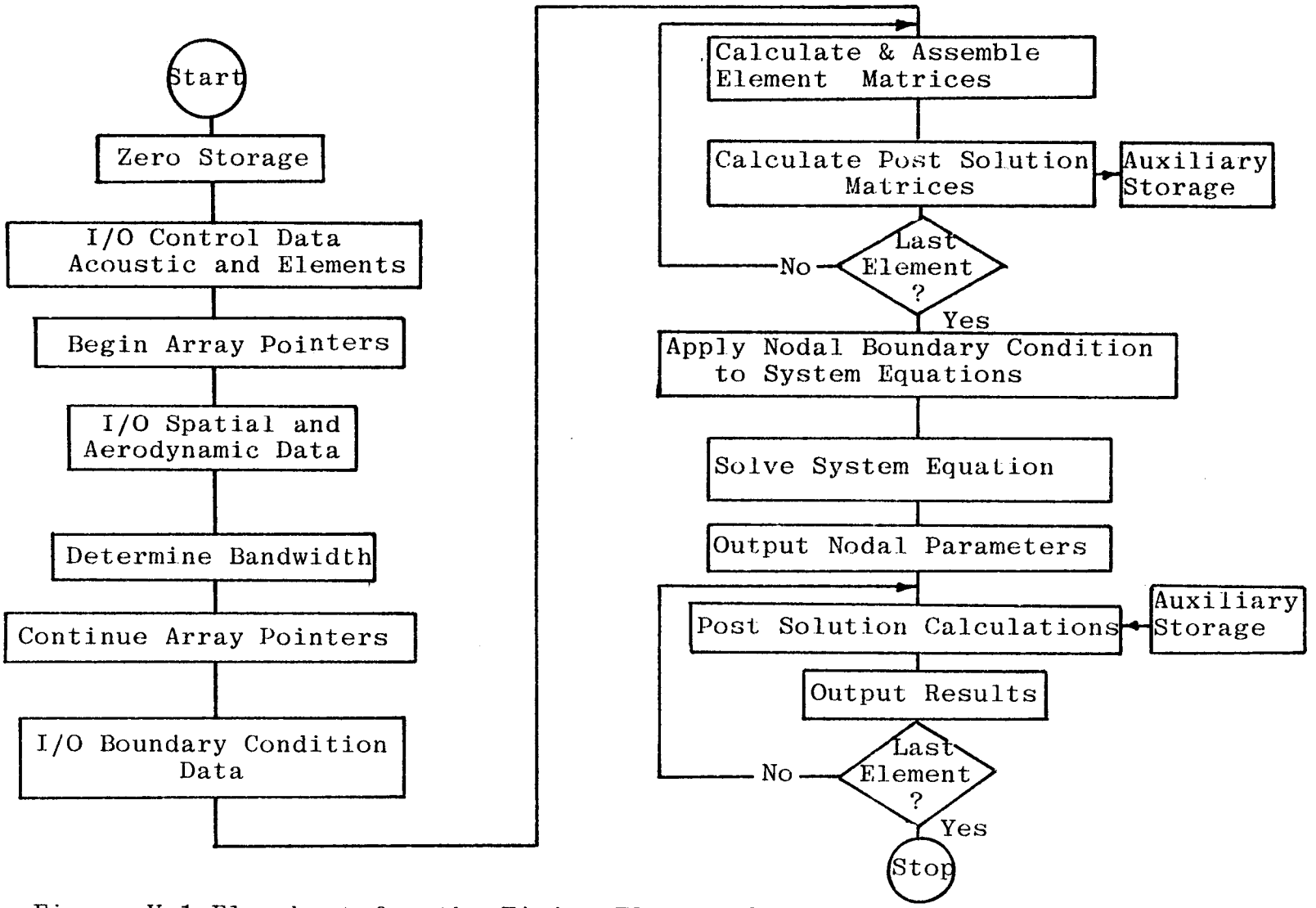


Figure V.1 Flowchart for the Finite Element Computer Program

the element square matrices is non-hermitian and non-positive definite. The assembly algorithm results in a banded form which is stored in a compact form by subroutine STRBND. The solution of the resulting system is solved efficiently using Gauss' elimination technique and then the solution is obtained by back substitution. The computer program can be coupled with a mesh generator program for complicated and irregular geometries. In this study, however, the program generated its own mesh and determined the element connectivity for each element under consideration. In the axisymmetric configurations a nonuniform distribution of elements is considered allowing smaller elements near the outer boundary and larger ones closer to the centerline to maintain reasonable accuracy in the radial direction. In acoustic related problems, the program handles different variables such as duct area changes, multisectioned soft walls, hard walls, reflective and non-reflective boundary conditions, variable frequency higher order modes and high subsonic one and/or two dimensional flows. In this analysis, in order to compare the finite element results with the experimental ones, hard-wall ducts with one-dimensional flows are considered only.

A. Program Description and Subroutines

1. SUBROUTINE MODEL

This subroutine zeros a complex, a real and

an integer vectors then reads a solution code, two-dimensional or axisymmetric case; also acoustic data such as exciting frequency and circumferential wave number are read in.

This information is printed out. Another read statement follows describing mesh data, number of nodes, number of elements, number of degrees of freedom per node, number of nodes per element, dimension of space, number of boundary segment for flux boundary condition and number of nodes per boundary segment. This information is printed out after it is read in. The number of degrees of freedom per element and the total number of degrees of freedom required for SUBROUTINE POINTR are calculated from input data. In addition to calling SUBROUTINE POINTR, this subroutine calls also other subroutines INPUT, SYSBAN, POINT, INFLUX, ASYMBL, APLYBC, DECOMP, SOLVE, WRTPT and POST. The function of each one of these subroutines is explained and discussed in the following section.

2. SUBROUTINE ZEROZ and SUBROUTINE ZERO

The first one ZEROZ, zeros a variable size complex vector and the second ZERO zeros real and integer vectors.

3. SUBROUTINE POINTR

After establishing the total number of degrees of freedom and the number of the degrees of freedom per element, this subroutine assigns dynamic storage both for the real and the integer variables and thus allow efficient

utilization of the available computer storage. This dynamic storage scheme allows the expansion and the contraction of the dimension statement of the variables according to the input data of a specified problem (i.e) number of elements and number of nodes. Maximum size of storage is generally governed by computer capacity.

4. SUBROUTINE INPUT

This subroutine reads in mean flow conditions, axial and transverse Mach number and their spatial derivatives obtained from a potential flow program. In this study, one-dimensional steady flow is considered. Mass flow rate and stagnation conditions are read in along with duct geometry. Subroutine Mach calculates the Mach number using the Newton-Raphson method, then the calculated Mach number is smoothed using subroutine SMOOTH and finally the spatial derivative of the Mach number is calculated using subroutine DERIVT based on the following formulae, Reference(40).

$$f'(x_o) = \frac{1}{12h}\,[-25f(x_o) + 48f(x_1) - 36f(x_2) + 16f(x_3) - 3f(x_4)]$$

$$f'(x_1) = \frac{1}{12h}\,[-3f(x_o) - 10f(x_1) + 18f(x_2) - 6f(x_3) + f(x_4)]$$

$$f'(x_2) = \frac{1}{12h}\,[f(x_o) - 8f(x_1) + 8f(x_2) - f(x_3)]$$

$$f'(x_3) = \frac{1}{12h}\,[-f(x_o) - 16f(x_1) + 36f(x_2) - 48f(x_3) + 25f(x_4)]$$

where

h is the axial spacing.

Subroutine INPUT constructs a mesh based on uniform distribution of the number of elements across a two-dimensional duct and a nonuniform distribution for an axisymmetric duct. The non-uniformity allows smaller elements to be located close to the wall and larger ones close to the centerline of the duct; this has been accomplished by considering equal annular areas across the duct. After constructing the mesh, nodes are numbered and their coordinates are calculated and printed out along with the values of Mach number and the spatial derivative of the Mach number for each specified node. Boundary nodes, where the forced boundary condition is applied are also identified in this subroutine.

Element connectivity data is then calculated as a function of the numbering scheme for each element. It is to be mentioned here that element bandwidth is influenced by the nodal numbering scheme. Element connectivity information is printed out.

5. SUBROUTINE SYSBAN

After establishing the element connectivity data, subroutine SYSBAN calculates the half bandwidth associated with each element and then identifies the one with the highest half bandwidth. Subroutines LNODES and ELBAND are called in this subroutine to determine the nodes

associated with a specified element and then to determine the half bandwidth associated with this element. The expression used to calculate the half bandwidth HBW for a typical element e is

$$HBW = NG * (NDIFF + 1)$$

where NG is the number of degrees of freedom per node and NDIFF is the absolute value of the maximum difference in node numbers of the node associated with the element e.

If HBW is the maximum half bandwidth, then the associated maximum bandwidth is

$$MAXBAN = 2 * HBW - 1$$

which specifies the bandwidth of the global matrix.

6. SUBROUTINE POINT

The function of this subroutine is in allocating dynamic storage for variables. It calculates the dimensions needed for the element square matrix, the global matrix, system column vector and degrees of freedom vector.

7. SUBROUTINE INFLUX

This subroutine reads flux boundary data for each boundary segment and calls subroutine BFLUXS to calculate the contribution to the system square matrix from each boundary segment based on linear or quadratic interpolation. Calculating segment contributions is followed by calling subroutines INDXEL and STRBND. The former determines the degrees of freedom associated with

the element under consideration and the later stores element contributions in a banded system.

8. SUBROUTINE ASYMBL

The assembly operation of the different element contributions is performed by subroutine ASYMBL which extracts for each element the element's node number using subroutine LNODES, nodal coordinates and properties using subroutine ELCORD, then calculates the degree of freedom numbers associated with the element from subroutine INDXEL, generates the element square matrix of the element using subroutine ELSQ and stores the element square matrix contributions in a banded form using subroutine STRBND.

9. SUBROUTINE APLYBC

The forced boundary condition is introduced using subroutine APLYBC which in turn calls subroutine INDXPT and MODIFY. Subroutine INDXPT determines the degrees of freedom associated with the nodal point at which there is a forced boundary condition; the value (and/or the values) at this point is introduced into the global system by subroutine MODIFY.

V.4 Input Specified Flux Components on Boundary Segments

The flux boundary condition for the acoustic equation under study leads to contribution to the system square matrix [S]. The addition of the flux contribution is accomplished by subroutine ASYMBL. Subroutine INFLUX

reads the flux boundary condition data for each boundary segment. Calculations of the flux contributions is done by subroutine BFLUXS. In this analysis, specified flux components are in the normal and tangential directions to the segment. The boundary square matrix is defined as

$$[S^b] = F \int_S [H^b]^T [H^b] dS$$

where F is the specified flux component.

V.5 Element Square Matrix

Subroutine ELSQ evaluates the volume integral

$$\int_V r(1-V^2)\left[\frac{\partial H^e}{\partial r}\right]^T \left[\frac{\partial H^e}{\partial r}\right] + r(1-U^2)\left[\frac{\partial H^e}{\partial z}\right]^T \left[\frac{\partial H^e}{\partial z}\right]$$

$$- 2rUV \left[\frac{\partial H^e}{\partial z}\right]^T \left[\frac{\partial H^e}{\partial r}\right]$$

$$+ r\left(-\frac{2i\omega}{C} V + (\gamma+1)VV_r + 2UU_r + \frac{\gamma-1}{r} V^2 + (\gamma-1)U_z V\right)$$

$$\left[\frac{\partial H^e}{\partial r}\right]^T [H^e]$$

$$+ r\left(-\frac{2i\omega}{C} U + (\gamma+1)UU_z + 2VV_z + \frac{\gamma-1}{r} UV + (\gamma-1)V_r U\right)$$

$$\left[\frac{\partial H^e}{\partial z}\right]^T [H^e]$$

$$+ r\left(\frac{1}{C^2}\frac{m^2}{r^2} - \frac{\omega^2}{C^2} - \frac{i\omega}{C}(\gamma-1)\left[V_r + \frac{1}{r}V + U_z\right]\right.$$

$$\left.[H^e]^T[H^e]\right\}dV$$

Such an integral is difficult to solve in a closed form particularly for the cases of variable area ducts; therefore numerical integration schemes are introduced as will be explained later. In this subroutine, the Mach number and its derivative are considered to vary linearly over the element under study. The variation of radius r over the element is also linear. In this program, the element square matrix is generated for each and every element in the system and then assembled in the global matrix one at a time. In calculating the derivatives, calculations must be performed on a global coordinate system rather than a local one. In the case where isoparametric elements are encountered such a transformation is explicitly included.

V.6 Assembly of Element Equations into System Equations

Assembly algorithm is one of the important operations in finite element methodology. One of the most efficient schemes is the direct assembly technique which requires a definition for the relationship between local number and system degree of freedom numbers. This relationship is determined by subroutine INDXPT. Subroutine INDXEL

determines the degrees of freedom associated with an element provided that the degrees of freedom associated with a node are known from subroutine INDXPT.

Subroutine STRBND converts the subscripts of the degrees of freedom associated with an element to the subscripts of the global system according to the relation

$$S^{e}_{I,J} \rightarrow S_{II,JJ}$$

where I and J are the local subscripts in the element square matrix and II,JJ are the corresponding subscripts of the system equation coefficient. Direct conversion means that

II = INDEX(I) and

JJ = INDEX(J) - INDEX(I) + HBW

This scheme allows a global banded matrix of dimension (NDFREE,(2*HBW-1)), and thus the global matrix is stored in a rectangular array.

V.7 Application of Nodal Parameter Boundary Conditions

After the system of equations has been fully assembled, forced boundary conditions are applied before the equations are solved for the unknown nodal parameters. The boundary condition considered in this study is generally in the form

$$X_j = b$$

where X_j represents system degree of freedom number j and b is the specified value assigned to that degree of freedom, and it is a complex number. The system of equations before modification is written as [S]{X} = {0}, or, upon expansion

$$\begin{array}{c} \\ 1 \\ \\ \\ j \\ \\ \\ k \\ \\ \\ p \end{array} \begin{array}{c} \begin{array}{cccccccc} 1 & & j & & k & & \end{array} \\ \begin{bmatrix} S_{11} & \cdots & S_{1j} & \cdots & S_{1k} & \cdots & S_{1p} \\ \vdots & & & & & & \\ S_{j1} & \cdots & S_{jj} & \cdots & S_{jk} & \cdots & S_{jp} \\ \vdots & & & & & & \\ S_{k1} & \cdots & S_{kj} & \cdots & S_{kk} & \cdots & S_{kp} \\ \vdots & & & & & & \\ S_{p1} & \cdots & S_{pj} & \cdots & S_{pk} & \cdots & S_{pp} \end{bmatrix} \end{array} \begin{Bmatrix} X_1 \\ \vdots \\ X_j \\ \vdots \\ X_k \\ \vdots \\ X_p \end{Bmatrix} = \begin{Bmatrix} 0 \\ \vdots \\ 0 \\ \vdots \\ 0 \\ \vdots \\ 0 \end{Bmatrix}$$

After applying the boundary conditon the system takes the form

$$\begin{array}{c} \\ 1 \\ \\ \\ j \\ \\ \\ k \\ \\ \\ p \end{array} \begin{array}{c} \begin{array}{cccccccc} 1 & & j & & k & & p \end{array} \\ \begin{bmatrix} S_{11} & \cdots & 0 & & S_{1k} & & S_{1p} \\ \vdots & & \vdots & & \vdots & & \\ 0 & & 1 & & 0 & & 0 \\ \vdots & & \vdots & & \vdots & & \\ S_{k1} & & 0 & & S_{kk} & & S_{kp} \\ \vdots & & \vdots & & \vdots & & \\ S_{p1} & & 0 & & S_{pk} & & S_{pp} \end{bmatrix} \end{array} \begin{Bmatrix} X_1 \\ \vdots \\ X_j \\ \vdots \\ X_k \\ \vdots \\ X_p \end{Bmatrix} = \begin{Bmatrix} -b\ S_{1j} \\ \vdots \\ b \\ \vdots \\ -b\ S_{kj} \\ \\ -b\ S_{pj} \end{Bmatrix}$$

V.8 Equation Solving Technique

The system of equations resulting from the assembly algorithm and after applying the forced boundary condition can be written as

$$[S]\{X\} = \{C\}$$

where {X} and {C} are the unknown complex vector and the complex column vector, respectively. [S] is a non-hermitian non-positive definite banded matrix stored in a rectangular form.

Solution is accomplished in three steps:

1. The coefficient matrix [S] triangularized using Gauss elimination technique.
2. The column vector {C} is modified in a similar fashion as that of step 1.
3. The solution is obtained using back substitution.

The first step is done in subroutine DECOMP; steps 2 and 3 are accomplished in subroutine SOLVE.

To obtain the upper triangular matrix an elimination scheme is implemented such that

$$S_{ij}^{(n)} = S_{ij}^{(n-1)} - S_{in}^{(n-1)} \frac{S_{nj}^{(n-1)}}{S_{nn}^{(n-1)}} \qquad i,j > n$$

where n is the number of reductions or eliminations.

One important property for this reduction scheme is that whenever $S_{in}^{(n-1)}$ or $S_{nj}^{(n-1)}$ is zero, $S_{ij}^{(n)} = S_{ij}^{(n-1)}$. This property results in great savings in computer times when dealing with large systems of equations. The resulting triangular matrix is stored in a rectangular form of dimension (NDFREE,HBW), where HBW is the half bandwidth including the diagonal. It should be mentioned also, that during the reduction process, the number of equations involved in the reduction process is equal to the half bandwidth HBW which results in a considerable saving of computer time.

Subroutine SOLVE modifies the column according to

$$C_i^{(n)} = C_i^{(n-1)} - S_{in}^{(n-1)} \frac{C_n^{(n-1)}}{S_{nn}^{(n-1)}} \qquad i > n$$

and then determines the solution using back substitution.

V.9 Isoparametric Elements and Numerical Quadrature

A. Isoparametric Elements

Isoparametric elements are formulated on a local coordinate basis. If we let the local coordinates be denoted by (R,S,T) and the correponding global coordinates by (X,Y,Z), then for any variable, X can be defined by its nodal values

$$X(R,S,T) = \sum_{i=1}^{N} H_i(R,S,T)X_i^e = [H(R,S,T)]\{X^e\} \qquad (V.9.1)$$

X in Equation (V.9.1) defines the global coordinates of a point

or $$[X\ Y\ Z] = [H(R,S,T)][X^e\ Y^e\ Z^e] \qquad (V.9.2)$$

Now if we consider the isoparametric quadrilateral element in Figure (V.2), H_i can be derived from

$$H_i(R,S) = \frac{1}{4}(1 + RR_i)(1 + SS_i) \qquad (V.9.3)$$

where

$$i = 1,2,3,4$$

$$R_i = -1,+1,+1,-1$$

and

$$S_i = -1,-1,+1,+1$$

It can be seen that

$$\sum_{i=1}^{N} H_i(R,S,T) = 1 \qquad (V.9.4)$$

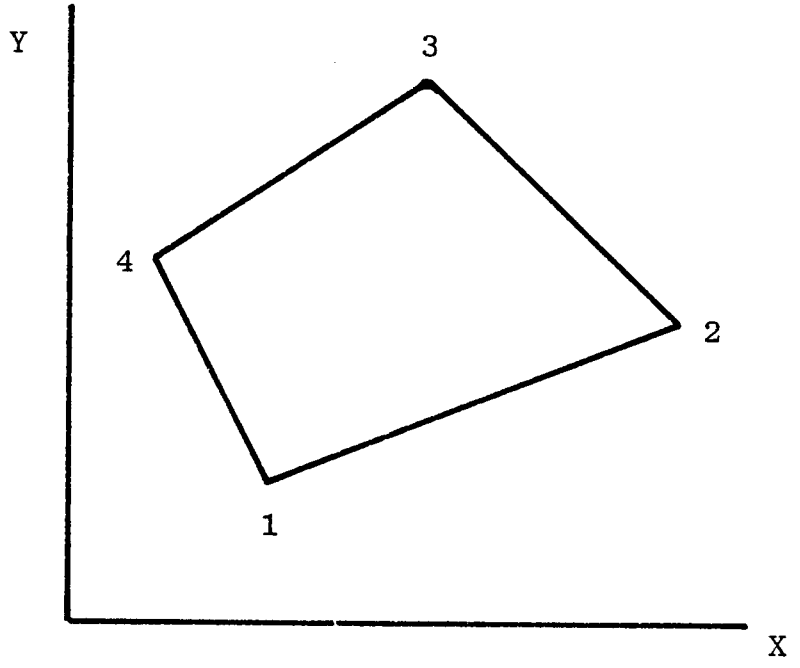
To obtain the global derivative from the local ones

$$\frac{\partial H_i}{\partial R} = \frac{1}{4} R_i(1 + SS_i) \qquad (V.9.5)$$

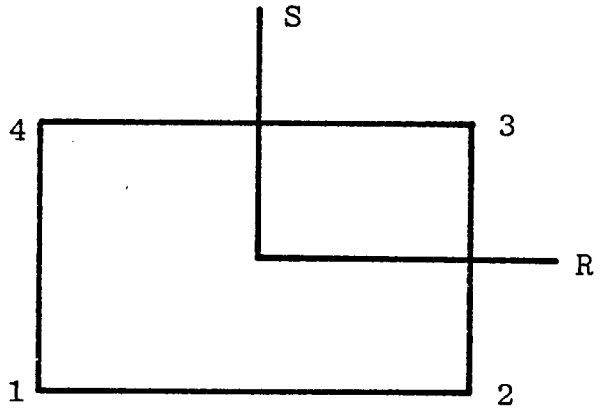
$$\frac{\partial H_i}{\partial S} = \frac{1}{4} S_i(1 + RR_i) \qquad (V.9.6)$$

If we let the local derivatives be denoted by

$$[\Delta(R,S,T)] \equiv \begin{bmatrix} \frac{\partial}{\partial R}[H] \\ \frac{\partial}{\partial S}[H] \\ \frac{\partial}{\partial T}[H] \end{bmatrix} \qquad (V.9.7)$$



Global Coordinate System, X,Y



Local Coordinate System R,S

Figure V.2 Isoparametric Quadrilateral Element

and since

$$\frac{\partial}{\partial R} = \frac{\partial X}{\partial R}\frac{\partial}{\partial X} + \frac{\partial Y}{\partial R}\frac{\partial}{\partial Y} + \frac{\partial Z}{\partial R}\frac{\partial}{\partial Z} \tag{V.9.8}$$

$$\frac{\partial}{\partial S} = \frac{\partial X}{\partial S}\frac{\partial}{\partial X} + \frac{\partial Y}{\partial S}\frac{\partial}{\partial Y} + \frac{\partial Z}{\partial S}\frac{\partial}{\partial Z} \tag{V.9.9}$$

$$\frac{\partial}{\partial T} = \frac{\partial X}{\partial T}\frac{\partial}{\partial X} + \frac{\partial Y}{\partial T}\frac{\partial}{\partial Y} + \frac{\partial Z}{\partial T}\frac{\partial}{\partial Z} \tag{V.9.10}$$

Equations (V.9.8) - (V.9.10) can be written as

$$\begin{Bmatrix} \frac{\partial}{\partial R} \\ \frac{\partial}{\partial S} \\ \frac{\partial}{\partial T} \end{Bmatrix} = \begin{bmatrix} \frac{\partial X}{\partial R} & \frac{\partial Y}{\partial R} & \frac{\partial Z}{\partial R} \\ \frac{\partial X}{\partial S} & \frac{\partial Y}{\partial S} & \frac{\partial Z}{\partial S} \\ \frac{\partial X}{\partial T} & \frac{\partial Y}{\partial T} & \frac{\partial Z}{\partial T} \end{bmatrix} \begin{Bmatrix} \frac{\partial}{\partial X} \\ \frac{\partial}{\partial Y} \\ \frac{\partial}{\partial Z} \end{Bmatrix} \tag{V.9.11}$$

or symbolically,

$$\{\partial(\ )\}_{\ell} = [J(R,S,T)]\{\partial(\ )\}_{g} \tag{V.9.12}$$

Then for the variable V

$$\{\partial V\}_{\ell} = J\ \{\partial V\}_{g} \tag{V.9.13}$$

Solving for the global derivative, we have

$$\{\partial V\}_{g} = [J]^{-1}\ \{\partial V\}_{\ell} \tag{V.9.14}$$

where

[J] stands for the Jacobian,

ℓ stands for the local derivative,

g stands for the global derivative.

Thus, to obtain the global derivative to be used in the integral statement

$$\{\partial V\}_g = [J]^{-1} \{\partial V\}_\ell \qquad \text{(V.9.15)}$$

and to use the isoparametric element, we must convert to a local coordinate integral expressing an elemental volume $dv = dXdYdZ = |J|drdsdt$. Now the $\int_V [B^e]dv$ can be evaluated as

$$\int [B^e]|J|dSdRdT$$

in the local coordinate system using numerical quadrature and can then be transformed into the global coordinate system.

B. Gaussian Quadrature

Consider a three-dimensional integration in the form

$$I = \int_{-1}^{+1} \int_{-1}^{+1} \int_{-1}^{+1} \phi(R,S,T)dRdSdT \qquad \text{(V.9.16)}$$

Then using Gauss' quadrature, I can be written as

$$I \simeq \sum_{i=1}^{n} \sum_{j=1}^{n} \sum_{k=1}^{n} W_i W_j W_k \, \phi(R_i, S_i, T_i) \qquad \text{(V.9.17)}$$

where the W's are the tabulated one-dimensional Gauss coefficients.

To program an isoparametric element, the following steps are to be considered.

For each and every quadrature point NQP

1. Get values for W_i, R_i, S_i and T_i using subroutine GAUSCO.
2. Formulate the interpolation functions $[H]_i$ using subroutine SHP4Q and their derivatives $[\Delta]_i$ using subroutine DER4Q.
3. Formulate the Jacobian $[J]_i$ by multiplying $[\Delta]_i[COORD]$ using subroutine JACOB.
4. Form $[J]_i^{-1}$ and the determinant of the Jacobian $|J|$ using subroutine I2BY2.
5. Form the global derivative of $[H]_i$ using subroutine GDERIV.
6. Add current terms to form the summation and complete the numerical integration.

CHAPTER VI

EXPERIMENTAL INVESTIGATION OF THE INFLUENCE OF HIGH-SPEED FLOW ON SOUND PROPAGATION

VI.1 Introduction

In this chapter, the experimental investigation of the influence of high-speed flow on sound propagation in variable area ducts is considered. The noise source is a spinning mode synthesizer located at one end of a variable area duct carrying high subsonic Mach number flows. A choked inlet is located on the compressor to suppress the undesirable noise generated by the compressor.

Spinning mode synthesizer SMS generated the required plane wave and/or spinning modes with variable frequency and intensity. The test section contains the variable area duct mounted on a constant area spool piece where the SMS is located. The SMS is constructed of eight sound drivers located circumferentially and equally spaced. The arrangement of the drivers has the capability of generating the plane wave, and two circumferential modes, mainly (1,0) and (2,0). Downstream of the constant area spool piece, a choked inlet with translating centerbody is located and connected to another adaptor piece which is directly hooked to the compressor flange. The purpose of the choked inlet is to choke all the noise generated by the compressor. The fine adjustment of the

centerbody location of the choked inlet eliminated upstream propagation of compressor noise.

In other words, the compressor provided a quiet high-speed flow in the test section. The compressor is of the transonic type and located in NASA-Langley anechoic chamber. All measuring equipment is remotely controlled from the operating room.

VI.2 Description of Inlets and Test Facility

A. Inlets

Four inlets were tested describing four different axial velocity gradients. The first is a constant area duct representing a zero velocity gradient inlet; the second has its maximum velocity gradient far from the inlet throat; the third inlet has a constant velocity gradient; and the fourth one has its maximum velocity gradient near the throat. Figure VI.1 shows the Mach number variation of these four inlets. The design of these inlets was optimized to minimize boundary layer separation and to maximize pressure recovery by a suitable choise of length/diameter ratio.

B. Test Facility

The inlets were tested in the anechoic chamber transonic compressor facility of the NASA-Langley Research Center. The test vehicle was a 30.5 cm-tip diameter single-stage transonic compressor with 19 rotor blades. Figure VI.2 shows the anechoic chamber facility with one

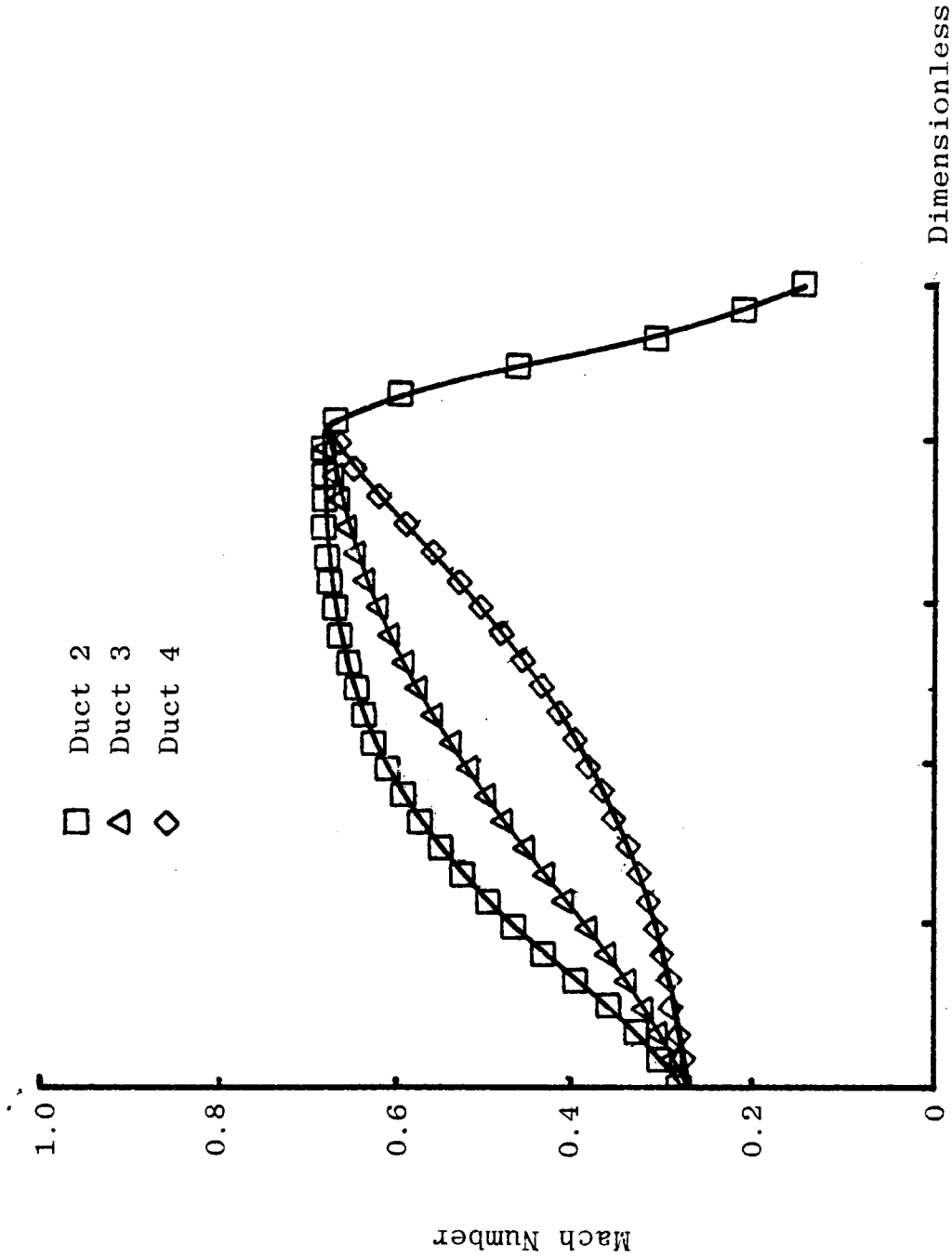


Figure VI.1 Mach Number Distribution for 18 lb_m/sec

NASA
L-76-2381

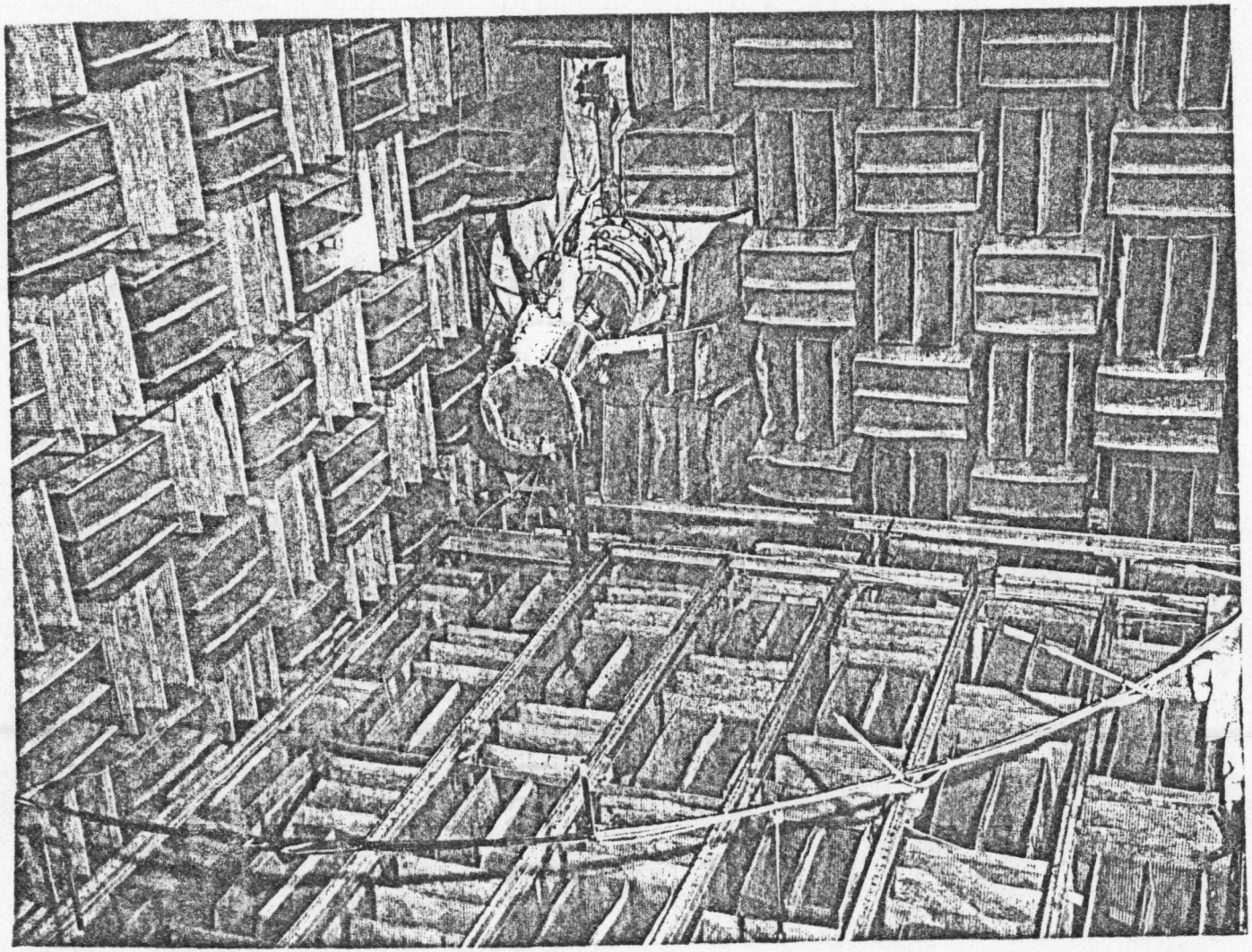


Figure VI.2 Experimental Setup to Determine the Influence of High-Speed Flow on Noise Attenuation

of the test sections in place. Also shown in the figure are the wall microphones, the acoustic drivers, the choked inlet, static pressure taps, the spinning mode synthesizer and the acoustic traverse probe.

C. Intrumentation and Test Procedure

Figure VI.3 is a schematic of the inlet arrangement showing the positions of the wall microphones. Figure VI.4 is a schematic of the two inlet section showing the positions of the pressure probes for aerodynamic measurements. In additon to the eight 1/4-inch wall microphones, nine 1/2-inch far-field microphones were used to obtain data in the radiation field. Aerodynamic output was recorded on VIDAR from the scanivalve system with on-line chart output as well as magnetic tape. The far-field data were taken on-line with a 1/3-octave real-time analyzer.

The following aerodynamic instrumentation was used:

1. Seventy-two static pressure taps were located axially on the two inlets (36 each) for obtaining the Mach number distribution along the walls. In addition, four static taps distributed circumferentially at two axial locations were used to determine the circumferential pressure variation.
2. One total pressure probe at the exit of the test section was used to determine the

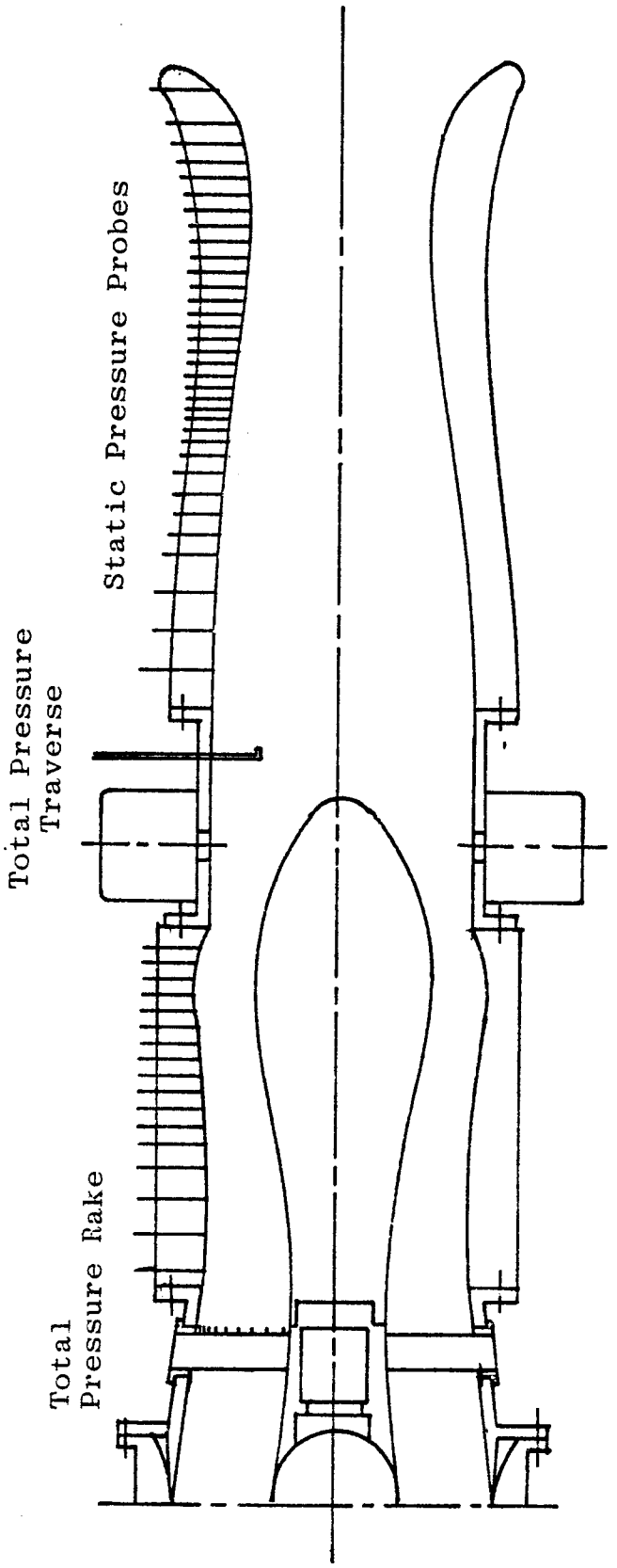


Figure VI.3 Schematic of Experimental Apparatus
Showing Two Inlets with Aerodynamic
Instrumentation

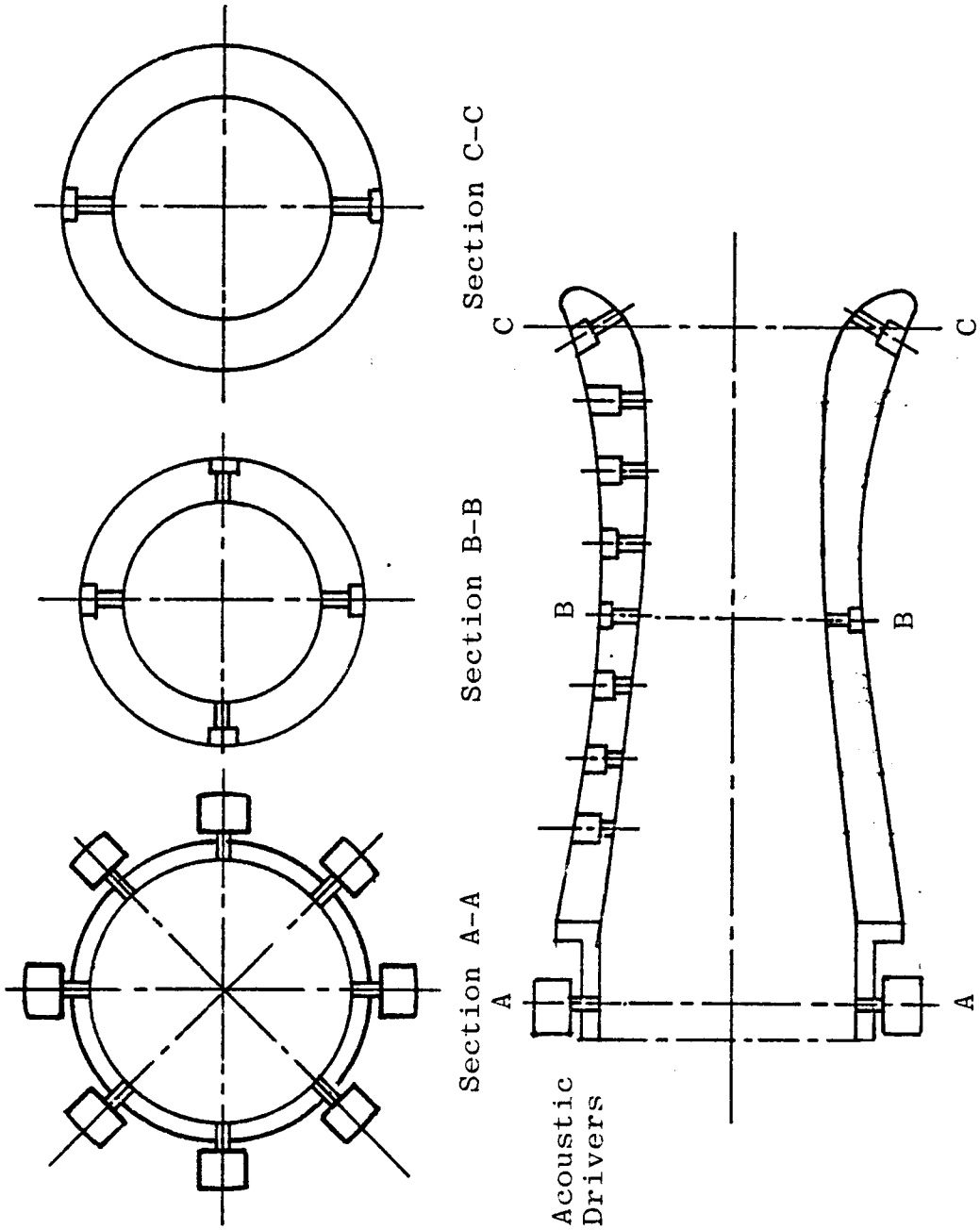


Figure VI.4 Schematic of Typical Test Section Showing the Microphone and Sound Driver Positions

pressure loss and mass flow.

3. The centerbody of the second inlet was controlled by a hydraulic cylinder, and its position was indicated by a digital voltmeter in the control room.

The acoustic instrumentation consisted of the following:

1. Nine 1/2-inch condenser microphones located 4.57 cm from the inlet plane, reading at every 10 degrees, but excluding the 90-degree position were used to obtain far-field acoustic data.
2. Eight B & K 1/4-inch condenser microphones were located axially in the first duct (test section) to determine the in-duct pressure distribution.
3. Halfway along the axis of the first inlet, four 1/4-inch condenser microphones located circumferentially were used for monitoring if the waves generated by the drivers were of the mode desired.
4. Eight acoustic drivers (ID-60, Universal Sound Units, 60 Watts, 16 Ohms) were used to construct the spinning mode synthesizer needed to generate the desired modes. The arrangement of the drivers together with the monitoring system is shown in Figure VI.5

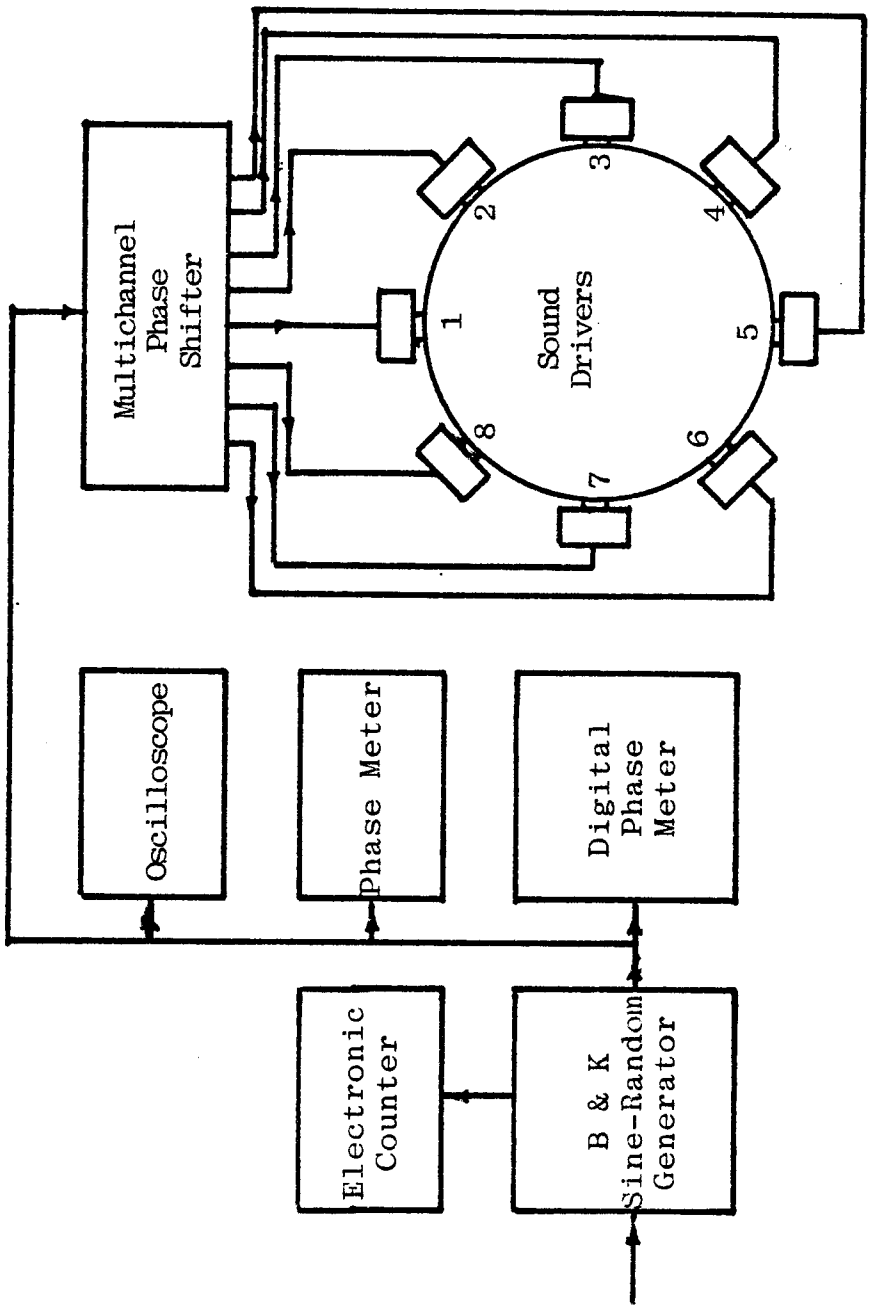


Figure VI.5 Monitoring System for Acoustic Drivers

All microphones were calibrated before each test. Prior to starting the compressor, a no-flow test was conducted for each frequency and mode. Frequencies on the sine-random generator (B & K 1022) were selected for each case above the cut-off for that particular mode. The frequencies were:

Mode (0,0)	Mode (1,0)	Mode (2,0)
500 Hz	764 Hz	1223 Hz
680 Hz	1000 Hz	1490 Hz
1000 Hz	1600 Hz	2000 Hz

The outlet signal from the sine-random generator was fed into an eight-channel phase shifter where each channel is separately adjusted in phase and amplitude. The three modes were generated by the eight-channel phase shifter by placing the sound drivers in accordance with the following table:

Sound Driver Mode Number	1	2	3	4	5	6	7	8
(0,0) degrees	0	0	0	0	0	0	0	0
(1,0) degrees	0	45	95	135	180	225	270	315
(2,0) degrees	0	90	180	270	0	90	180	270

Phase adjustments to produce any mode of order (m,0) are given by

$$\Theta = \frac{360\ m(i-1)}{8} \quad \text{degrees}$$

where $i = 1,2,...8$ (number of drivers).

The output from each channel was fed into the phase meter to measure the phase angle. The output level to each sound driver was monitored using the digital voltmeter which measured the voltage output from each channel. Four circumferential microphones located at two axial positions were used to monitor the output from the drivers to ensure that the desired modes were generated. Typical results are given in Figures VI.6 and VI.7. Before starting the compressor, a static test was conducted. For the tests with flow, the centerbody of the second inlet was in the retracted position, and the compressor was accelerated until choking in the inlet occured. A typical curve showing the tone from the acoustic drivers before and after choke is given in Figure VI.8. After data collection in this position, the centerbody was translated consecutively to several prescribed positions to give different desired axial Mach numbers to the first inlet while maintaining choked flow in the second inlet. The rpm of the compressor was reduced accordingly.

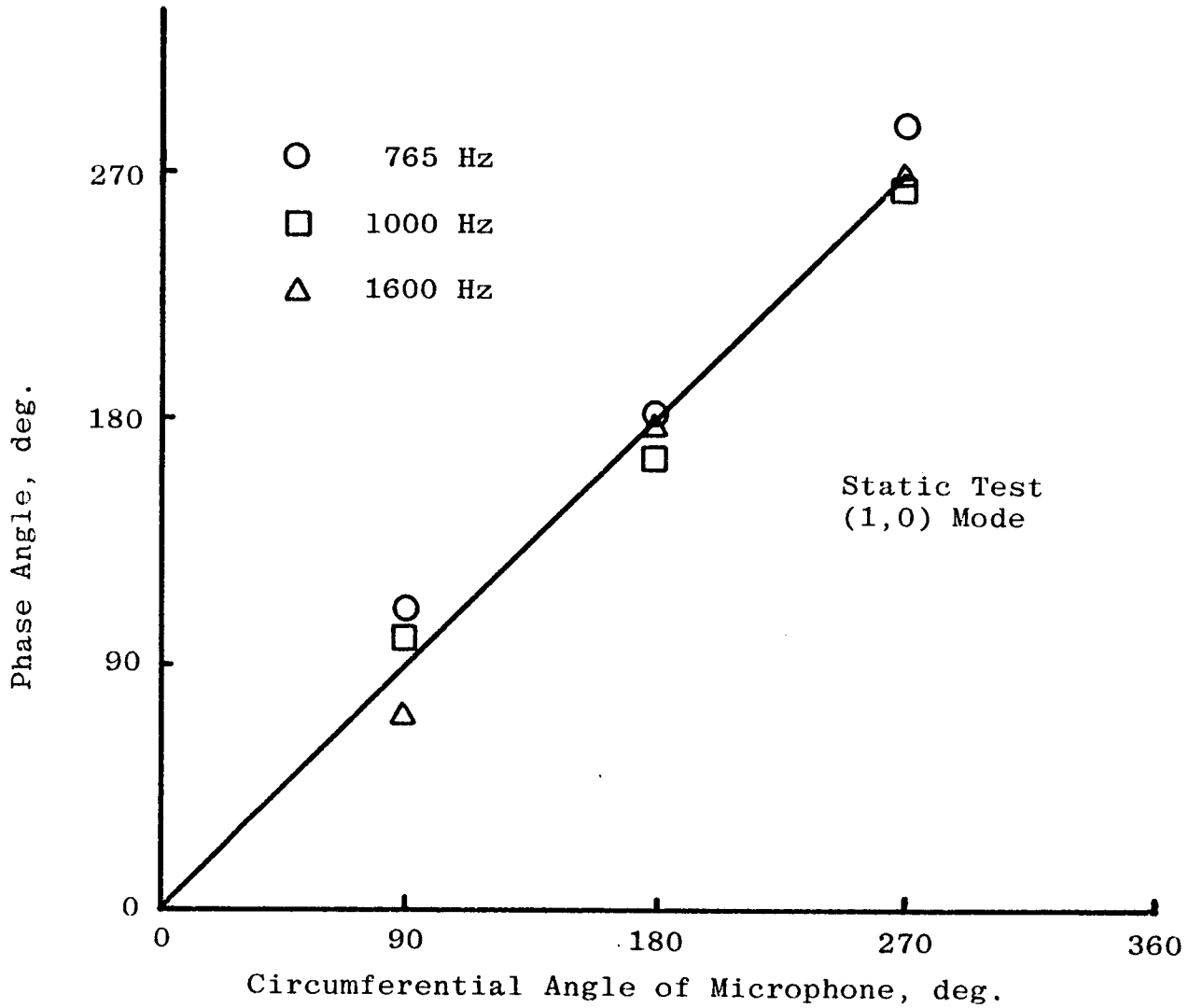


Figure VI.6 Variation of Phase Angle with Microphone Position (1.0) Mode

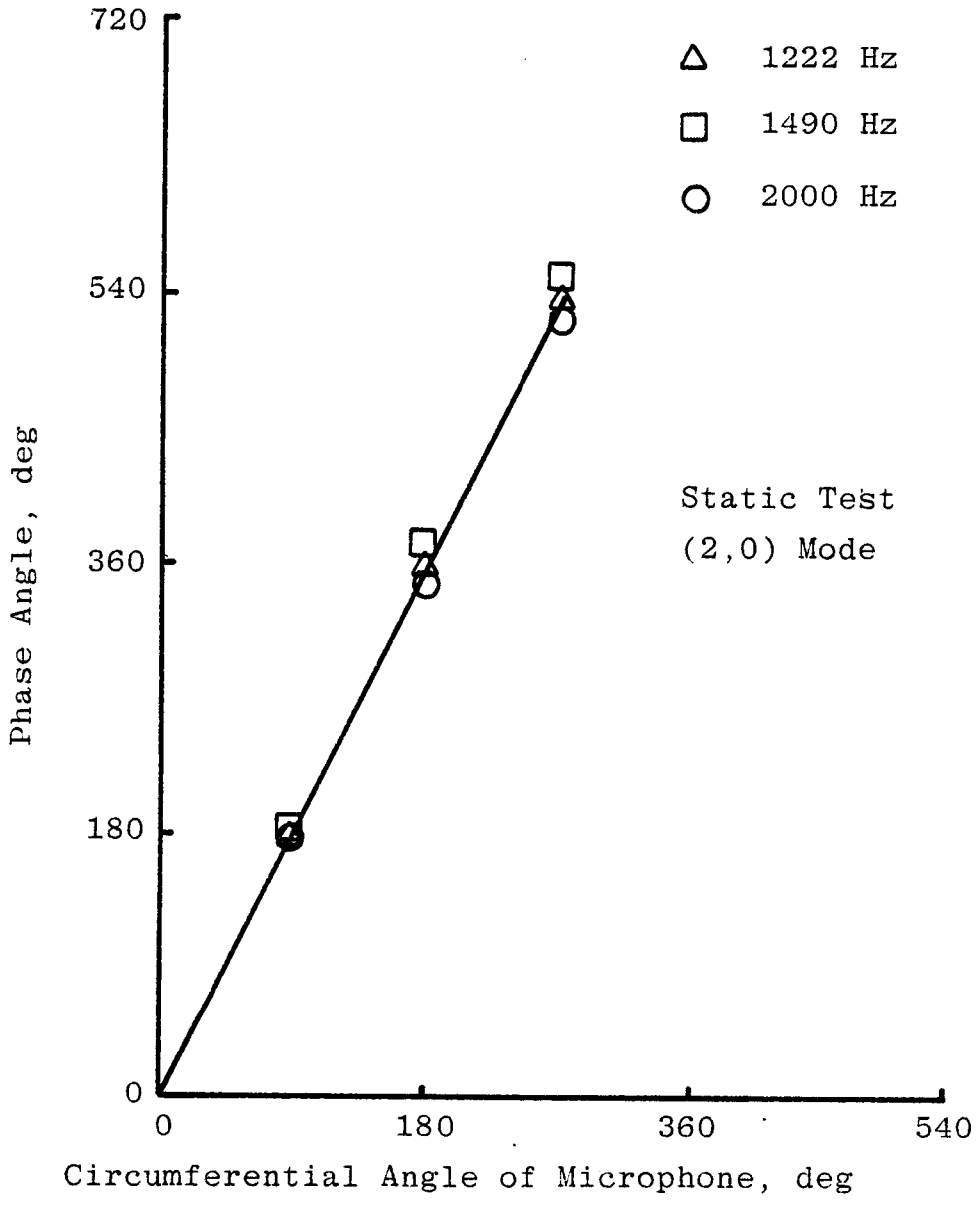


Figure VI.7 Variation of Phase Angle with Microphone Position (2,0) Mode

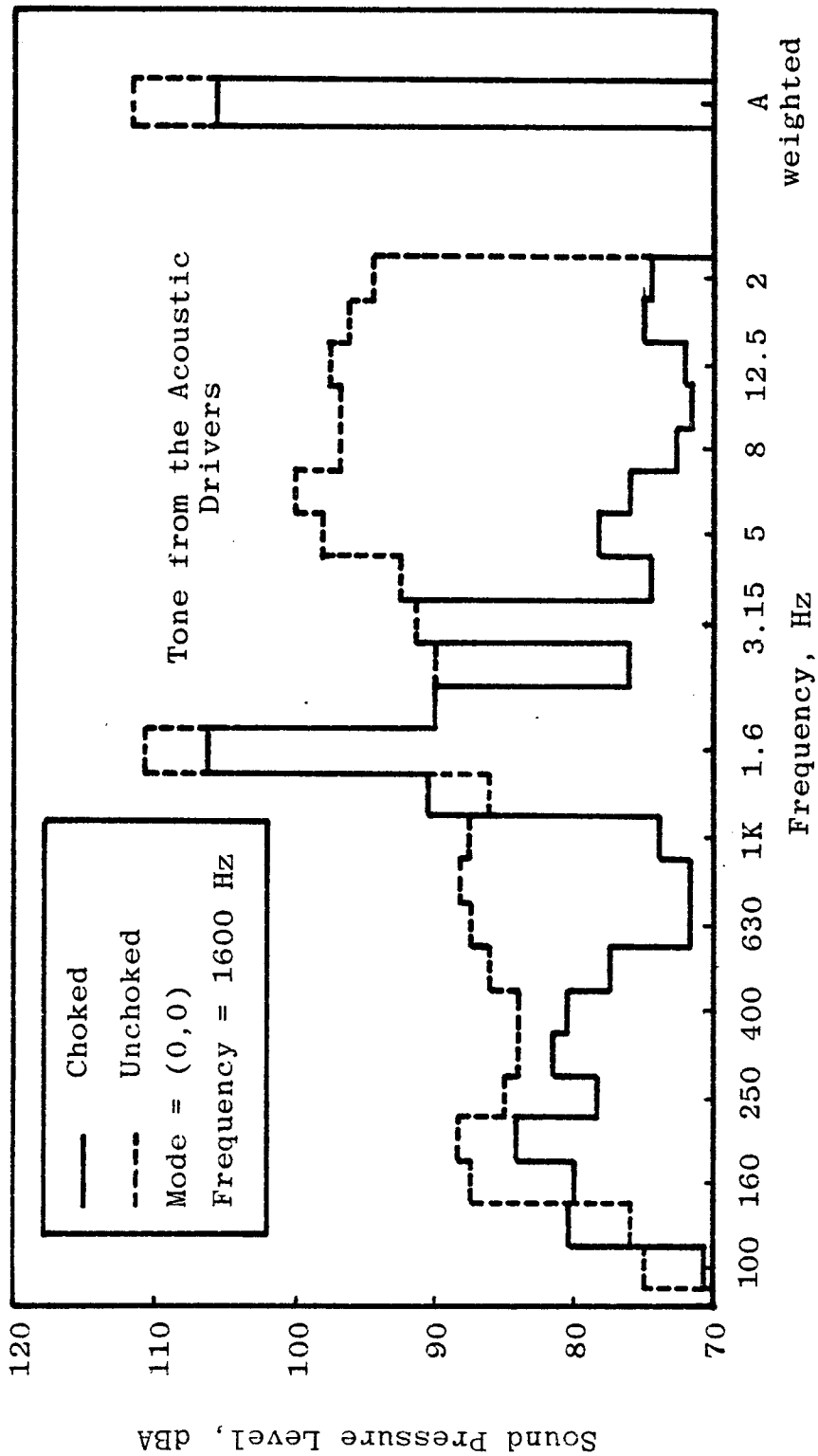


Figure VI.8 Influence of Choking on the Signal-to-Noise Ratio of Eight Acoustic Drivers

CHAPTER VII

DISCUSSION OF RESULTS, CONCLUSION AND RECOMMENDATIONS

In this chapter, finite element predictions and the experimental results are presented and compared for different duct geometries, different exciting frequencies and different mode numbers. Figure VII.1 shows the finite element (FE) solution and the exact solution for the real part of the acoustic velocity potential in a hard-wall constant area duct for different Mach number flows. Agreement is excellent for no flow, 0.15 and 0.68 Mach number flows when a plane wave source is applied at one end and a non-reflection boundary condition is applied at the other end of the duct.

Discussion of results is divided into two parts, no flow results and flow results.

VII.1 No Flow Results

Three duct geometries are considered in this analysis, duct number 3 of mild velocity gradients and ducts number 2 and 4 of velocity gradients far from and near to the duct throat area, respectively. Three exciting modes are compared: plane wave (0,0) mode, and two higher order modes (1,0) and (2,0) for different frequencies.

Figures VII.2 - VII.4 give the normalized acoustic pressure amplitude along the duct wall versus the non-

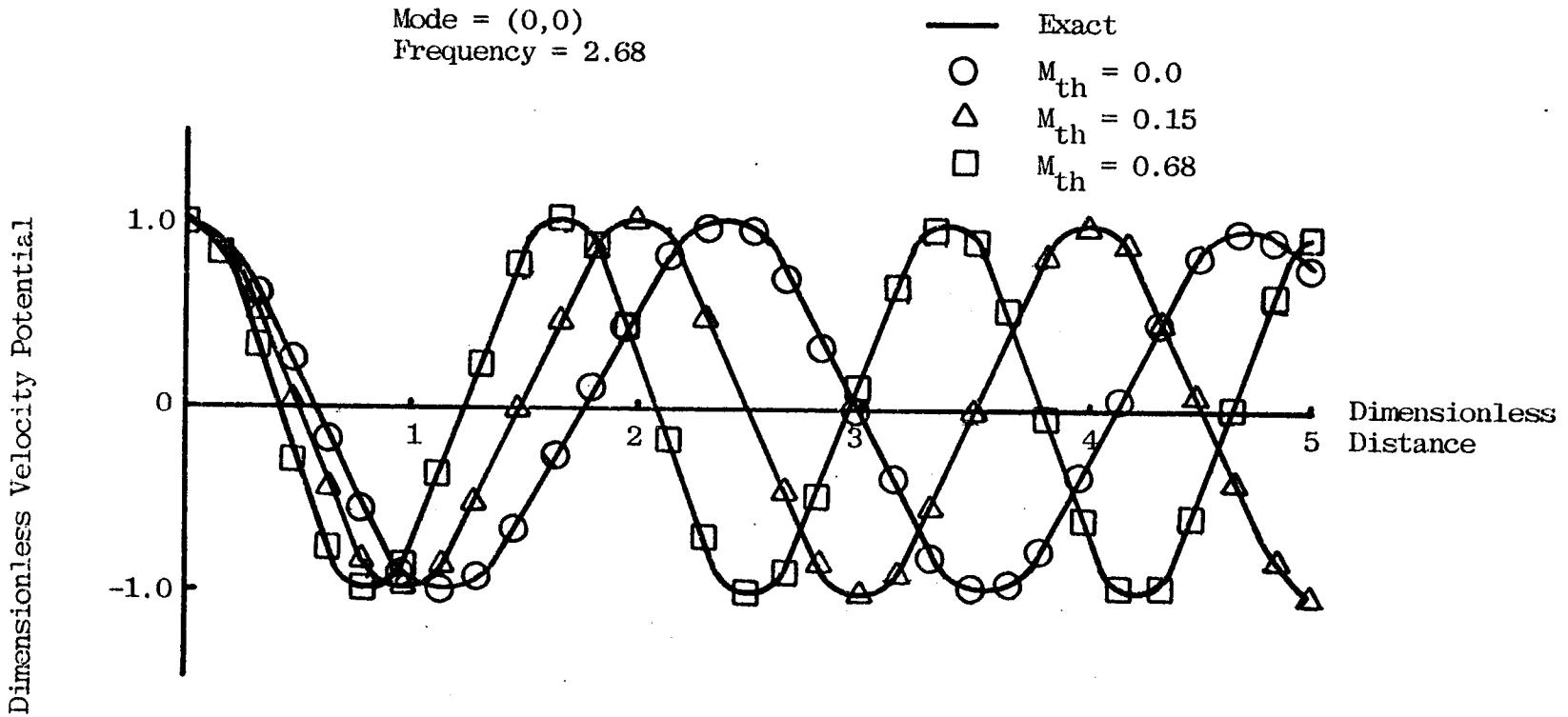


Figure VII.1 Exact and Finite Element Solutions for Wave Progagation in a Constant Area Duct

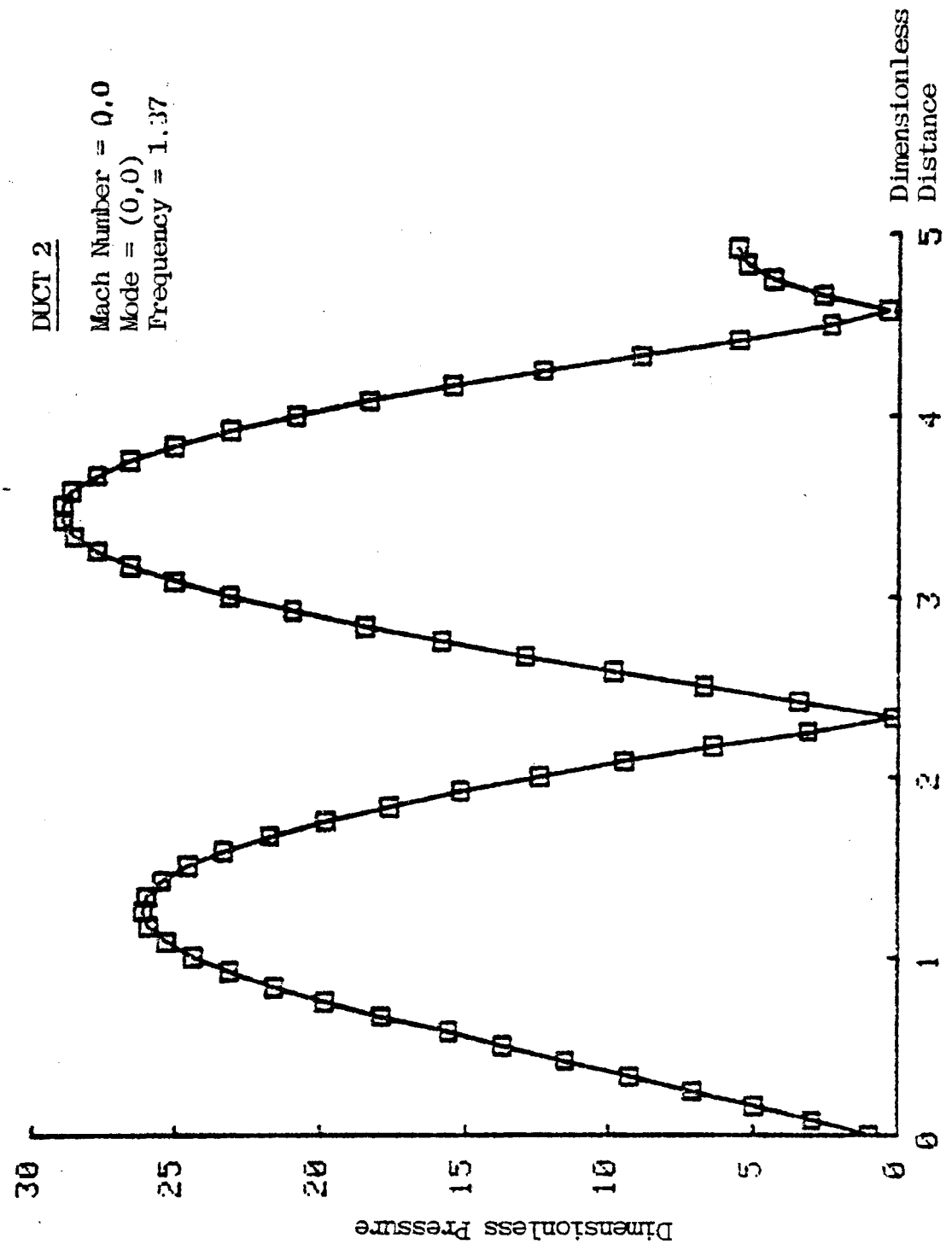


Figure VII.2 Pressure Distribution Along Duct Wall
(Duct 2, Mach Num=0.0, Mode=(0,0), Freq=1.37)

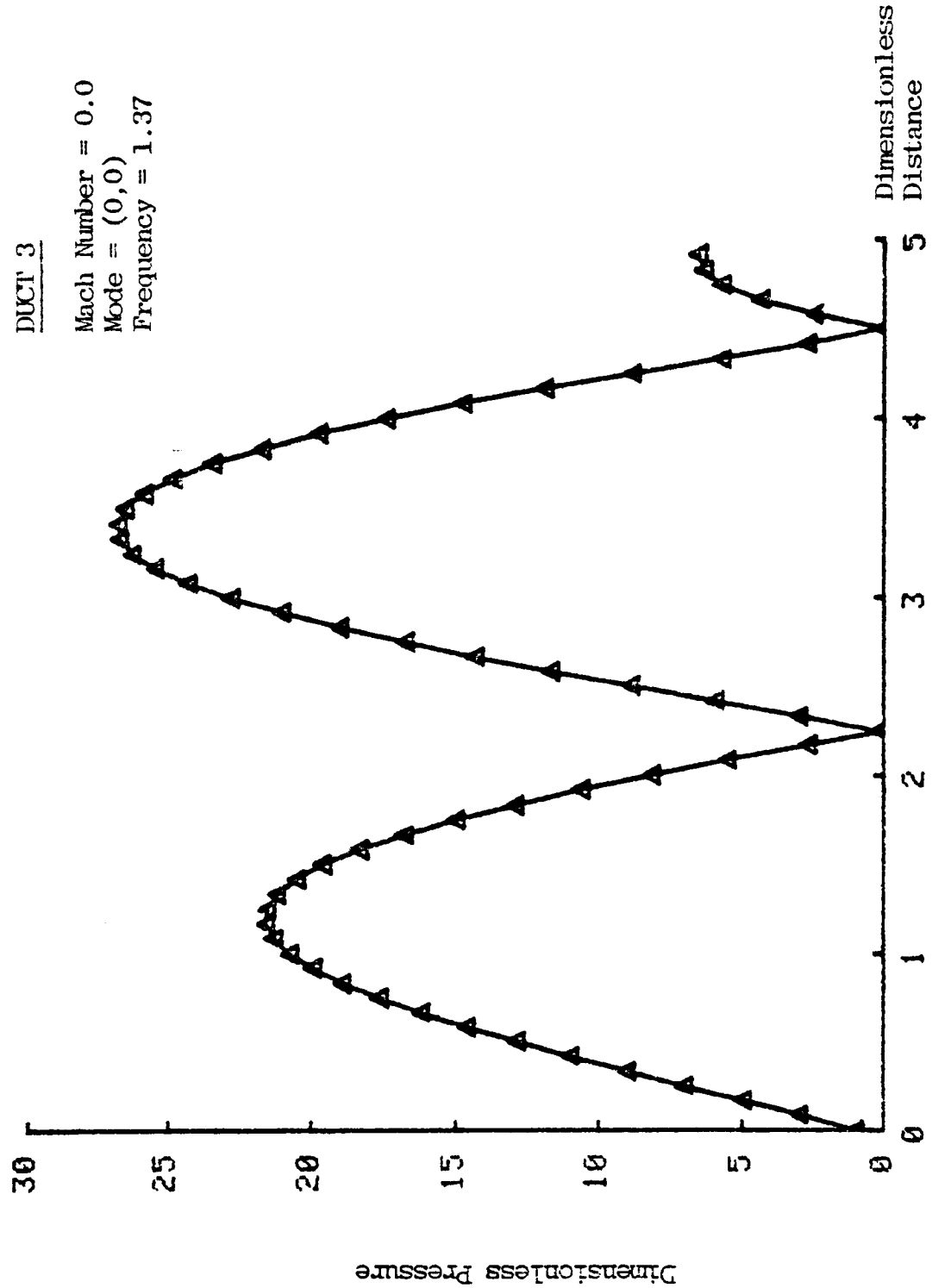


Figure VII.3 Pressure Distribution Along Duct Wall
(Duct 3, Mach Num=0.0, Mode=(0,0), Freq=1.37)

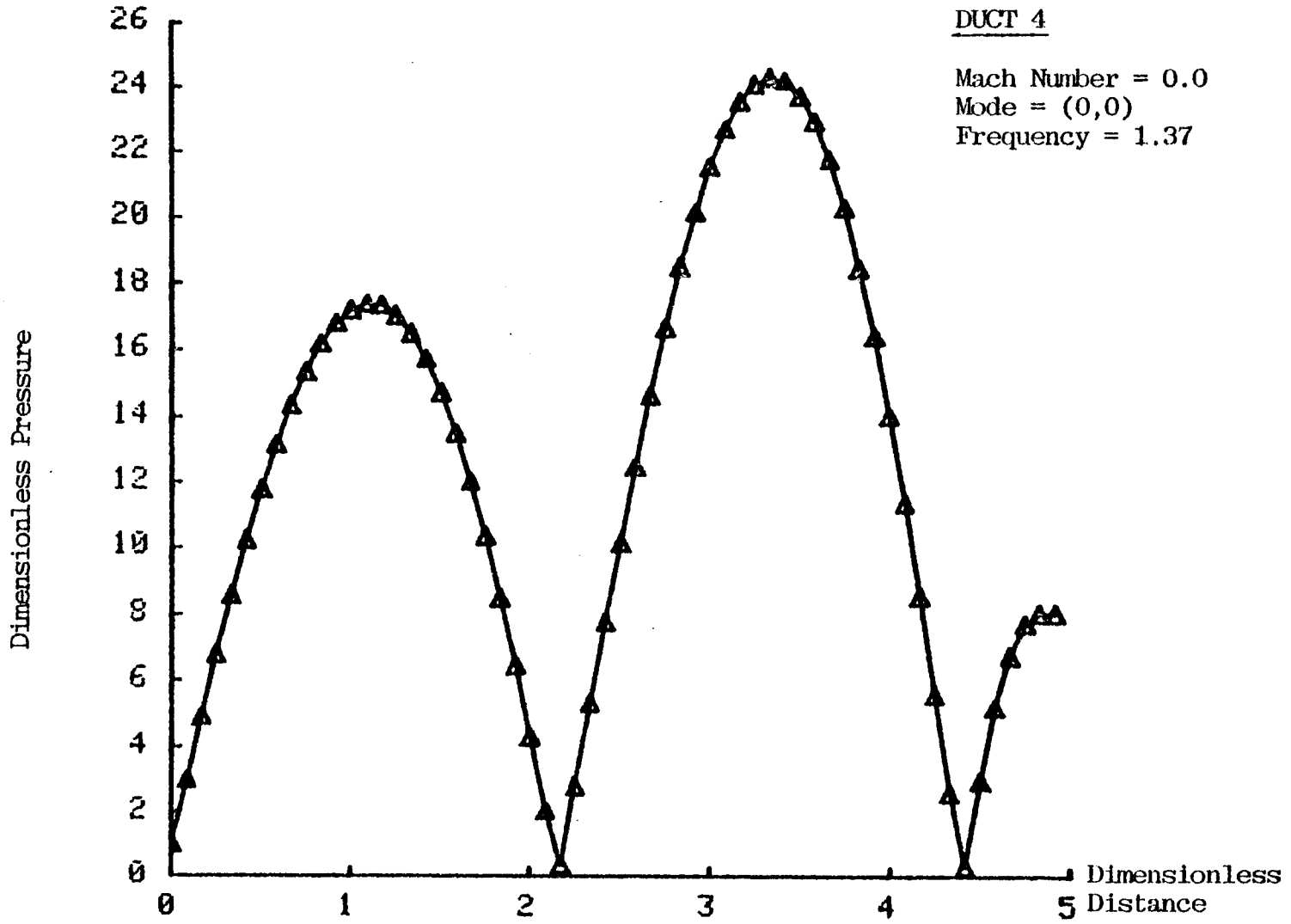


Figure VII.4 Pressure Distribution Along Duct Wall
(Duct 4,Mach Num=0.0,Mode=(0,0),Freq=1.37)

dimensional axial distance for the three variable area ducts under consideration: ducts 2, 3 and 4, respecitvely for plane wave excitation of 500 Hz (1.37 non-dimensional frequency). Acoustic pressure peaks near the throat area for all the ducts. The difference between the peak magnitudes for duct 4 is much higher than that for ducts 3 and 2. Maximum value of the pressure amplitude for the three ducts is about the same near the throat (in agreement with experimental results) which shows that there is no remarkable difference in the far-field sound pressure levels for the three ducts as can be seen in Figure VII.5. When the exciting frequency is doubled, the same trend is observed for inlets number 3 and 4 with higher levels near the throat in duct 4 as shown in Figures VII.6 and VII.7. The far-field attenuation, Figure VII.8, shows more attenuation due to duct 3 compared to 2 and 4; this might be due to the lower pressure levels in duct 3 as seen in Figures VII.6 and VII.7.

For this frequency, duct geometry has no effect on changing the effective wave length inside the duct as demonstrated in Figures VII.9 and VII.10, which give the variation of the real part of the acoustic velocity potential along duct walls for inlets 3 and 4.

For higher order modes, Figures VII.11, VII.12 and VII.13 show the wave inside the duct when the (1,0) mode of 765 Hz frequency is excited in ducts 2, 3 and 4.

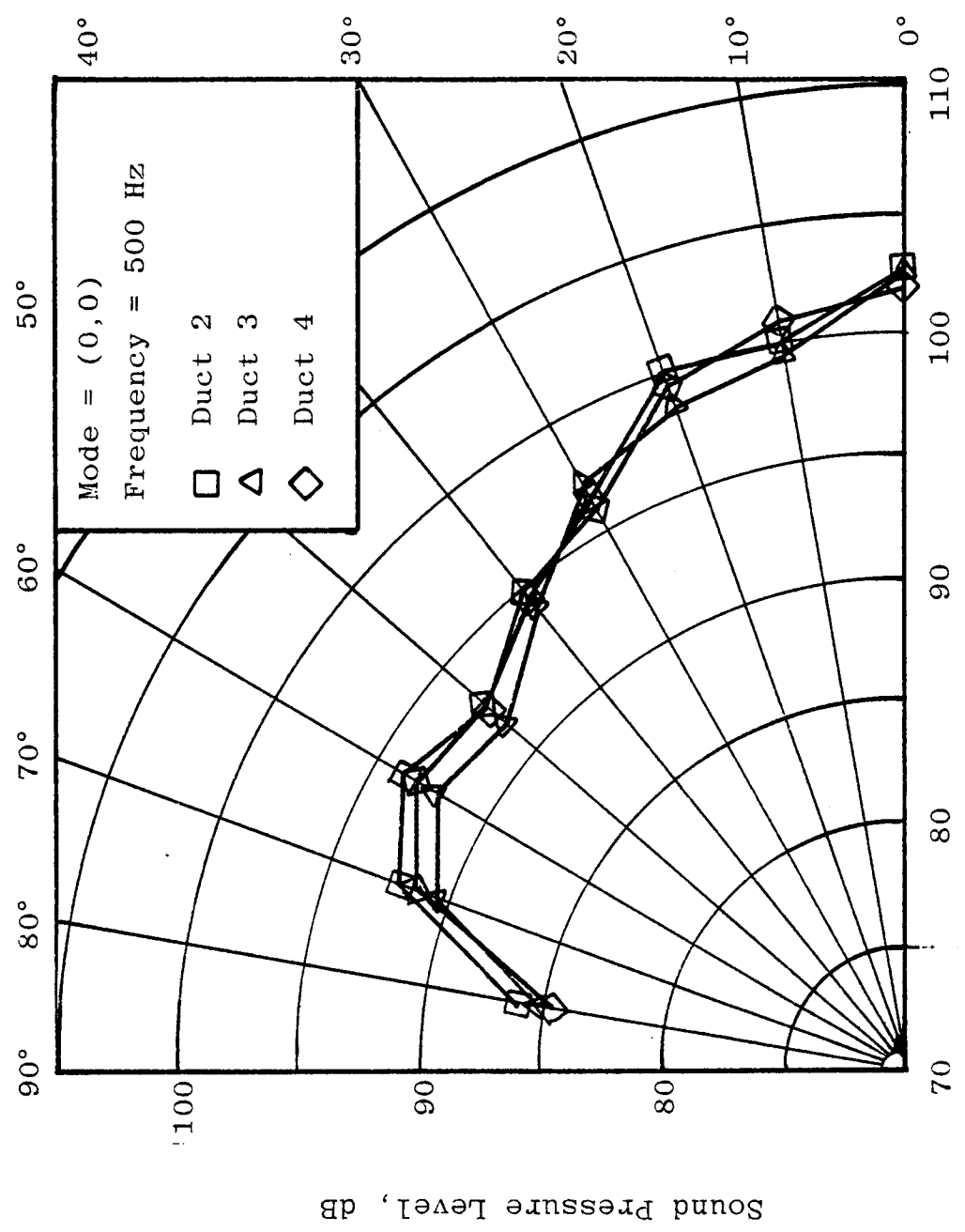


Figure VII.5 Far-Field Sound Pressure Level Under Static Conditions (Mode=(0,0),Freq=500 Hz)

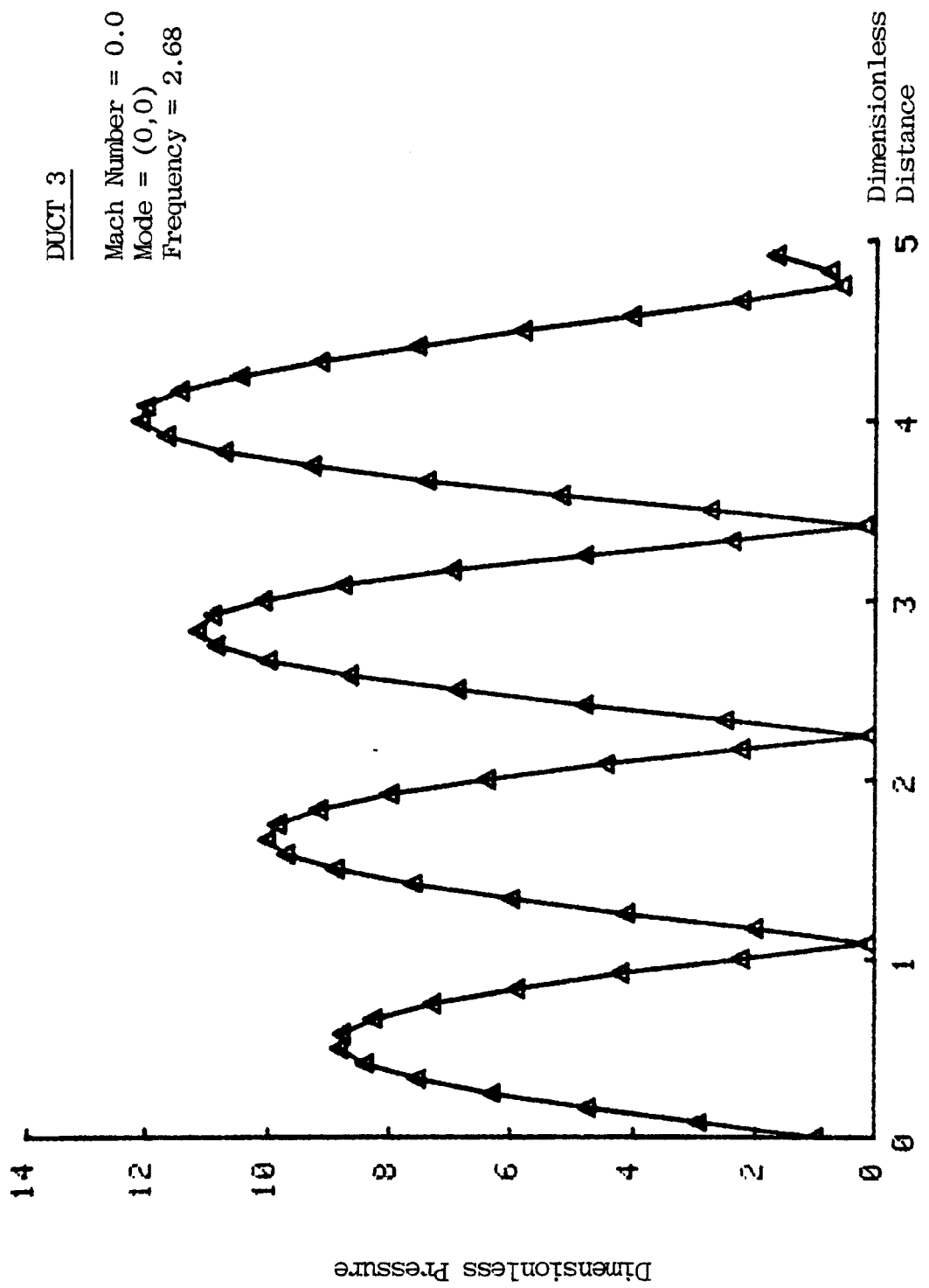


Figure VII.6 Pressure Distribution Along Duct Wall
(Duct 3, Mach Num=0.0, Mode=(0,0), Freq=2.68)

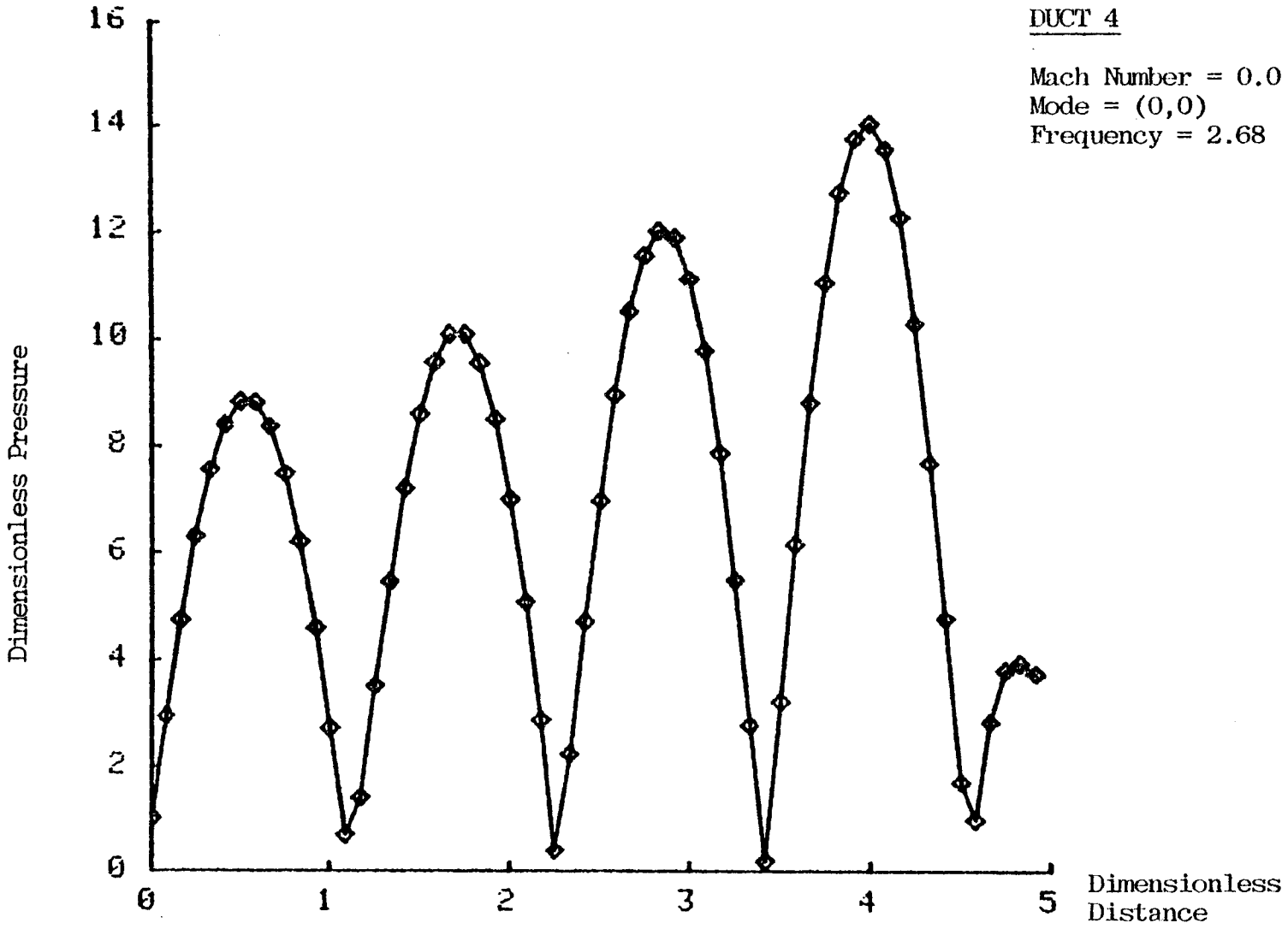


Figure VII.7 Pressure Distribution Along Duct Wall
(Duct 4, Mach Num=0.0, Mode=(0,0), Freq=2.68)

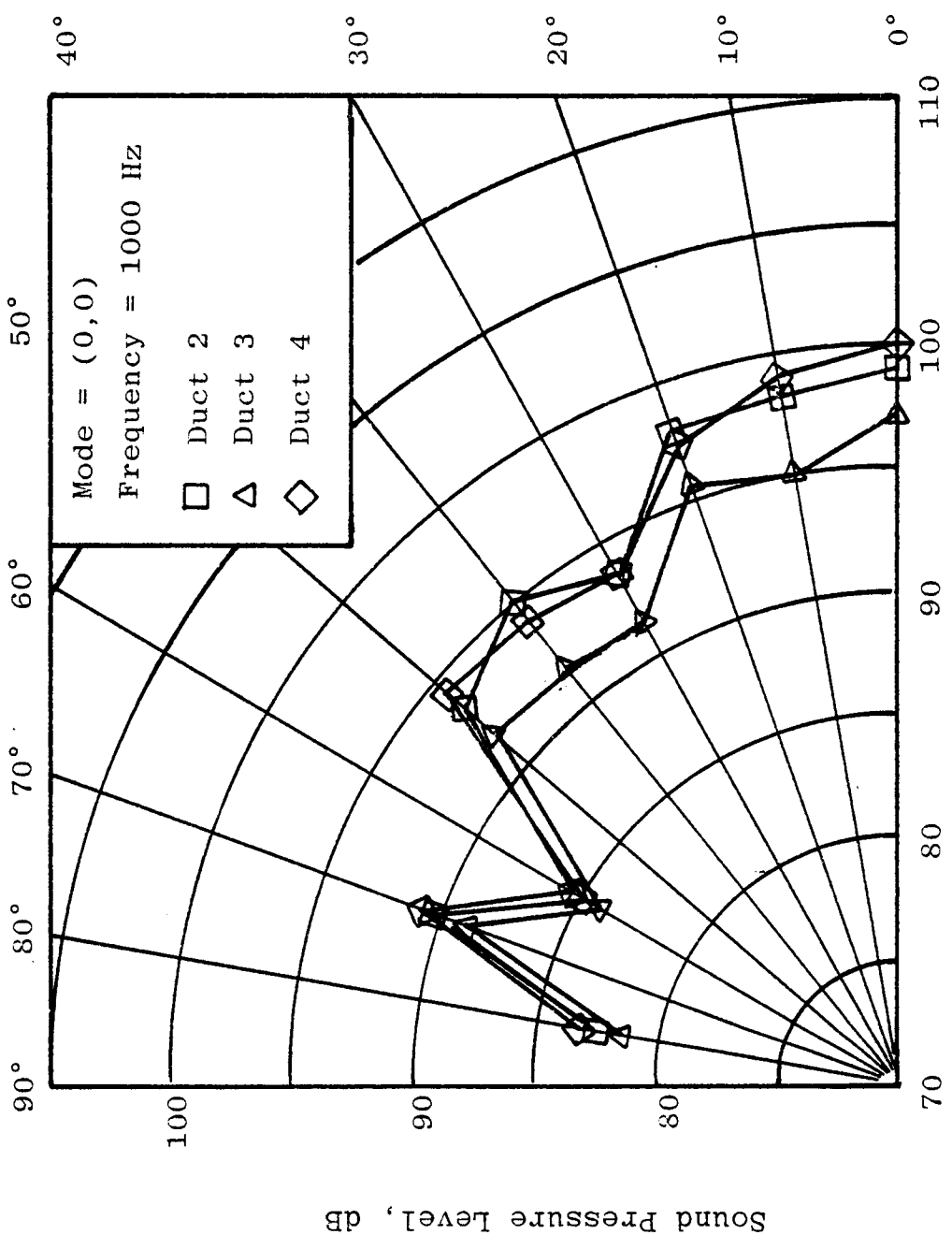


Figure VII.8 Far-Field Sound Pressure Level Under Static Conditions (Mode=(0,0),Freq=1000 Hz)

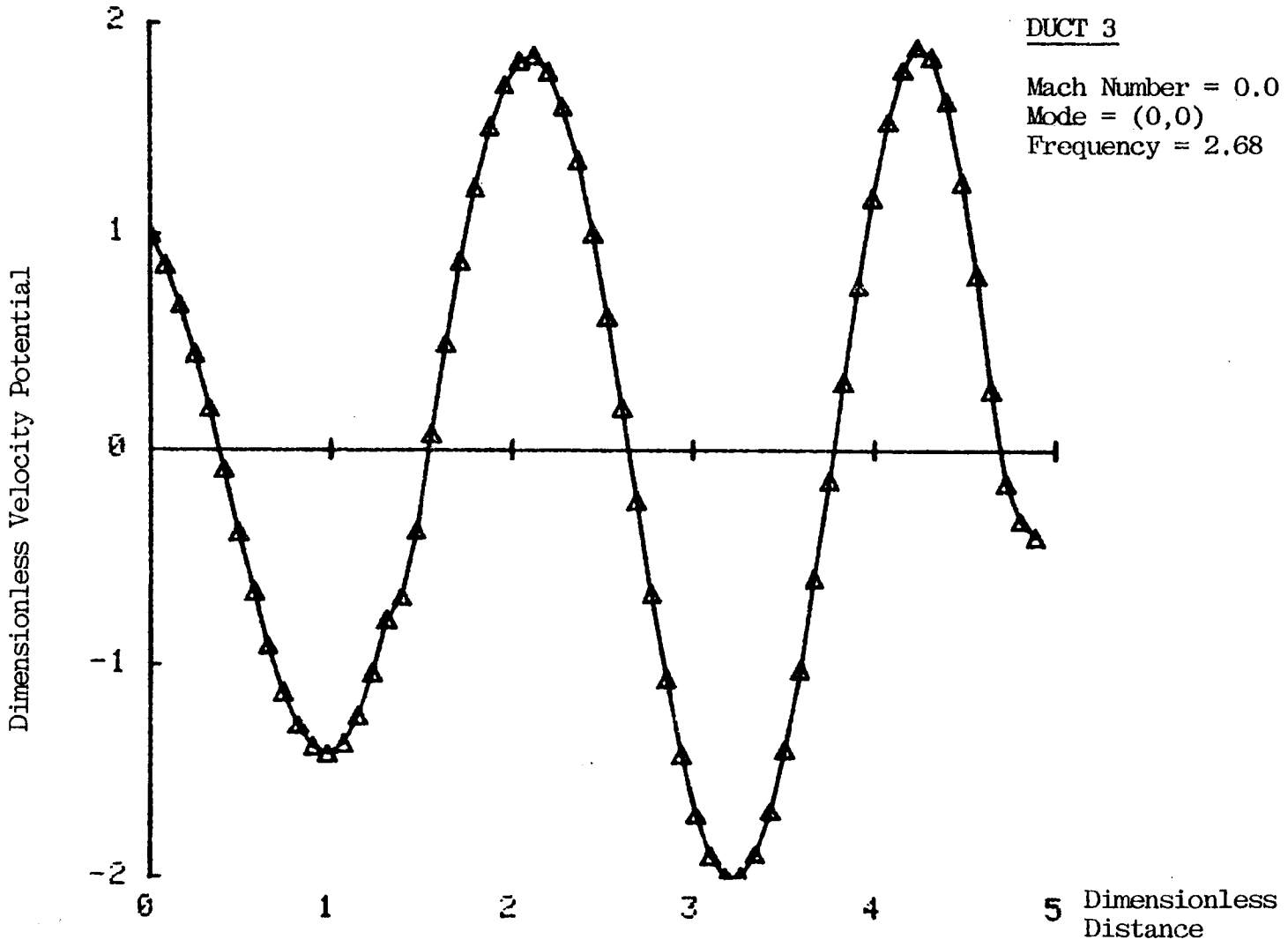


Figure VII.9 Acoustic Velocity Potential (Real Part) Along Duct Wall
(Duct 3,Mach Num=0.0,Mode=(0,0),Freq=2.68)

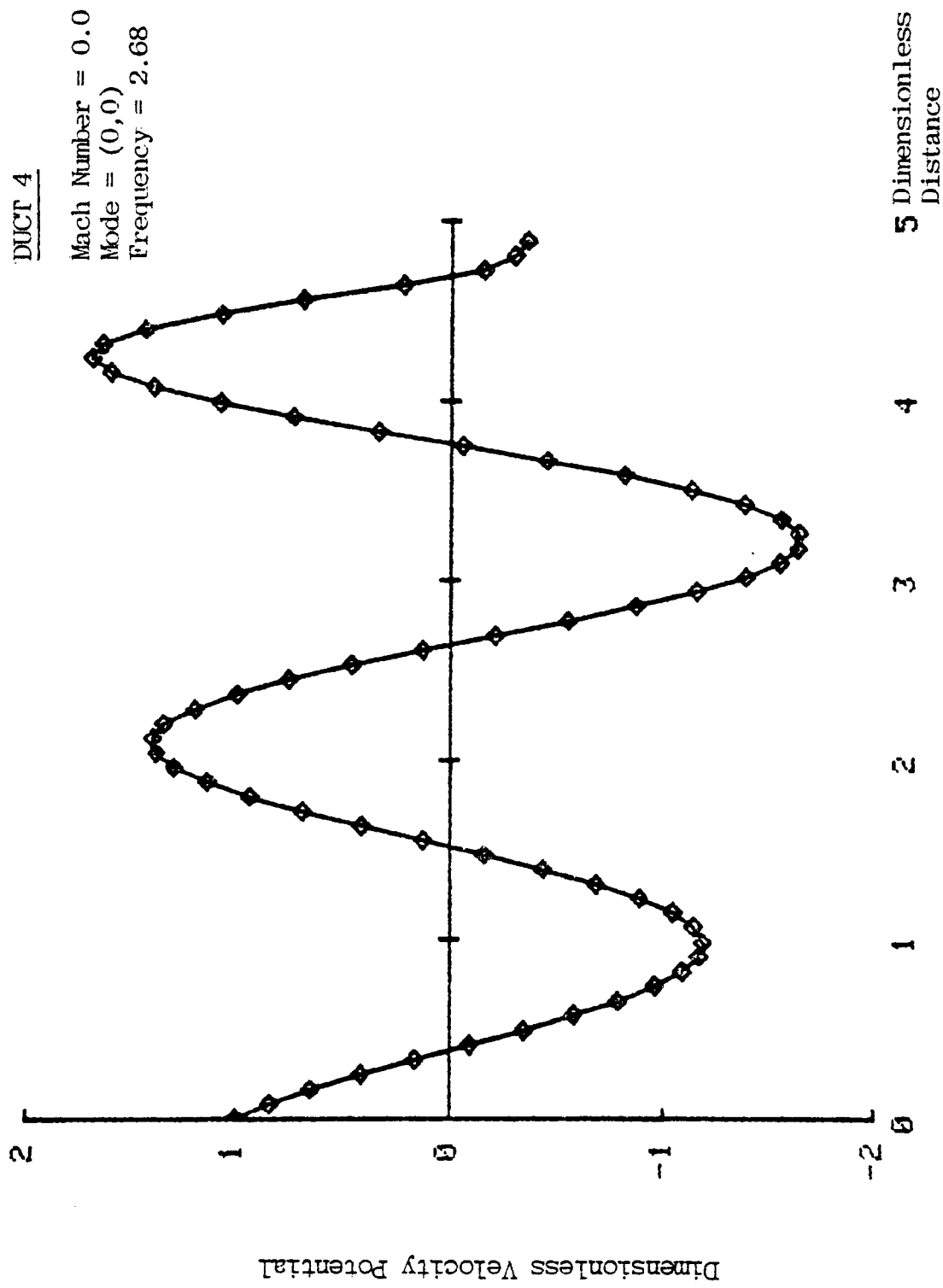


Figure VII.10 Acoustic Velocity Potential (Real Part) Along Duct Wall
(Duct 4, Mach Num=0.0, Mode=(0,0), Freq=2.68)

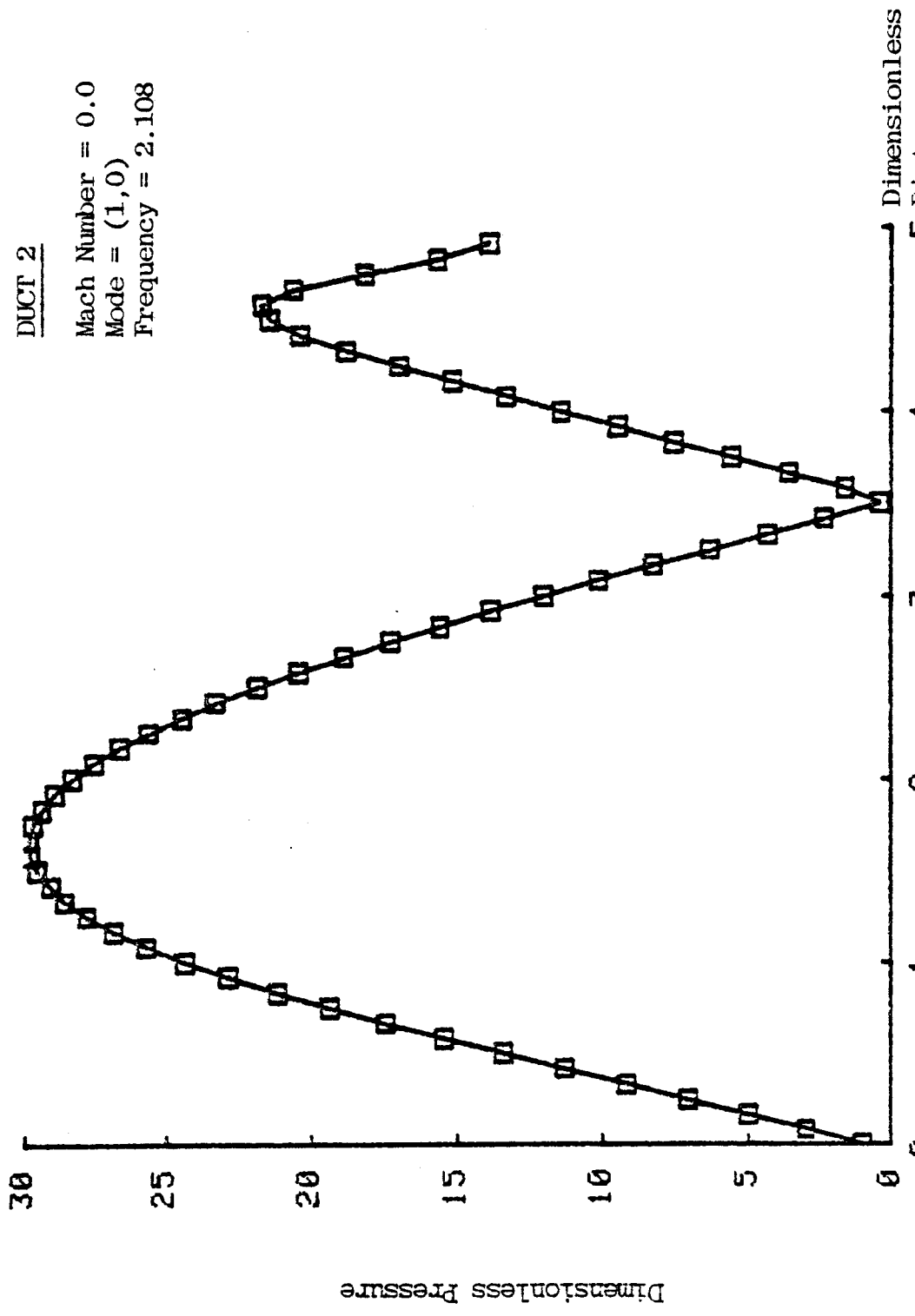


Figure VII.11 Pressure Distribution Along Duct Wall
(Duct 2, Mach Num=0.0, Mode=(1,0), Freq=2.108)

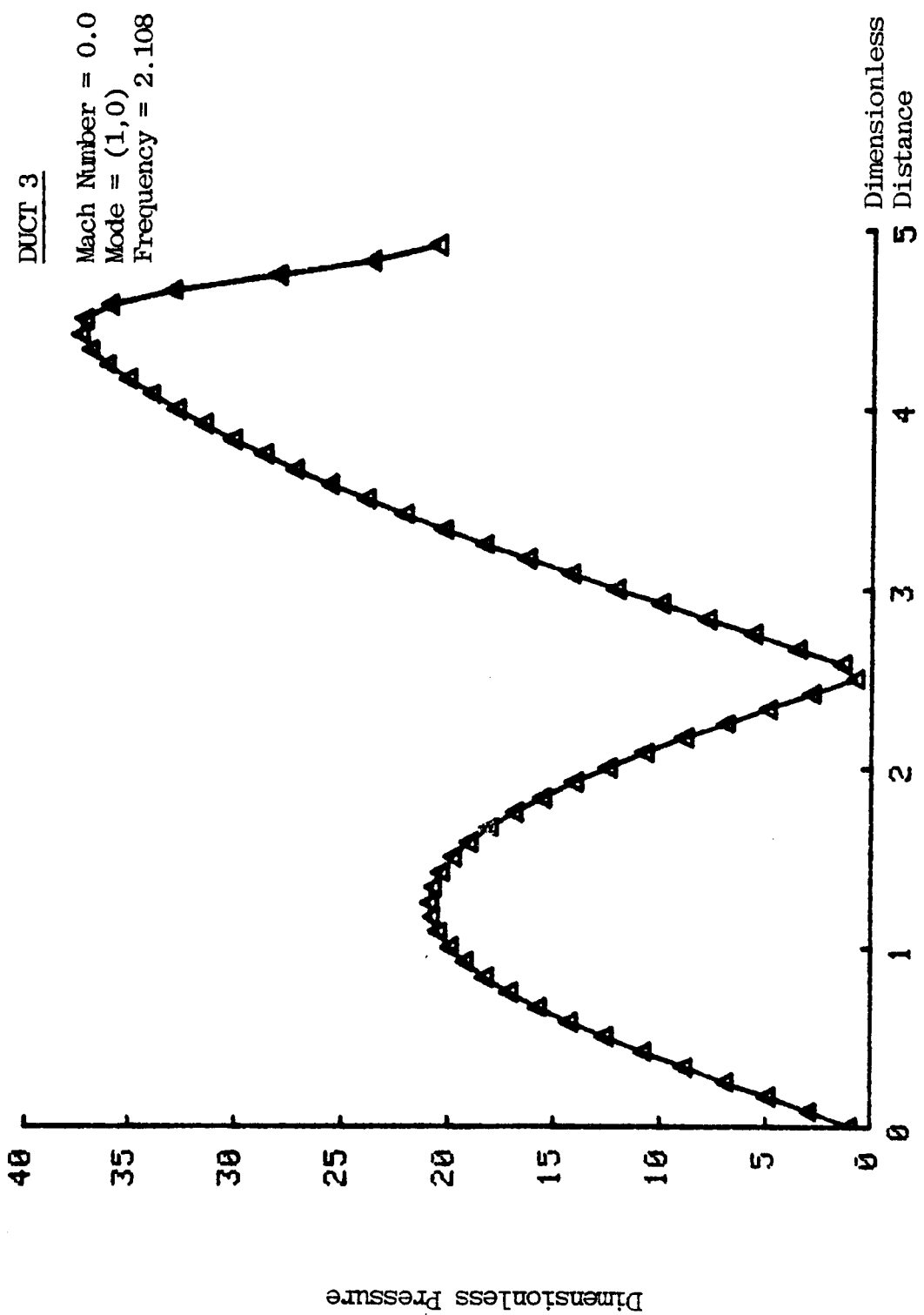


Figure VII.12 Pressure Distribution Along Duct Wall
(Duct 3, Mach Num=0.0, Mode=(1,0), Freq=2.108)

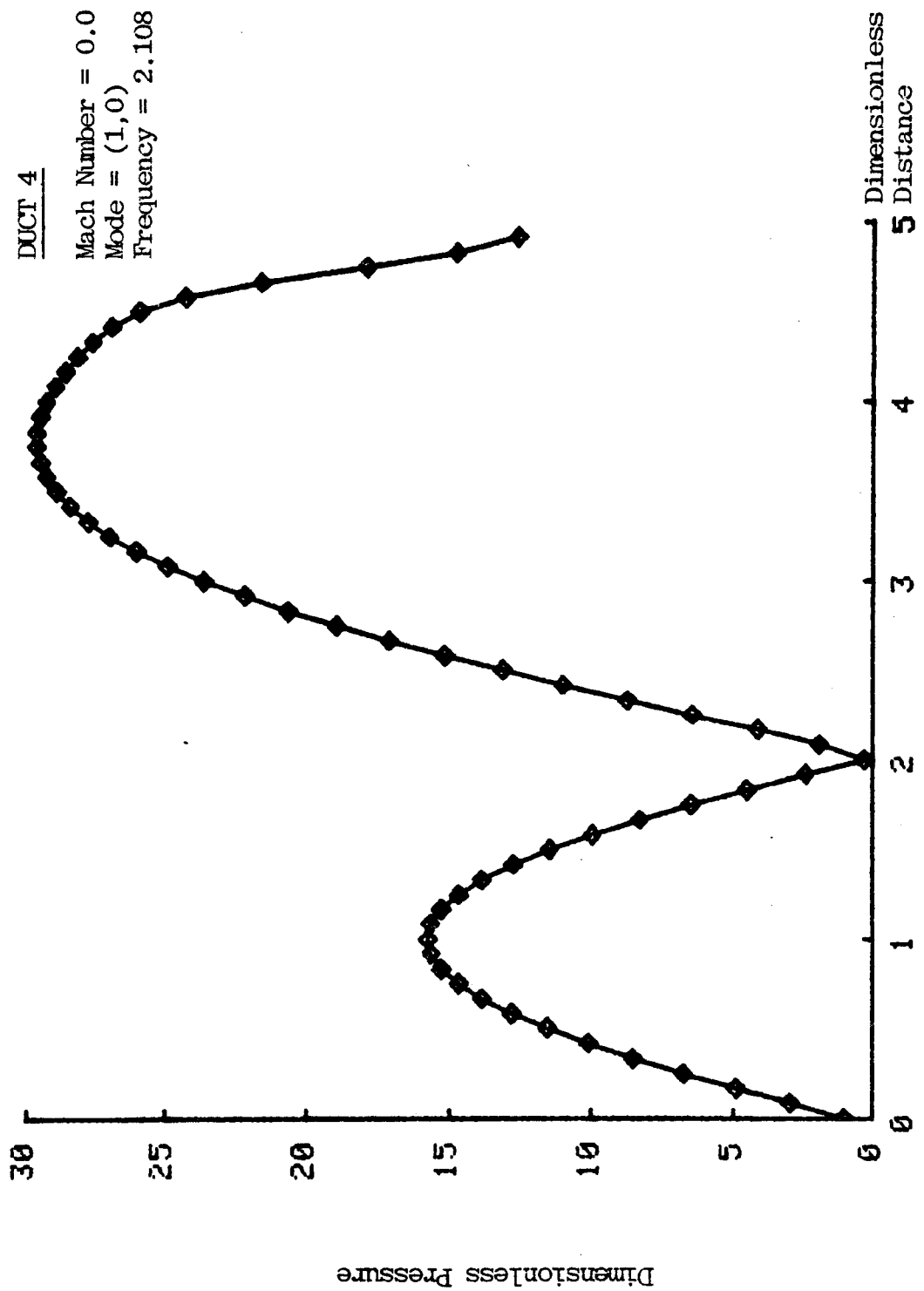


Figure VII.13 Pressure Distribution Along Duct Wall
(Duct 4, Mach Num=0.0, Mode=(1,0), Freq=2.108)

The distorted shape of the wave inside ducts 3 and 4 indicate that the exciting frequency is near the cutoff frequency of these ducts and hence, a wave decay results and can be clearly seen in the far-field experimental results, Figure VII.14. Figure VII.11, on the other hand, shows an undistorted wave inside duct 2 which started to propagate as seen in Figure VII.14.

Increasing the exciting frequency to 1000 Hz caused all the waves to propagate as shown in Figures VII.15, VII.16 and VII.17 with relatively equal maximum pressure values; consequently, no remarkable difference in the far-field attenuation is expected. Figure VII.18 shows experimental far-field attenuation for the (1,0) mode with no appreciable differences.

For higher frequencies, Figures VII.19, VII.20 and VII.21 give the normalized pressure wave for 4.2 dimensionless frequency. Pressure levels are higher for duct number 3, compared to the levels of ducts 2 and 4 with the possibility of greater far-field attenuation for duct 3. Figure VII.22 shows the far-field attenuation for 1600 Hz exciting frequency with no distinct trend.

Figures VII.23, VII.24 and VII.25 give the variation of the real part of the acoustic velocity potential for 4.2 dimensionless frequency. No wave distortion and/or wave length changes are predicted.

For much higher frequencies, a phase shift is

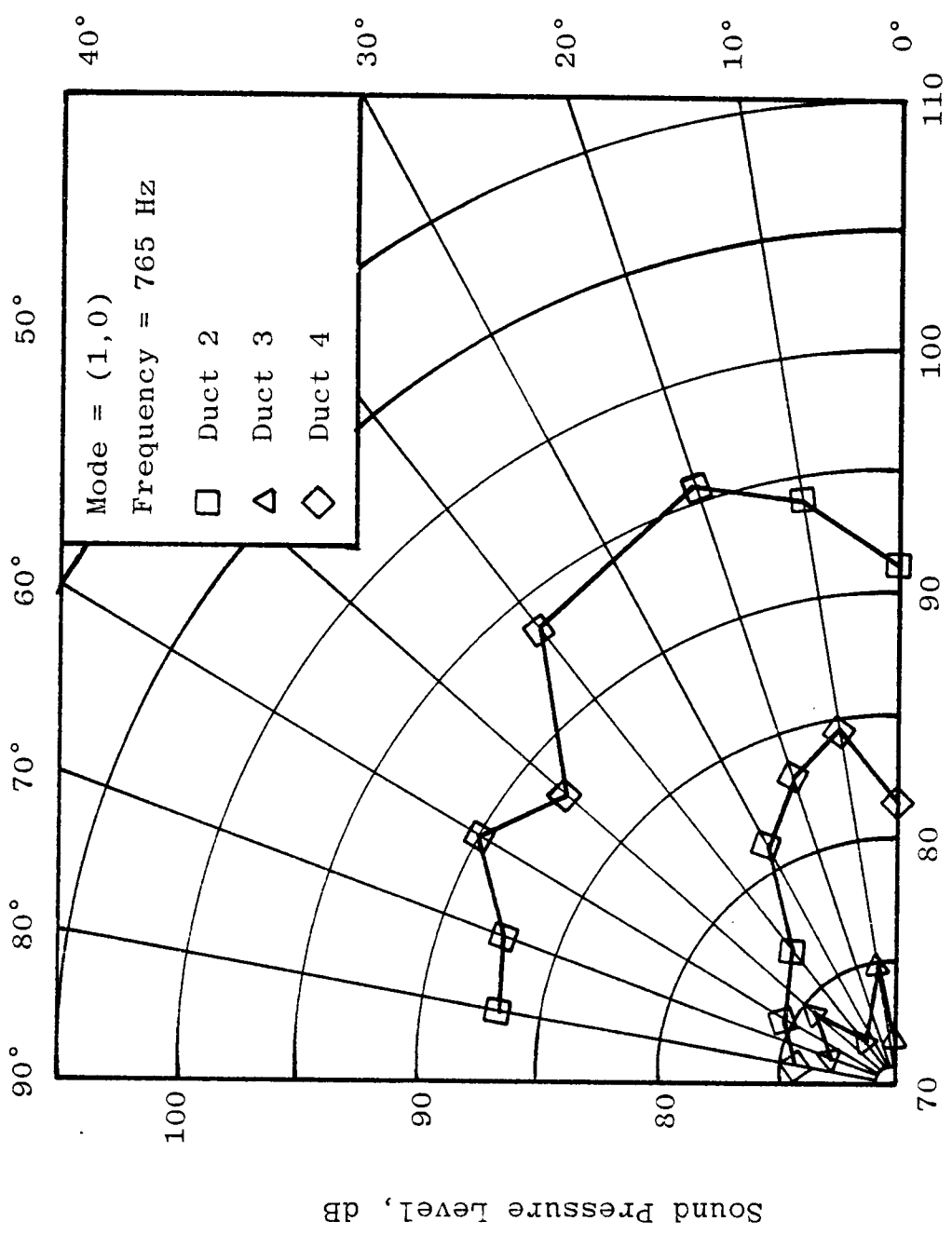


Figure VII.14 Far-Field Sound Pressure Level Under Static Conditions (Mode=(1,0),Freq=765 Hz)

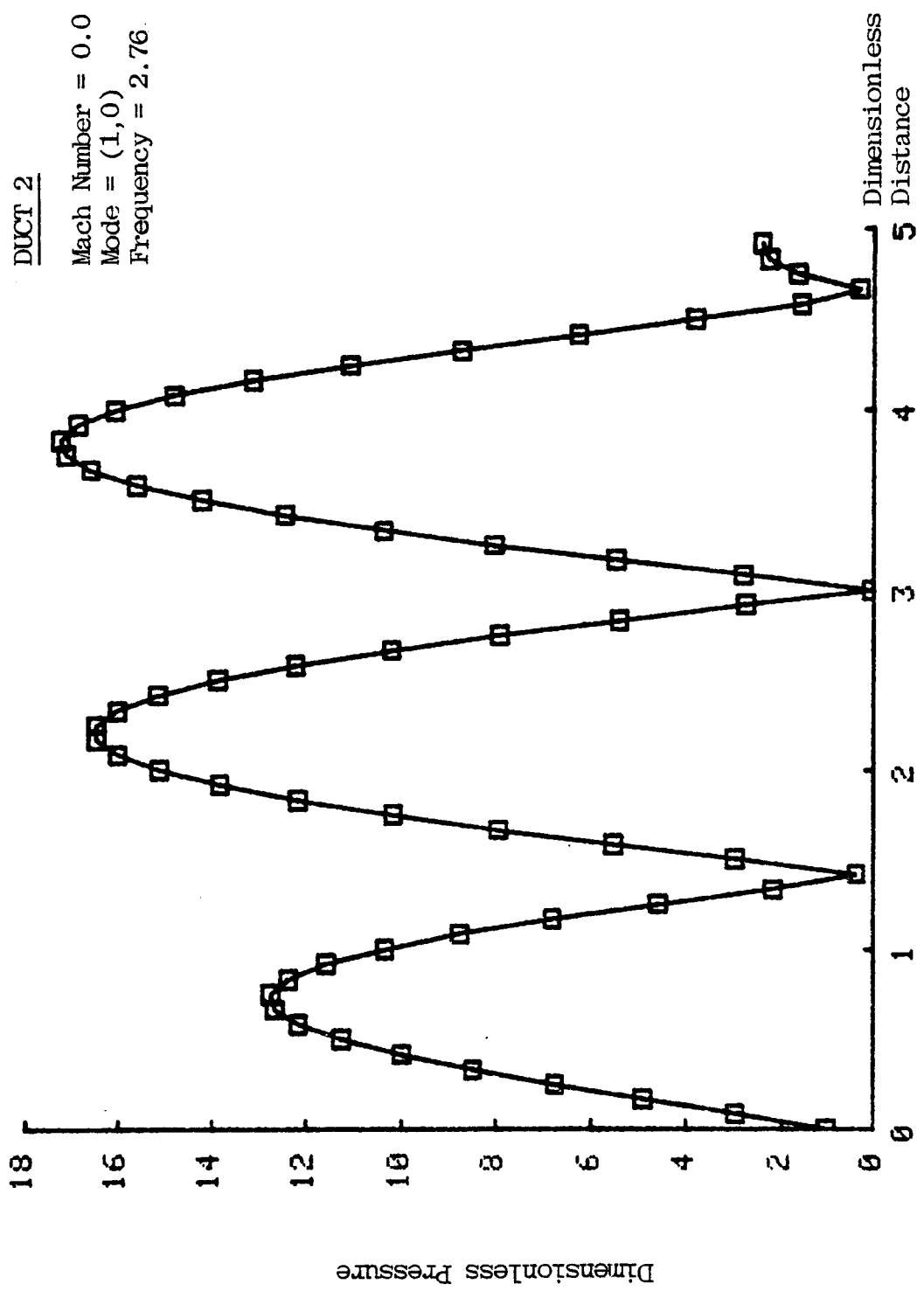


Figure VII.15 Pressure Distribution Along Duct Wall
(Duct 2,Mach Num=0.0,Mode=(1,0),Freq=2.76)

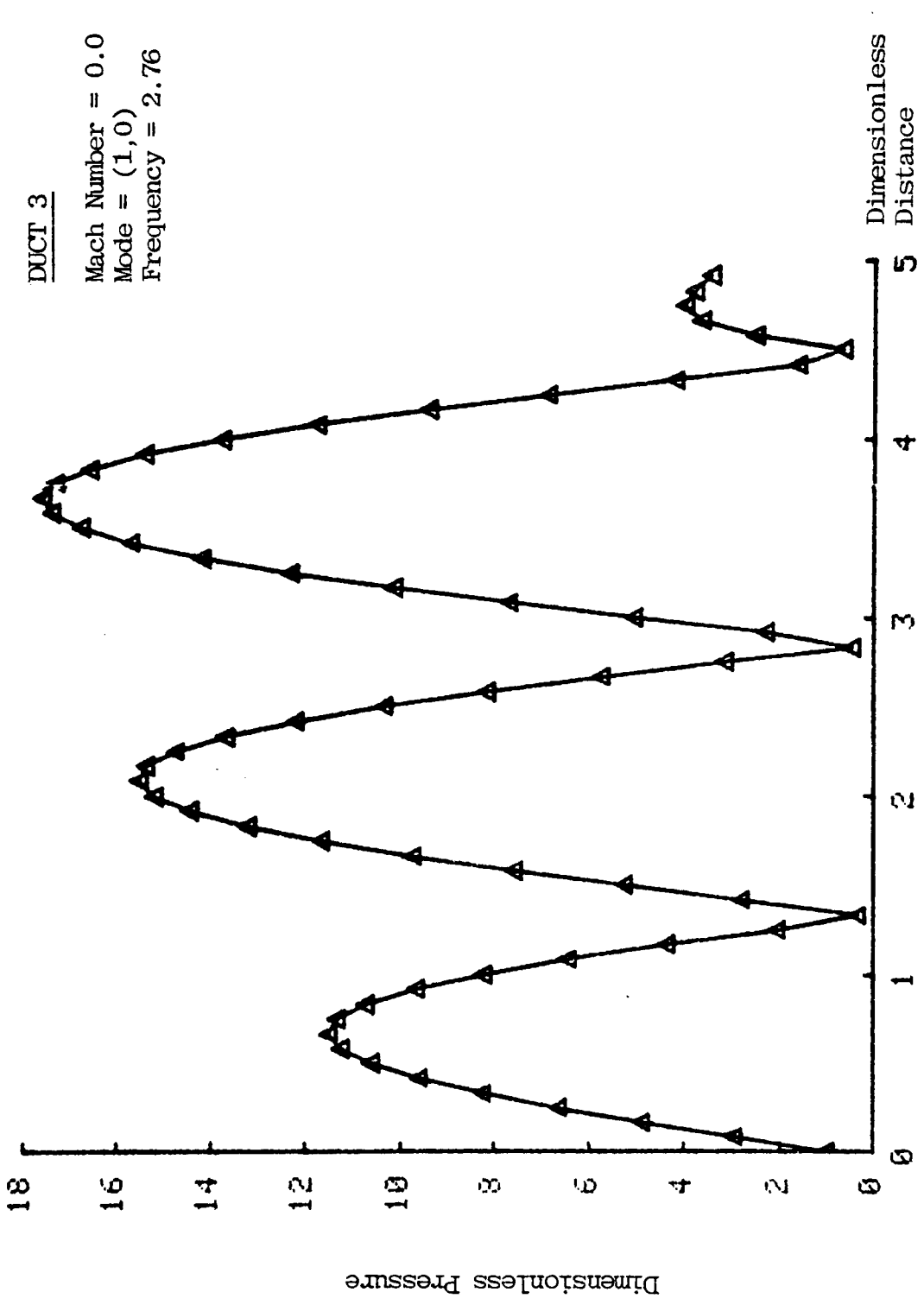


Figure VII.16 Pressure Distribution Along Duct Wall
(Duct 3, Mach Num=0.0, Mode=(1,0), Freq=2.76)

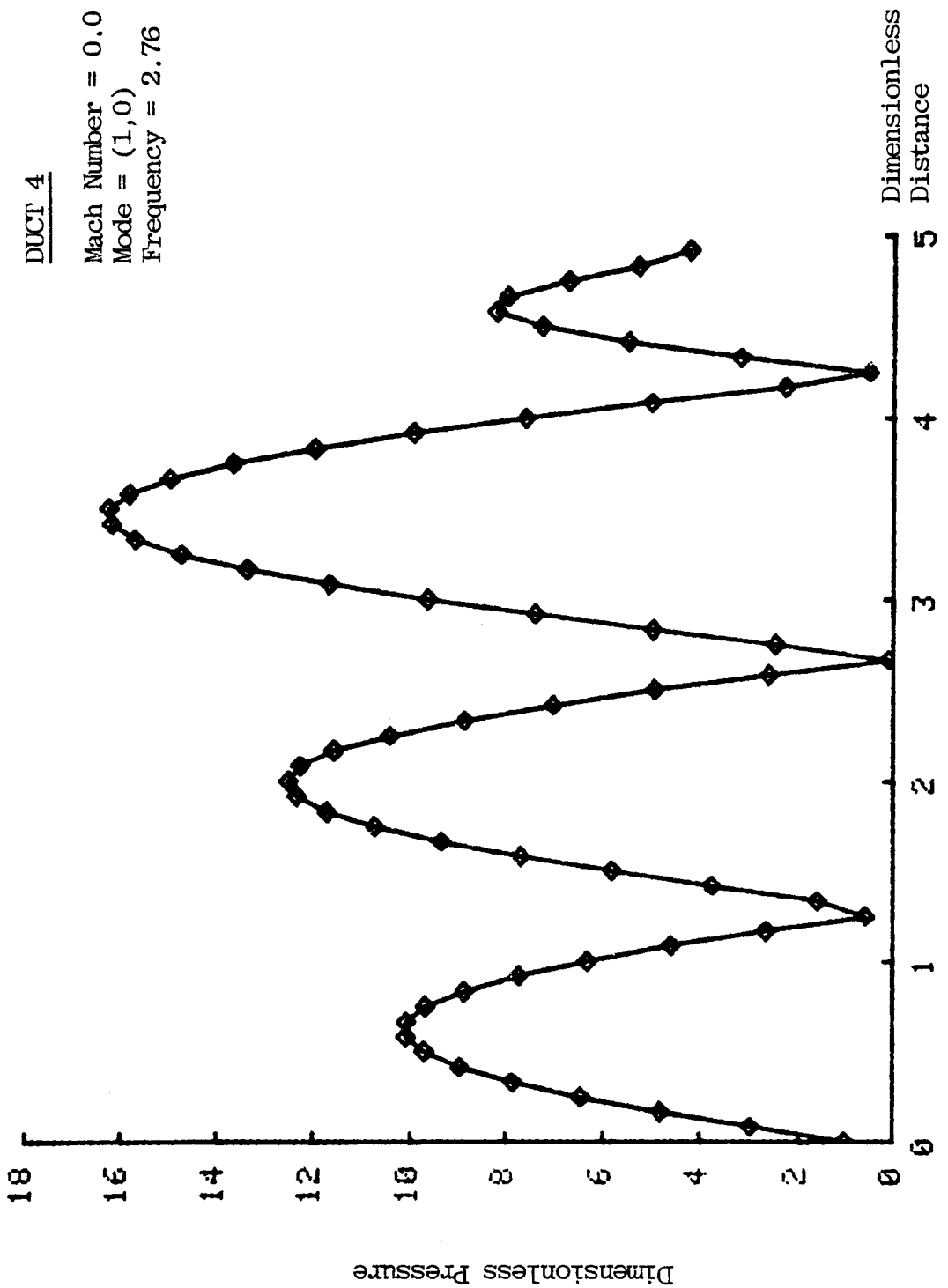


Figure VII.17 Pressure Distribution Along Duct Wall
(Duct 4,Mach Num=0.0,Mode=(1,0),Freq=2.76)

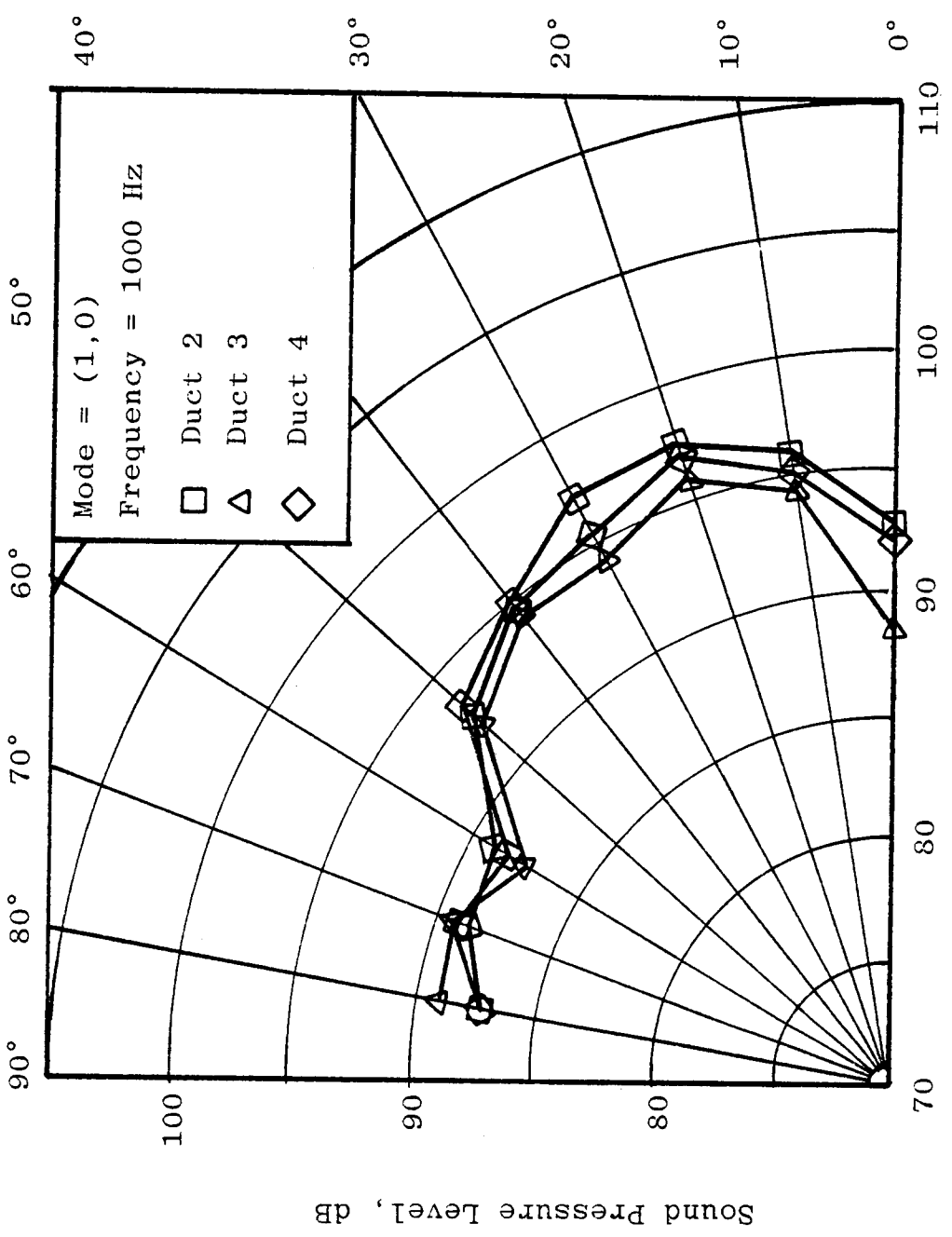


Figure VII.18 Far-Field Sound Pressure Level Under Static Conditions (Mode=(1,0),Freq=1000 Hz)

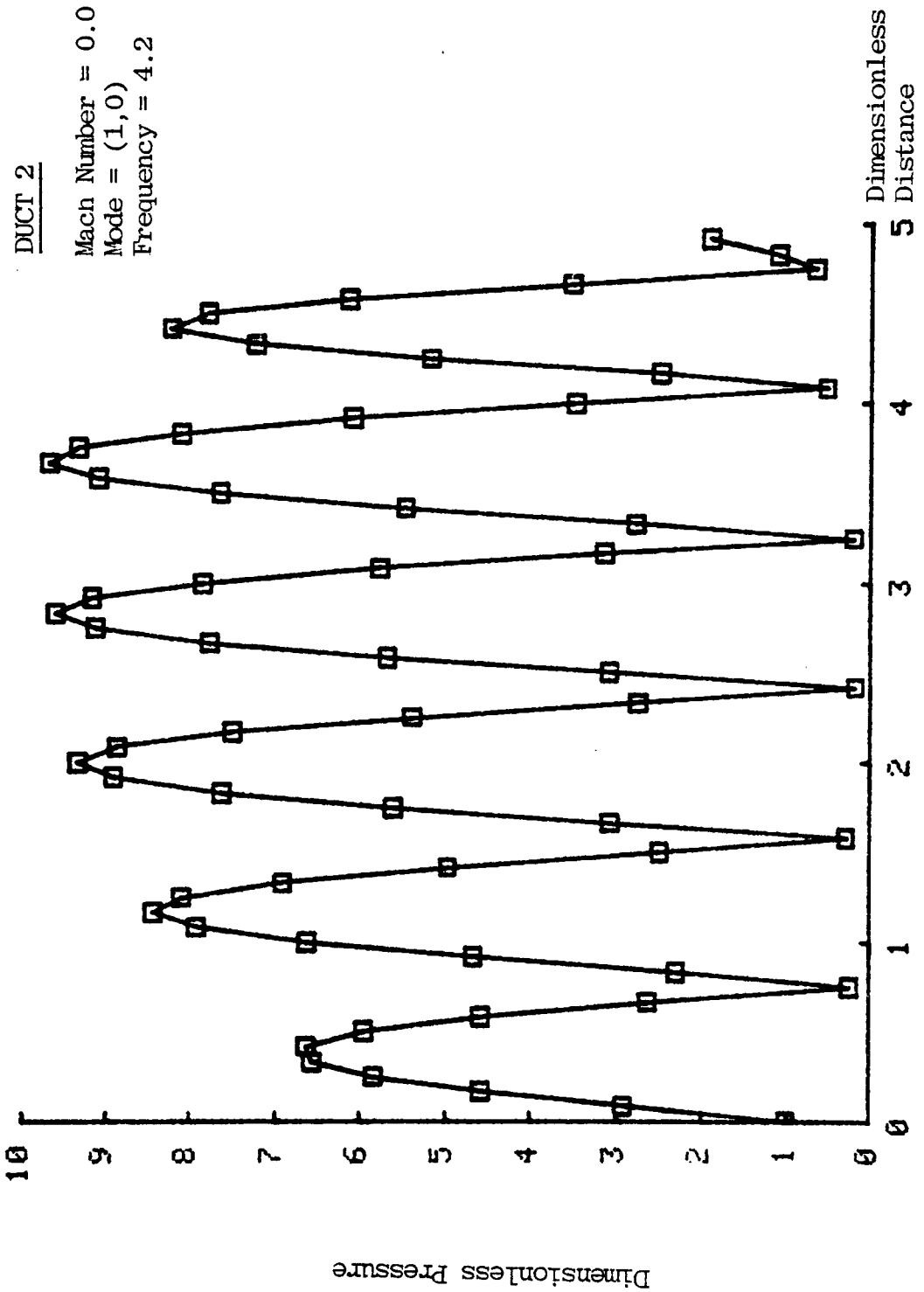


Figure VII.19 Pressure Distribution Along Duct Wall
(Duct 2,Mach Num=0.0,Mode=(1,0),Freq=4.2)

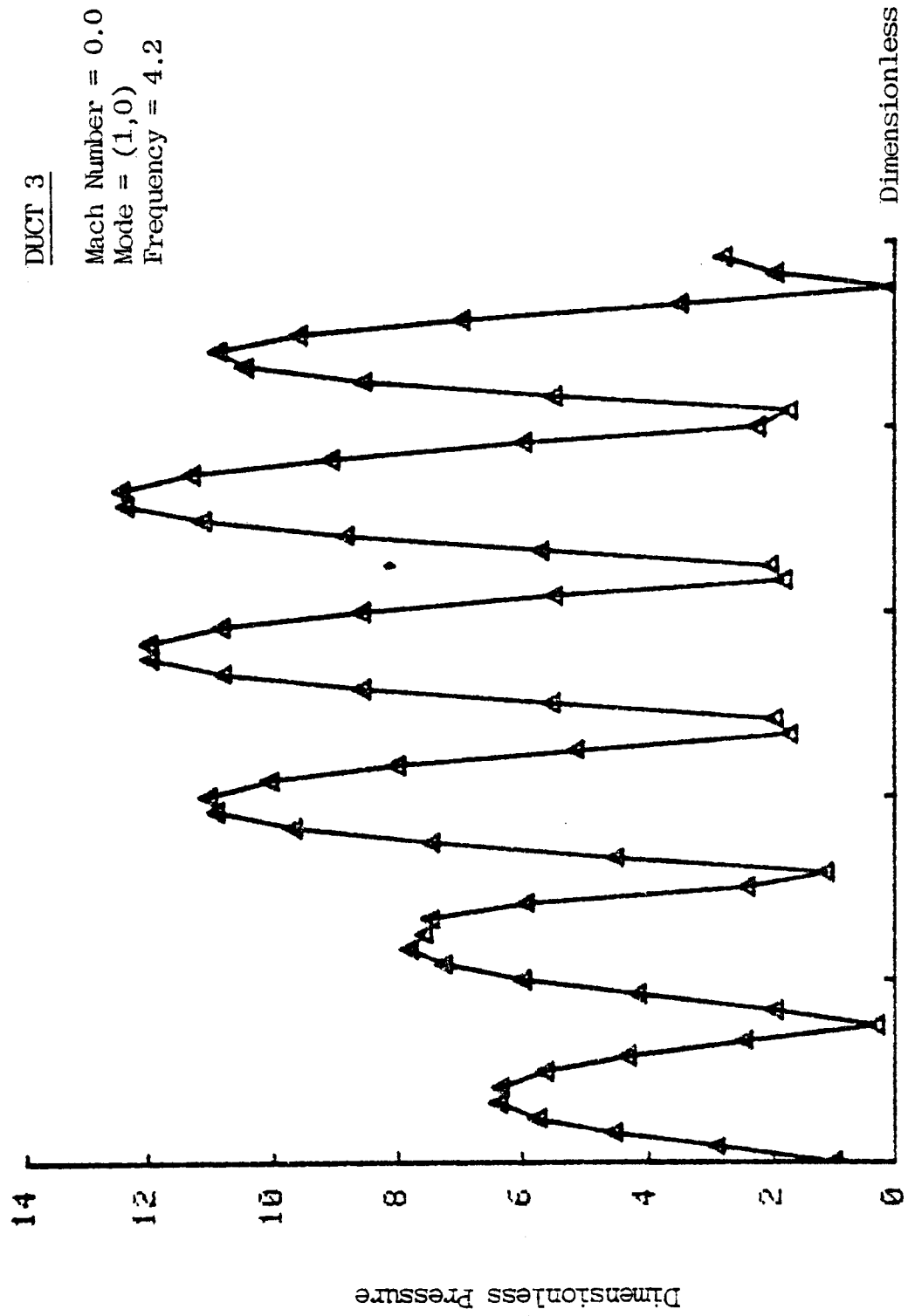


Figure VII.20 Pressure Distribution Along Duct Wall
(Duct 3, Mach Num=0.0, Mode=(1,0), Freq=4.2)

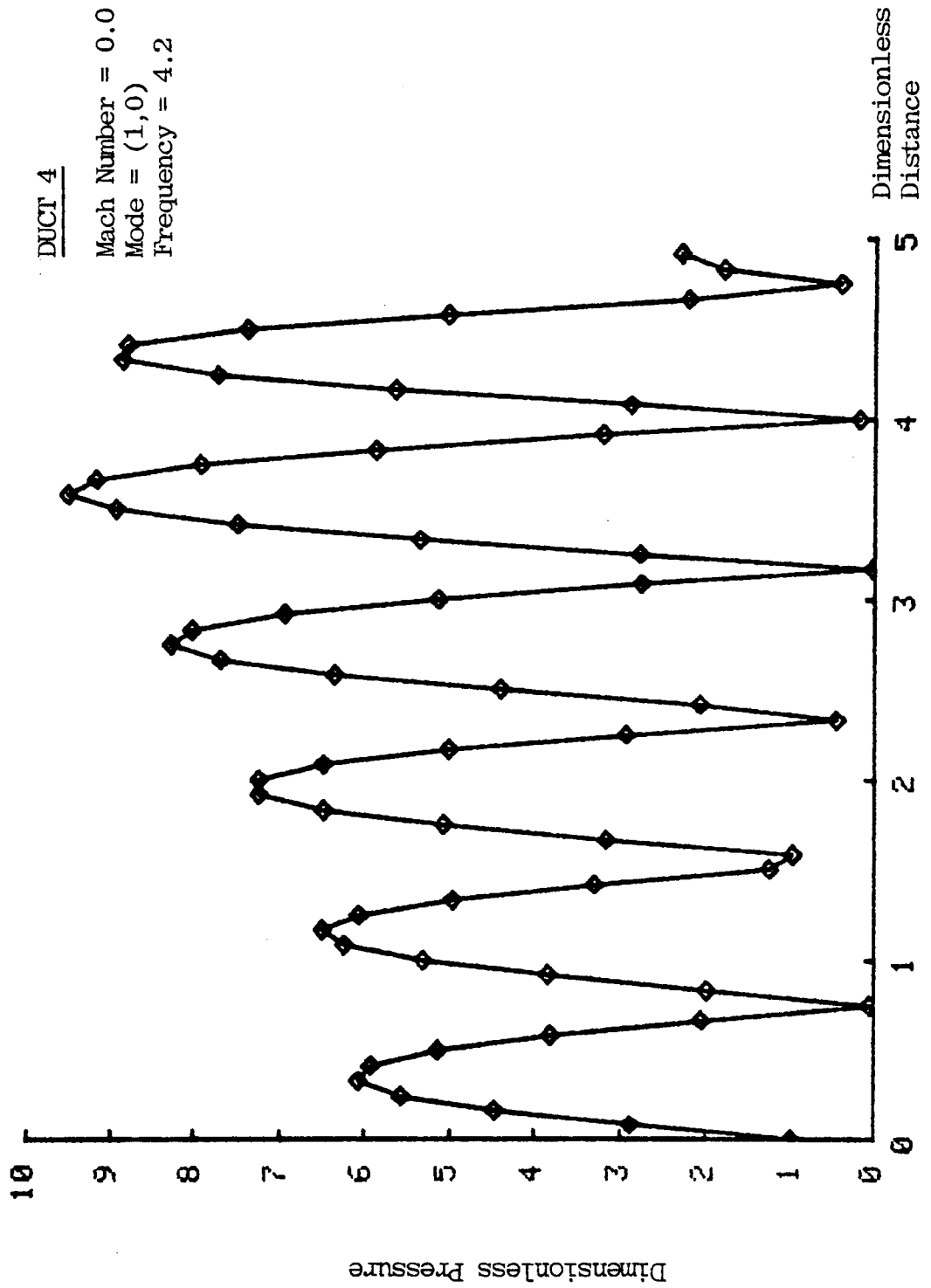


Figure VII.21 Pressure Distribution Along Duct Wall
(Duct 4,Mach Num=0.0,Mode=(1,0),Freq=4.2)

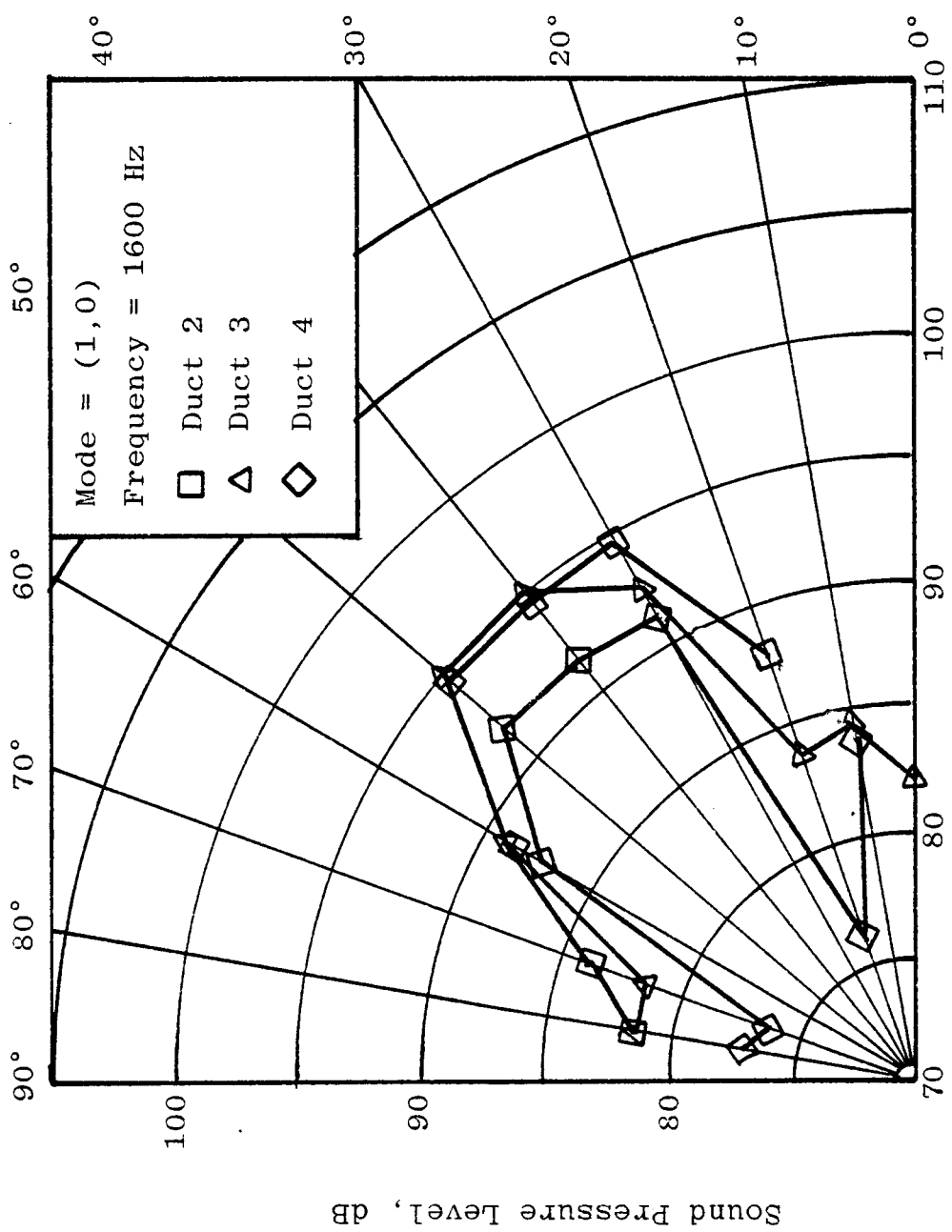


Figure VII.22 Far-Field Sound Pressure Level Under Static Conditions (Mode=(1,0),Freq=1600 Hz)

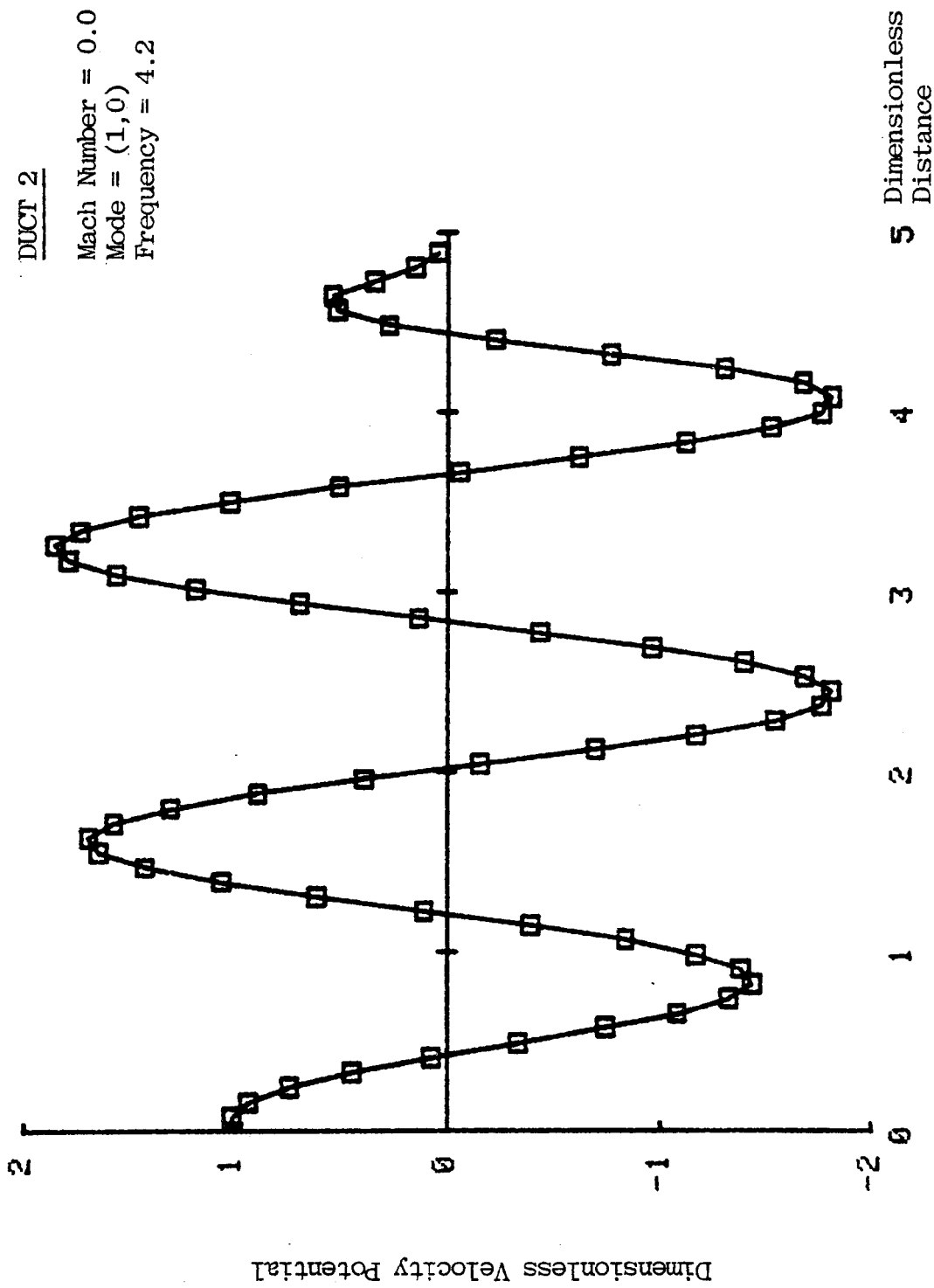


Figure VII.23 Acoustic Velocity Potential (Real Part) Along Duct Wall
(Duct 2,Mach Num=0.0,Mode=(1,0),Freq=4.2)

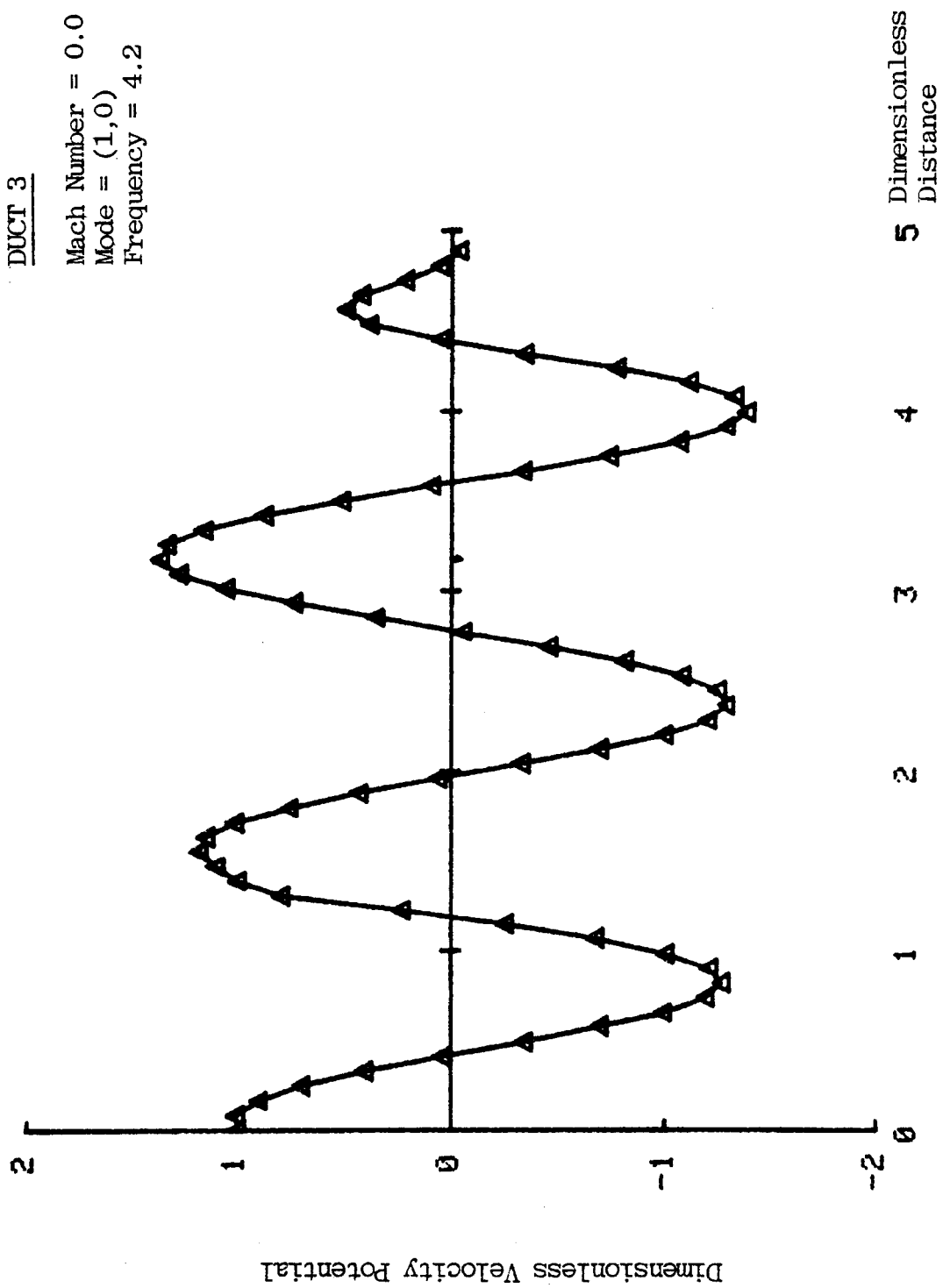


Figure VII.24 Acoustic Velocity Potential (Real Part) Along Duct Wall
(Duct 3, Mach Num=0.0, Mode=(1,0), Freq=4.2)

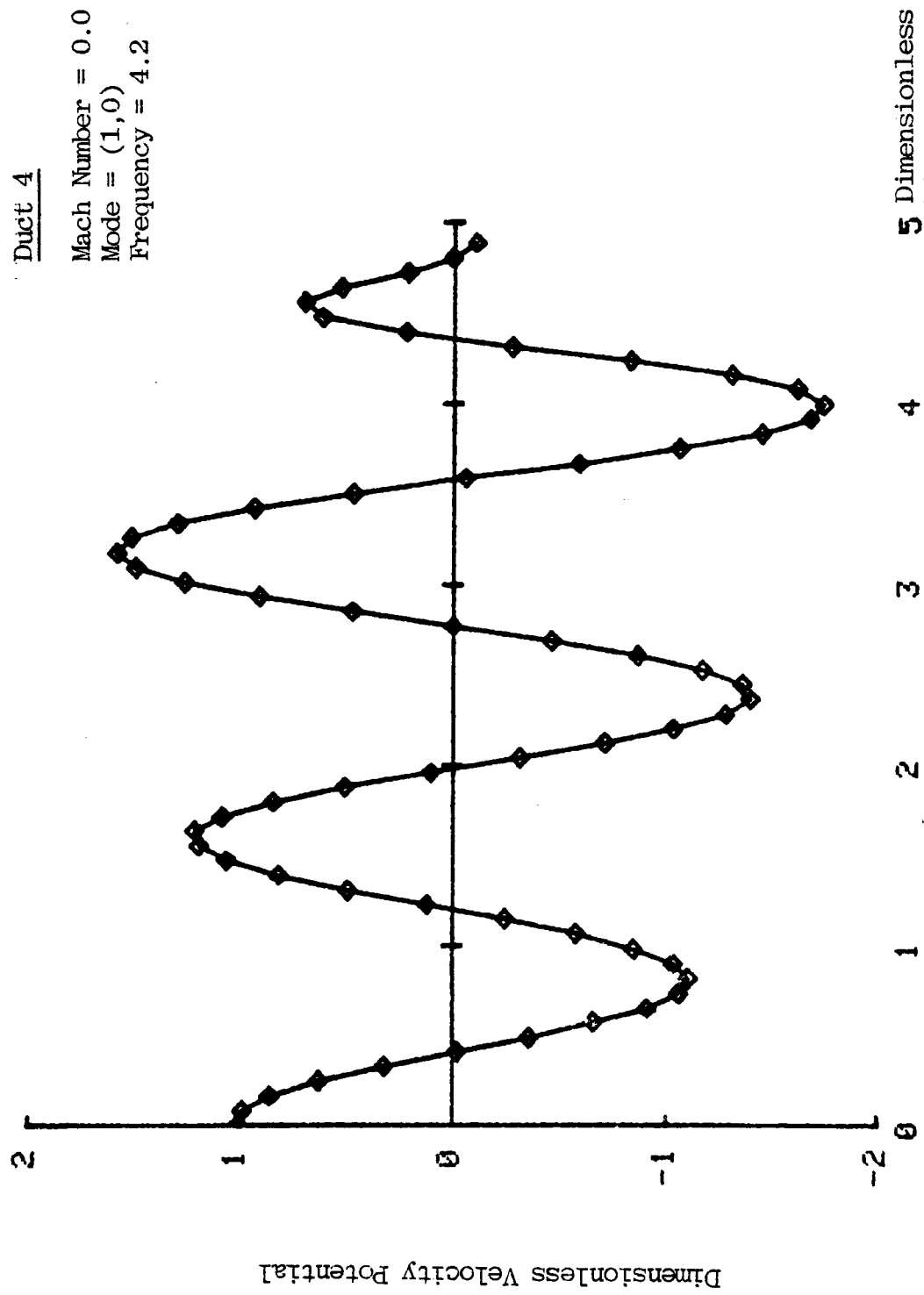


Figure VII.25 Acoustic Velocity Potential (Real Part) Along Duct Wall
(Duct 4, Mach Num=0.0, Mode=(1,0), Freq=4.2)

predicted for duct 2 as can be seen in Figures VII.26, VII.27 and VII.28 for 5.36 dimensionless frequency. The phase shift of inlet 2 is not accompanied by any changes in the effective wave length as shown in Figures VII.29, VII.30 and VII.31, which give the variation of the real part of the acoustic velocity potential along the duct wall.

For the (2,0) mode, a dimensionless frequency of 3.375 which is equivalent to 1223 Hz caused a decaying wave for inlets 2 and 4 as seen in Figures VII.32, VII.33 and VII.34. Experimental results of Figure VII.35 show that in duct 3, the wave started to propagate, (i.e. for this configuration, the applied frequency is higher than the cutoff frequency which is different than that of a constant area duct).

Doubling the frequency has caused the acoustic waves to propagate as shown in Figures VII.36, VII.37 and VII.38 with the higher pressure amplitudes in duct 3 causing more far-field attenuation depicted in the experimental results in Figure VII.39. For the (2,0) mode, duct 2 shows a phase shift compared to ducts 3 and 4 as shown in Figures VII.40, VII.41 and VII.42. There is no change in the effective wave length, however.

As the frequency increases to 8.58 dimensionless frequency, pressure values peak near the throat for duct 4 and closer to the sound source for ducts 2 and 3 with

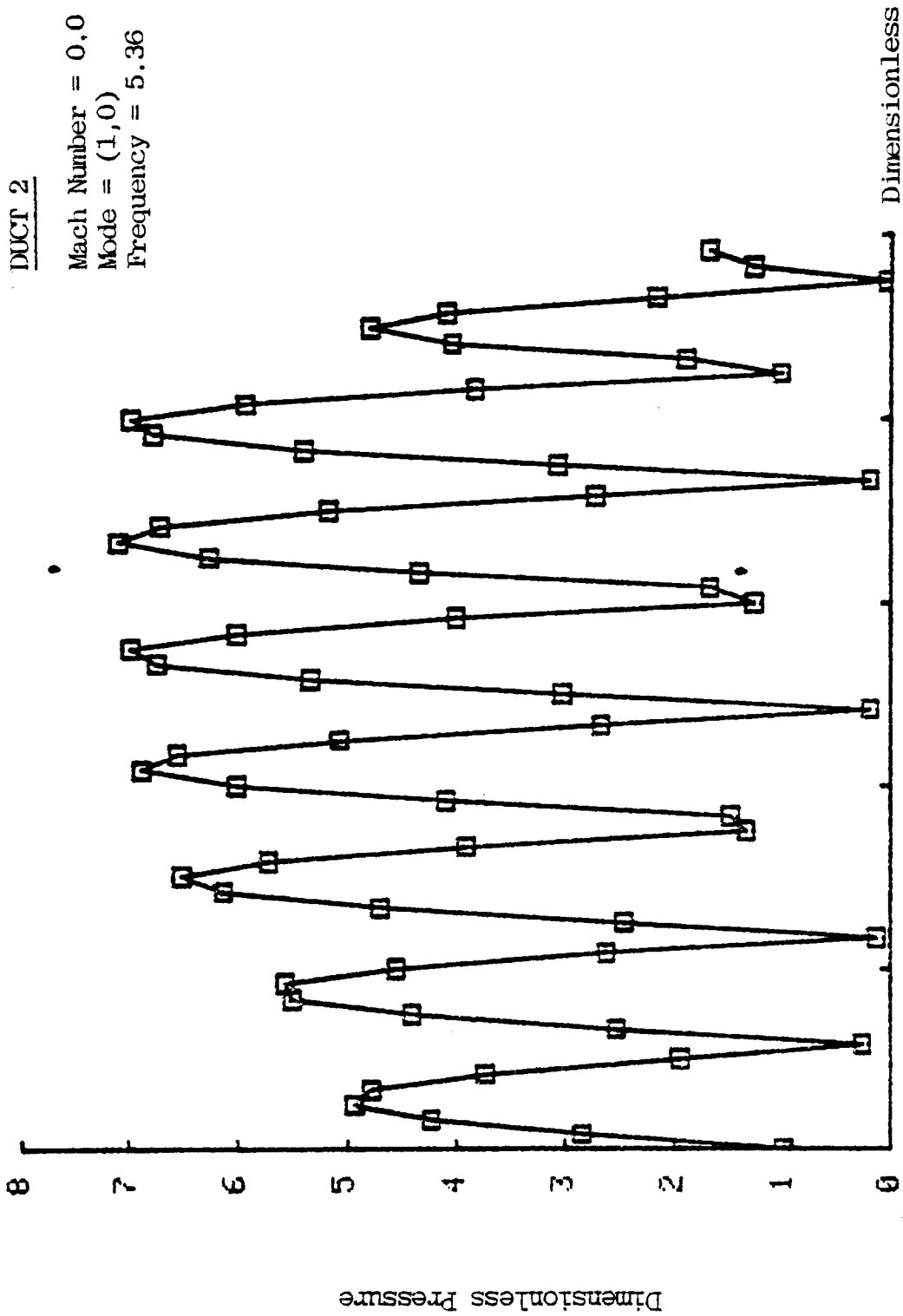


Figure VII.26 Pressure Distribution Along Duct Wall
(Duct 2, Mach Num=0.0, Mode=(1,0), Freq=5.36)

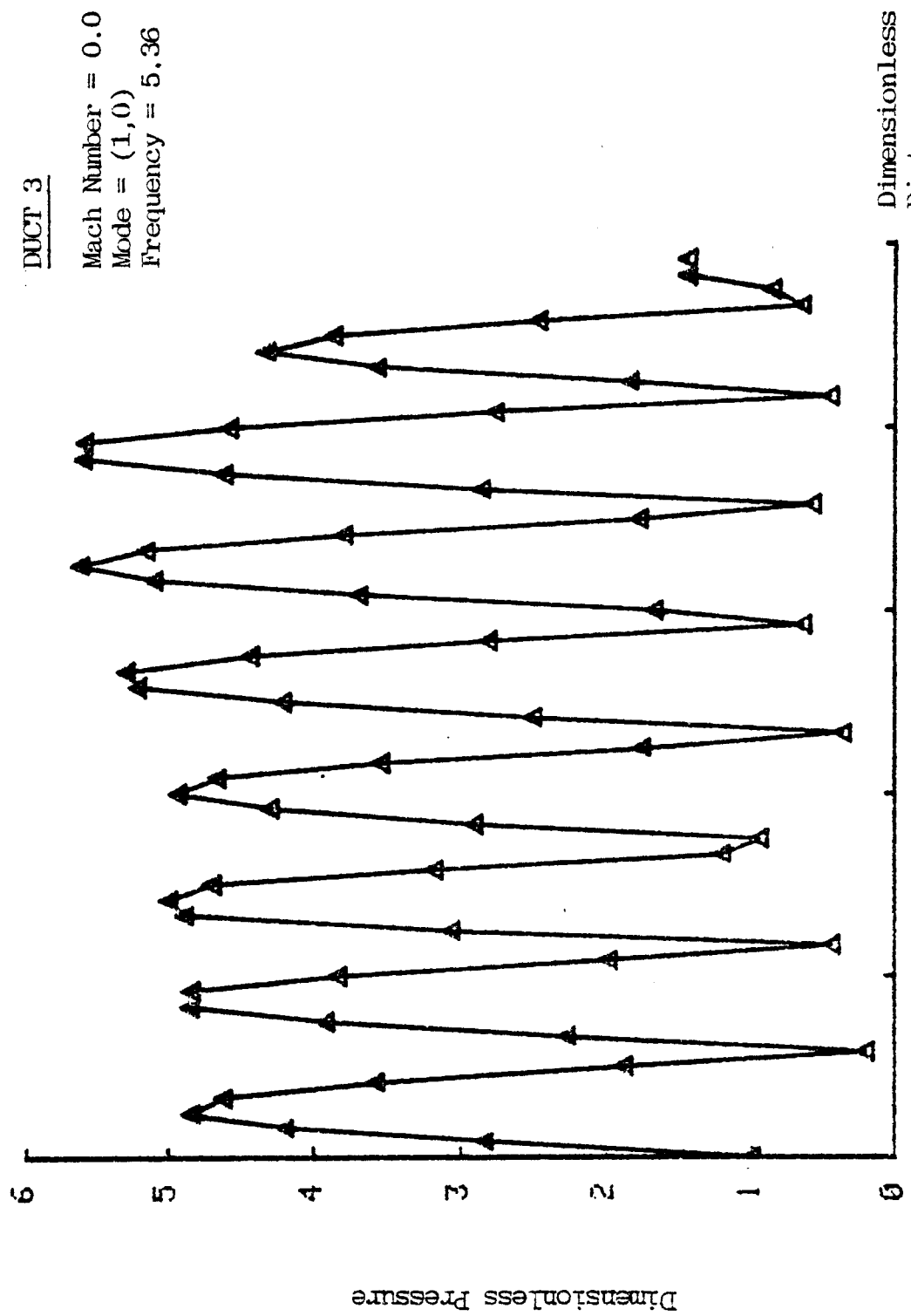


Figure VII.27 Pressure Distribution Along Duct Wall
(Duct 3, Mach Num=0.0, Mode=(1,0), Freq=5.36)

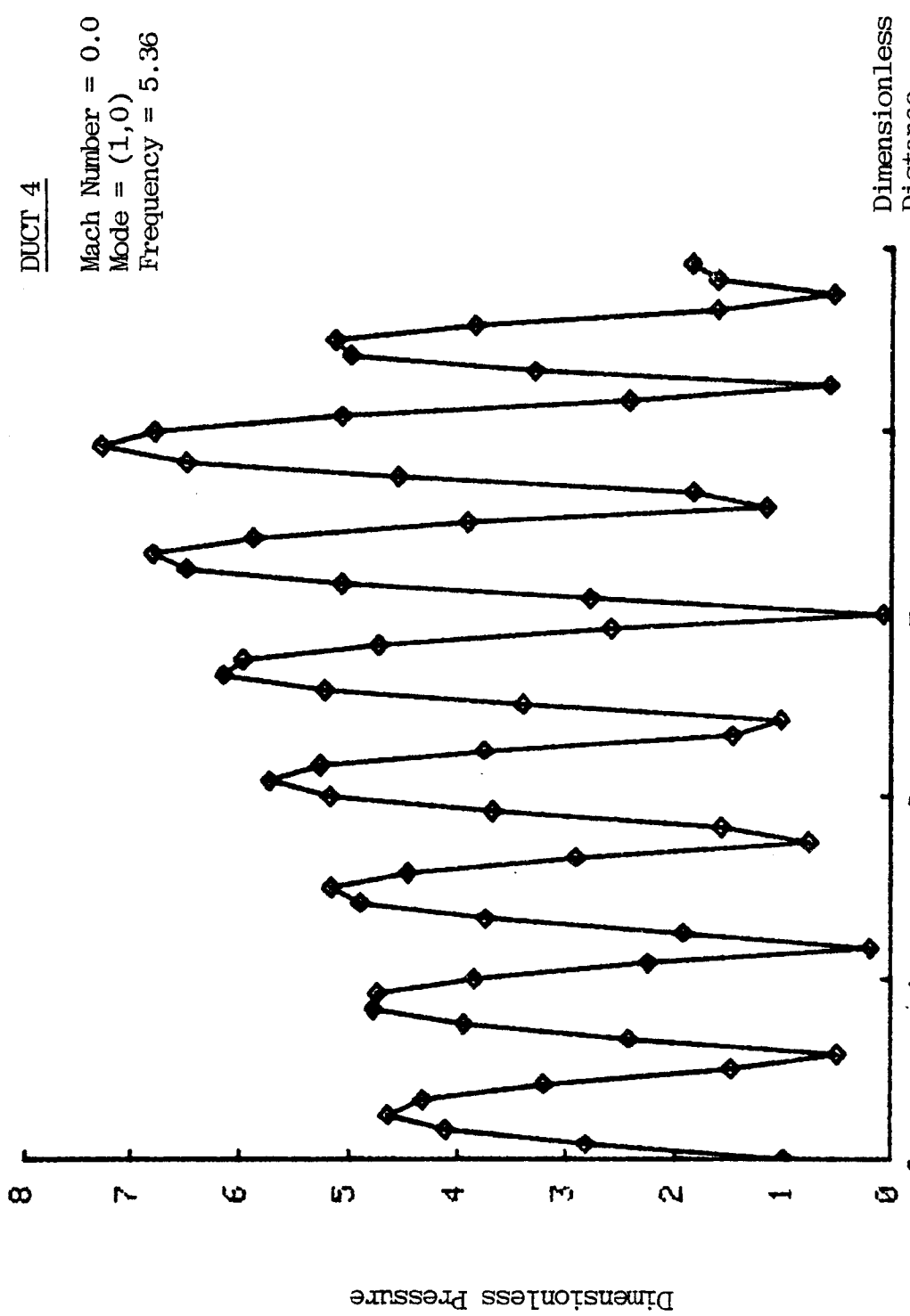


Figure VII.28 Pressure Distribution Along Duct Wall
(Duct 4, Mach Num=0.0, Mode=(1,0), Freq=5.36)

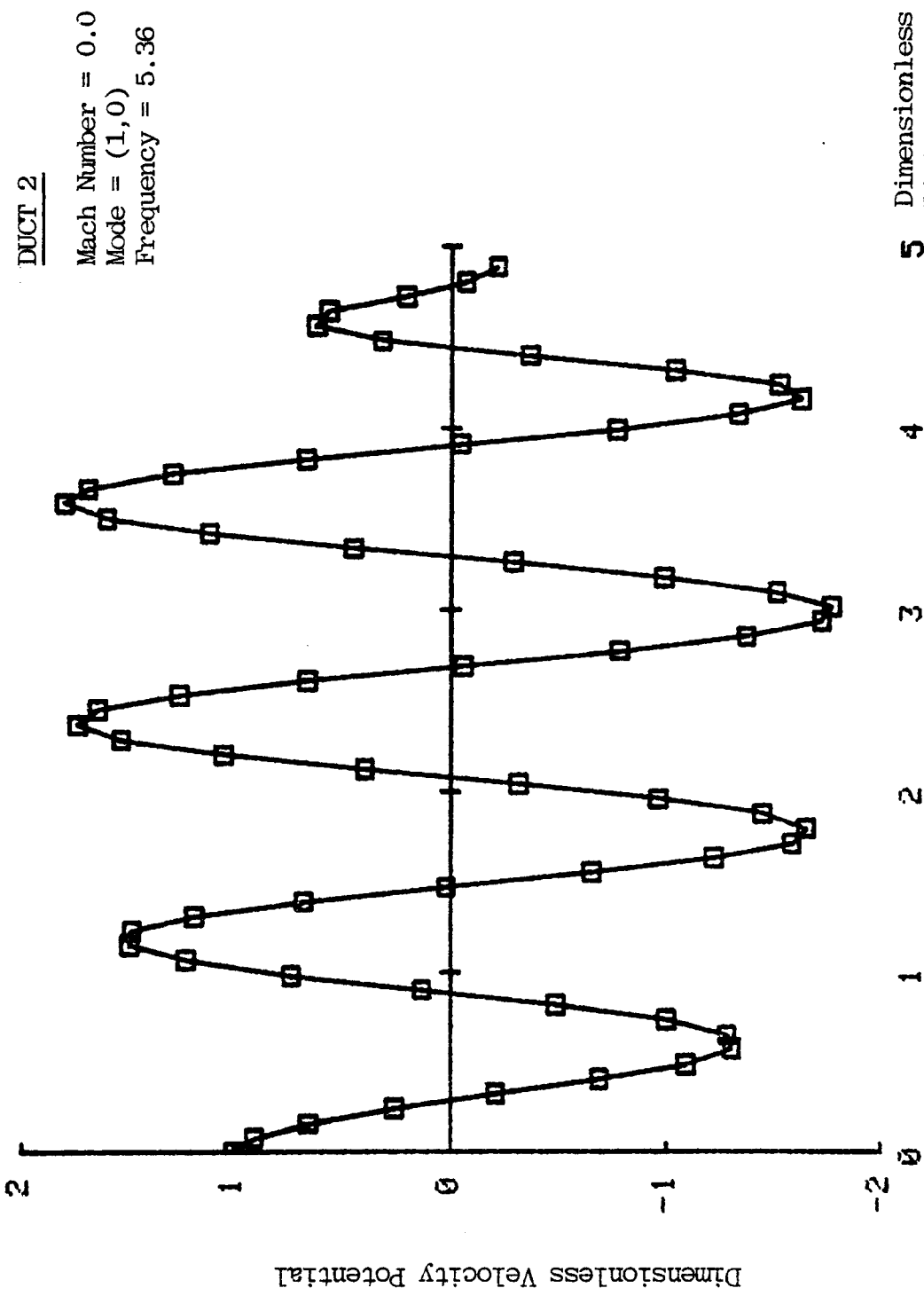


Figure VII.29 Acoustic Velocity Potential (Real Part) Along Duct Wall
(Duct 2,Mach Num=0.0,Mode=(1,0),Freq=5.36)

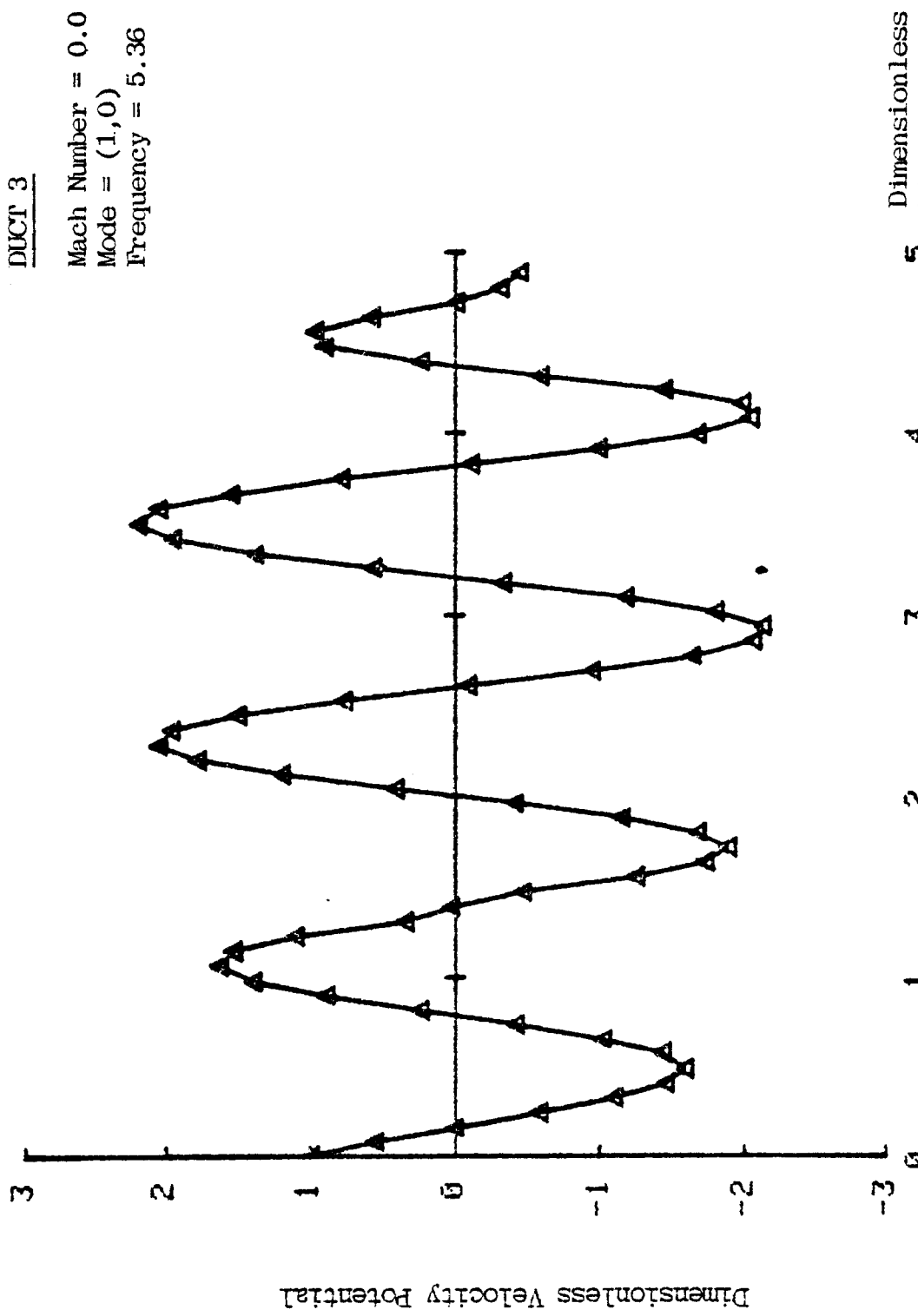


Figure VII.30 Acoustic Velocity Potential (Real Part) Along Duct Wall
(Duct 3, Mach Num=0.0, Mode=(1.0), Freq=5.36)

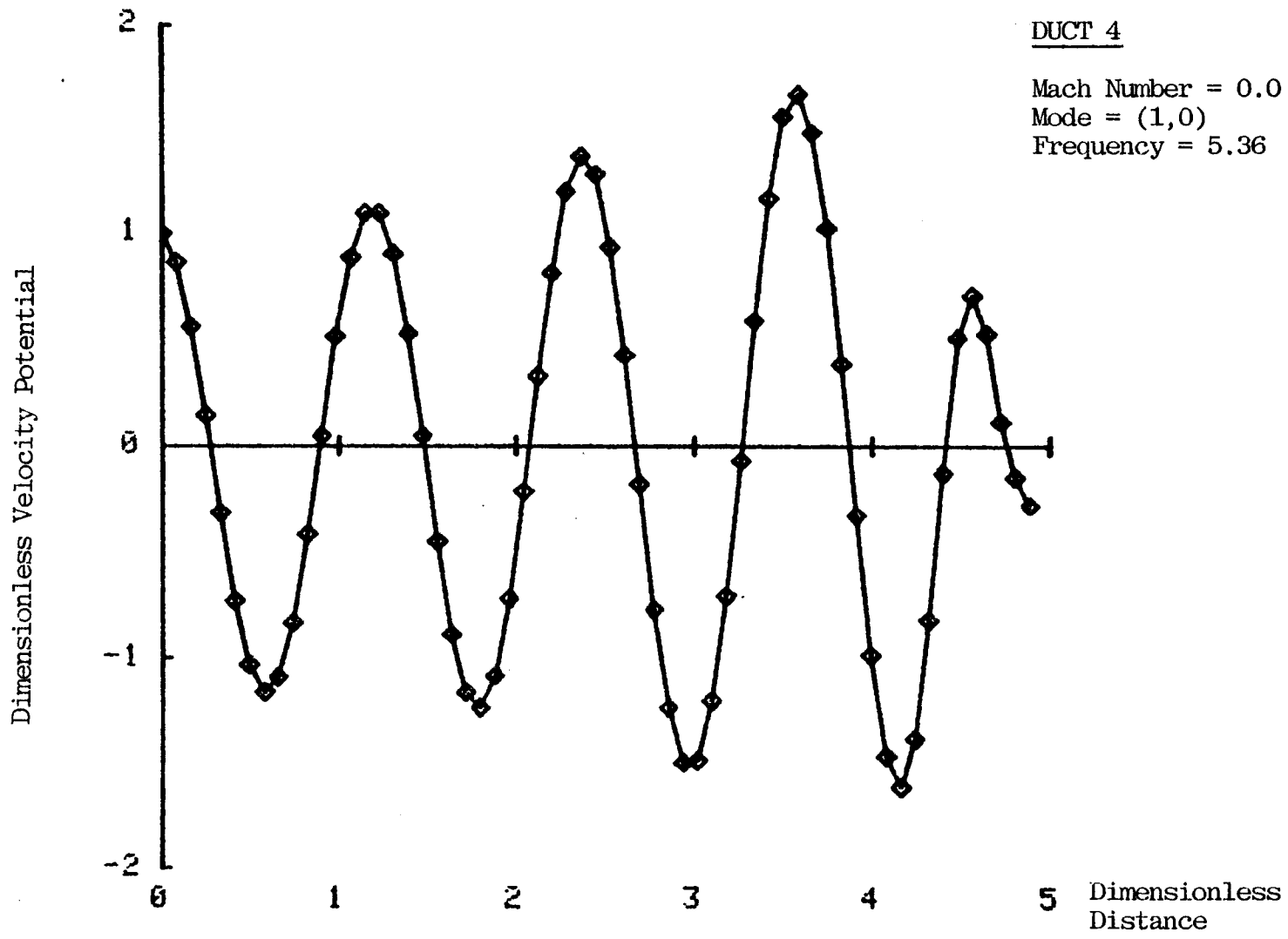


Figure VII.31 Acoustic Velocity Potential (Real Part) Along Duct Wall (Duct 4,Mach Num=0.0,Mode=(1,0),Freq=5.36)

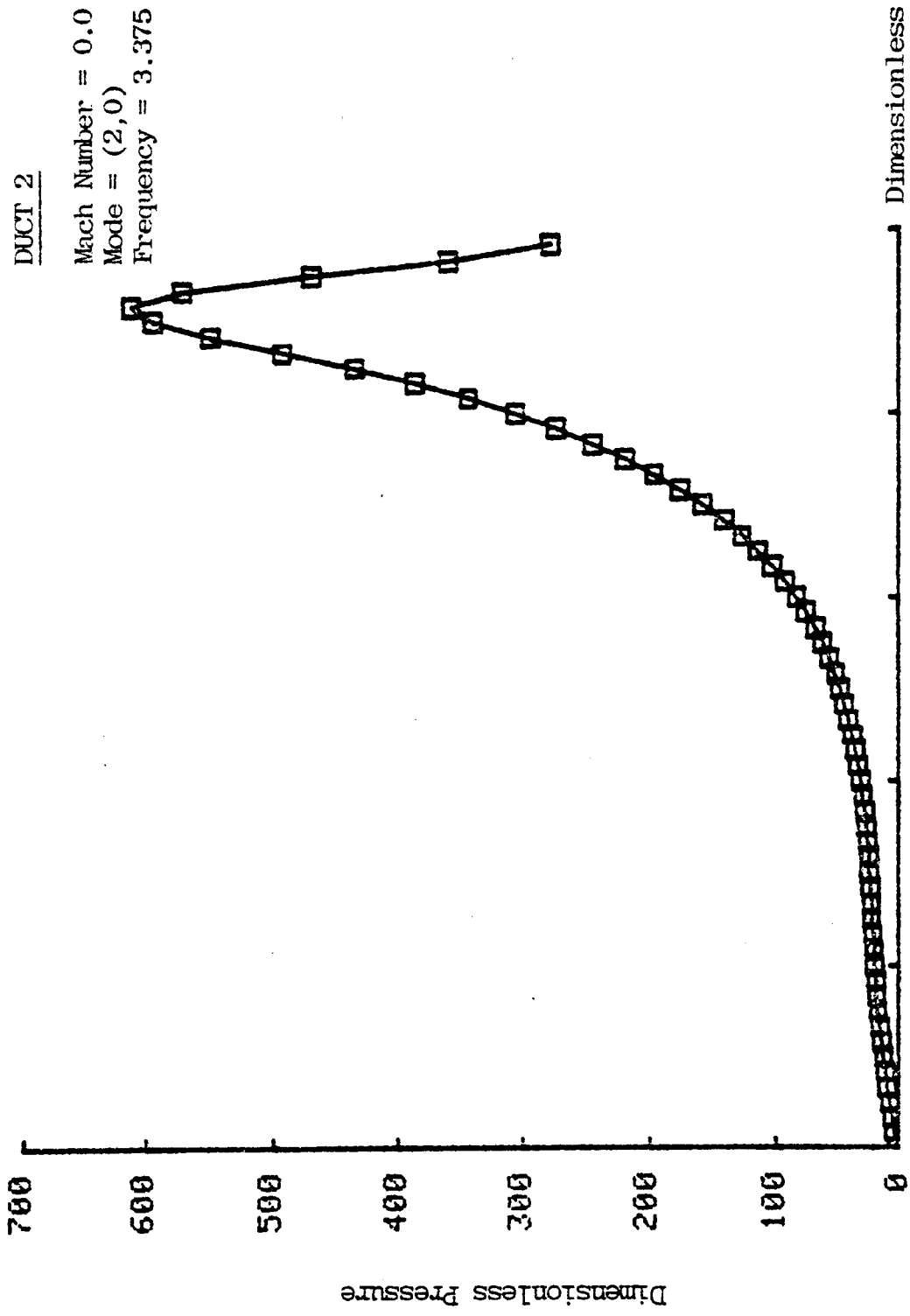


Figure VII.32 Pressure Distribution Along Duct Wall
(Duct 2, Mach Num=0.0, Mode=(2,0), Freq=3.375)

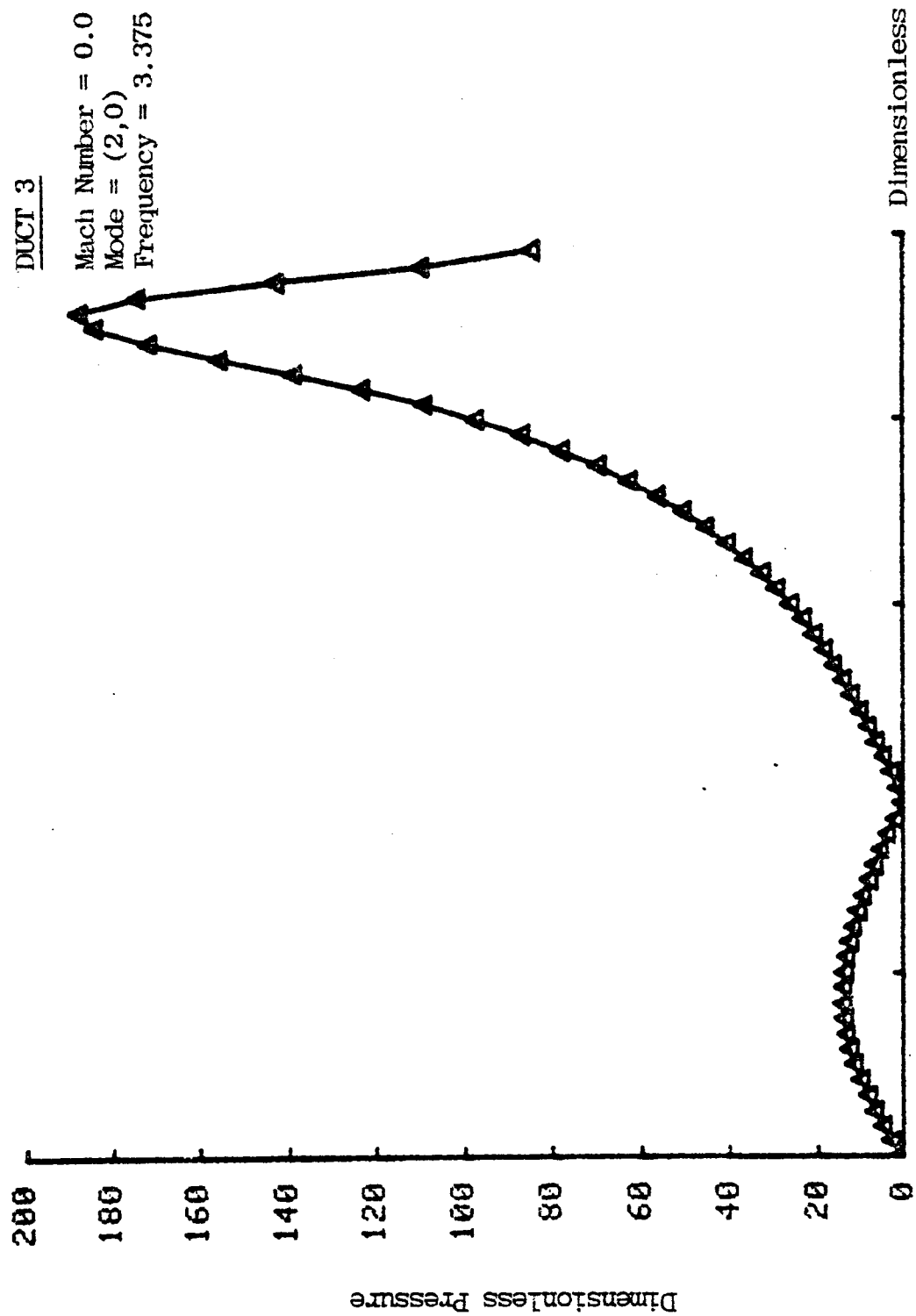


Figure VII.33 Pressure Distribution Along Duct Wall
(Duct 3, Mach Num=0.0, Mode=(2,0), Freq=3.375)

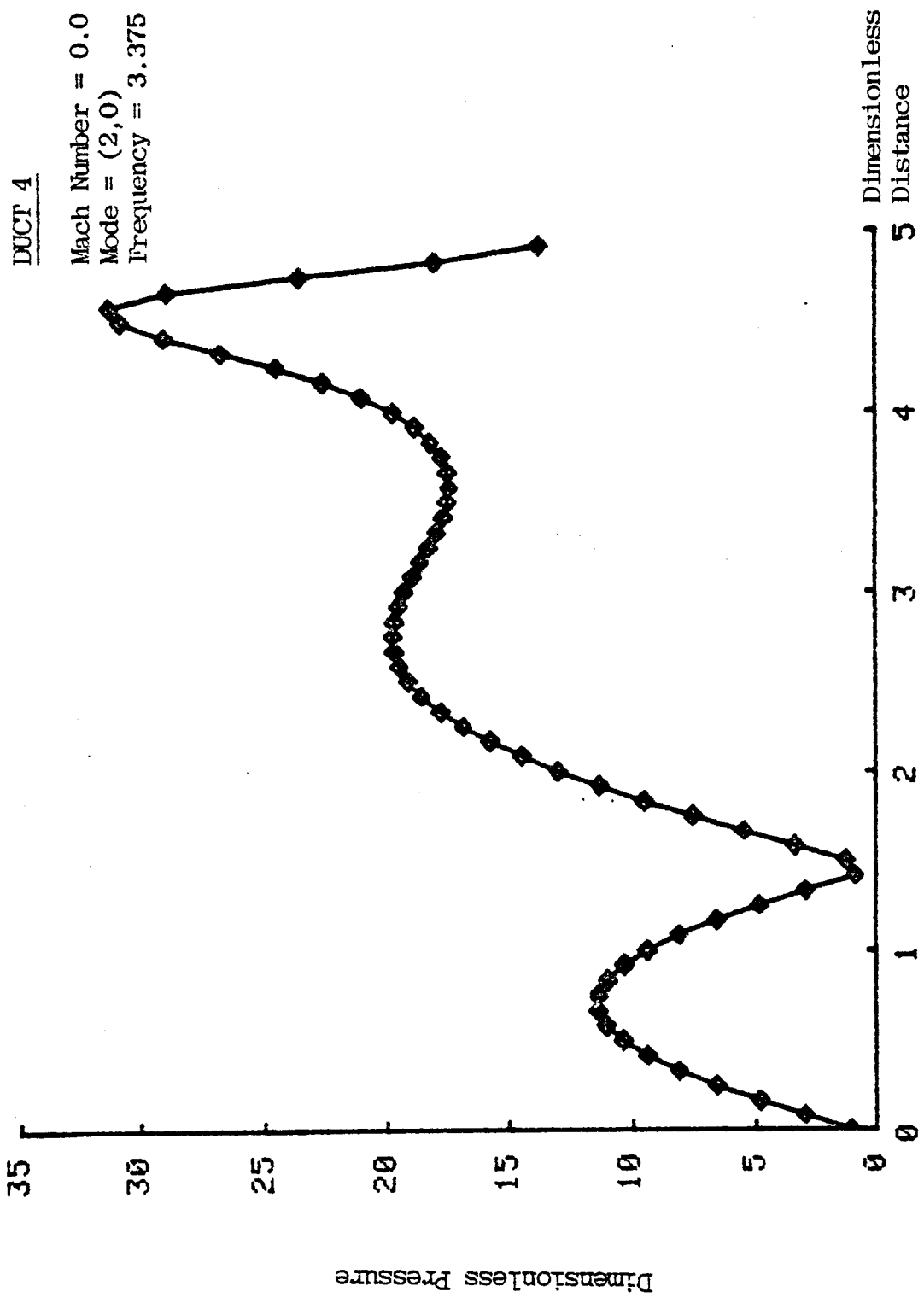


Figure VII.34 Pressure Distribution Along Duct Wall
(Duct 4, Mach Num=0.0, Mode=(2,0), Freq=3.375)

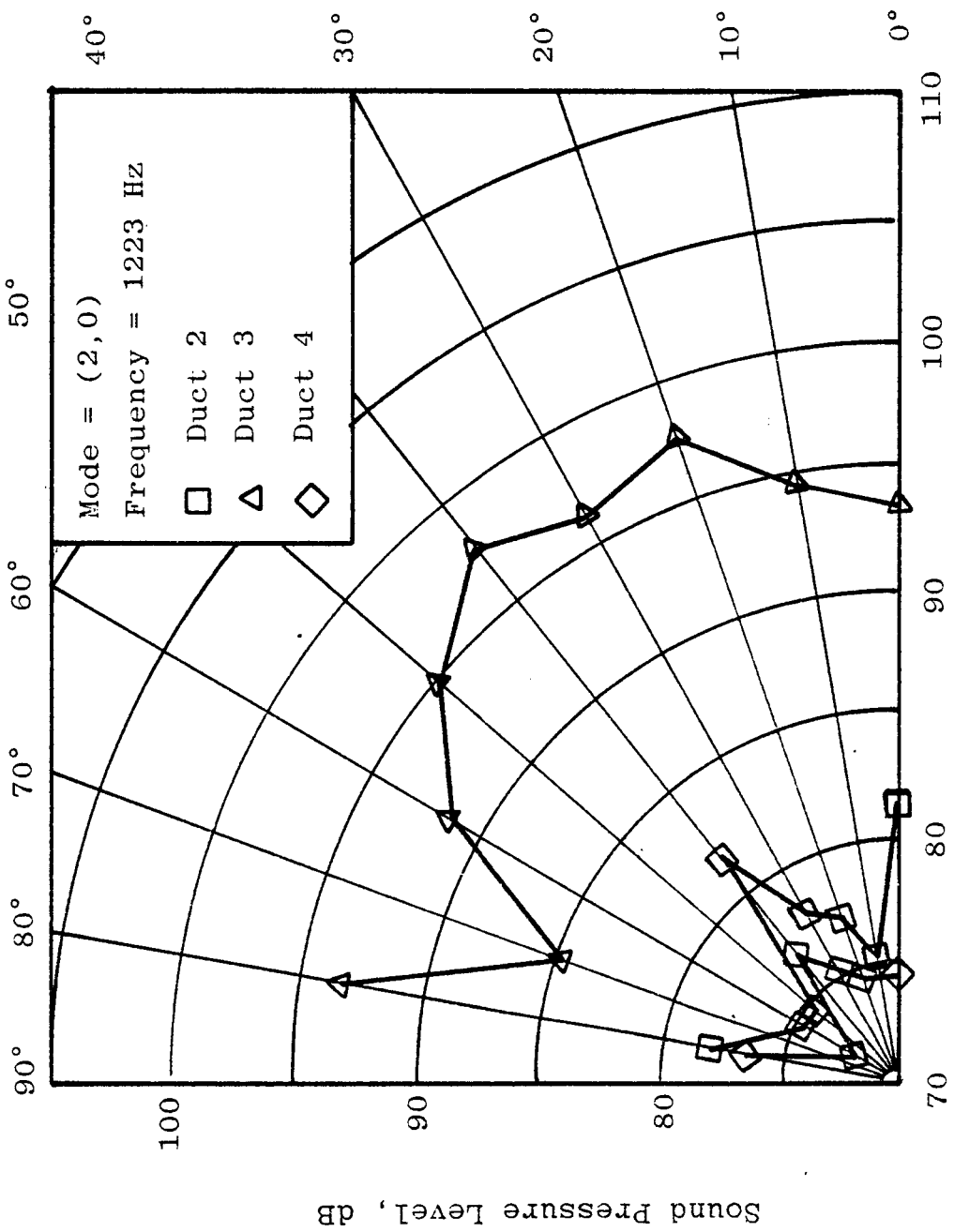


Figure VII.35 Far-Field Sound Pressure Under Static Conditions (Mode=(2,0),Freq=1223 Hz)

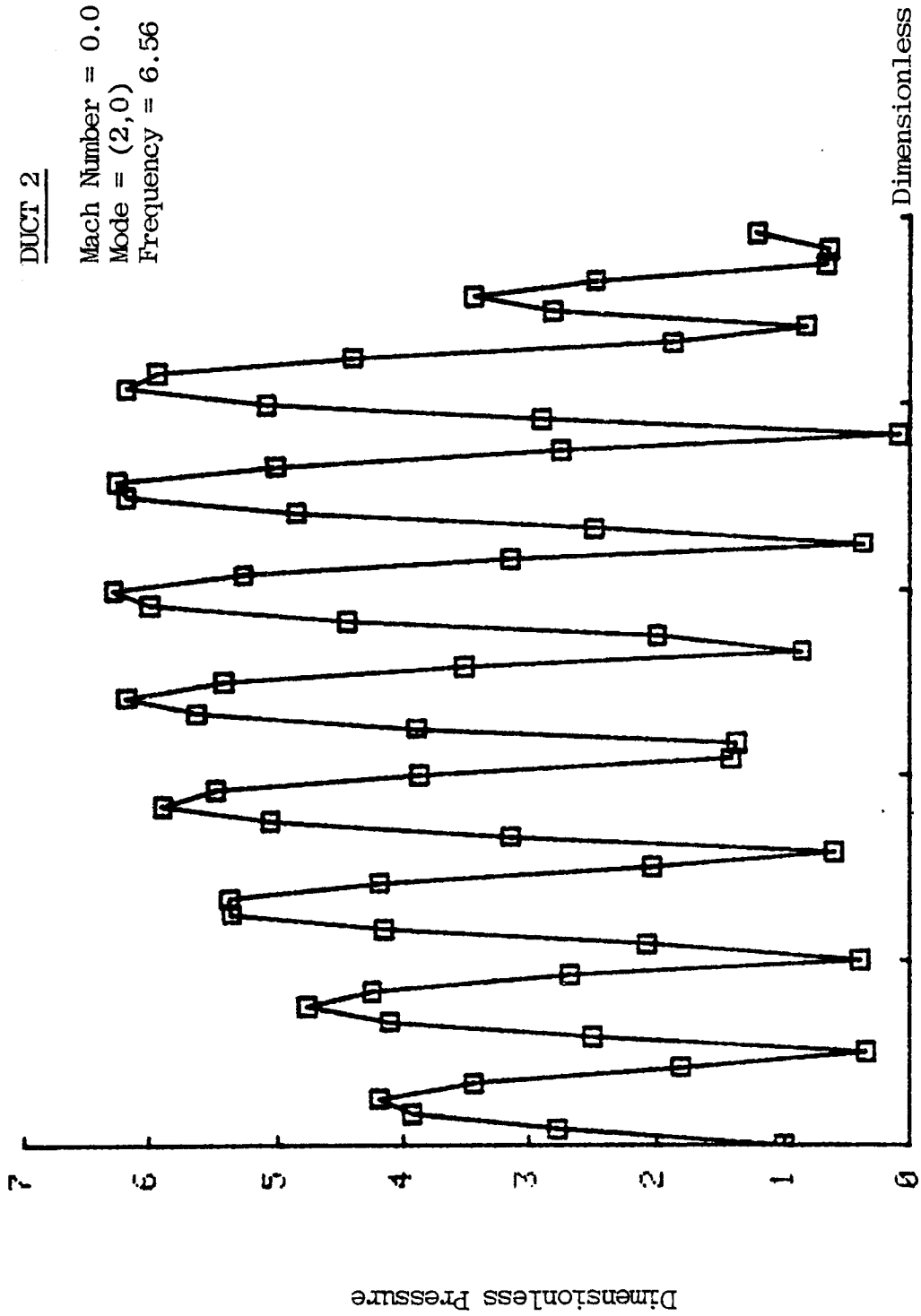


Figure VII.36 Pressure Distribution Along Duct Wall
(Duct 2, Mach Num=0.0, Mode=(2,0), Freq=6.56)

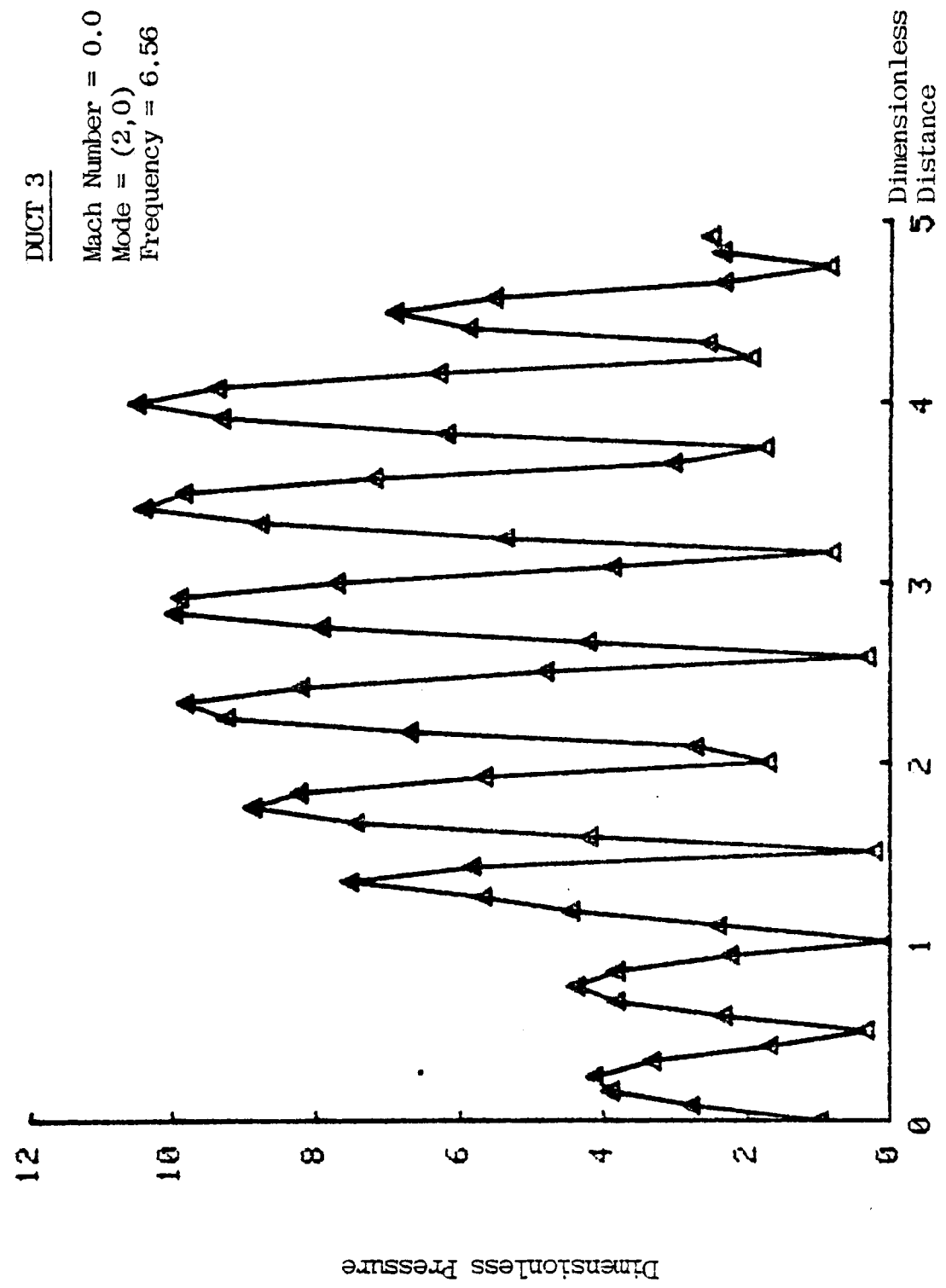


Figure VII.37 Pressure Distribution Along Duct Wall
(Duct 3, Mach Num=0.0, Mode=(2,0), Freq=6.56)

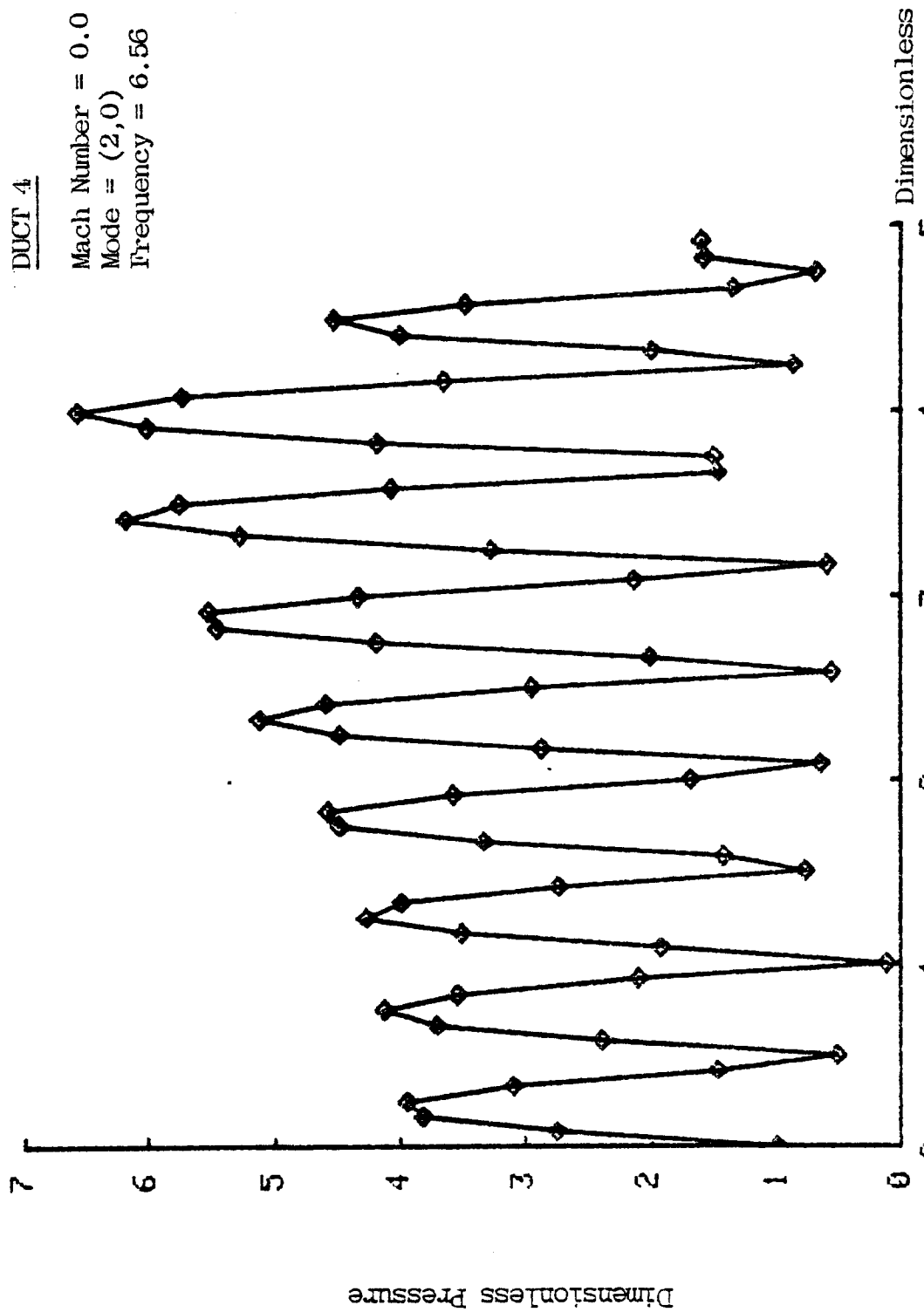


Figure VII.38 Pressure Distribution Along Duct Wall
(Duct 4, Mach Num=0.0, Mode=(2,0), Freq=6.56)

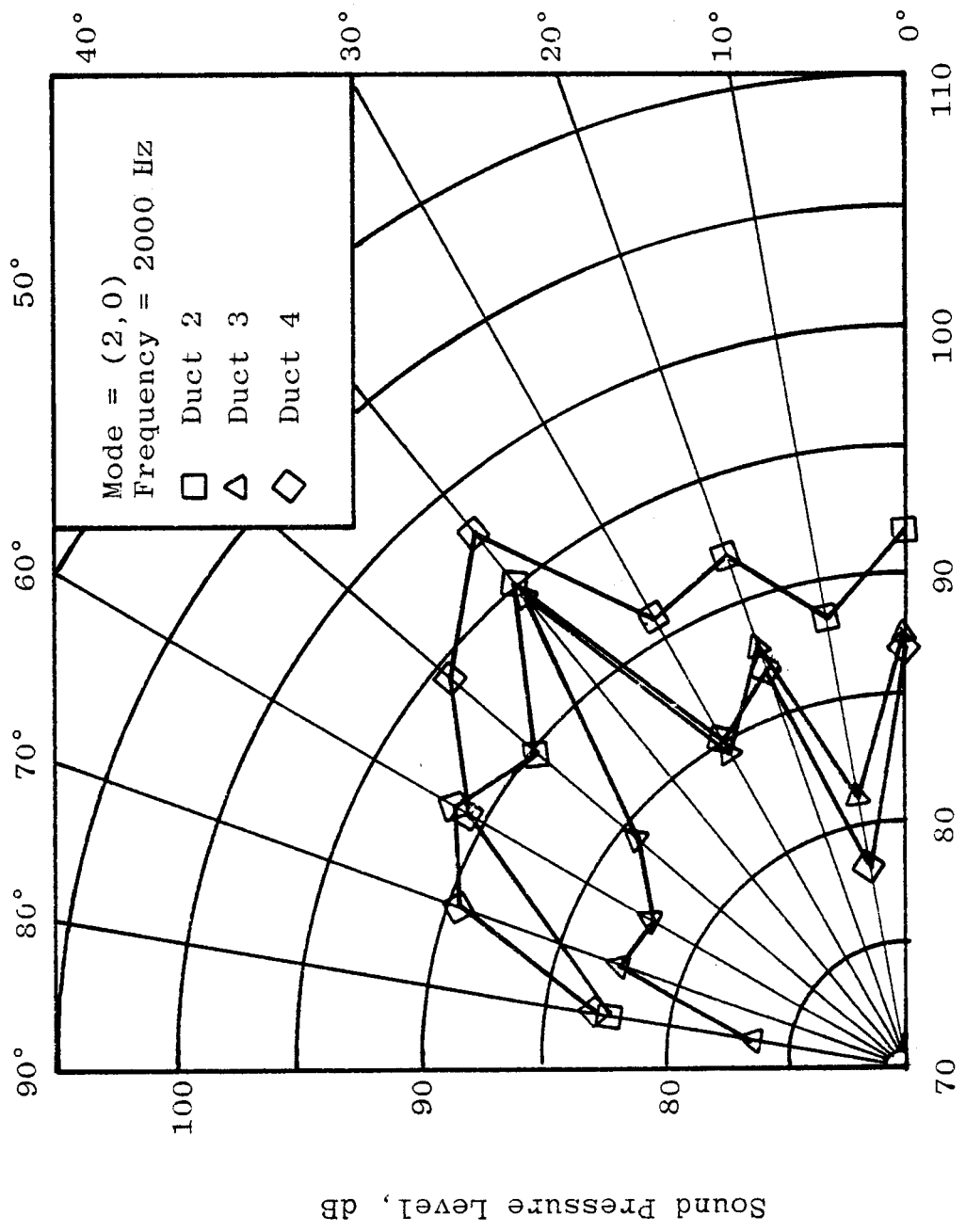


Figure VII.39 Far-Field Sound Pressure Level Under Static Conditions (Mode=(2,0),Freq=2000 Hz)

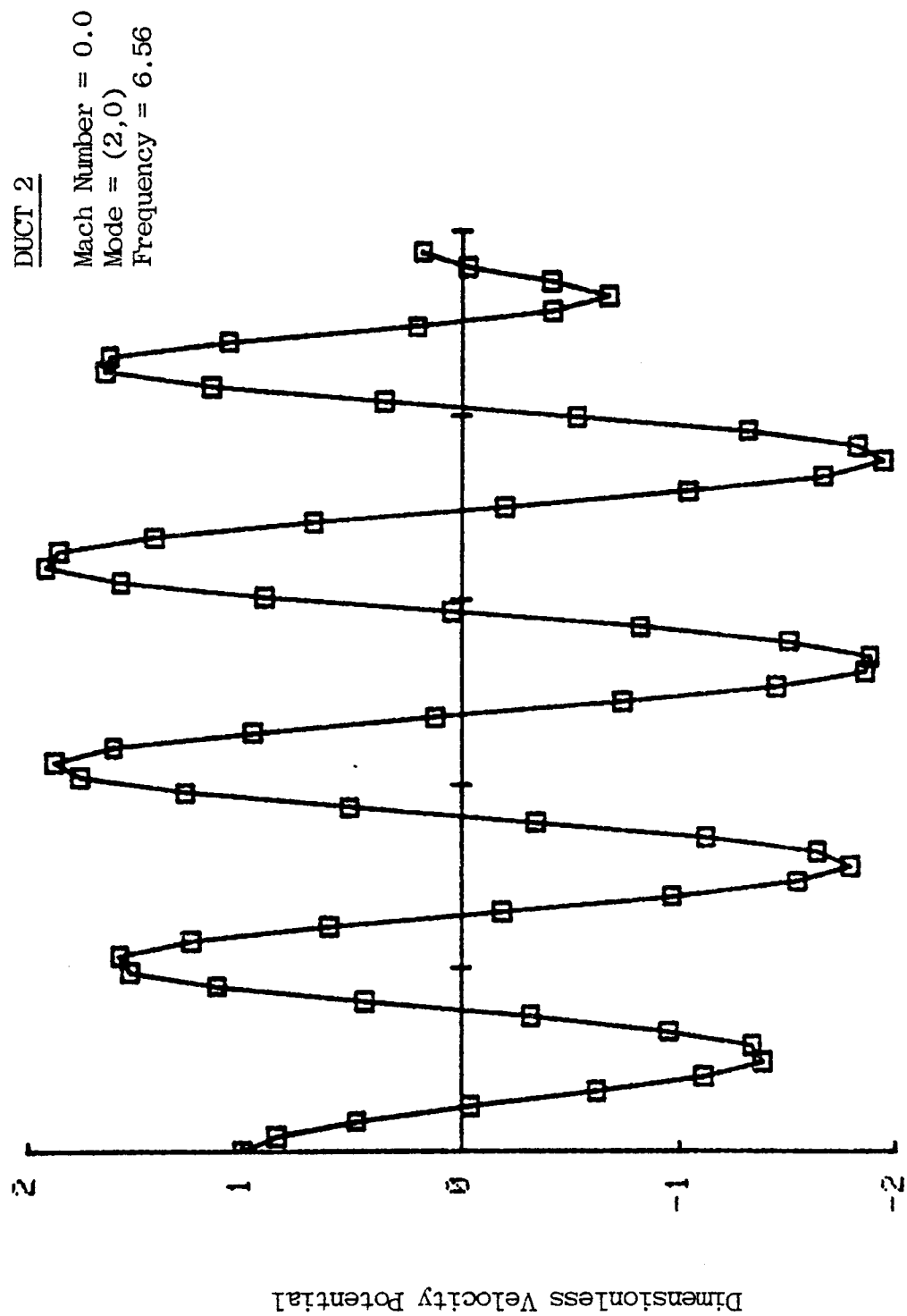


Figure VII.40 Acoustic Velocity Potential(Real Part) Along Duct Wall
(Duct 2,Mach Num=0.0,Mode=(2,0),Freq=6.56)

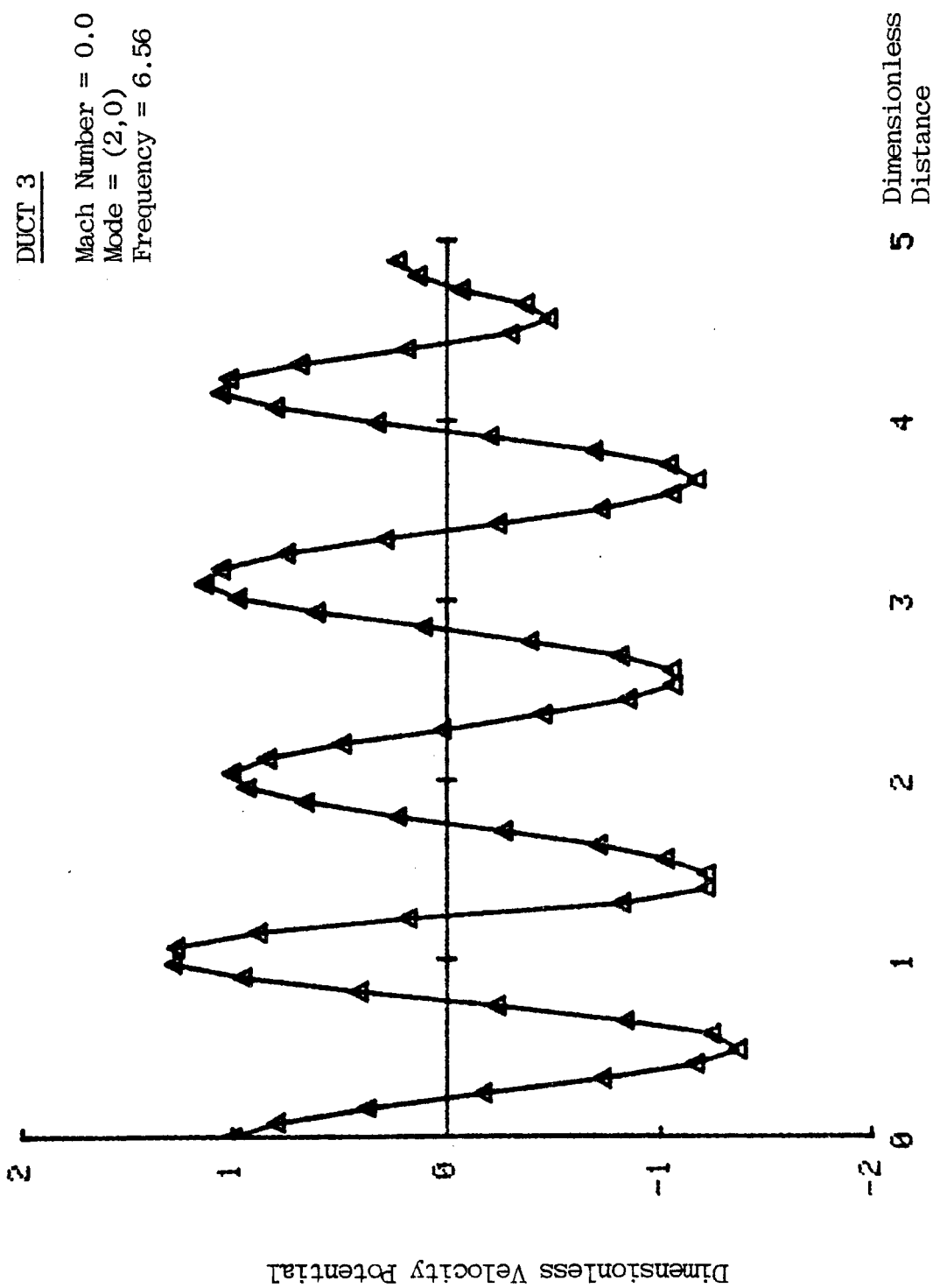


Figure VII.41 Acoustic Velocity Potential (Real Part) Along Duct Wall
(Duct 3, Mach Num=0.0, Mode=(2,0), Freq=6.56)

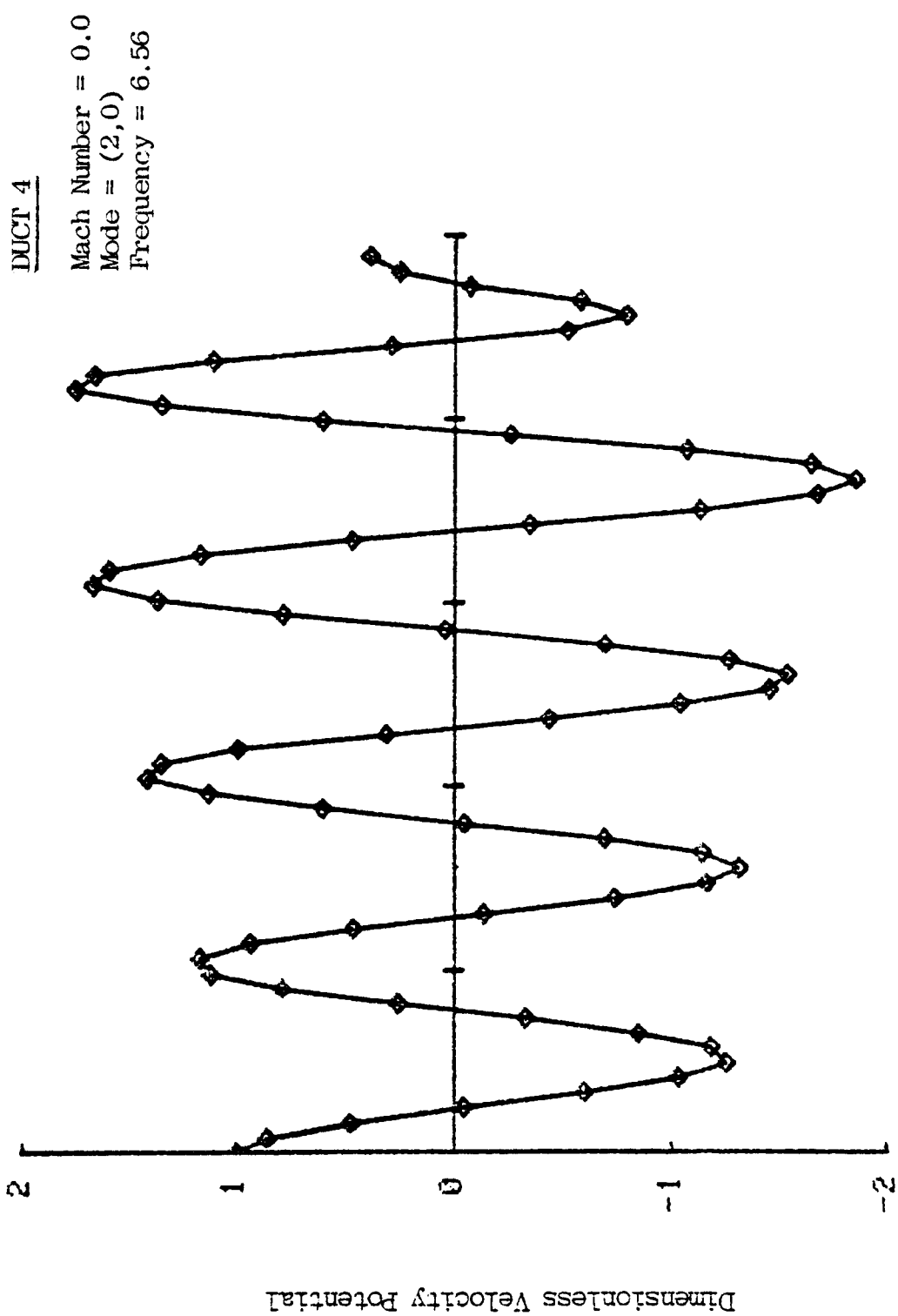


Figure VII.42 Acoustic Velocity Potential (Real Part) Along Duct Wall
(Duct 4, Mach Num=0.0, Mode=(2,0), Freq=6.56)

higher values in duct 3 as shown in Figures VII.43, VII.44 and VII.45. Although there is no pattern for the pressure distribution, it is expected that duct 3 would give a higher far-field attenuation.

For this frequency 8.58, there is no remarkable phase shift in duct 2 when it is compared with ducts 3 and 4 as shown in Figures VII.46, VII.47 and VII.48.

VII.2 Flow Cases

Two cases are considered; first is the case when the mass flow is 18 lb_m/sec which gives a throat Mach number of 0.68. The second case is for the much higher throat Mach number of 0.95 when 19.95 lb_m/sec is considered.

Figure VII.49 and Figure VII.50 give the pressure distribution for the (0,0) mode for 1.37 dimensionless frequency for duct 2 when the mass flow rates are 18 and 19.95 lb_m/sec. The build up of pressure near the throat for high Mach numbers is quite remarkable along with the decrease of the effective wave length due to the presence of flow, particularly for the 19.95 lb_m/sec flow case. It is believed that the far-field attenuation due to the high subsonic Mach number flows is due to the build up of the pressure near the throat. Experimentally, flow separation caused by high-speed flow prevented us from maintaining high subsonic Mach numbers for inlet 2. Theoretically, sizeable attenuation can be achieved using duct 2. Experimentally, boundary layer control is to be

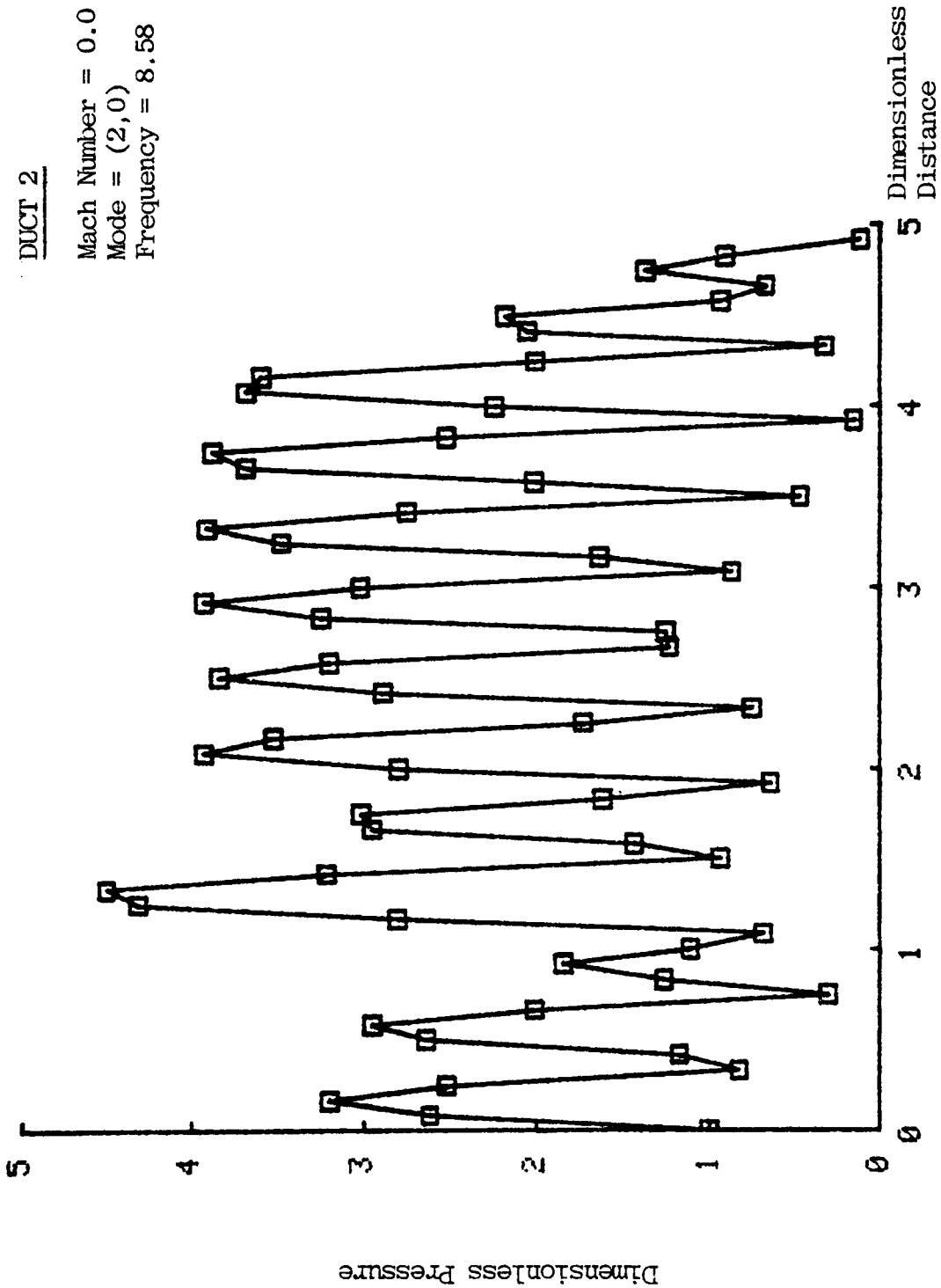


Figure VII.43 Pressure Distribution Along Duct Wall
(Duct 2, Mach Num=0.0, Mode=(2,0), Freq=8.58)

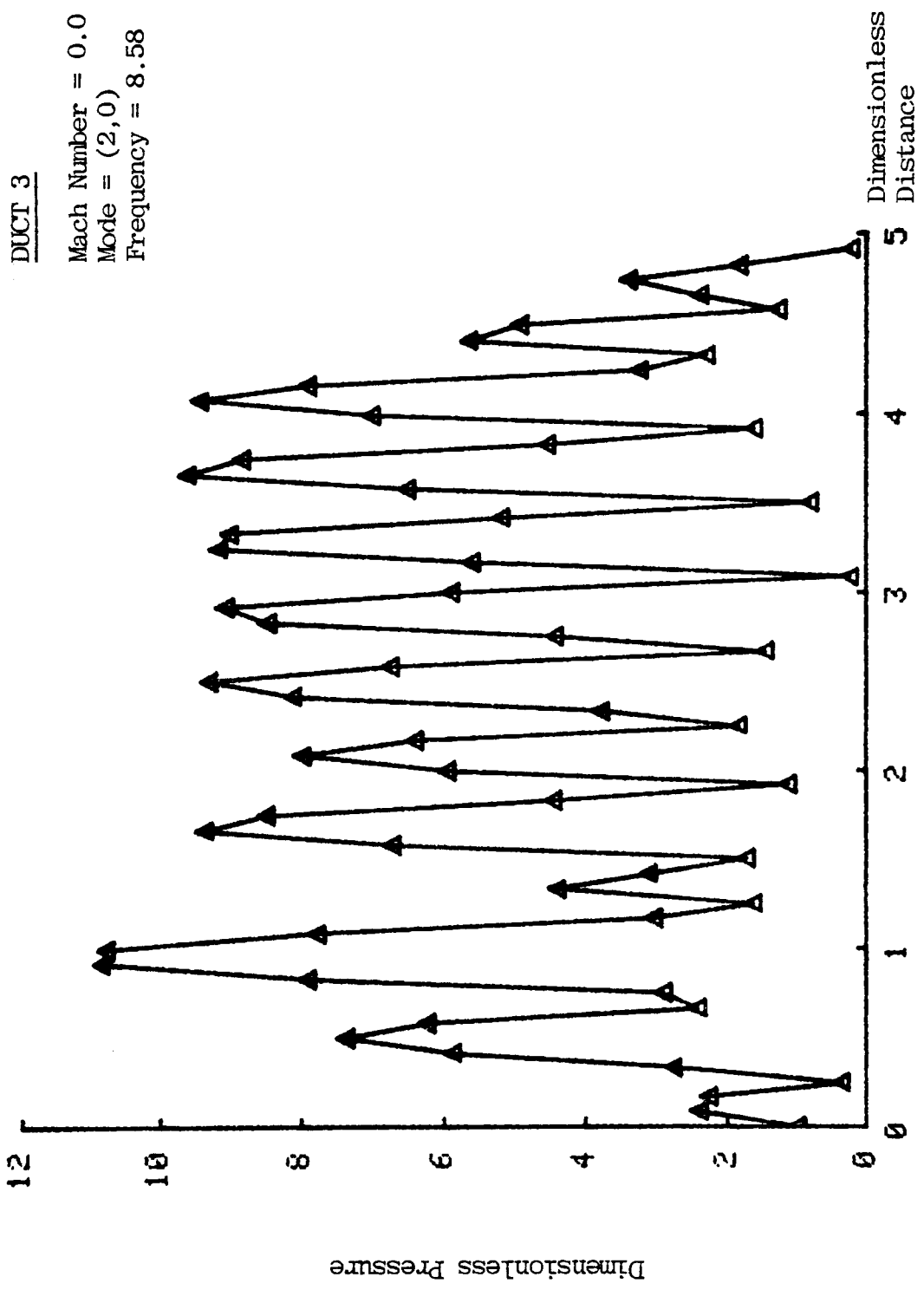


Figure VII.44 Pressure Distribution Along Duct Wall
(Duct 3, Mach Num=0.0, Mode=(2,0), Freq=8.58)

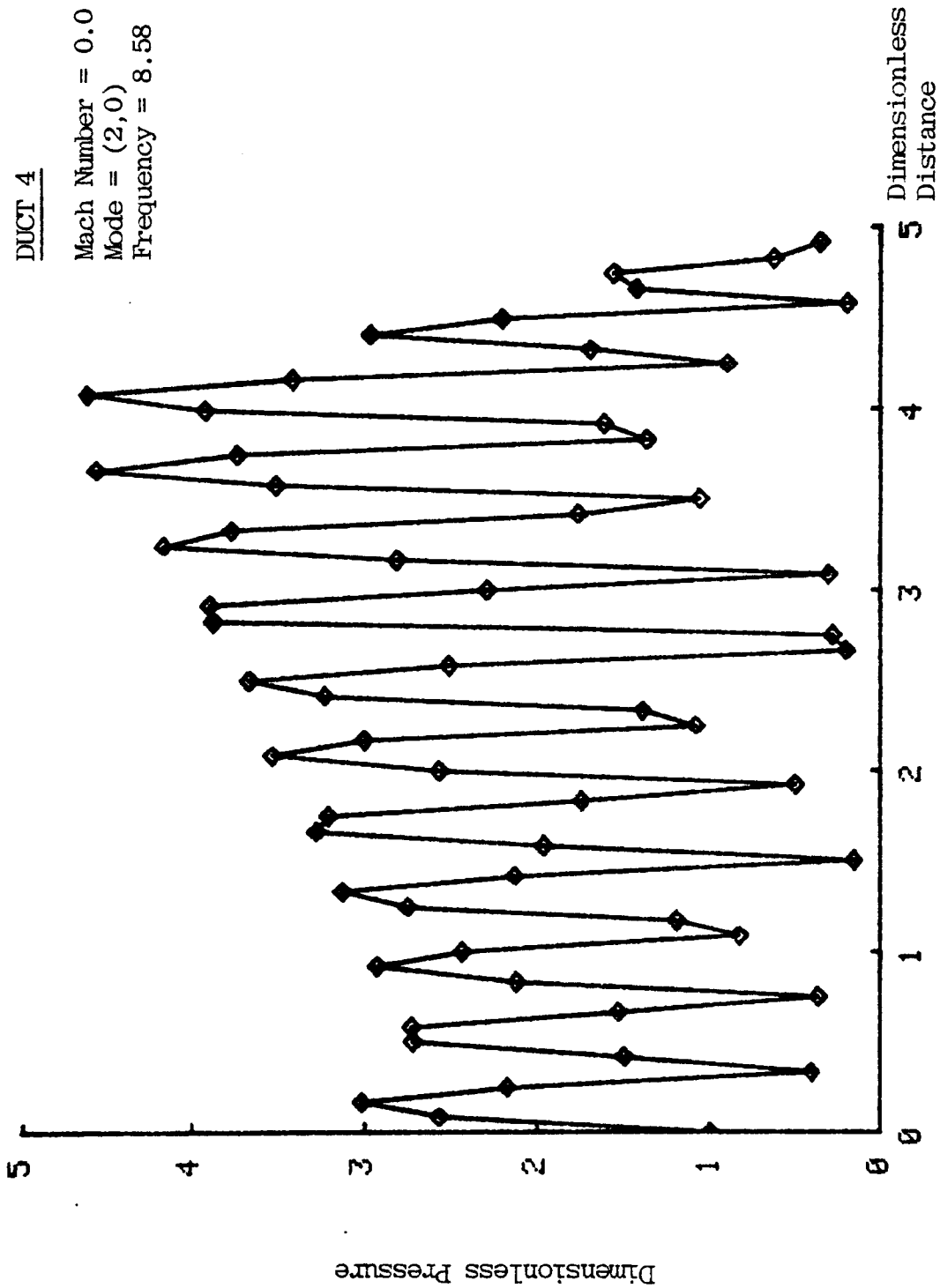


Figure VII.45 Pressure Distribution Along Duct Wall
(Duct 4, Mach Num=0.0, Mode=(2,0), Freq=8.58)

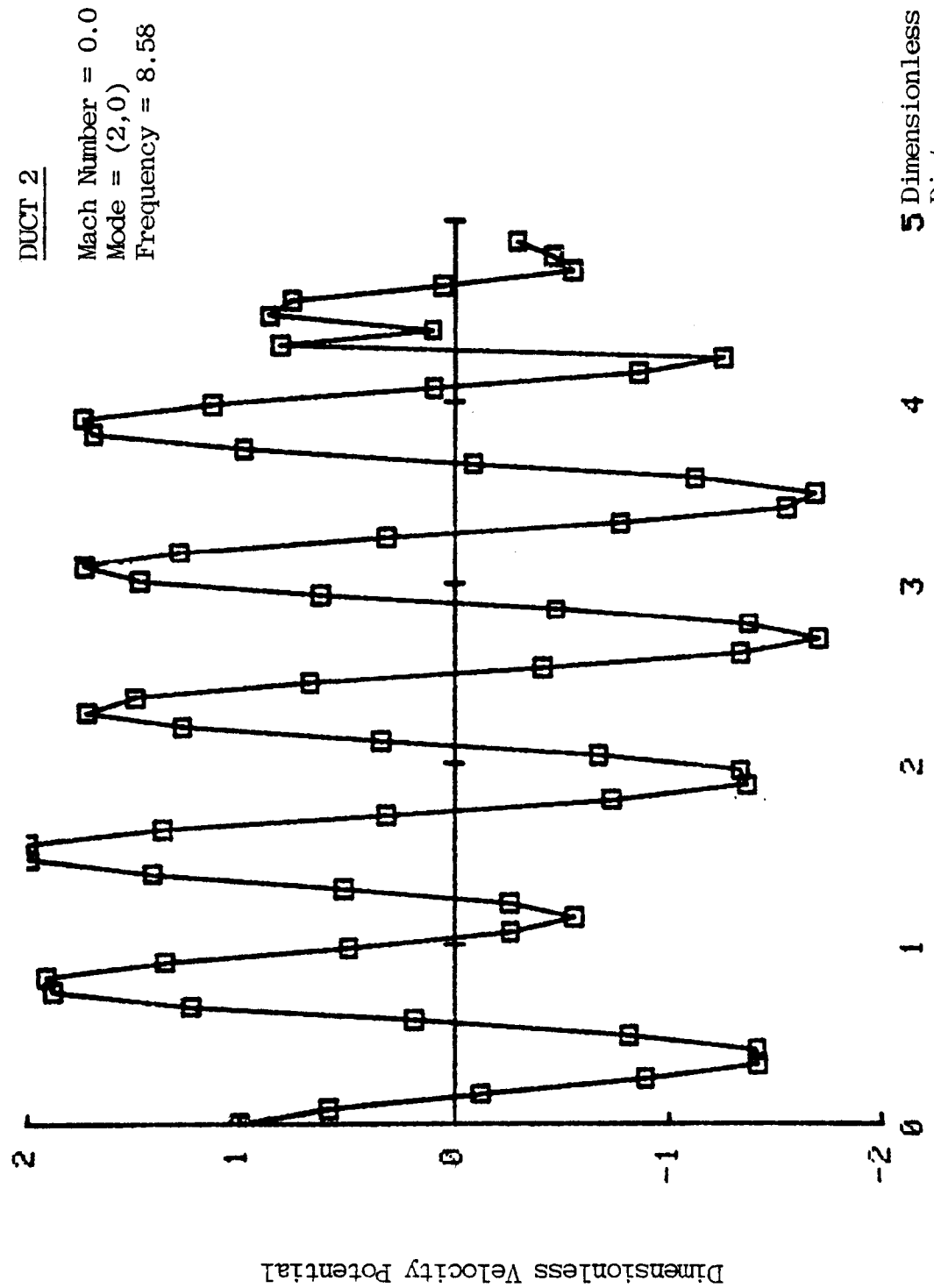


Figure VII.46 Acoustic Velocity Potential (Real Part) Along Duct Wall
(Duct 2, Mach Num=0.0, Mode=(2,0), Freq=8.58)

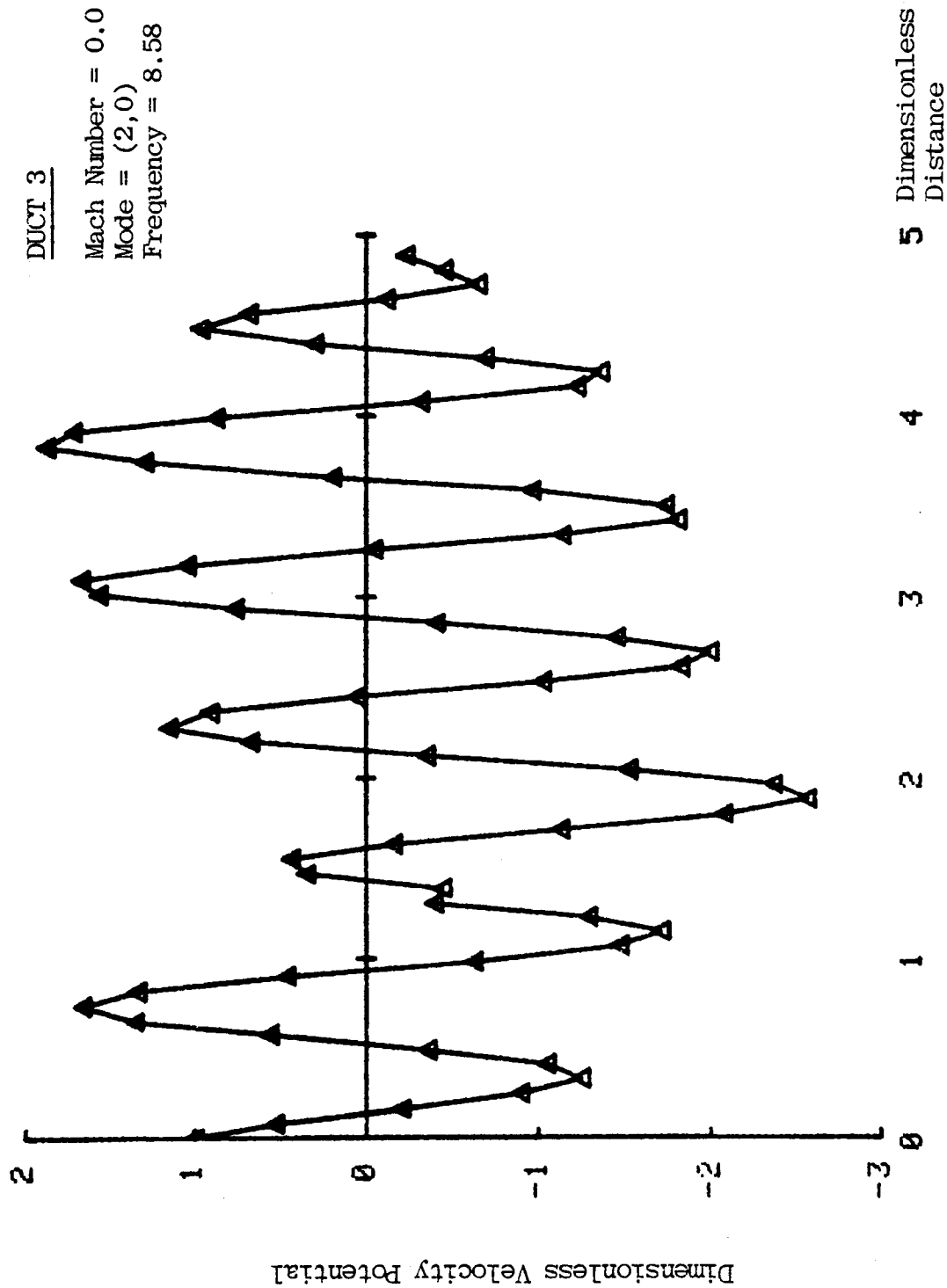


Figure VII.47 Acoustic Velocity Potential (Real Part) Along Duct Wall
(Duct 3, Mach Num=0.0, Mode=(2,0), Freq=8.58)

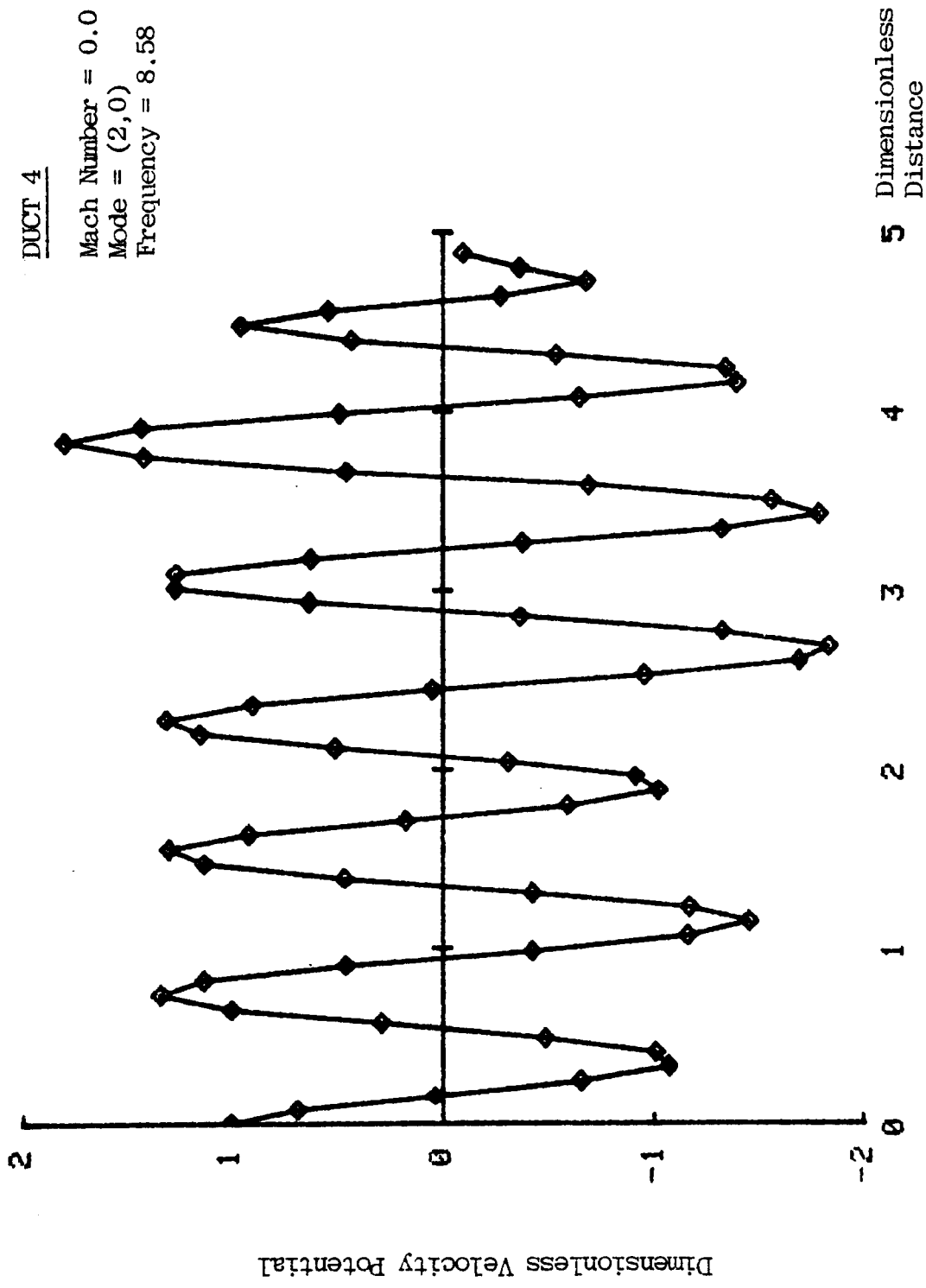


Figure VII.48 Acoustic Velocity Potential (Real Part) Along Duct Wall
(Duct 4, Mach Num=0.0, Mode=(2,0), Freq=8.58)

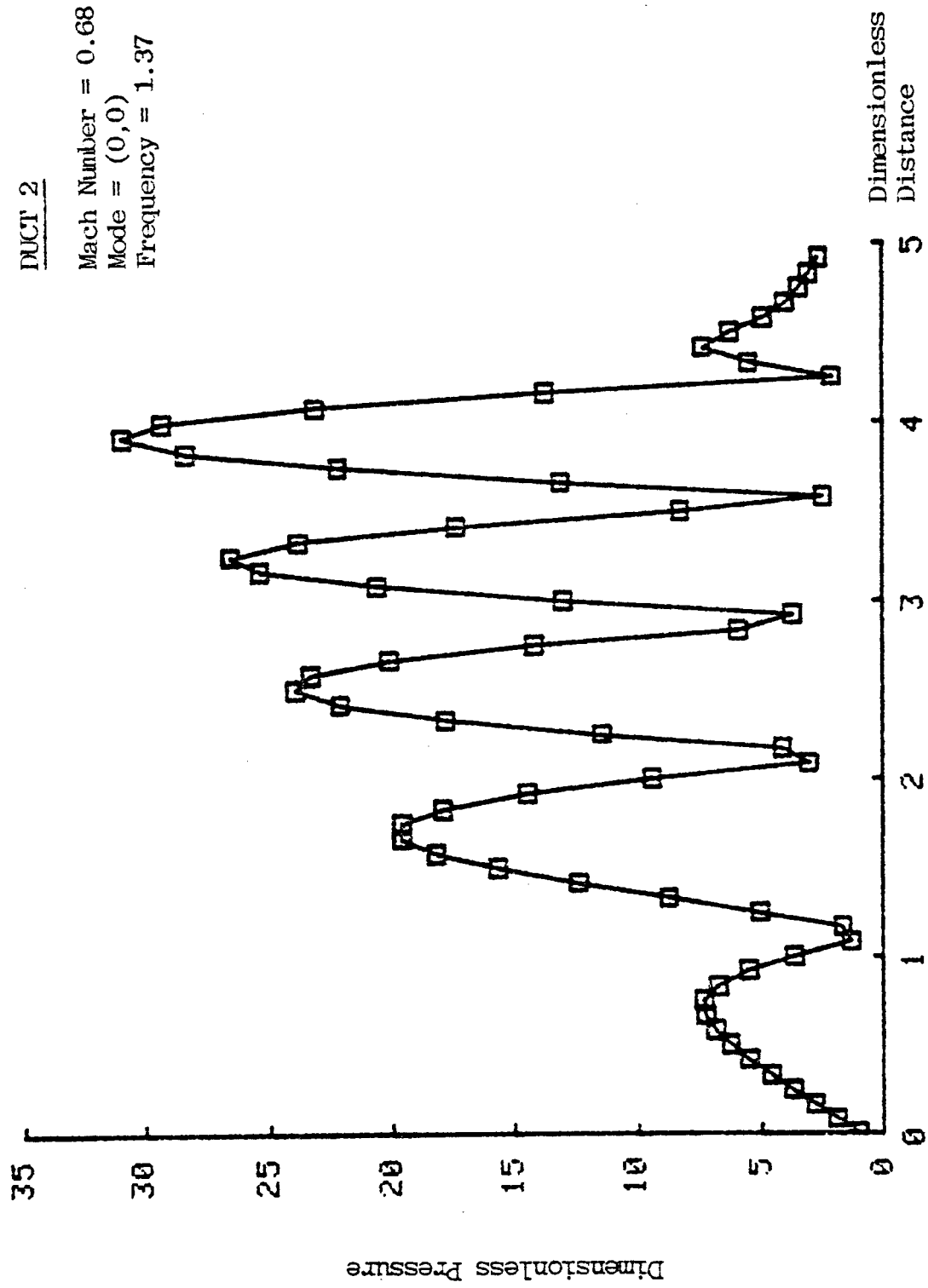


Figure VII.49 Pressure Distribution Along Duct Wall
(Duct 2, Mach Num=0.68, Mode=(0,0), Freq=1.37)

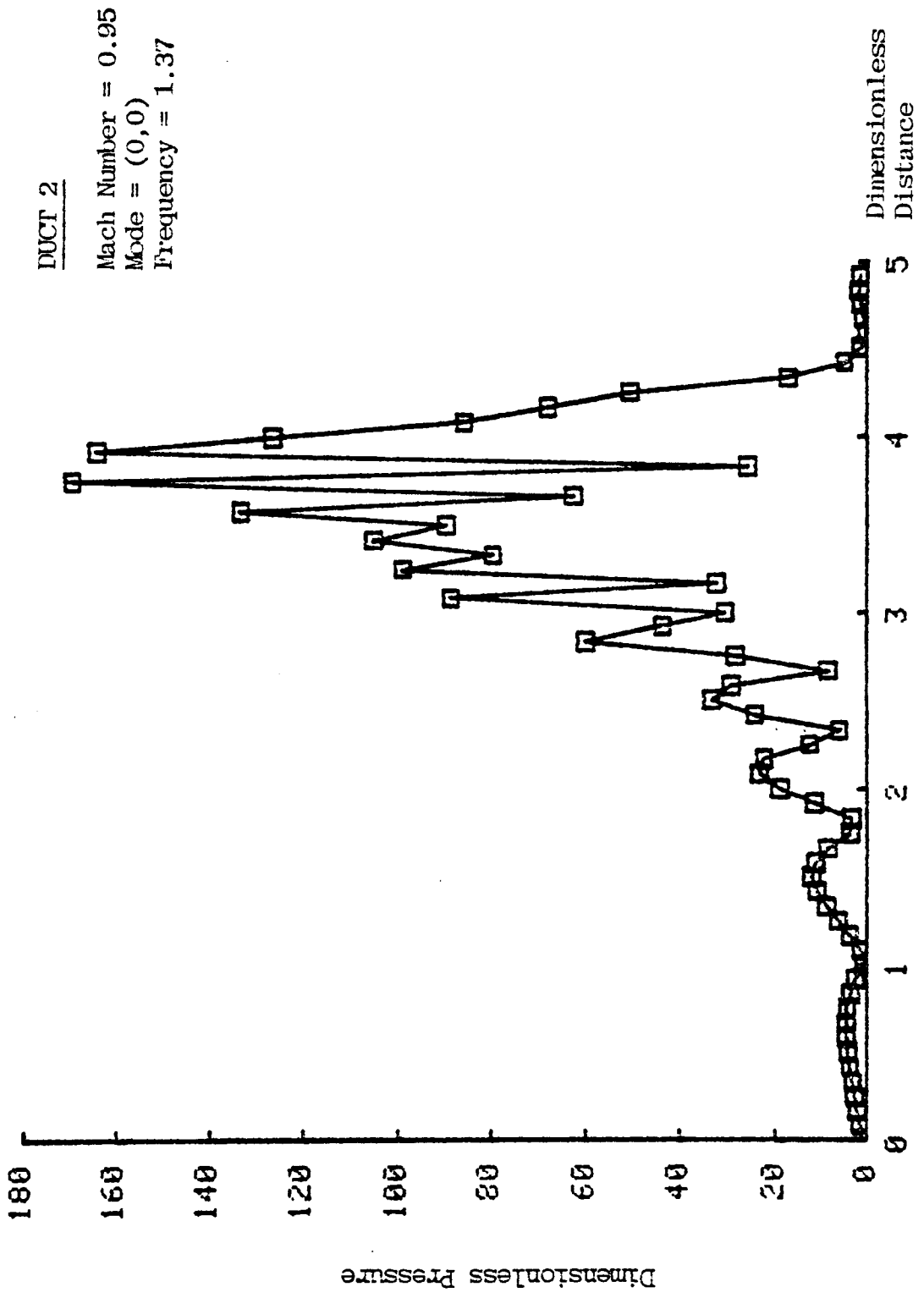


Figure VII.50 Pressure Distribution Along Duct Wall
(Duct 2, Mach Num=0.95, Mode=(0,0), Freq=1.37)

introduced to support high Mach number flows.

Duct 3 with a mild gradient shows the same trend with much higher pressure values near the throat which could be the reason for the high far-field attenuation obtained with duct 3 as can be seen in Figures VII.51 and VII.52

Figures VII.53 and VII.54 demonstrate the same trend with higher effective wave length when compared to ducts 2 and 3. This change in the effective frequency would affect the far-field attenuation as well.

For the (1,0) mode and 2.76 dimensionless frequency, a comparison is made between inlets 3 and 4 for 18 and 19.95 lb_m/sec mass flow.

Figures VII.55 - VII.58 show that the trend for the (0,0) mode holds. In addition, for the 19.95 lb_m/sec flow case the wave is attenuated sharply along duct 4 with maximum pressure at the throat. It is anticipated that duct 4 would give a maximum far-field attenuation. The decrease of the effective wave length can be seen also from Figures VII.56 and VII.58.

For the (2,0) mode case, Figures VII.59 - VII.62 demonstrate the same trend with the (1,0) mode; here again the near-field attenuation is quite remarkable for the 19.95 lb_m/sec flow case in duct 4 which provides a basis to conclude that acoustically duct 4 would give a maximum far-field attenuation if the flow is aerodynamically stable. On the other hand, duct 3 with a mild gradient gave

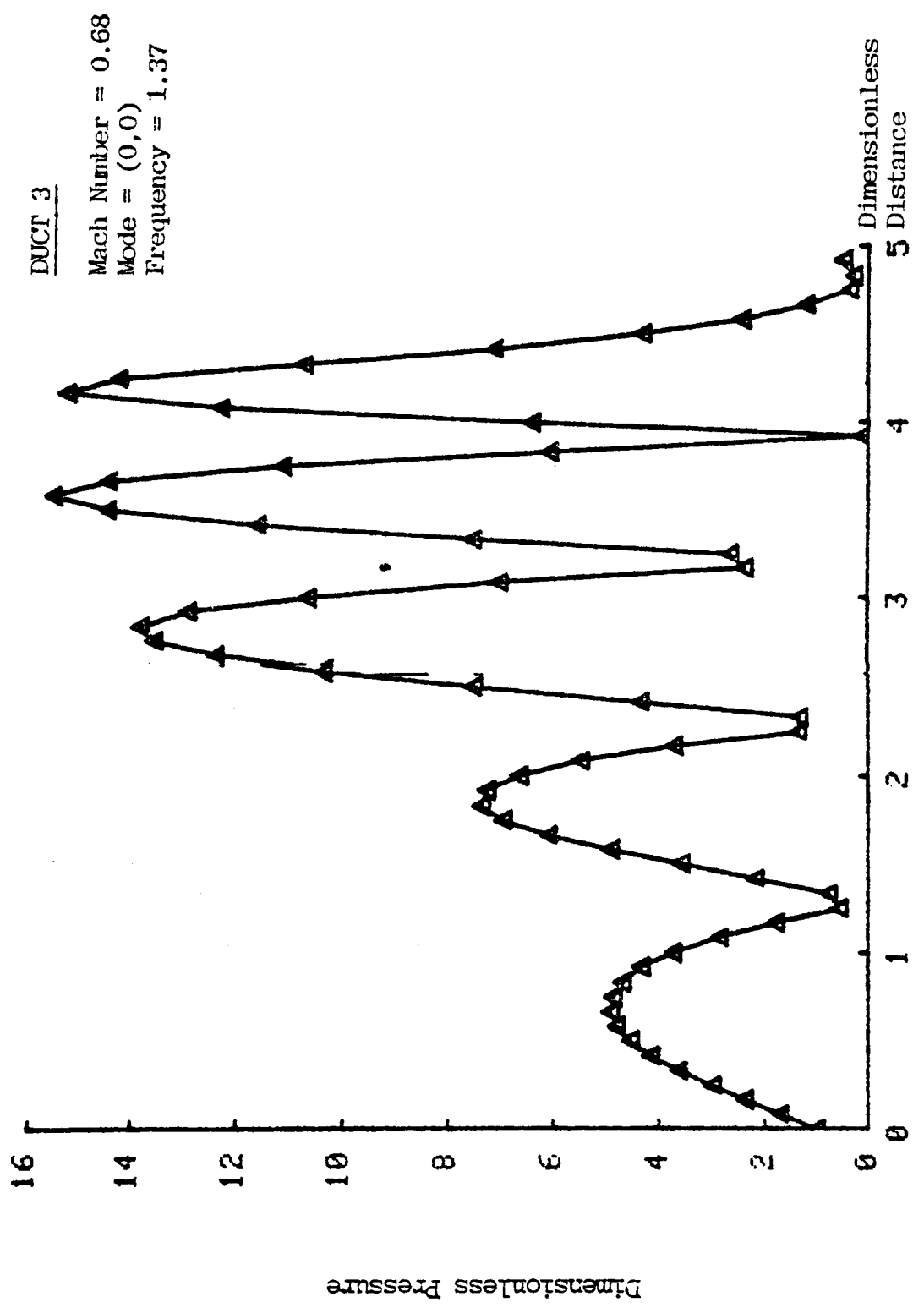


Figure VII.51 Pressure Distribution Along Duct Wall
(Duct 3, Mach Num=0.68, Mode=(0,0), Freq=1.37)

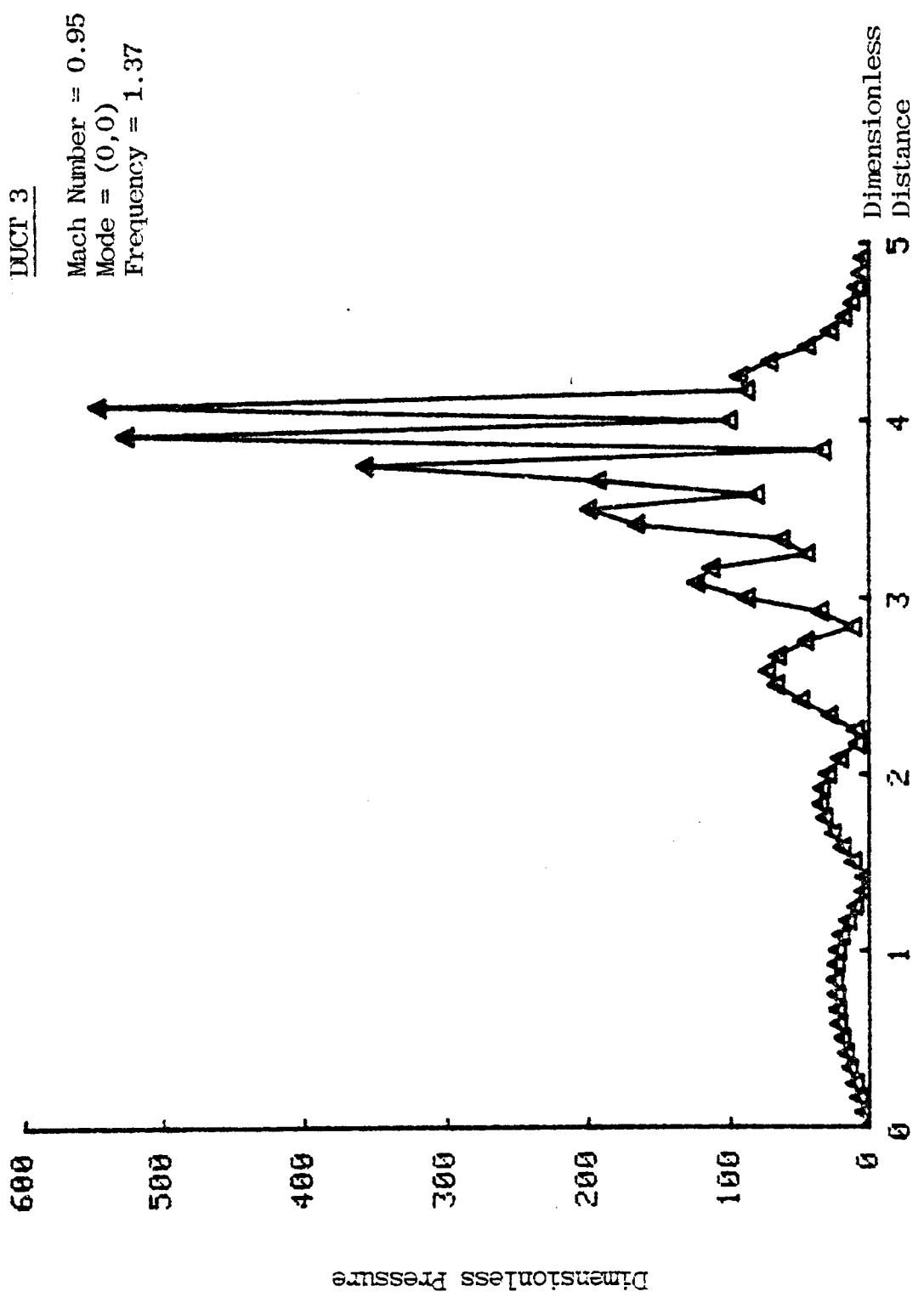


Figure VII.52 Pressure Distribution Along Duct Wall
(Duct 3, Mach Num=0.95, Mode=(0,0), Freq=1.37)

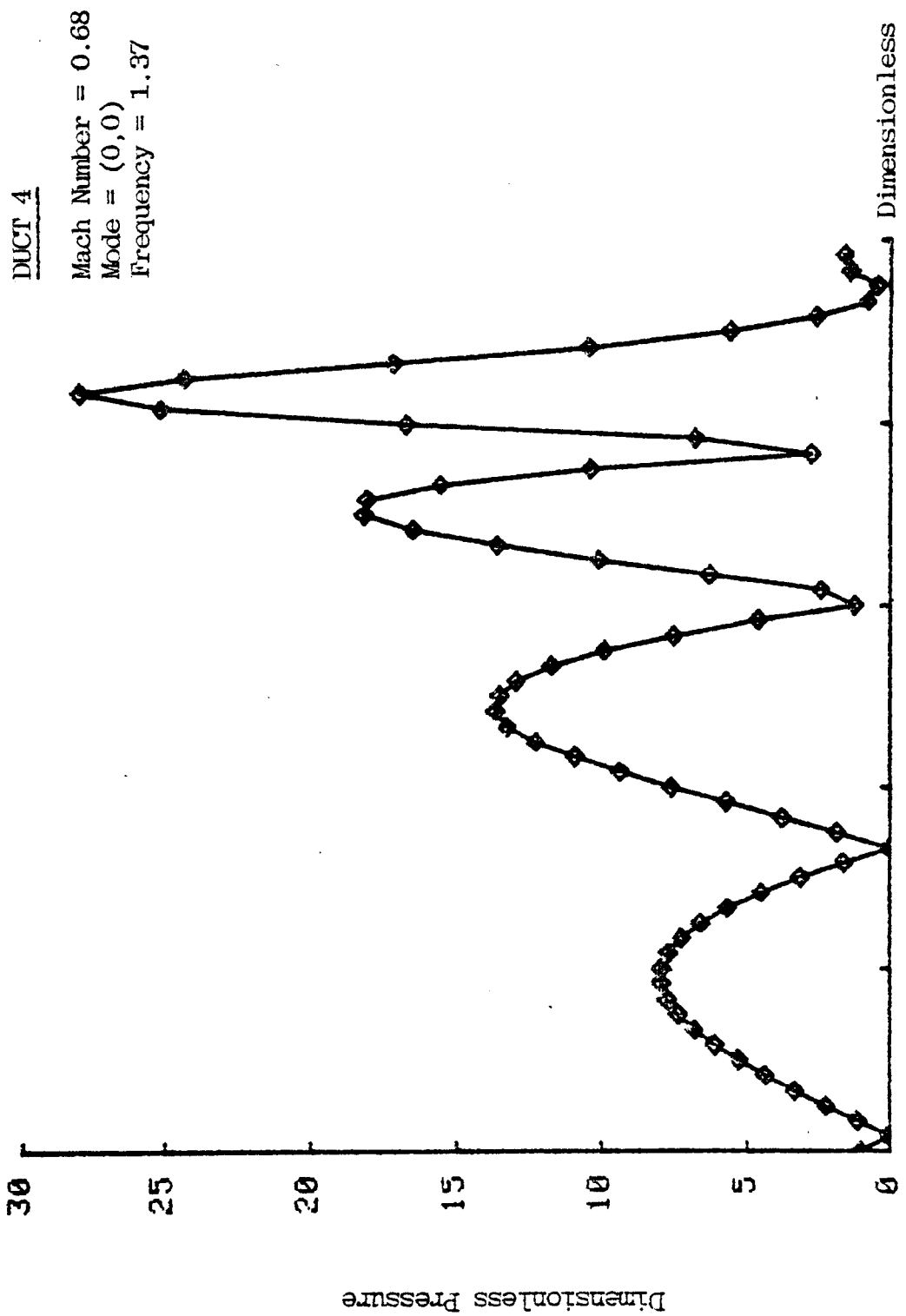


Figure VII.53 Pressure Distribution Along Duct Wall
(Duct 4, Mach Num=0.68, Mode=(0,0), Freq=1.37)

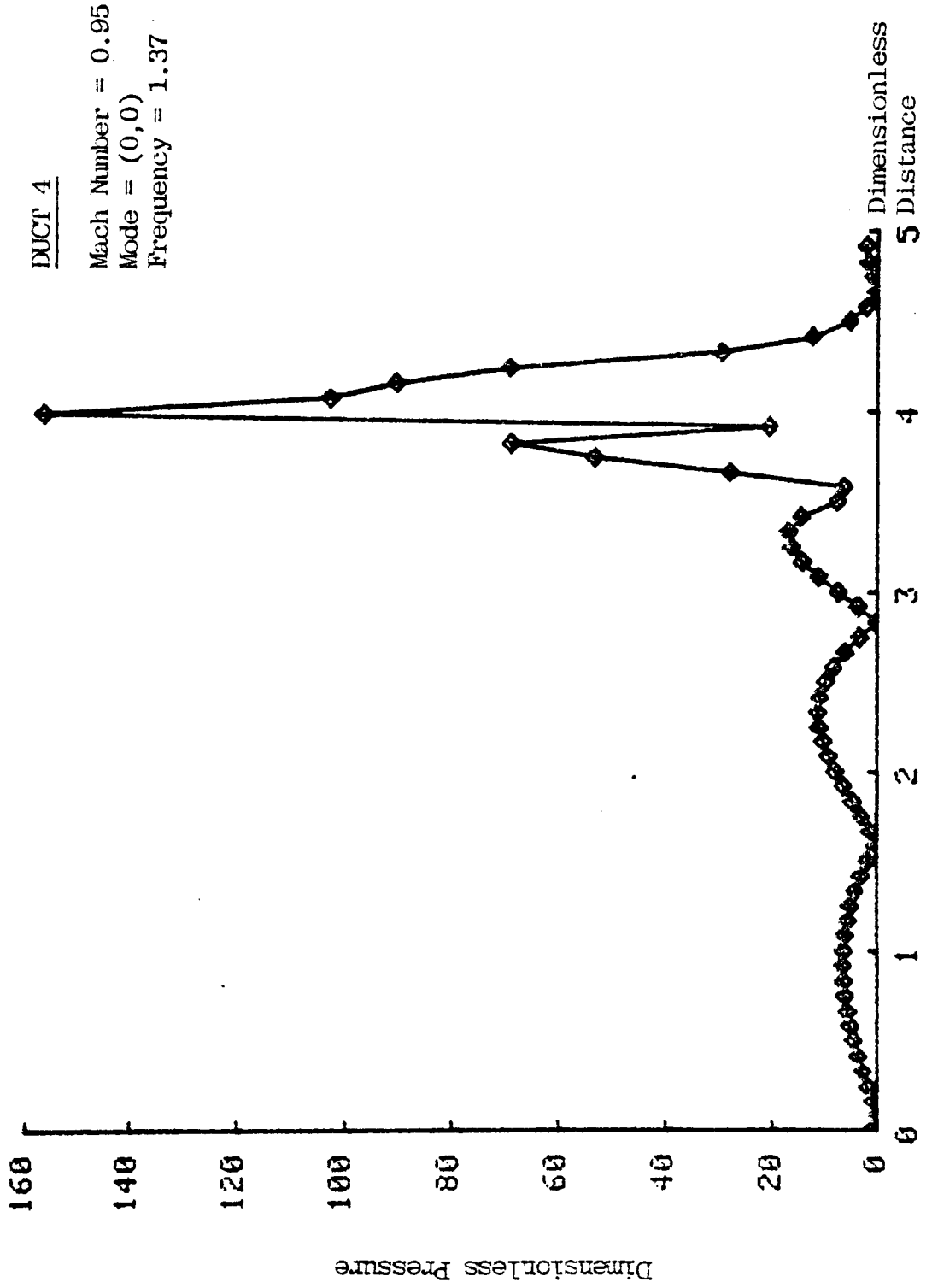


Figure VII.54 Pressure Distribution Along Duct Wall
(Duct 4, Mach Num=0.95, Mode=(0,0), Freq=1.37)

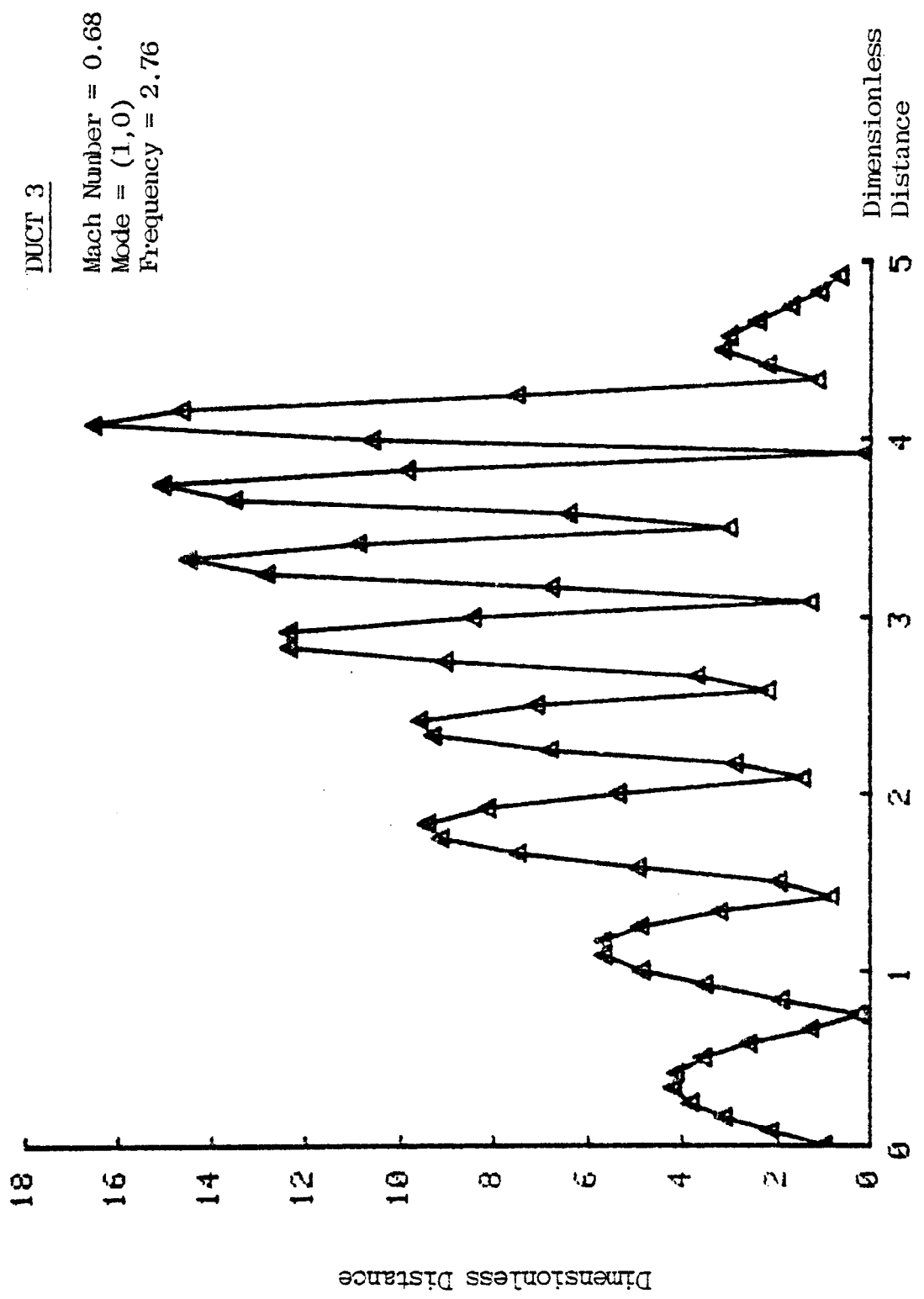


Figure VII.55 Pressure Distribution Along Duct Wall
(Duct 3, Mach Num=0.68, Mode=(1,0), Freq=2.76)

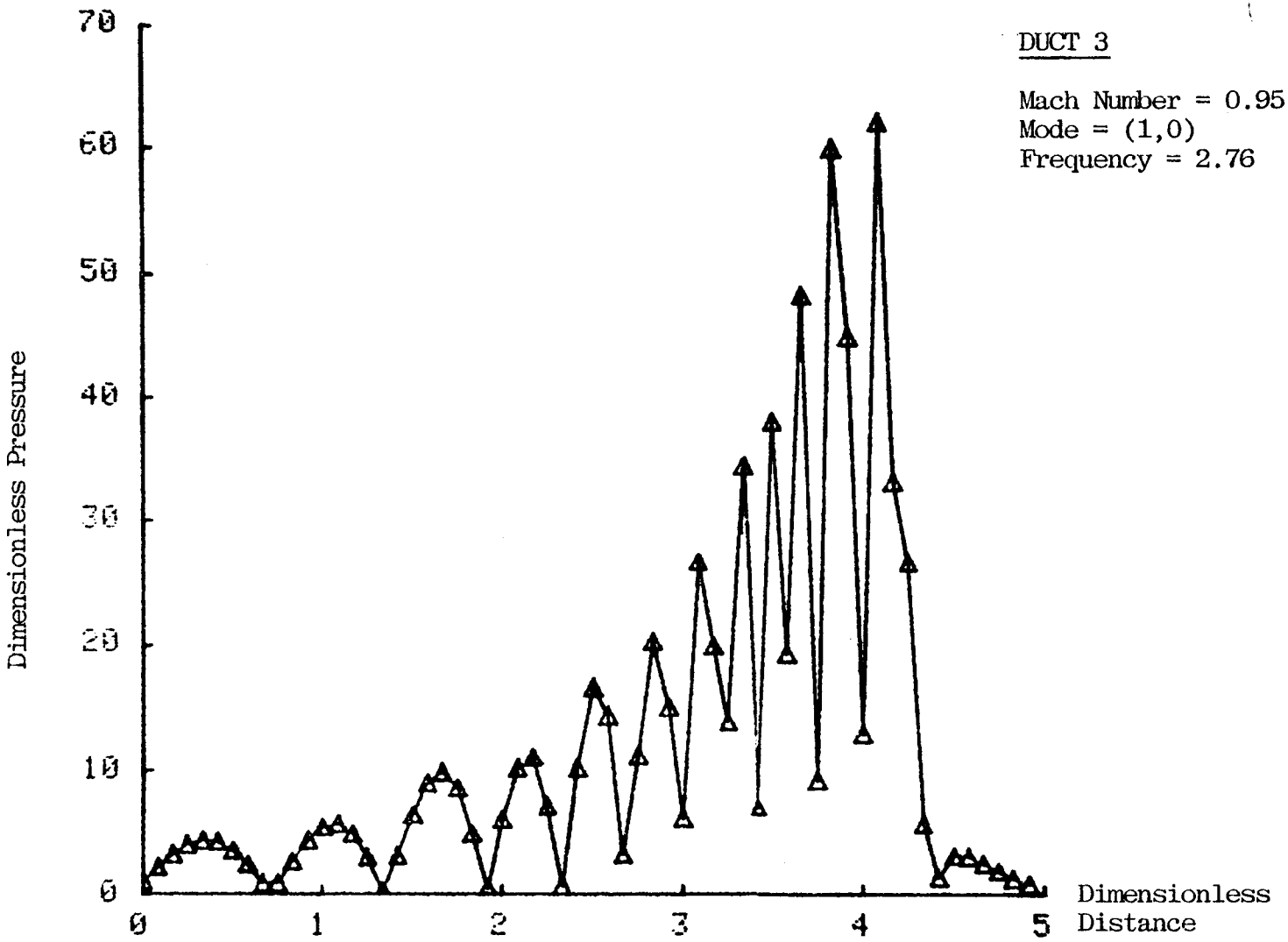


Figure VII.56 Pressure Distribution Along Duct Wall
(Duct 3,Mach Num=0.95,Mode=(1,0),Freq=2.76)

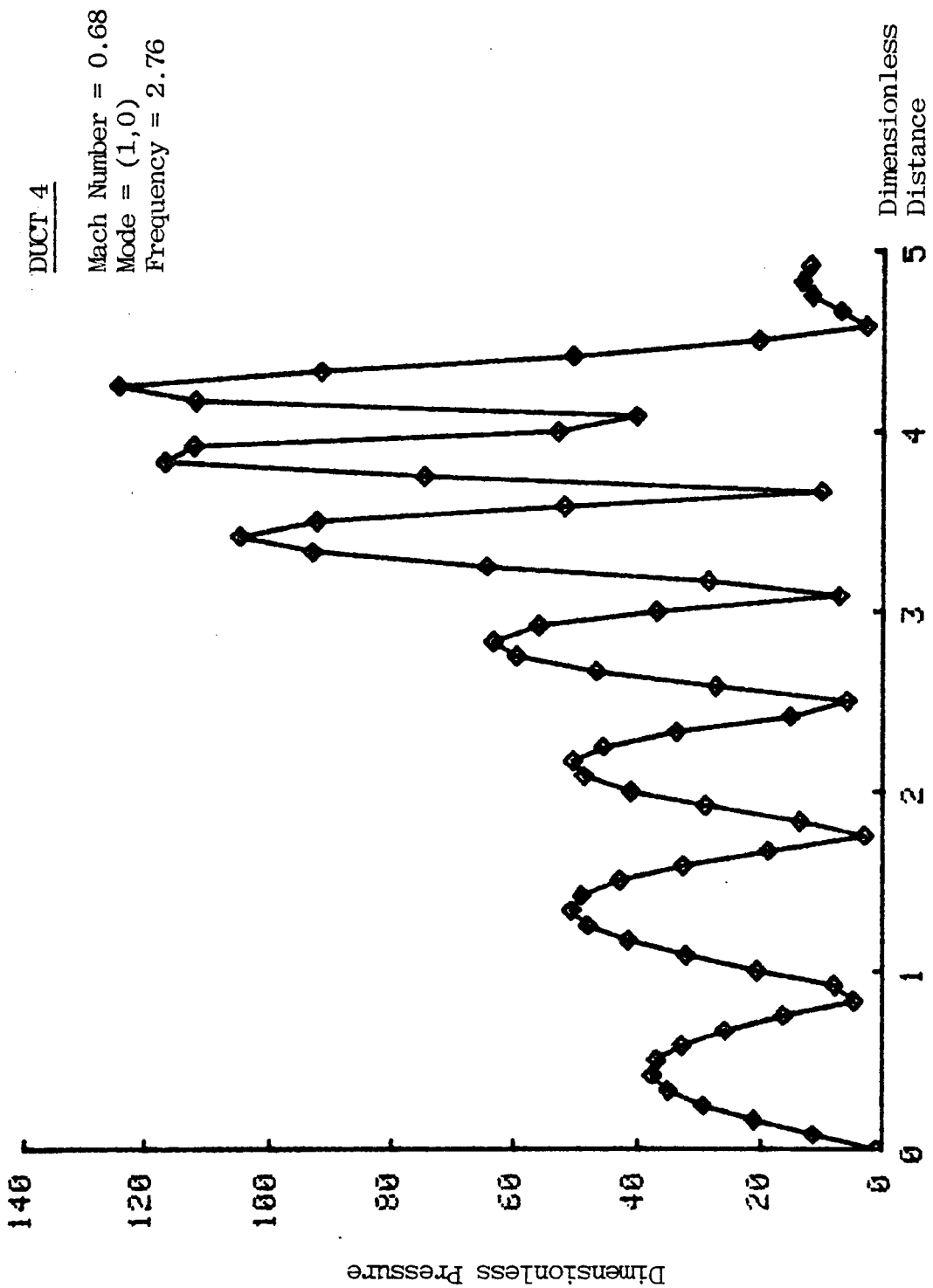


Figure VII.57 Pressure Distribution Along Duct Wall
(Duct 4, Mach Num=0.68, Mode=(1,0), Freq=2.76)

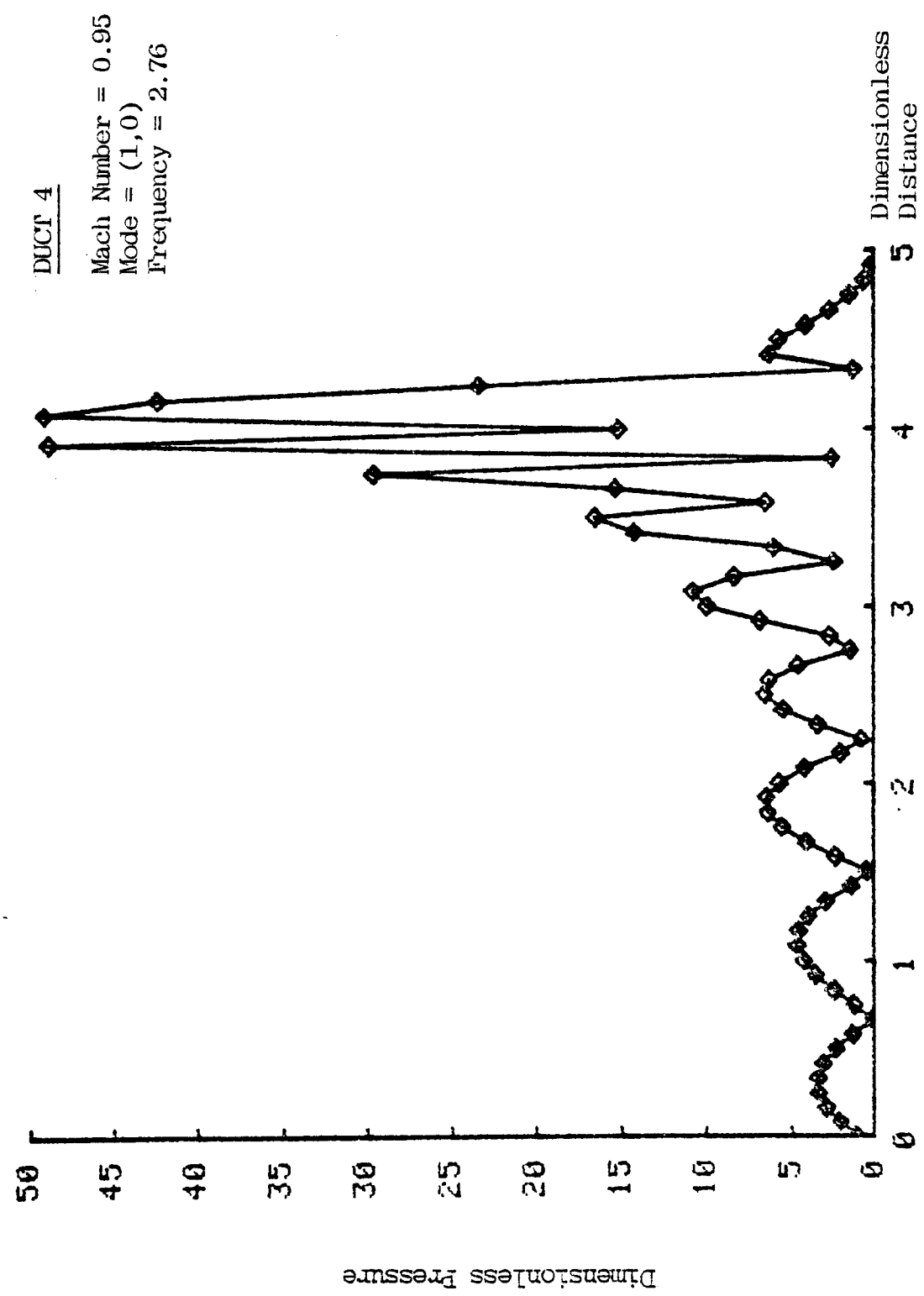


Figure VII.58 Pressure Distribution Along Duct Wall
(Duct 4,Mach Num=0.95,Mode=(1,0),Freq=2.76)

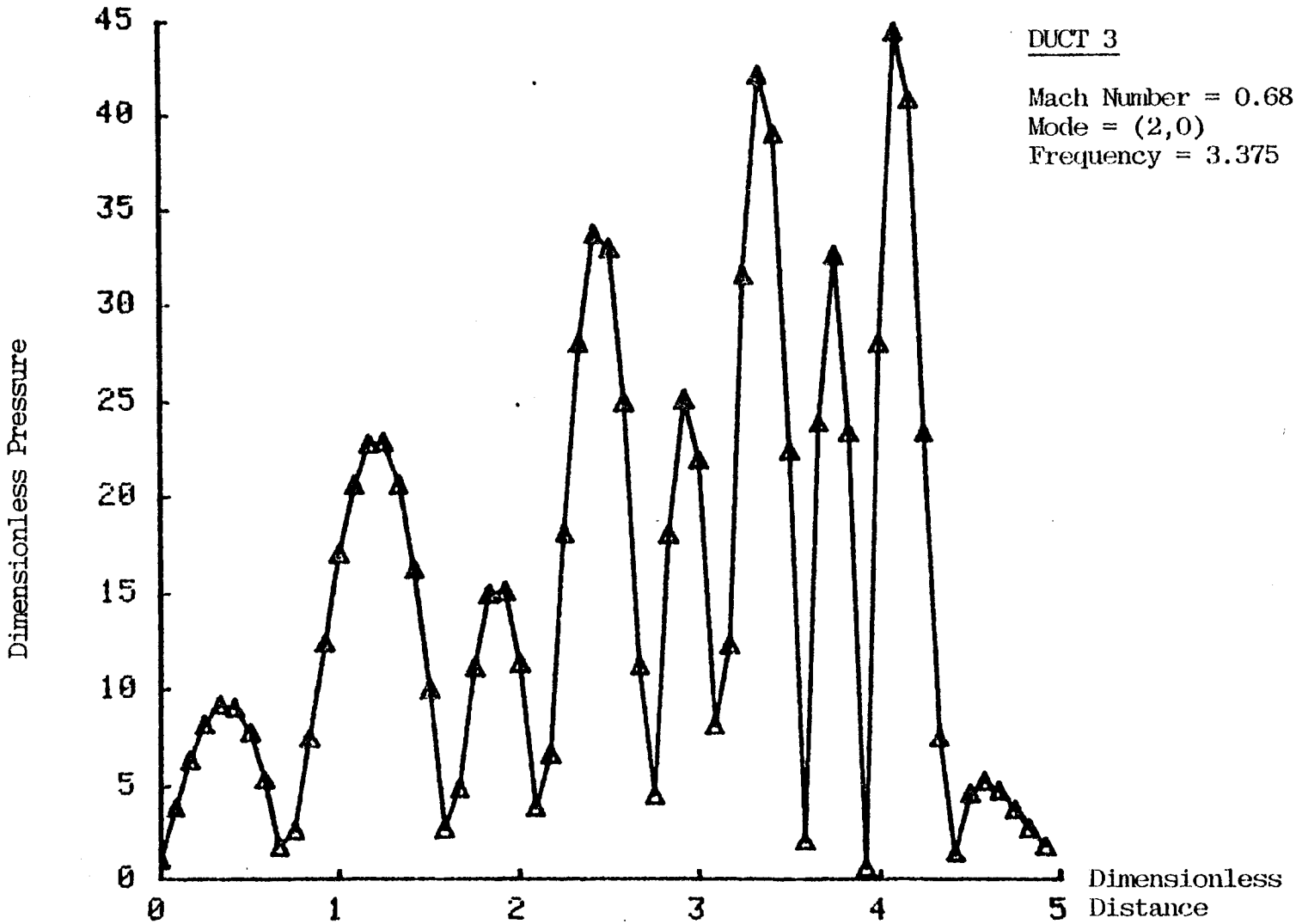


Figure VII.59 Pressure Distribution Along Duct Wall
(Duct 3,Mach Num=0.68,Mode=(2,0),Freq=3.375)

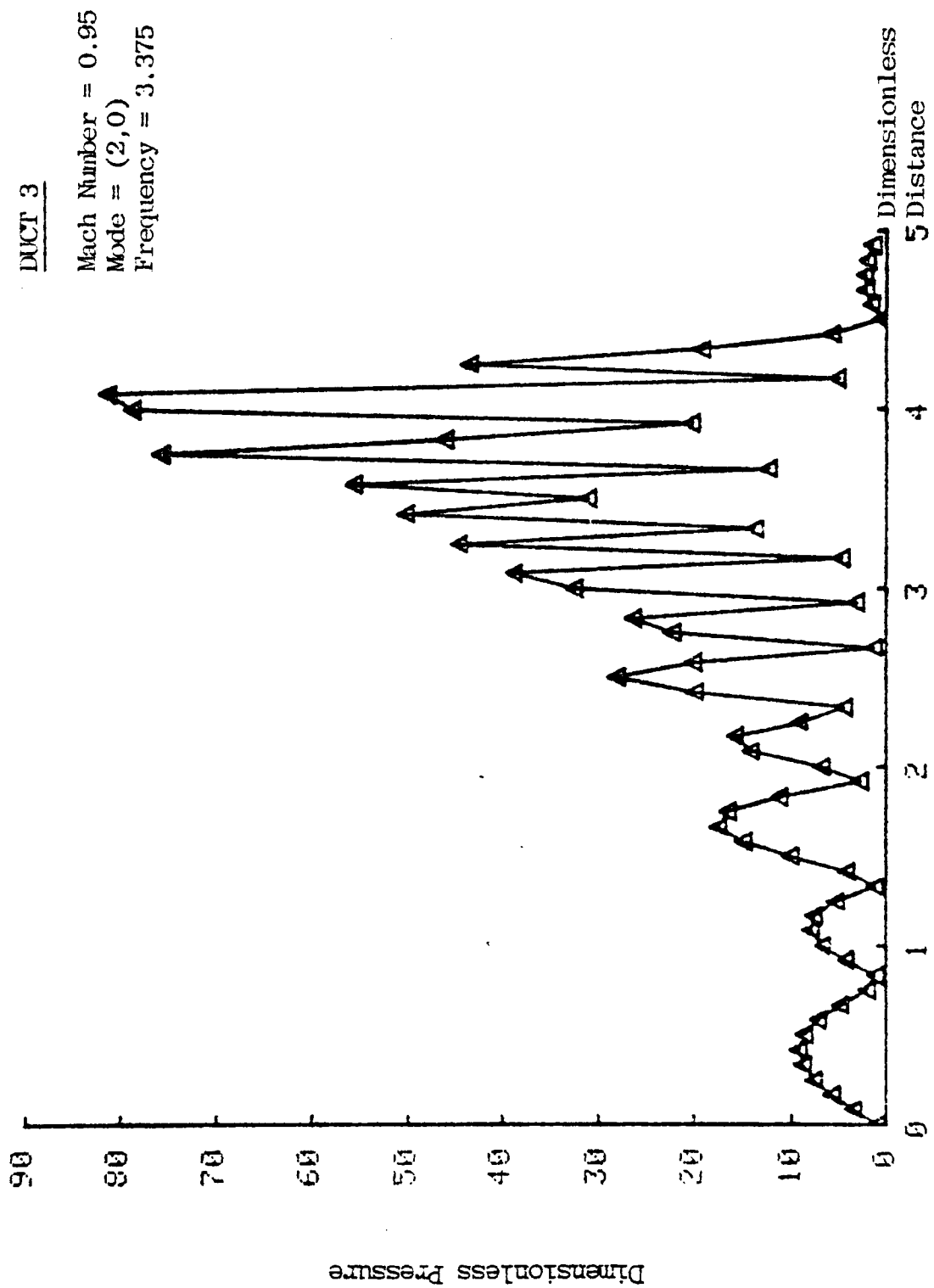


Figure VII.60 Pressure Distribution Along Duct Wall
(Duct 3, Mach Num=0.95, Mode=(2,0), Freq=3.375)

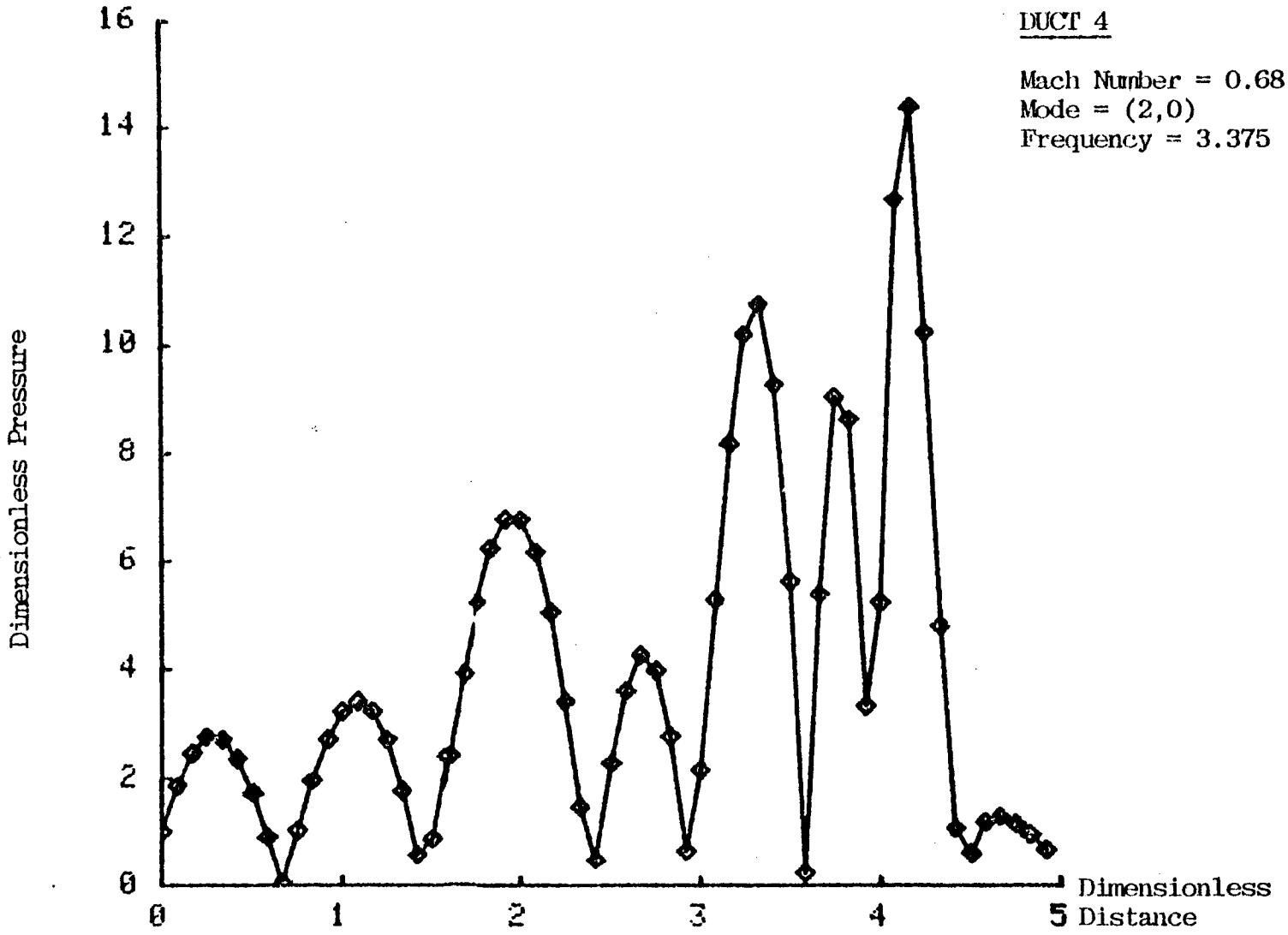


Figure VII.61 Pressure Distribution Along Duct Wall
(Duct 4,Mach Num=0.68,Mode=(2,0),Freq=3.375)

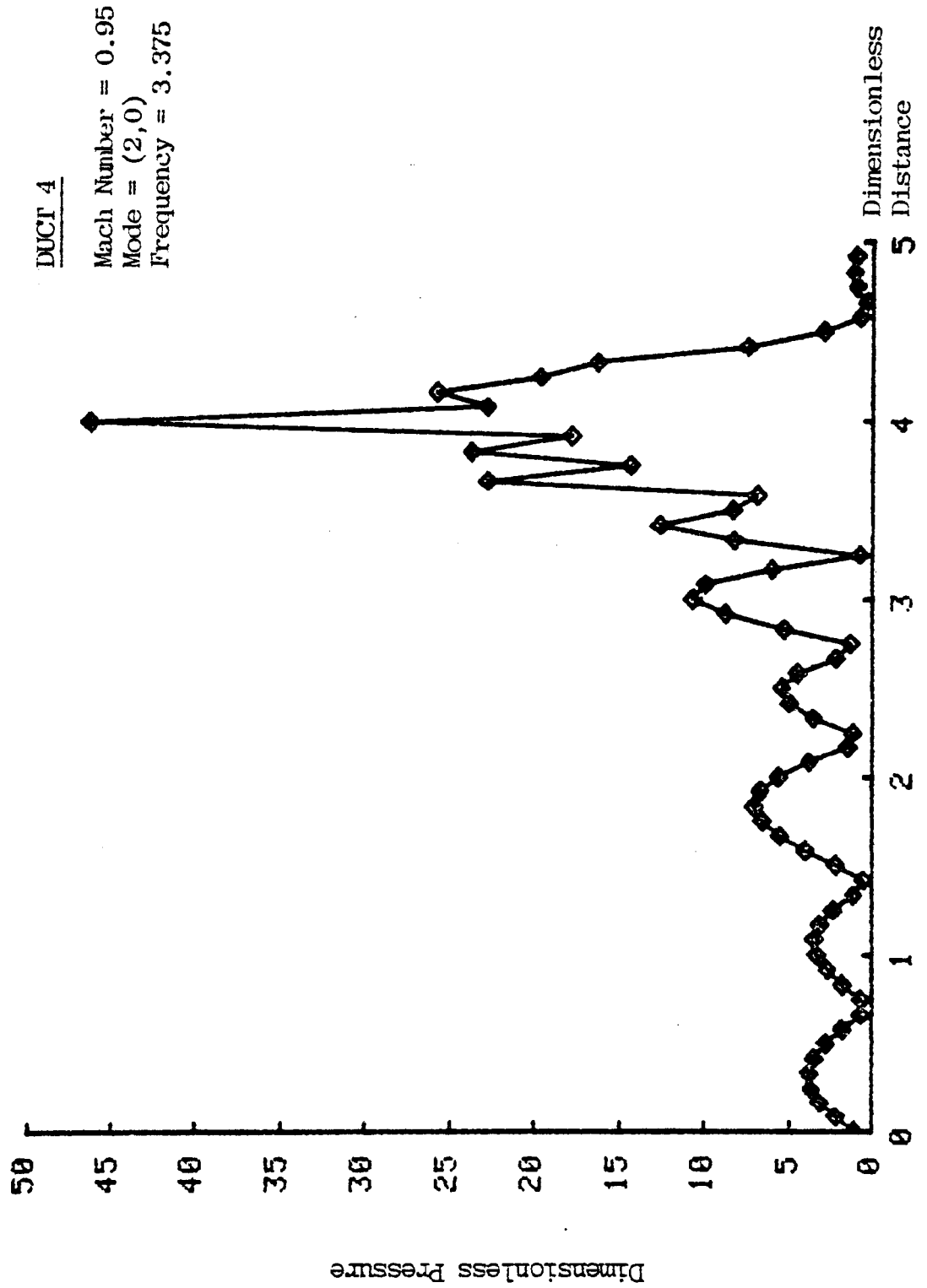


Figure VII.62 Pressure Distribution Along Duct Wall
(Duct 4, Mach Num=0.95, Mode=(2,0), Freq=3.375)

relatively stable flow and consequently the far-field sound attenuation has been higher than that of duct 4 (with velocity gradient near the throat) as can be seen in Figure VII.63.

VII.3 Conclusion

In the design of a quiet jet engine air intake, three duct geometries are considered, mild velocity gradient and steep gradients near and far from the throat area. For no flow cases, duct geometry has very little effect for the (0,0) mode and for higher order modes if the exciting frequency is above the cutoff frequency of the variable area duct. Cutoff frequency for a variable area duct is not as distinct as for a constant area duct.

A sizeable far-field attenuation is achieved when a high subsonic Mach number flow is present.

Theoretically, a steep gradient near the throat is more effective than the mild and/or the steep gradient far from the throat. Experimentally, for no flow control a mild gradient is favorable acoustically and aerodynamically.

The effective wave length depends on throat Mach numbers as well as duct geometries.

Implementing finite element techniques to solve the general wave equation proved to be accurate, reliable and efficient.

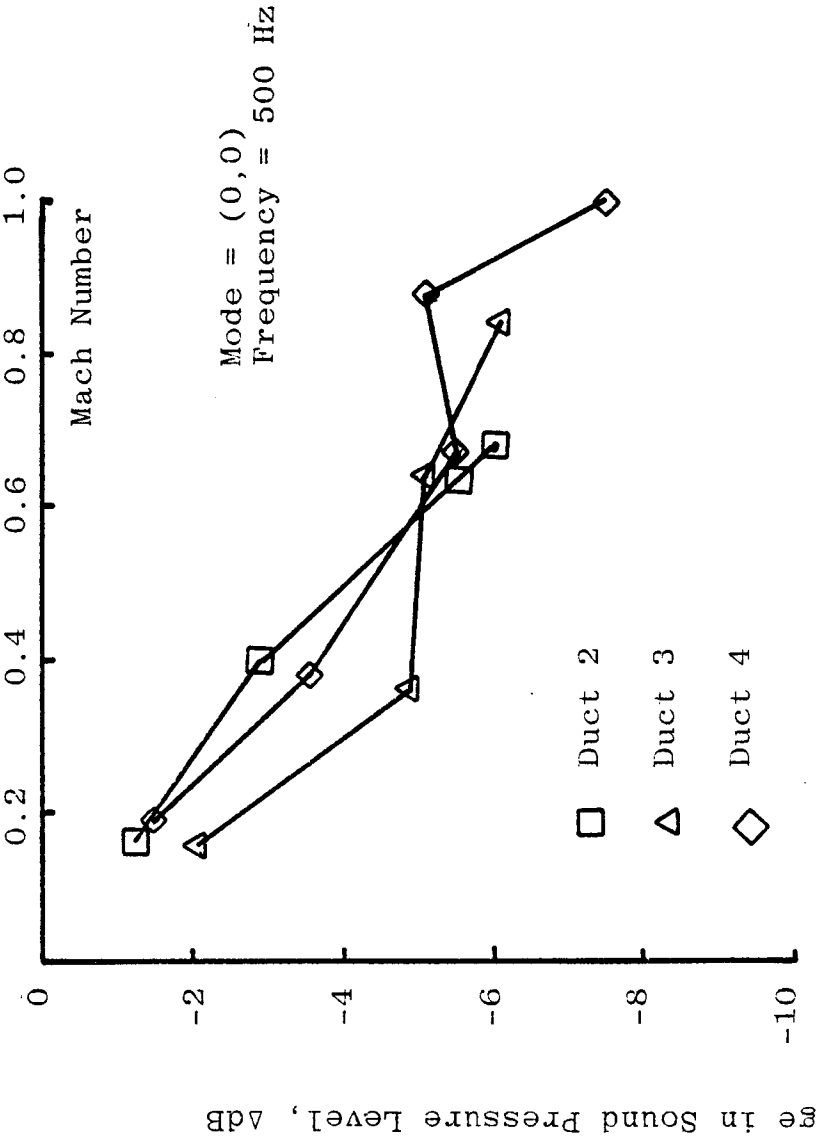


Figure VII.63 Comparison of Sound Attenuation Due to Flow for Three Inlets

VII.4 Recommendations for Future Work

Possible future work may include the following:

1. Eight node curved isoparametric elements can be introduced to improve accuracy.
2. Three-dimensional effects for the linear problem can be introduced in the finite element scheme.
3. The phenomenon of cutoff frequency in a variable area duct can be analyzed using the available finite element program.
4. The radiated field and the far-field attenuation can be coupled with the present analysis.
5. The non-linear terms eliminated in the work can be reconsidered and introduced in the analysis.
6. An axial microphone traverse is to be introduced in the experimental setup in order to better compare the near-field experimental results with numerical predictions.

REFERENCES

REFERENCES

1. Nayfeh, A., Kaiser, J., and Telionis, D., "Acoustics of Aircraft Engine-Duct Systems," AIAA Journal, Vol. 13, No. 2, 1975.

2. Alfredson, R. J., "A Note on the Use of the Finite Difference Method for Predicting Steady State Sound Fields," Acoustica, Vol. 28, 1973.

3. Baumeister, K. J., and Bittner, E. C., "Numerical Simulation of Noise Propagation in Jet Engine Ducts," NASA TN D-7339, 1973.

4. Baumeister, K. J., and Rice, E. J., "A Difference Theory for Noise Propagation in an Acoustically Lined Ducts with Mean Flow," AIAA Paper No. 73-1007, 1973.

5. Baumeister, K. J., "Analysis of Sound Propagation in Ducts Using the Wave Envelope Concept," NASA TN D-7719, 1974.

6. Quinn, D. W., "A Finite Difference Method for Computing Sound Propagation in Nonuniform Ducts," AIAA Paper No. 75-130, 1975.

7. Bell, W. A., Meyer, W. L., and Zinn, B. T., "An Integral Approach for Determining the Resonant Frequencies and Natural Modes of Arbitrarily Shaped Ducts," Third Interagency Symposium on University Research in Transportation Noise, University of Utah, 1975.

8. Quinn, D. W.,"An Integral Equation Method for Duct Acoustics with Varying Cross Sections and Axially Varying Impedance," AIAA Paper No. 76-495, 1976.

9. Unruh, J. F., and Eversman, W., "The Utility of the Galerkin Method for the Acoustic Transmission in an Attenuating Duct," Journal of Sound and Vibration, Vol. 23 (2), 1972.

10. Beckemeyer, R. J., and Eversman, W., "Computational Methods for Studying Acoustic Propagation in Nonuniform Waveguides," AIAA Paper No. 73-1006, 1973.

11. Eversman, W., Cook, E. L., and Beckemayer, R. J., "A Method of Weighted Residuals for the Investigation of Sound Transmission in Nonuniform Ducts without Flow," Journal of Sound and Vibration, Vol. 38 (1), 1975.

12. Eversman, W., "A Multimodal Solution for the Transmission of Sound in Nonuniform Ducts," AIAA Paper No. 76-497, 1976.

13. Watson, W., and Lansing, D. L., "A Comparison of Matrix Methods for Calculating Eigenvalues in Acoustically Lined Ducts," NASA TN D-8186, 1976.

14. Gladwell, G. M. L., "A Finite Element Method for Acoustics," 5e Congrés International D'Acoustique, Liège, France, 1965.

15. Mason, V., "The Finite Element Technique Applied to an Acoustic Damping Problem," Institute of Sound and Vibration Research Report No. 161, 1967.

16. Herting, D. N., and Joseph, J. A., "Acoustic Analysis of Solid Rocket Motor Cavities by Finite Element Method," NASA TM-X 2378, 1971.

17. Craggs, A., "The Use of Simple Three-Dimensional Acoustic Finite Elements for Determining the Natural Modes and Frequencies of Complex Shaped Enclosures," Journal of Sound and Vibration, Vol. 23 (3), 1972.

18. Craggs, A., "An Acoustic Finite Element Approach for Studying Boundary Flexibility and Sound Transmission between Irregular Enclosures," Journal of Sound and Vibration, Vol. 30 (3), 1973.

19. Craggs, A., "Some Practical Applications of Acoustic Finite Elements," Journal of Sound and Vibration, Vol. 49 (3), 1976.

20. Shuku, T. and Ishihara, K., "The Analysis of the Acoustic Field in Iregularly Shaped Rooms by the Finite Element Method," Journal of Sound and Vibration, Vol. 29 (1), 1973.

21. Davies, J. B., "Waveguides, Numerical Methods," Proc. IEEE, Vol. 119, No. 1, 1972.

22. Sigman, R. K., Majjigi, R. K., and Zinn, B. T., "Use of Finite Element Techniques in the Determination of the Acoustic Properties of Turbofan Inlets," AIAA Paper No. 77-18, 1977.

23. Abrahamson, A. L., "A Finite Element Algorithm for Sound Propagation in Axisymmetric Ducts Containing Compressible Mean Flow," AIAA Paper No. 77-1301.

24. Eversman, W., Astley, R. J., and Thanh, V. P., "Transmission in Nonuniform Ducts - A Comparative Evaluation of Finite Element and Weighted Residuals Computational Schemes," AIAA Paper No. 77-1299, 1977.

25. Lumsdaine, E., "Noise Suppression with Sonic and Near Sonic Inlets," Proceedings Second Interagency Symposium on University Research in Transportation Noise, North Carolina State University, 1974.

26. Plumblee, H. E., and Dean, P. D., "Sound Measurements within and in the Radiated Field of an Annular Duct with Flow," Journal of Sound and Vibration, Vol. 28 (4), 1973.

27. Akin, J. E., and Stoddart, W. C., "Computer Programs for Implementing the Finite Element Method," Report ESM 75-1, The University of Tennessee, 1975.

28. Baker, A. J., Finite Elements in Fluid-Thermal System Analysis, Manuscript in Preparation.

29. Segerlind, L. J., Applied Finite Element Analysis, John Wiley, 1976.

30. Sen Gupta, S. K., "A Finite Element Solution of Pucher's Equation," Ph.D. Dissertation, The University of Tennessee, 1975.

31. Strang, G. and Fix, G. J., An Analysis of the Finite Element Method, Prentice Hall, 1973.

32. Westlake, J. R., A Handbook of Numerical Matrix Inversion and Solution of Linear Equations, John Wiley, 1968.

33. Zaiser, J. N., "Non-Linear Vibrations of a Moving Threadline," Ph.D. Dissertation, University of Delaware, 1964.

34. Ames, W. F., Non-Linear Partial Differential Equations in Engineering, Academic Press, 1965.

35. Lumsdaine, E., and Ragab, S., "Effect of Flow on Quasi-One-Dimensional Acoustic Wave Propagation in a Variable Area Duct of Finite Length," Journal of Sound and Vibration, Vol. 53 (1), 1977.

36. Lumsdaine, E., "Calculation of Pressure Reflection Ratio." Journal of Sound and Vibration, Vol.52 (1), 1977.

37. Callegari, A. J., and Myers, M. K., "Non-linear Effects on Sound in Nearly Sonic Duct Flows," AIAA Paper No. 77-1296, 1977.

38. Lumsdaine, E., Cherng, J. G., and Tag, I., "Noise Suppression with High Mach Number Inlets," NASA CR-2708, 1976.

39. Lumsdaine, E., Cherng, J. G. and Tag, I., "Influence of High-Speed Flow on Sound Propagation and Radiation," to be published.

40. Carnahan, B., Luther, H. A., and Wilkes, J. O., Applied Numerical Methods, John Wiley, 1969.

APPENDIXES

APPENDIX A

THE TWO-DIMENSIONAL WAVE EQUATION

The propagation of sound in a two-dimensional rectangular duct as shown in Figure A.1 is described by a solution of the continuity and momentum equations with the appropriate boundary conditions.

A. Governing Equation

The linearized continuity equation takes the form

$$\frac{\partial p'}{\partial t} + U\left(\frac{\partial p'}{\partial x}\right) + \varsigma C^2\left[\left(\frac{\partial u'}{\partial x'}\right) + \frac{\partial v'}{\partial y'}\right] = 0 \qquad (A.1)$$

The linearized momentum equation in the x and y directions can be written as

x - Momentum

$$\left(\frac{\partial u'}{\partial t}\right) + U\left(\frac{\partial u'}{\partial x}\right) = -\frac{1}{\varsigma}\left(\frac{\partial p'}{\partial x'}\right) \qquad (A.2)$$

y - Momentum

$$\frac{\partial v'}{\partial t} + U\left(\frac{\partial v'}{\partial x'}\right) = \frac{1}{\varsigma}\left(\frac{\partial p'}{\partial y'}\right) \qquad (A.3)$$

For steady state conditions, upon introducing harmonic time dependency, we have

$$p'(x,y,t) = p'_o(x,y)e^{i\omega t} \qquad (A.4)$$

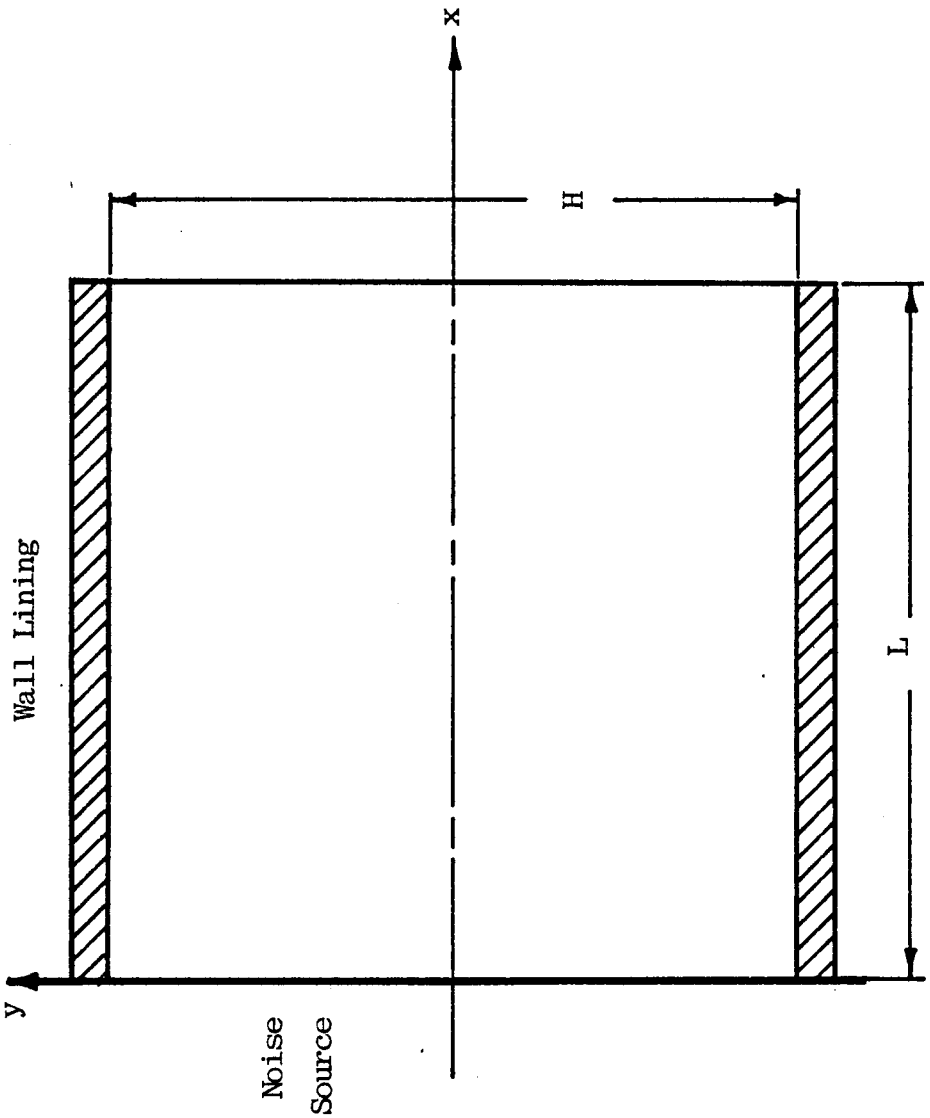


Figure A.1 Two-Dimensional Duct with Lining

$$u'(x',y',t) = u'_o(x',y')e^{i\omega t} \tag{A.5}$$

$$v'(x',y',t) = v'_o(x',y')e^{i\omega t} \tag{A.6}$$

Introducting the dimensionless quantities

$$p = \frac{p'_o}{p_A} \tag{A.7}$$

$$u = (\frac{\zeta\omega H}{p_A})u'_o \tag{A.8}$$

$$v = (\frac{\zeta\omega H}{p_A})v'_o \tag{A.9}$$

$$x = \frac{x'}{H} \tag{A.10}$$

$$y = \frac{y'}{H} \tag{A.11}$$

and substitution of Equations (A.4) - (A.11) into Equations (A.1) - (A.3) yields

$$p - (\frac{iM}{2\pi\eta})(\frac{\partial p}{\partial x}) - \frac{i}{(2\pi\eta)^2}[\frac{\partial u}{\partial x} + \frac{\partial v}{\partial y}] = 0 \tag{A.12}$$

$$u = i(\frac{\partial p}{\partial x}) + (\frac{iM}{2\pi\eta})(\frac{\partial u}{\partial x}) \tag{A.13}$$

$$v = i(\frac{\partial p}{\partial y}) + (\frac{iM}{2\pi\eta})(\frac{\partial v}{\partial x}) \tag{A.14}$$

where η is the dimensionless frequency defined as

$$\eta = (\frac{H}{2\pi})(\frac{\omega}{C}) = \frac{Hf}{C} \tag{A.15}$$

Substitution of Equations (A.13) and (A.14) into Equation (A.12) gives,

$$(1-M^2)\left(\frac{\partial^2 p}{\partial x^2}\right) + \left(\frac{\partial^2 p}{\partial y^2}\right) - 2i(2\pi\eta)M\left(\frac{\partial p}{\partial x}\right) + (2\pi\eta)^2 p = 0 \qquad (A.16)$$

Equation (A.16) describes the dimensionless acoustic pressure in a constant area duct carrying uniform mean flow.

B. Boundary Conditions

1. At the sound source, and for a uniform acoustic pressure profile, one writes

$$p(0,y) = 1. \qquad (A.17)$$

2. At duct termination x = L/H, the no reflection boundary condition with a ζC exit impedance can be derived from the x-momentum equation, Equation (A.13):

$$Z = \frac{p'_o}{u'_o} = \zeta C \qquad (A.18)$$

Introducing Equations (A.7) and (A.8) gives,

$$\frac{p}{u} = \frac{1}{2\pi\eta} \qquad (A.19)$$

Using Equation (A.19) into Equation (A.13) yields

$$\frac{\partial p}{\partial x} = -i\,\frac{2\pi\eta}{1+M}\,p \qquad (A.20)$$

Equation (A.20) is a gradient boundary condition.

3. At the wall, for no lining,

$$\frac{\partial p}{\partial y} = 0 \tag{A.21}$$

Equation (A.21) is a natural boundary condition.

C. Axial Acoustic Intensity

The non-dimensional acoustic intensity takes the form

$$I = \frac{2\zeta C}{p_A^2} I' = \text{Real} \left\{ \frac{p^* u}{2\pi\eta} + \frac{M}{2} \left[p^* p + \frac{1}{(2\pi\eta)^2} (u^* u + v^* v) \right] \right\} \tag{A.22}$$

For no flow cases,

$$I = \frac{1}{2\pi\eta} \text{Real} \{p^* u\} \tag{A.23}$$

D. Acoustic Power

The total dimensionless acoustic power is defined as

$$E_x = \int_0^1 I(x,y)dy \tag{A.24}$$

E. Sound Attenuation

By definition, sound attenuation between two stations x = 0 and x takes the form

$$\Delta db = 10 \log_{10}\left(\frac{E_x}{E_o}\right) \qquad (A.25)$$

APPENDIX B

SOME ASPECTS OF THE CALCULUS OF VARIATION

In a multidimensional space (n) Euler-Lagrange equation can be written as

$$\sum_{i=1}^{n} \frac{\partial}{\partial x_i} \left(\frac{\partial f}{\partial w_{,i}}\right) - \frac{\partial f}{\partial w} - 0 \qquad \text{(B.1)}$$

where

w is the solution of the given differential equation.

$w_{,i}$ is the gradient of w in the x_i direction.

Equation (B.1) is the partial differential for w that can be expressed in terms of the functional $f(x_i, w, w_{,i})$ which extremizes the integral

$$I = \int_R f(x_i, w, w_{,i}) d\tau \qquad \text{(B.2)}$$

in the domain R and the closure ∂R when $w(x_i)$ is known everywhere on the closure.

Generalizing Equation (B.2) to account for normal derivative which is constrained by

$$\bar{f}(\bar{x}_i, w, w_{,i}) = 0 \qquad \text{(B.3)}$$

and introducing Lagrange multiplier λ, the integral (B.2) can be written as

$$I = \int_R f(x_i, w, w_{,i}) d\tau - \lambda \int_{\partial R_1} g(\bar{x}_i, w, w_{,i}) d\sigma \tag{B.4}$$

Extremizing (B.4) with respect to $w(x_i)$ yields that the function which extremizes (B.4) satisfies the Euler-Lagrange equation and in addition satisfies the relation

$$\int_{\partial R_1} \left(\frac{\partial f}{\partial w_{,i}} + \lambda \frac{\partial g}{\partial w}\right) \cdot n_i d\sigma = 0 \tag{B.5}$$

on ∂R_1 of ∂R where Equation (B.3) applies i.e.,

$$\bar{f}(\bar{x}_i, w, w_{,i}) = \frac{\partial f}{\partial w_{,i}} + \lambda \frac{\partial g}{\partial w} \tag{B.6}$$

On the remainder ∂R_2 of ∂R the dependent variable satisfies the equation

$$w(\bar{x}_i) = C \tag{B.7}$$

where C is a specified constant.

Equation (B.6) determines an appropriate value for λ.

Given $p(x_i)$ to be the solution in R to the equation

$$\nabla^2 p + (2\pi\eta)^2 p = 0 \tag{B.8}$$

and on ∂R_1 satisfies

$$p_n + \frac{i(2\pi\eta)}{Z} p = 0 \tag{8.9}$$

while on ∂R_2 the acoustic pressure is fixed as

$$p(\bar{x}_i) = p_b \tag{B.10}$$

where p is complex, then the functionals f and g are determined by inspection as

$$f(x_i,p) = \frac{1}{2} (\nabla p \cdot \nabla p) - \frac{1}{2} (2\pi\eta)^2 p^2 \tag{B.11}$$

$$g(\bar{x}_i,p) = \frac{1}{2} i \frac{(2\pi\eta)}{Z} p^2 \tag{B.12}$$

and

$$\lambda = 1$$

Functional I in Equation (B.4) can be written as

$$I = \int_R \{\nabla p \cdot \nabla p - (2\pi\eta)^2 p^2\} d\tau + \frac{i(2\pi\eta)}{Z} \int_{\partial R_1} p^2 d\sigma \tag{B.13}$$

Equation (B.13) is the three-dimensional variational statement for the acoustic equation.

APPENDIX C

SOME RESULTS FOR RIGHT ANGLE AND CIRCULAR BENDS OF RECTANGULAR CROSS SECTIONS

The problem of predicting steady state sound fields in circular bends and/or right angle bends in a hard or soft wall rectangular duct carrying no mean flow is considered and solved using the present finite element techniques. Results are presented in this appendix to illustrate the versatility of the finite element methods in solving the wave equation when the geometry of the sound field and/or the boundary conditions are irregular.

Figure C.1, in this appendix shows two duct geometries; circular and rectangular bends with or without wall treatment.

Figures C.2 and C.3 give the distribution of the acoustic pressure along the duct centerline, and the inner and outer walls for rectangular and circular bends with and without wall treatment. In the rectangular bend case, lining has caused appreciable attenuation at all locations and particularly at the outer wall. For the circular bend, segmented wall lining caused more attenuation at the outer wall than at the centerline or the inner wall. More studies are needed to efficiently locate the lining material in the circular bend case.

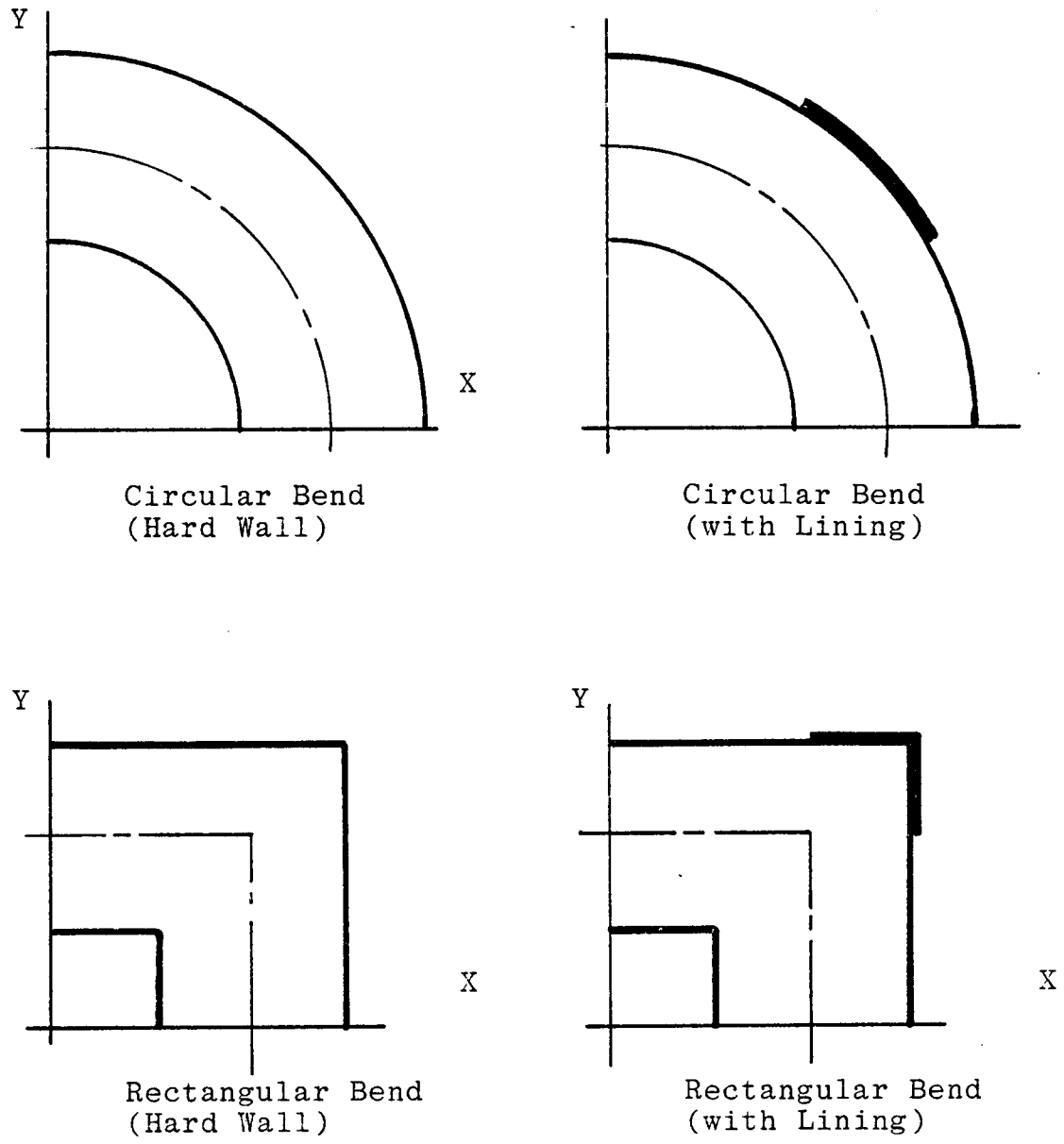


Figure C.1 Circular and Rectangular Bends with and without Lining

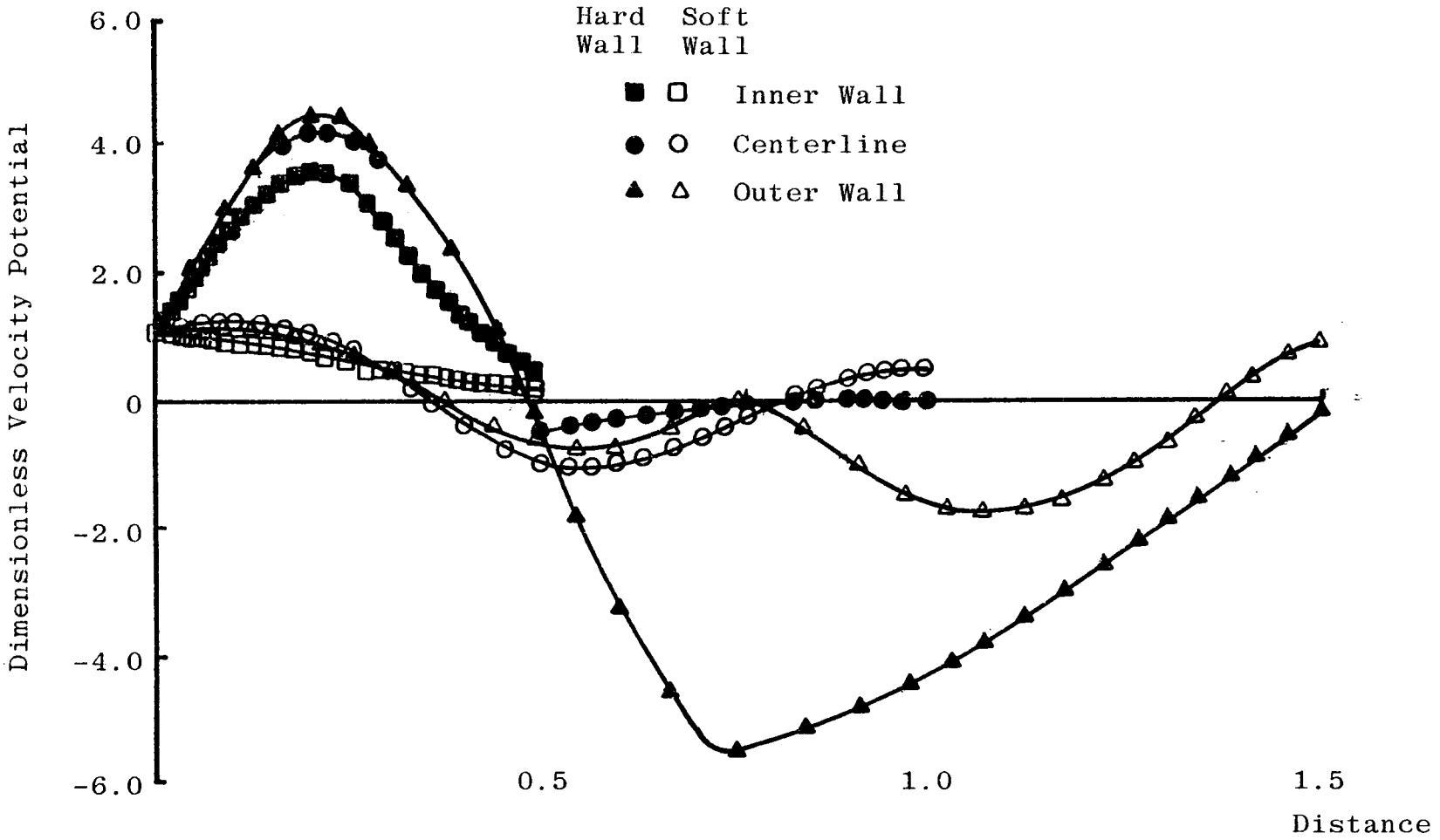


Figure C.2 Acoustic Pressure Distribution (Real Part) in a Rectangular Bend

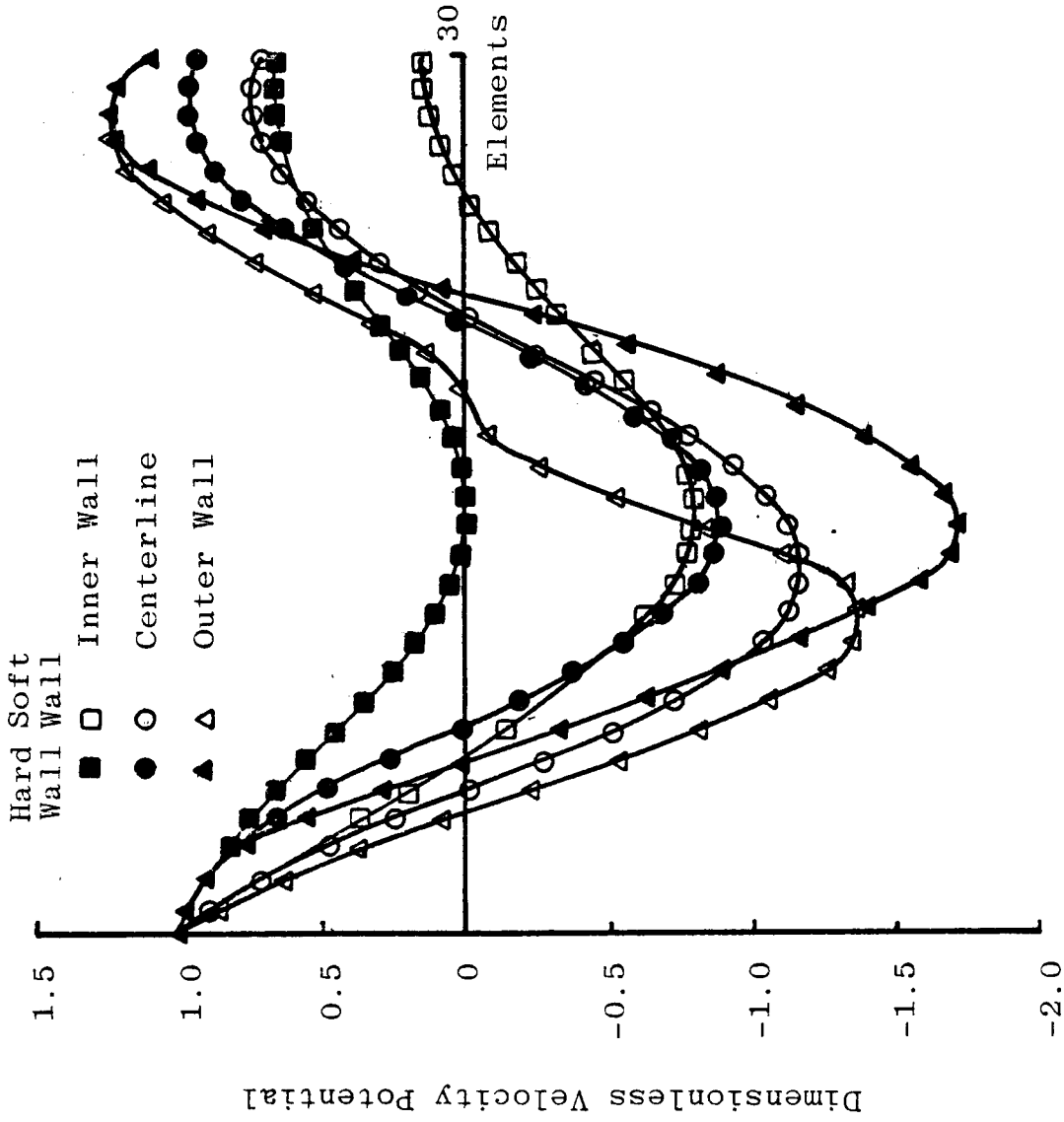


Figure C.3 Acoustic Pressure Distribution (Real Part) in a Circular Bend

APPENDIX D

DERIVATION OF THE POTENTIAL EQUATION IN A DUCT

In this appendix, the potential flow equation for a gas flowing in a duct is derived from the continuity and momentum equations along with the isentropic relationship and the assumption of irrotational flow:

Continuity equation

$$\frac{\partial \zeta'}{\partial t'} + \nabla' \cdot (\zeta' \bar{V}') = 0 \tag{D.1}$$

Momentum equation

$$\frac{\partial \bar{V}'}{\partial t'} + \frac{1}{2} \nabla'(\bar{V}' \cdot \bar{V}') + (\nabla' \times \bar{V}') \times \bar{V}' + \frac{1}{\zeta'} \nabla' p' = 0 \tag{D.2}$$

Isentropic relationship

$$\frac{p'}{\zeta'^{\gamma}} = \text{constant} \tag{D.3}$$

Irrotational condition

$$\nabla' \times \bar{V}' = 0 \tag{D.4}$$

The momentum equation reduces to

$$\frac{\partial \bar{V}'}{\partial t'} + \frac{1}{2} \nabla'(V'^2) + \frac{\nabla' p'}{\zeta'} = 0 \tag{D.5}$$

To non-dimensionalize the above equations, we introduce

$$\bar{V} = \frac{\bar{V}'}{C_o'}$$

$$t = \frac{C_o' t'}{R'}$$

$$\nabla = R'\nabla'$$

$$p = \frac{p'}{p_o'}$$

$$\zeta = \frac{\zeta'}{\zeta_o'}$$

where C_o', p_o', ζ_o' and R' are reference quantities.

Rewriting Equations (D.1) and (D.5) in non-dimensional form, we get

$$\frac{\partial \zeta}{\partial t} + \nabla \cdot (\zeta \bar{V}) = 0 \qquad \text{(D.6)}$$

and

$$\frac{\partial \bar{V}}{\partial t} + \frac{1}{2} \nabla(V^2) + \frac{\nabla p}{\gamma \zeta} = 0 \qquad \text{(D.7)}$$

The isentropic relationship becomes

$$p = \zeta^{\gamma} \qquad \text{(D.8)}$$

Since the flow is irrotational, a velocity potential can be defined such that

$$\bar{V} = \nabla \Phi \qquad \text{(D.9)}$$

Substitution in Equation (D.7) gives

$$\nabla\Phi_t + \nabla\left(\frac{V^2}{2}\right) + \frac{\nabla p}{\gamma\zeta} = 0 \qquad (D.10)$$

Introducing the isentropic relationship into Equation (D.10)

$$\frac{\nabla p}{\gamma\zeta} = \frac{1}{\gamma-1}\,\nabla(p/\zeta) \qquad (D.11)$$

Substitution of Equation (D.11) into Equation (D.10) yields

$$\nabla\left(\Phi_t + \frac{V^2}{2} + \frac{1}{\gamma-1}\,p/\zeta\right) = 0 \qquad (D.12)$$

Integrating Equation (D.12) gives

$$\Phi_t + \frac{V^2}{2} + \frac{1}{\gamma-1}\,p/\zeta = f(t) \qquad (D.13)$$

where $f(t)$ is an arbitrary function in time and can be determined from stagnation conditions

$$f(t) = \text{constant} = \frac{1}{\gamma-1}$$

Equation (D.13) can be rewritten as

$$\Phi_t + \frac{V^2}{2} + \frac{1}{\gamma-1}\,p/\zeta = \frac{1}{\gamma-1} \qquad (D.14)$$

Differentiation with respect to t gives

$$\zeta_t\Phi_t + \zeta\Phi_{tt} + \zeta_t\,\frac{V^2}{2}$$

$$+ \zeta\bar{V}\cdot\frac{\partial\bar{V}}{\partial t} + \frac{\gamma}{\gamma-1}\,\zeta^{\gamma-1}\,\zeta_t$$

$$- \frac{1}{\gamma-1}\,\zeta_t = 0 \qquad (D.15)$$

Using Equation (D.14) into Equation (D.15) gives

$$\Phi_{tt} + \frac{1}{2}\frac{\partial V^2}{\partial t} + \frac{\zeta_t}{\zeta}\frac{p}{\zeta} = 0 \tag{D.16}$$

From the continuity equation and using the relation $\nabla \cdot (\zeta\bar{V}) = \bar{V} \cdot \nabla\zeta + \zeta\nabla \cdot \bar{V}$ we get

$$\frac{\zeta_t}{\zeta} = -\left(\nabla^2\Phi + \nabla\Phi \cdot \frac{\nabla\zeta}{\zeta}\right) \tag{D.17}$$

From Equation (D.8),

$$\frac{\nabla\zeta}{\zeta} = \frac{1}{\gamma}\frac{\nabla p}{p} \tag{D.18}$$

Hence, Equation (D.16) becomes

$$\Phi_{tt} + \frac{1}{2}\frac{\partial V^2}{\partial t} - \frac{p}{\zeta}\left(\nabla^2\Phi + \nabla\Phi \cdot \frac{\nabla p}{\gamma p}\right) = 0$$

or

$$\Phi_{tt} + \frac{1}{2}\frac{\partial V^2}{\partial t} - \frac{p}{\zeta}\nabla^2\Phi - \nabla\Phi \cdot \frac{\nabla p}{\gamma\zeta} = 0 \tag{D.19}$$

From the momentum equation and Equation (D.14),

$$\nabla^2\Phi - \Phi_{tt} = 2\nabla\Phi \cdot \nabla\Phi_t + \frac{1}{2}(\gamma-1)\nabla^2\Phi(\nabla\Phi \cdot \nabla\Phi)$$

$$+ (\gamma-1)\nabla^2\Phi\Phi_t + \frac{1}{2}\nabla\Phi \cdot \nabla(\nabla\Phi \cdot \nabla\Phi) \tag{D.20}$$

Equation (D.20) is the non-linear potential flow equation for a gas in a duct.

Equation (D.20) can be rewritten in the more familiar form

$$C^2\nabla^2\Phi = \Phi_{tt} + 2\nabla\Phi \cdot \nabla\Phi_t + \frac{1}{2}\nabla\Phi \cdot \nabla(\nabla\Phi \cdot \nabla\Phi) \qquad (D.21)$$

where

$$C^2 = 1 - (\gamma-1)[\Phi_t + \frac{1}{2}(\nabla\Phi \cdot \nabla\Phi)]$$

and is defined as the local speed of sound.

APPENDIX E

INSTRUCTIONS FOR USING THE FINITE ELEMENT COMPUTER PROGRAM AND A PROGRAM LISTING

In this appendix, input statements (READ statements) of the computer program are explained along with the FORMAT statements for the input data. The computer program is a FORTRAN IV program prepared to be implemented on the IBM 360 Model 65 computer. The program consists of a main routine and several subroutines.

Input Data and Format:

The following are the input data contained in each data card together with the reading FORMAT used.

Card No. 1 (Acoustic Parameters)

Column	1-5	6-10	11-20
Format	I5	I5	F10.5
Variable	NCASE	MODE	FREQCY

NCASE = IF 0 one and two-dimensional cases

IF 1 axisymmetric cases

MODE = Mode number 0, 1, 2, ..., m

FREQCY = Noise source dimensionless frequency

Card No. 2 (Mesh Data Parameters)

Column	1-5	6-10	11-15	16-20	21-25	26-30	31-35
Format	←			(7I5)			→
Variable	M	NE	NG	N	NSPACE	NSEG	LBN

M = Number of nodes

NE = Number of elements

NG = Number of degrees of freedom per node

N = Number of nodes per element

NSPACE = Dimension of space

NSEG = Number of boundary segments where the flux boundary condition is present

LBN = Number of nodes on a boundary segment

Card No. 3 (Steady Flow Parameters)

Column	1-10	11-20	21-30
Format	←(3F10.5)→		
Variable	FLOW	PRESS	TEMP

FLOW = Rate of mass flow in the duct lb_m/sec

PRESS = Stagnation pressure lb_f/in^2

TEMP = Stagnation temperatue °R

Card No. 4 (Mesh Generator Data)

Column	1-5	6-10
Format	I5	I5
Variable	NROW	NCOL

NROW = Number of rows across duct centerline and wall

NCOL = Number of columns along duct centerline

Card No. 5

Column	1-10	11-20	21-30	31-40	...	...	71-80
Format	←		(8F10.5)				→
Variable	DL	DH(1)	DH(2)	DH(3)	...	...	DH(NCOL)

DL = Non-dimensional duct length

DH(1), DH(2), ..., DH(NCOL)

= Non-dimensional duct heights or radii at NCOL points

Additional cards of the same format as Card No. 5 are needed, depending on the value of NCOL.

Card No. 6 (Flux Boundary Condition Data)

Column	1-5	6-10	...	76-80
Format	←	(16I5)		→
Variable	LNODE(1)	LNODE(2)	...	LNODE(LBN)

LNODE(1), LNODE(2), ..., LNODE(LBN)

= the LBN incidences of boundary segment

Additional cards of the same format as that of Card No. 6 are needed for each boundary segment ISEG = 1, 2, ..., NSEG.

Card No. 7 (Flux Values)

Column	1-10	11-10	21-30	31-40
Format	←	(4F10.4)		→
Variable	FLUX(1,1)	FLUX(1,2)	FLUX(2,1)	FLUX(2,2)

FLUX(1,1), FLUX(1,2)

= Specified components of flux at the first boundary node (real part of impedance ratio)

FLUX(2,1) FLUX(2,2)

= Specified components of the flux at the second boundary node (imaginary part of impedance ratio)

Additional cards of the same format as Card No. 7 are needed for each boundary segment ISEG = 1, 2, ..., NSEG.

A listing of the finite element program is included at the end of this appendix.

```
      COMPLEX ZD
      DIMENSION ZD(15000)
      DIMENSION AD(15000)
      DIMENSION ID(9000)
      KCOMPX=15000
      KFLOAT=15000
      KFIXED=9000
      CALL MODEL (KCOMPX,KFLOAT,KFIXED,ZD,AD,ID)
      STOP
      END



      SUBROUTINE MODEL (KCOMPX,KFLOAT,KFIXED,ZD,AD,ID)
      COMPLEX ZD
      DIMENSION ZD(KCOMPX)
      DIMENSION AD(KFLOAT)
      DIMENSION ID(KFIXED)
      CALL ZEROZ (KCOMPX,ZD)
      CALL ZERO (KFLOAT,KFIXED,AD,ID)
      READ(5,1100) NCASE,MODE,FREQCY
 1100 FORMAT (2I5,F10.5)
      WRITE (6,2300)
 2300 FORMAT ('    ACOUSTIC DATA'/'    ************'//)
      WRITE(6,2200)NCASE,MODE,FREQCY
 2200 FORMAT ('     CASE = ',I5,'  IF ZERO TWO DIMENSIONAL , ONE AXISYMME
     1TRIC '/'     MODE = ( ',I2 ,',0)'/'     FREQCY= ',F10.4///)
      READ (5,1000) M,NE,NG,N,NSPACE,NSEG,LBN
 1000 FORMAT (7I5)
      WRITE(6,2400)
 2400 FORMAT ('    MESH AND DEGREES OF FREEDOM DATA'/'    ***************
     1****************'//)
      WRITE (6,2000) M,NE,NG,N,NSPACE,NSEG,LBN
      WRITE(6,3000)
 2000 FORMAT('    NC OF NODES = ',I5/'    NO OF ELEMENTS = ',I5/'    NO OF
     1PARAM/NODE= ',I5/'    NO OF NODES /ELEMENT= ',I5/'    DIMENSION OF S
     1PACE = ',I5/'    NO OF BOUNRY SEGMENTS =',I5/'    NO OF NODES ON A B
     1OUNDRY SEGMENT = ',I5)
      NGPLUS=NG+1
      NOFREE=NG*M
      NELFRE=N*NG
      CALL POINTR (M,N,NE,NG,NELFRE,NOFREE,NSPACE,LBN,NSEG,N1,N2,N3,N4,
     1M1,M2,M3,M4,M5,M6,M7,M8,M9,M10)
      AMACH=0.0
      CALL INPUT (M,N,NE,NG,NELFRE,NOFREE,NSPACE,ID(N1),ID(N2),AD(M1),
     1AD(M2),AD(M5),AD(M6),AD(M7),AMACH)
      IBW=1
      CALL SYSBAN (NE,N,NG,IBW,ID(N2),ID(N3),LID)
      MAXBAN=2*IBW-1
      WRITE(6,2100) MAXBAN,LID
 2100 FORMAT ( ' EQUATION      BANDWIDTH = ' ,I5/ ' AND OCCURS IN ELEMEN
     1T NUMBER ' , I5/)
      WRITE(6,3000)
      CALL POINT       (K1,K3,K4,K5,K6,NELFRE,NOFREE,MAXBAN,K7)
      IF (NSEG.GT.0) CALL INFLUX (ZD(K1),ZD(K3),AD(M1),AD(M4),AD(M3),
     1ID(N3),ID(N4),M,NSPACE,LBN,NSEG,NELFRE,NOFREE,NG,NCASE,FREQCY
     1,MAXBAN,AMACH)
```

```
      CALL ASYMBL (ZD(K1),ZD(K3),AD(M1),AD(M4),FREQCY,M,N,NE,NG,NSPACE,
     1NELFRE,ID(N2),ID(N3),ID(N4),NDFREE,AD(M5),AD(M6),AD(M7),MODE
     1,AD(M8),AD(M9),AD(M10),NCASE,MAXBAN)
      CALL APLYBC (ZD(K3),ZD(K4),AD(M2),ID(N1),ID(N4),M,NG,NGPLUS,NELFRE
     1,NDFREE,MAXBAN)
      CALL DECOMP (ZD(K3),NDFREE,MAXBAN,ZD(K4))
      CALL SOLVE (ZD(K3),ZD(K4),ZD(K5),NDFREE,MAXBAN,IBW,ZD(K7))
      WRITE(6,3000)
 3000 FORMAT(///)
      CALL WRTPT (ZD(K5),NDFREE)
      REWIND 10
      CALL POST (NE,N,NG,NELFRE,NSPACE,NDFREE,ID(N2),ID(N3),ID(N4)
     1,ZD(K6),ZD(K5),AD(M8),AD(M5),M,FREQCY)
      RETURN
      END



      SUBROUTINE ZPRINT (A,NR,NC,IOPT)
      COMPLEX A
      DIMENSION A(1),NCOL(4)
      DO 50 J=1,NC,4
      JL1=J-1
      MAXCOL=MIN0(K,4)
      MXCLL1=MAXCOL-1
      DO 10 L=1,MAXCOL
   10 NCOL(L)=L+JL1
      WRITE(6,5000) (NCOL(N),N=1,MAXCOL)
 5000 FORMAT(' C ROW/COL ',I13,7I14)
      DO 40 N=1,NR
      NL=N+(J-1)*NR
      NH=NL+MXCLL1*NR
      IF (IOPT) 30,20,30
   20 WRITE(6,5010) N,(A(I),I=NL,NH,NR)
 5010 FORMAT(I6,8F14.5)
      GO TO 40
   30 WRITE (6,5020) N,(A(I),I=NL,NH,NR)
 5020 FORMAT (I6,8(1PE14.5))
   40 CONTINUE
   50 CONTINUE
      RETURN
      END



      SUBROUTINE POINTR (M,N,NE,NG,NELFRE,NDFREE,NSPACE,LBN,NSEG,N1,N2,
     1N3,N4,M1,M2,M3,M4,M5,M6,M7,M8,M9,M10)
      N1=1
      N2=N1+M
      N3=N2+NE*N
      N4=N3+N
      M1=1
      M2=M1+M*NSPACE
      M3=M2+M*NG
      M4=M3+LBN*NSPACE
      M5=M4+N*NSPACE
      M6=M5+M*NSPACE
```

```
      M7=M6+M*NSPACE
      M8=M7+M*NSPACE
      M9=M8+N*NSPACE
      M10=M9+N*NSPACE
      RETURN
      END



      SUBROUTINE POINT (K1,K3,K4,K5,K6,NELFRE,NOFREE,MAXBAN,K7)
      K0=0
      K1=K0+1
      K3=K1+NELFRE*NELFRE
      K4=K3+NOFREE*MAXBAN
      K5=K4+NOFREE
      K6=K5+NOFREE
      K7=K6+NOFREE
      RETURN
      END



      SUBROUTINE SYSBAN(NE,N,NG,IBW,NODES,LNODE,LMAX)
      DIMENSION  NODES(NE,N), LNODE(N)
      LMAX=1
      IBW=1
      LBW=1
      DO 20 I=1,NE
      CALL LNODES(I,NE,N,NODES,LNODE)
      CALL ELBAND(N,NG,LBW,LNODE)
      IF (LBW-IBW) 20,20,10
   10 IBW=LBW
      LMAX=I
   20 CONTINUE
      RETURN
      END



      SUBROUTINE ELBAND(N,NG,IBW,LNODE)
      DIMENSION LNODE(N)
      IBW=1
      NLESS=N-1
      DO 20 I=1,NLESS
      II=I+1
      LNI=LNODE(I)
      DO 10 J=II,N
      NEW=NG*(IABS(LNODE(J)-LNI)+1)
      IF(NEW.GT.IBW) IBW=NEW
   10 CONTINUE
   20 CONTINUE
      RETURN
      END
```

```
      SUBROUTINE INPUT (M,N,NE,NG,NELFRE,NDFREE,NSPACE,IBC,NODES,X,BC
     1,PROP1,PROP2,PROP3,AMACH)
      DIMENSION PROP1(M,NSPACE),PROP2(M,NSPACE),PROP3(M,NSPACE)
      DIMENSION IBC(M),X(M,NSPACE),NODES(NE,N),BC(M,NG)
      DIMENSION R(15),DY(10,80),DH(80)
      DIMENSION AM(80),DM(80)
      READ (5,1050) FLOW,PRESS,TEMP
 1050 FORMAT (3F10.5)
      WRITE (6,2030) FLOW,PRESS,TEMP
 2030 FORMAT('    FLOW DATA'/'    *********'//'    MASS FLOW = ',F10.4/'
     1STAG PRESS = ',F10.4/'    STAG TEMP = ',F10.4////)
      READ (5,1030) NROW,NCOL
 1030 FORMAT (2I5)
      READ (5,1040) DL,(DH(I),I=1,NCOL)
      CALL MACH (FLOW,PRESS,TEMP,NCOL,AM,DH)
      CALL SMOOTH (AM,NCOL)
      AMACH=AM(NCOL)
      DL=DL/DH(1)
      DOHH=DH(1)
      DO 200 I=1,NCOL
  200 DH(I)=DH(I)/DOHH
      BYE = 4.*ATAN(1.)
      DX=DL/(NCOL-1)
      CALL DERIVT (DX,AM,DM,NCOL)
      NROWL=NROW-1
      DO 30 I=1,NCOL
      AREA = BYE*(DH(I)**2)/(NROWL)
      DY(1,I)=SQRT(AREA/BYE)
      R(1)=DY(1,I)
      DO 30 J=2,NROWL
      JJ=J-1
      DY(J,I)=AREA/(2.*BYE*R(JJ))
      R(J)=R(JJ)+DY(J,I)
   30 CONTINUE
      DO 80 I=1,M
   80 IBC(I)=0
      DO 90 I=1,NROW
   90 IBC(I)=1
      DO 110 L=1,NG
      DO 100 J=1,M
      BC(J,L)=0.0
  100 CONTINUE
  110 CONTINUE
      DO 120 J=1,NROW
      BC(J,1)=1.
  120 CONTINUE
      K=0
      DO 50 J=1,NCOL
      SUM=0.0
      DO 40 I=1,NROW
      KK=I+K
      PROP1(KK,1)=AM(J)
      PROP1(KK,2)=0.0
      PROP2(KK,1)=DM(J)
      PROP2(KK,2)=0.0
      PROP3(KK,1)=0.0
      PROP3(KK,2)=0.0
      X(KK,1)=DX*(J-1)
```

```
      X(KK,2)=SLM
      IF (I.EQ. NROW) GO TO 40
      SUM=SUM+DY(I,J)
   40 CONTINUE
      K=KK
   50 CONTINUE
      WRITE (6,2040)
 2040 FORMAT(' NODE   IBC  X-COORD    R-COORD    B.COND     MACH-X     MACH-R
     1    D(MX)/DX  D(MR)/DR  D(MX)/DR  D(MR)/DX            '/' ****  ***
     1*******   *******   *******     ******     ******    ********  *******
     1*  ********  ********'/)
      DO 10 J=1,M
   10 WRITE(6,2010) J,IBC(J),(X(J,K),K=1,NSPACE),(BC(J,L),L=1,NG)
     1,(PROP1(J,K),K=1,NSPACE),(PROP2(J,K),K=1,NSPACE),(PROP3(J,K),K=1,
     1NSPACE)
 2010 FORMAT (2I5,(10F10.6))
      NR=NROW-1
      NN=M-NR-NROW
      K=0
      DO 70 J=1,NN,NROW
      DO 60 I=1,NR
      K=K+1
      NODES(K,1)=I-1+J
      NODES(K,2)=NODES(K,1)+NROW
      NODES(K,3)=NODES(K,2)+1
      NODES(K,4)=NODES(K,1)+1
   60 CONTINUE
   70 CONTINUE
      WRITE(6,3000)
 1010 FORMAT (2I5,(7F10.6))
      WRITE (6,2050)
 2050 FORMAT (' ELEMENT CONECTIVITY'/'  NO.   FOUR   NODES     '/'  ***
     1  ****   *****'/)
      DO 20 J=1,NE
   20 WRITE(6,2020) J,(NODES(J,K),K=1,N)
      WRITE(6,3000)
 1020 FORMAT(I5,(15I5))
 1040 FORMAT (8F10.4)
 2020 FORMAT(I5,(15I5))
 3000 FORMAT(///)
      RETURN
      END



      SUBROUTINE MACH (FLOW,P,T,N,AM,DH)
      DIMENSION AM(N),DH(N)
      CONS=0.3464*FLOW*SQRT(T)/P
      XOLD=.1
      DO 20 I=1,N
      CONST=CONS/DH(I)**2
   10 GAM=(1.+.2*(XOLD)**2)**3
      FM=CONST-XOLD/GAM
      DFM=-(GAM-1.2*(XOLD**2)*(GAM**0.666667))
      XNEW=XOLD - FM/DFM
      IF (XNEW .GE. 1.0 ) GO TO 30
      IF(ABS(XNEW-XOLD) .LE. 1.E-4) GO TO 30
      XOLD=XNEW
      GO TO 10
```

```
 30 AM(I)=XNEW
    XOLD=XNEW
20  CONTINUE
    RETURN
    END



    SUBROUTINE SMOOTH (Y ,NN)
    DIMENSION Y(NN)
    NJ=NN-1
    NK=NN-2
    B=1.666666667*(5.*Y(1)+Y(2)+Y(2)-Y(3))/10.
    C=1.66666667*(5.*Y(NN)+Y(NJ)+Y(NJ)-Y(NK))/10.
    DO 10 I=3,NN
    J=I-1
    K=I-2
    A=B
    B=0.33333333*(Y(K)+Y(J)+Y(I))
 10 Y(K)=A
    Y(NJ)=B
    Y(NN)=C
    RETURN
    END



    SUBROUTINE DERIVT (H,Y,Z,NN)
    DIMENSION Y(NN),Z(NN)
    NJ=NN-1
    NL=NN-2
    NM=NN-3
    NK=NN-4
    HH=1./(12.*H)
    YY=Y(NK)
    B=HH*(-25.*Y(1)+48.*Y(2)-36.*Y(3)+16.*Y(4)-3.*Y(5))
    C=HH*(-3.*Y(1)-10.*Y(2)+18.*Y(3)-6.*Y(4)+Y(5))
    DO 10 I=5,NN
    N1=I-1
    N2=I-2
    N3=I-3
    N4=I-4
    A=B
    B=C
    C=HH*(Y(N4)-Y(N1)+8.*(Y(N2)-Y(N3)))
10  Z(N4)=A
    A=HH*(-YY+6.*Y(NM)-18.*Y(NK)+10.*Y(NJ)+3.*Y(NN))
    Z(NN)=HH*(3.*YY-16.*Y(N4)+36.*Y(NL)-48.*Y(NJ)+25.*Y(NN))
    Z(NJ)=A
    Z(NL)=C
    Z(NM)=B
    RETURN
    END
```

```
      SUBROUTINE ZERO (N1,N2,A,I)
      DIMENSION A(N1),  I(N2)
      DO 10 J=1,N1
   10 A(J)=0.0
      DO 20 J=1,N2
   20 I(J)=0
      RETURN
      END



      SUBROUTINE ZEROZ (N,Z)
      COMPLEX Z
      DIMENSION Z(N)
      DO 10 J=1,N
   10 Z(J)=(0.0,0.0)
      RETURN
      END



      SUBROUTINE INFLUX (S,SS,X,COORD,FLUX,LNODE,INDEX,M,NSPACE,LBN,NSEG
     1,NELFRE,NDFREE,NG,NCASE,FREQCY,MAXBAN,AMACH)
      COMPLEX S,SS
      DIMENSION S(2,2),SS(NDFREE,MAXBAN),X(M,NSPACE),
     1FLUX( LBN,NSPACE),LNODE(LBN),INDEX(LBN)
      DIMENSION COORD (LBN,NSPACE)
      NFLUX=LBN*NG
      WRITE (6,2060)
 2060 FORMAT ('     BOUNDARY FLUX AND IMPEDANCE'/'     ******** **** *** *
     1********'/)
      DO 30 ISEG=1,NSEG
      READ(5,1030) (LNODE(L),L=1,LBN)
 1030 FORMAT (16I5)
      READ (5,1040)((FLUX(K,IS),IS=1,NSPACE),K=1,LBN)
 1040 FORMAT(8F10.4)
      WRITE(6,2030) ISEG,(LNODE(L),L=1,LBN)
 2030 FORMAT(1218)
      DO 5 L=1,LBN
    5 WRITE(6,2040)  (FLUX(L,IS),IS=1,NSPACE),AMACH
 2040 FORMAT(6F15.4)
      DO 20 L=1,LBN
      K=LNODE(L)
      IF(K.GT.M) WRITE(6,2050)
 2050 FORMAT('   DATA ERROR IN SUBROUTINE INFLUX  ')
      DO 10 IS=1,NSPACE
   10 COORD(L,IS)= X(K,IS)
   20 CONTINUE
      CALL BFLUXS (FLUX,COORD,LBN,NSPACE,NFLUX,NG,S,AMACH,FREQCY,NCASE)
      CALL INDXEL (LBN,NFLUX,NG,LNODE,INDEX)
      CALL STRBND (NDFREE,NFLUX,MAXBAN,INDEX,S,SS)
   30 CONTINUE
      RETURN
      END
```

```
      SUBROUTINE BFLUXS (FLUX,COORD,LBN,NSPACE,NFLUX,NG,S,AMACH,FREQCY
     1,NCASE)
      COMPLEX S,CONS
      DIMENSION S(2,2),FLUX(LBN,NSPACE),COORD(LBN,NSPACE),SB(2,2)
      DATA SB/2.0,1.0,1.0,2.0/
      GAMMA=1.4
      SPEED=(1.-((GAMMA-1.)/2.)*AMACH**2)**.5
      R=((COORD(1,2)+COORD(2,2))/2.)**2
      IF(NCASE.EQ.0) R=1.0
      DX=COORD(2,1)-COORD(1,1)
      DY=COORD(2,2)-COORD(1,2)
      DL=(DX*DX+DY*DY)**.5
      F=FREQCY/SPEED
      Z1=(FLUX(1,1)+FLUX(1,2))/2.
      Z2=(FLUX(2,1)+FLUX(2,2))/2.
      ZM1=Z1+AMACH
      A=F*(1.-AMACH**2)*Z2/(Z1**2 + Z2**2)
      B=F*(1.-AMACH**2)*ZM1/(ZM1**2 + Z2**2)
      C1=R*A*DL/6.
      C2=R*B*DL/6.
      CONS=CMPLX(C1,C2)
      DO 20 J=1,2
      DO 10 I=1,2
   10 S(I,J)=CONS*SB(I,J)
   20 CONTINUE
      RETURN
      END



      SUBROUTINE INDXEL (N,LEMFRE,NG,LNODE,INDEX)
      DIMENSION INDEX(LEMFRE),LNODE(N)
      DO 20 K=1,N
      NGNM1=NG*(LNODE(K)-1)
      NGKM1=NG*(K-1)
      DO 10 IG=1,NG
      IELM=NGKM1+IG
   10 INDEX(IELM)=NGNM1 + IG
   20 CONTINUE
      RETURN
      END



      SUBROUTINE STRBND (NDFREE,NELFRE,IBW,INDEX,S,SS)
      COMPLEX S,SS
      DIMENSION S(NELFRE,NELFRE),SS(NDFREE,IBW),INDEX(NELFRE)
      DO 10 L=1,NELFRE
      I=INDEX(L)
      DO 10 K=1,NELFRE
      J=INDEX(K)
      JJ=((IBW+1)/2) + J - I
      SS(I,JJ)=SS(I,JJ) + S(L,K)
   10 CONTINUE
```

```
      RETURN
      END



      SUBROUTINE ASYMBL (S,SS,X,COORD,FREQCY,M,N,NE,NG,NSPACE,NELFRE,
     1NODES,LNODE,INDEX,NOFREE,PROP1,PROP2,PROP3,MODE,SPEED,DSPEED,
     1DSPEEC,NCASE,MAXBAN)
      COMPLEX S,SS
      DIMENSION NODES(NE,N),LNODE(N),INDEX(NELFRE),X(M,NSPACE),COORD(N,
     1NSPACE),S(NELFRE,NELFRE),SS(NOFREE,MAXBAN)
     1,PROP1(M,NSPACE),PROP2(M,NSPACE),PROP3(M,NSPACE),SPEED(N,NSPACE)
     1,DSPEED(N,NSPACE),DSPEEC(N,NSPACE)
      DO 10 IE=1,NE
      CALL LNODES (IE,NE,N,NODES,LNODE)
      CALL ELCORD (IE,M,N,NSPACE,X,COORD,LNODE)
      CALL ELCORD (IE,M,N,NSPACE,PROP1,SPEED ,LNODE)
      CALL ELCORD (IE,M,N,NSPACE,PROP2,DSPEED,LNODE)
      CALL ELCORD (IE,M,N,NSPACE,PROP3,DSPEEC,LNODE)
      CALL INDXEL (N,NELFRE,NG,LNODE,INDEX)
      CALL ELSC (N,NELFRE,NSPACE,COORD,SPEED,DSPEED,DSPEEC,FREQCY,S,MODE
     1,NCASE)
      CALL STRBNC (NOFREE,NELFRE,MAXBAN,INDEX,S,SS)
   10 CONTINUE
      RETURN
      END



      SUBROUTINE LNODES (LIC,NE,N,NODES,LNODE)
      DIMENSION NODES(NE,N), LNODE(N)
      DO 10 I=1,N
   10 LNODE(I)=NODES(LIC,I)
      RETURN
      END



      SUBROUTINE ELCORD (LIC,M,N,NSPACE,X,COORD,LNODE)
      DIMENSION X(M,NSPACE),COORD(N,NSPACE),LNODE(N)
      DO 20 I=1,N
      LNI=LNODE(I)
      DO 10 K=1,NSPACE
   10 COORD(I,K)=X(LNI,K)
   20 CONTINUE
      RETURN
      END



      SUBROUTINE ELSC (N,NELFRE,NSPACE,COORD,SPEED,DSPEED,DSPEEC,FREQCY,
     1S,MODE,NCASE)
      COMPLEX S
```

```
      COMPLEX D,E,G
      DIMENSION S(NELFRE,NELFRE),AJ(2,2),AJINV(2,2),DELTA(2,4),GLOBAL(2
     1,4),H(4),GPT(4),GWT(4),U(16),V(16),WT(16),COORD(N,NSPACE)
     1,SPEED(N,NSPACE),DSPEED(N,NSPACE),DSPEEC(N,NSPACE),UV(2),DUV(2),
     1DUVC(2),XY(2)
      GAMMA=1.4
      NQP=2
      LSQ=NELFRE*NELFRE
      CALL  GAUSCC (NQP,GPT,GWT)
      NIP = NQP*NQP
      K = 0
      DO 20  I = 1,NQP
      DO 10  J = 1,NQP
      K = K + 1
      WT(K) = GWT(I)*GWT(J)
      U(K) = GPT(J)
   10 V(K) = GPT(I)
   20 CONTINUE
      CALL ZEROZ (LSQ,S)
      WRITE (10) NIP
      DO 60  IP = 1,NIP
      CALL  DER4Q (U(IP),V(IP),DELTA)
      CALL  JACOB (N,NSPACE,DELTA,COORD,AJ)
      CALL  I2BY2 (AJ,AJINV,DET)
      DETWT = DET*WT(IP)
      CALL  GDERIV (NSPACE,N,AJINV,DELTA,GLOBAL)
      CALL SHP4C (U(IP),V(IP),H)
      CALL MMULT(H,COORD,XY,1,N,NSPACE)
      WRITE(10)       XY,GLOBAL
      R=XY(2)*XY(2)
      IF(NCASE.EQ.0) R=1.
      CALL MMULT (H,SPEED ,UV  ,1,N,NSPACE)
      CALL MMULT (H,DSPEED,DUV ,1,N,NSPACE)
      CALL MMULT (H,DSPEEC,DUVC,1,N,NSPACE)
      SPE=(1.-((GAMMA-1.)/2.)*(UV(1)**2+UV(2)**2))**.5
      F=FREQCY/SPE
      MODES=MCDE*MODE
      A=R*(1.0-UV(1)**2)
      B=R*(1.0-UV(2)**2)
      C=R*UV(1)*UV(2)
      D1=R*(-2.4*DUV(1)*UV(1) -2.*DUVC(1)*UV(2)-.4*DUVC(2)*UV(1)
     1-(.4*UV(1)*UV(2))/R**.5)
      D2=R*F*UV(1)
      E1=R*(-2.4*DUVC(2)*UV(2)-2.*DUVC(1)*UV(1)-(.4*UV(2)**2)/R**.5
     1-.4*UV(2)*DUV(1))
      E2=R*F*UV(2)
      FMODE=MCDES
      G1=R*(F**2-FMODE/R)
      G2=R*F*.4*(DUVC(2)+UV(2)/R**.5+DUV(1))
      D=CMPLX(D1,D2)
      E=CMPLX(E1,E2)
      G=CMPLX(G1,G2)
      DO 40 J=1,N
      DO 30 I=1,N
      S(I,J)=S(I,J)+(DETWT*(A*GLOBAL(1,I)*GLOBAL(1,J)+B*GLOBAL(2,I)*
     1GLOBAL(2,J) -C*GLOBAL(1,I)*GLOBAL(2,J) -C*GLOBAL(1,J)*GLOBAL(2,I)
     1+2.*D*H(J)*GLOBAL(1,I)
     1-   E*GLOBAL(2,I)*H(J)-   E*GLOBAL(2,J)*H(I)
     1-G*H(I)*H(J)))
   30 CONTINUE
   40 CONTINUE
```

```
60 CONTINUE
   RETURN
   END



   SUBROUTINE GAUSCO (N,A,W)
   DIMENSION A(N), W(N)
   A(1)=0.577350269189626
   A(2)=-A(1)
   W(1)=1.0
   W(2)=1.C
   RETURN
   END



   SUBROUTINE  SHP4Q (R,S,H)
   DIMENSICN H(4)
   RP=1.+R
   RM=1.-R
   SP=1.+S
   SM=1.-S
   H(1)=C.25*RM*SM
   H(2)=0.25*RP*SM
   H(3)=0.25*RP*SP
   H(4)=0.25*RM*SP
   RETURN
   ENC



   SUBROUTINE DER4Q (R,S,DELTA)
   DIMENSICN DELTA (2,4)
   RP=1.+R
   RM=1.-R
   SP=1.+S
   SM=1.-S
   DELTA(1,1)=-C.25*SM
   DELTA(1,2)=0.25*SM
   DELTA(1,3)=0.25*SP
   DELTA(1,4)=-0.25*SP
   DELTA(2,1)=-C.25*RM
   DELTA(2,2)=-0.25*RP
   DELTA(2,3)=0.25*RP
   DELTA(2,4)=0.25*RM
   RETURN
   END



   SUBROUTINE JACCB (N,NSPACE,DELTA,COORD,AJ)
   DIMENSICN DELTA(NSPACE,N), COORD(N,NSPACE), AJ(NSPACE,NSPACE)
```

```
      DO 30 I=1,NSPACE
      DO 20 J=1,NSPACE
      SUM=0.0
      DO 10 K=1,N
      SUM=SUM+DELTA(I,K)*COORD(K,J)
   10 CONTINUE
      AJ(I,J)=SUM
   20 CONTINUE
   30 CONTINUE
      RETURN
      END



      SUBROUTINE I2BY2 (A,AINV,DET)
      DIMENSION A(2,2), AINV(2,2)
      DET=A(1,1)*A(2,2) - A(1,2)*A(2,1)
      AINV(1,1) = A(2,2)/DET
      AINV(1,2)=-A(1,2)/DET
      AINV(2,1)=-A(2,1)/DET
      AINV(2,2)=A(1,1)/DET
      RETURN
      END



      SUBROUTINE GDERIV (NSPACE,N,AJINV,DELTA,GLOBAL)
      DIMENSION AJINV(NSPACE,NSPACE), DELTA(NSPACE,N), GLOBAL(NSPACE,N)
      DO 30 I=1,NSPACE
      DO 20 J=1,N
      SUM=0.0
      DO 10 K=1,NSPACE
      SUM=SUM + AJINV(I,K)*DELTA(K,J)
   10 CONTINUE
      GLOBAL(I,J)= SUM
   20 CONTINUE
   30 CONTINUE
      RETURN
      END



      SUBROUTINE APLYBC (SS,CC,BC,IBC,INDEX,M,NG,NGPLUS,NELFRE,NOFREE
     1,MAXBAN)
      COMPLEX SS,CC
      DIMENSION IBC(M),BC(M,NG),SS(NOFREE,MAXBAN),CC(NOFREE),INDEX(NG)
      DO 20 J=1,M
      CALL INDXPT (J,NG,INDEX)
      DO 10 IG=1,NG
      IF(IBC(J).NE.IG.AND.IBC(J).NE.NGPLUS) GO TO 10
      BCC=BC(J,IG)
      INDX=INDEX(IG)
      CALL MODIFY (SS,CC,NOFREE,MAXBAN,INDX,BCC)
   10 CONTINUE
   20 CONTINUE
```

```
      RETURN
      END



      SUBRCUTINE INDXPT (IPT,NG,INDEX)
      DIMENSICN INDEX (NG)
      NGIM1=NG*(IPT-1)
      DO 10 J=1,NG
   10 INDEX(J)=NGIM1 + J
      RETURN
      END



      SUBROUTINE MODIFY (SS,CC,NDFREE,MAXBAN,L1,BCC)
      COMPLEX SS,CC
      DIMENSICN SS(NDFREE,MAXBAN),CC(NDFREE)
      MBW=(MAXBAN+1)/2
      M1=MINO (L1,MBW)-1
      IF(M1.LT.1) GO TO 20
      DO  10  I=1,M1
      IROW=L1-I
      ICOL=I+MBW
      CC(IROW)=CC(IROW) - SS(IROW ,ICOL)*CMPLX(BCC,0.0)
   10 SS(IROW,ICOL)=(0.0,0.0)
   20 M1=MINO ((NDFREE+1-L1),MBW)
      DO 30 I=1,M1
      IROW=L1-1+I
      ICOL=I+MBW-1
      JCOL=MBW-I+1
      CC(IROW)=CC(IROW) - SS(IROW ,JCOL)*CMPLX(BCC,0.0)
      SS(IROW,JCOL)=(0.0,0.0)
   30 SS(L1,ICOL)=(0.0,0.0)
      DO 40 J=1,MAXBAN
   40 SS(L1,J)=(0.0,0.0)
      SS(L1,MBW)=(1.0,0.0)
      CC(L1)=CMPLX(BCC,0.0)
      RETURN
      END



      SUBROUTINE DECOMP (SS,NP,NBW,CC)
      COMPLEX SS
      COMPLEX CC
      DIMENSICN SS(NP,NBW)
      DIMENSICN CC(NP)
      NP1=NP-1
      NB=(NBW+1)/2
      DO 20 I=1,NP1
      MJ=I+NB-1
      IF(MJ .GT. NP) MJ=NP
      NJ=I+1
      ND=0
```

```
      K1=NB+1
      K2=NBW
      IF((NP-I+1) .LT. NB) K2=NP-I+NB
      DO 20 J=NJ,MJ
      K1=K1-1
      K2=K2-1
      ND=ND+1
      NL=NB+I-J
      CC(J)=CC(J) - SS(J,NL)*CC(I)/SS(I,NB)
      DO 20 K=K1,K2
      NK=ND+K
   20 SS(J,K)=SS(J,K) - SS(J,NL)*SS(I,NK)/SS(I,NB)
      RETURN
      END



      SUBROUTINE SOLVE (SS,C,X,NP,NB,NBW,S)
      COMPLEX S
      COMPLEX SS,C,X,SUM
      DIMENSION SS(NP,NB ),C(NP),X(NP),S(1,1)
      DO 10 I=1,NP
      DO 10 J=NBW,NB
      JJ=J-NBW+1
   10 SS(I,JJ)=SS(I,J)
      NP1=NP-1
      X(NP)=C(NP)/SS(NP,1)
      DO 2 K=1,NP1
      I=NP-K
      MJ=NBW
      IF((I+NBW-1).GT.NP) MJ=NP-I+1
      SUM=(0.0,0.0)
      DO 3 J=2,MJ
      N=I+J-1
    3 SUM=SUM+SS(I,J)*X(N)
    2 X(I)=(C(I)-SUM)/SS(I,1)
      RETURN
      END



      SUBROUTINE WRTPT (CC,NOFREE)
      COMPLEX CC
      DIMENSION CC(NOFREE)
      WRITE (6,2050)
 2050 FORMAT('       ACOUSTIC VELOCITY POTENTIAL'/'          **********
     1**********'//'    NODE                REAL                IMAGINARY
     1           MAGNITUDE'/'     ****                ****                *****
     1****            *********'/)
      DO 10 I=1,NOFREE
      O= REAL(CC(I))
      E=AIMAG(CC(I))
      F=CABS(CC(I))
   10 WRITE(6,2060) I,O,E,F
 2060 FORMAT(3X,I5,3F20.5)
      RETURN
      END
```

```
      SUBROUTINE POST(NE,N,NG,NELFRE,NSPACE,NDFREE,NODES,LNODE,INDEX,X,
     1XX,SPEED,PROP1,M,FREQCY)
      COMPLEX X,XX
      DIMENSION XX(NDFREE),PROP1(M,NSPACE),X(NELFRE),SPEED(N,NSPACE),
     1NODES(NE,N),LNODE(N),INDEX(NELFRE),XY(2),GLOBAL(2,4)
      DIMENSION P(180)
      DO 10 IE=1,NE
      CALL LNODES (IE,NE,N,NODES,LNODE)
      CALL INDXEL (N,NELFRE,NG,LNODE,INDEX)
      CALL ELFRE (NDFREE,NELFRE,X,XX,INDEX)
      CALL ELCORD (IE,M,N,NSPACE,PROP1,SPEED,LNODE)
      CALL POSTEL (X,SPEED,IE,NELFRE,M,NE,XY,GLOBAL,NSPACE,N,FREQCY,P)
   10 CONTINUE
      CALL OUTPUT (P,NE)
      RETURN
      END



      SUBROUTINE ELFRE (NDFREE,NELFRE,X,XX,INDEX)
      COMPLEX X,XX
      DIMENSION X(NELFRE),XX(NDFREE),INDEX(NELFRE)
      DO 10 I=1,NELFRE
   10 X(I)=XX(INDEX(I))
      RETURN
      END



      SUBROUTINE OUTPUT (P,NE)
      DIMENSION P(NE)
      READ (5,100) NROW
  100 FORMAT (I5)
      NL=NROW - 1
      WRITE (6,200)
  200 FORMAT (1H1)
      D1=P(NL)
      D2=P(1)
      DO 10 I=NL,NE,NL
      P(I)=ABS(P(I)/D1)
   10 WRITE (6,300) I,P(I)
  300 FORMAT (I5,F15.4)
      WRITE (6,200)
      NP=NE-(NL-1)
      DO 20 I=1,NP,NL
      P(I)=ABS(P(I)/D2)
   20 WRITE (6,300) I,P(I)
      RETURN
      END
```

```
      SUBROUTINE POSTEL (X,SPEED,IE,NELFRE,M,NE,XY,GLOBAL,NSPACE,N
     1,FREQCY,P)
      COMPLEX CXAVE,CYAVE,POT,PRESSA
      COMPLEX X,PRESS,GRAD
      DIMENSION P(NE)
      DIMENSION XY(2),GLOBAL(2,4),GRAD(2),X(NELFRE),SPEED(N,NSPACE)
      DATA KODE /1/
      IF (KODE.EQ.0) GO TO 10
      KODE=0
      WRITE(6,2000)
 2000 FORMAT('1         GLOBAL DERIVATIVE AT INTEGRATION POINTS AND ACOUS
     1TIC PRESSURE'/'          ****************************************
     1**********'//' POINT  X-COORD    Y-COORD  REAL D/DX  IMA
     1G D/DX  REAL D/DY  IMAG D/DY  REAL POT   IMAG POT   REAL PRESS IMA
     1G PRESS'/)
   10 CONTINUE
      WRITE (6,2100) IE
 2100 FORMAT (1H0,20X,' ELEMENT NUMBER ',I3)
      XAVE=0.0
      YAVE=0.0
      VEL=0.0
      CXAVE=(0.0,0.0)
      CYAVE=(0.0,0.0)
      POT=(0.0,0.0)
      PRESSA=(0.0,0.0)
      READ (10) NIP
      NPLUS=1+NIP
      DO 20 J=1,NIP
      READ (10) XY,GLOBAL
      CALL MMULTZ(GLOBAL,X,GRAD,2,NELFRE,1)
      XAVE=XAVE+XY(1)
      YAVE=YAVE+XY(2)
      CXAVE=CXAVE+GRAD(1)
      CYAVE=CYAVE+GRAD(2)
      VEL=VEL + SPEED(J,1)
      POT=POT + X(J)
      RHOS=1./(1.+.2*SPEED(J  ,1)**2)**2.5
      VELS=1./(SQRT(1.+.2*SPEED(J  ,1)**2))
      PRESS=RHOS*(CMPLX(0.0,FREQCY)*X(J) - SPEED(J,1)*VELS*GRAD(1))
      WRITE(6,2200) J,XY,GRAD,X(J  ),PRESS
 2200 FORMAT (I5,10E11.3)
   20 CONTINUE
      FNIP=NIP
      XAVE=XAVE/FNIP
      YAVE=YAVE/FNIP
      CXAVE=CXAVE/FNIP
      CYAVE=CYAVE/FNIP
      VEL=VEL/FNIP
      POT=POT/FNIP
      RHO = 1./(1.+.2*VEL**2)**2.5
      VE=1./(SQRT(1.+.2*VEL)**2)
      PRESSA=RHO*(CMPLX(0.0,FREQCY)*POT -VEL*VE*CXAVE)
      P(IE)=REAL(PRESSA)
      WRITE(6,2200) NPLUS,XAVE,YAVE,CXAVE,CYAVE,POT,PRESSA
      RETURN
      END
```

```
      SUBROUTINE MMULTZ (A,B,C,L,M,N)
      COMPLEX B,C,SUM,BKJ
      DIMENSION A(L,M),B(M,N),C(N,L)
      DO 30 I=1,L
      DO 20 J=1,N
      SUM=(0.0,0.0)
      DO 10 K=1,M
      BKJ=B(K,J)
      IF(CABS(BKJ).EQ.0.0) GO TO 10
      AIK=A(I,K)
      IF(AIK.EQ.0.0) GO TO 10
      SUM=SUM + AIK*BKJ
   10 CONTINUE
      C(J,I)= SUM
   20 CONTINUE
   30 CONTINUE
      RETURN
      END
```

APPENDIX F

NON-LINEAR EFFECTS ON SOUND PROPAGATION IN A VARIABLE AREA DUCT CARRYING HIGH SUBSONIC MACH NUMBER FLOWS

In a recent paper, Lumsdaine and Ragab[35] studied the effect of flow on quasi-one-dimensional acoustic wave propagation in a variable area duct of finite length by solving the linearized acoustic equation using the power series expansion method and the Runge-Kutta fourth-order method for harmonic time dependence. More recently, Callegari and Myers[37] studied the non-linear effects on sound of nearly sonic flows in variable area ducts; their theory is based on a quasi-one-dimensional model and the use of matched asymptotic expansions. The solution of Callegari and Myers is valid only for acoustic sources with a relatively low frequency located in the throat region of a slowly varying area duct. It is the purpose of this study to solve the one-dimensional non-linear equation for a variable area duct carrying high subsonic Mach number flows and avoiding the restrictions imposed on the solution of Callegari and Myers. The non-linear governing equation is presented here, normalized and solved using an implicit finite difference technique. A sinusoidal wave excitation is considered at one end of the duct and a non-reflection boundary condition at the other end.

Appropratie initial condition describing the function and its spatial derivative are assumed to initiate the solution.

The nature of the implicit scheme implemented in the solution guarantees unconditional stability.

An appropriate mesh ratio speeds up the convergance.

In order to assess the accuracy of the finite difference algorithm, the solution is compared with the exact solution of the linear initial boundary value problem and with the Runge-Kutta solution in which harmonic time-dependence is considered.

Mathematical Model and Solution Techniques:

The non-dimensional governing equation can be written as:

$$(1-M^2)\phi_{xx} - \frac{2M}{C}\phi_{xt} - \frac{1}{C^2}\phi_{tt} + f_1\phi_x + f_2\phi_t$$

$$+ f_3\phi_x\phi_{xx} + f_4\phi_x^2 + f_5\phi_x\phi_t + f_6\phi_x\phi_{xt}$$

$$+ f_7\phi_t\phi_{xx} + f_8\phi_x^2\phi_{xx} + f_9\phi_x^3 = 0 \qquad \text{(F.1)}$$

$$0 \leq x \leq 1 \quad , \quad 0 \leq t \leq T$$

where

$$f_1 = -\frac{(1+M^2) + (\gamma-1)M^4}{1 + \frac{\gamma-1}{2}M^2} \frac{1}{M}\frac{dM}{dx}$$

$$f_2 = -\frac{(\gamma-1)M^2}{(1 + \frac{\gamma-1}{2}M^2)^{1/2}} \frac{dM}{dx}$$

$$f_3 = \frac{(\gamma+1)M}{(1 + \frac{\gamma-1}{2} M^2)^{1/2}}$$

$$f_4 = \frac{(2-\gamma) + 3/2(\gamma-1)M^2}{(1 + \frac{\gamma-1}{2} M^2)^{1/2}} \frac{dM}{dx}$$

$$f_5 = -(\gamma-1) \frac{(1-M^2)}{M} \frac{dM}{dx}$$

$$f_6 = 2(1 + \frac{\gamma-1}{2} M^2)$$

$$f_7 = (\gamma-1)(1 + \frac{\gamma-1}{2} M^2)$$

$$f_8 = - \frac{(\gamma+1)}{2} (1 + \frac{\gamma-1}{2} M^2)$$

$$f_9 = \frac{\gamma-1}{2} \frac{(1-M^2)}{M} \frac{dM}{dx}$$

Boundary Conditions:

$$\phi(0,t) = h_o(t) \qquad (F.2)$$

$$\phi_x(1,t) = h_1(t) \qquad (F.3)$$

Initial Conditions:

$$\phi(x,0) = g_o(x) \qquad (F.4)$$

$$\phi_t(x,0) = g_1(x) \qquad (F.5)$$

In the analysis $h_o(t)$ represents a sinusoidal acoustic source located at one end of the duct and expressed in the form $A_o \sin \omega t$; for the non-reflection boundary

condition at the other end of the duct $h_1(t) = \frac{1}{C}\frac{1}{1-M}\frac{\partial\phi}{\partial t}$ is considered.

For the acoustic problem at hand, the initial conditions are written as

$$\phi(x,0) = \psi_o(x)$$

$$\phi_t(x,0) = \psi_1(x)$$

where $\psi_o(x)$ and $\psi_1(x)$ are the solution and its temporal derivative of the linearized problem obtained from Runge-Kutta method for harmonic time dependance.

The governing second order non-linear differential equation can be written in the form

$$\phi_{tt} + f(x,t,\phi,\phi_x,\phi_{xx})\phi_{xt} + g(x,t,\phi,\phi_x,\phi_{xx})\phi_t = p(x,t,\phi,\phi_x,\phi_{xx}) \qquad (F.6)$$

The Finite Difference Scheme:

If we let Ω_h be a rectangular lattice with mesh widths h and k fitted to the region

$$\Omega : 0 \leq x \leq 1 \quad , \quad 0 \leq t \leq T$$

this means that Ω_h is the set of all points of intersection of the coordinate lines

$$x = ih \quad , \quad i = 0, 1, \ldots, I$$

$$t = jk \quad , \quad j = 0, 1, \ldots, J$$

$$Ih = 1 \quad \text{and} \quad Jk = T$$

Thus, for a general point (i,j), and upon writing the finite difference algorithm for different derivatives, one obtains

$$\phi_x|_{i,j} = \frac{1}{2h}(\phi_{i+1,j} - \phi_{i-1,j}) + O(h^2)$$

$$\phi_t|_{i,j} = \frac{1}{2k}(\phi_{i,j+1} - \phi_{i,j-1}) + O(k^2)$$

$$\phi_{xx}|_{i,j} = \frac{1}{h^2}(\phi_{i+1,j} - 2\phi_{i,j} + \phi_{i-1,j}) + O(h^2) \qquad \text{(F.7)}$$

$$\phi_{tt}|_{i,j} = \frac{1}{k^2}(\phi_{i,j+1} - 2\phi_{i,j} + \phi_{i,j-1}) + O(k^2)$$

$$\phi_{xt}|_{i,j} = \frac{1}{4hk}(\phi_{i+1,j+1} - \phi_{i+1,j-1} - \phi_{i-1,j+1}$$

$$+ \phi_{i-1,j-1}) + O(h^2) + O(k^2)$$

Substitution of Equations (F.7) into Equation (F.6) yields,

$$a_i \phi_{i-1,j+1} + b_i \phi_{i,j+1} + C_i \phi_{i+1,j+1} = d_i \qquad \text{(F.8)}$$

where

$$a_i = - f_{i,j} \frac{1}{4hk}$$

$$b_i = (\frac{1}{k^2} + g_{i,j} \frac{1}{2k})$$

$$C_i = f_{i,j} \frac{1}{4hk} = -a_i$$

$$d_i = p_{i,j} + \frac{1}{4hk} f_{i,j}(\phi_{i+1,j-1} - \phi_{i-1,j-1})$$

$$+ \frac{1}{2k} g_{i,j}\, \phi_{i,j-1} + \frac{1}{k^2}(2\phi_{i,j} - \phi_{i,j-1})$$

and

$$f_{i,j} = -C^2 [f_6 \{\frac{\phi_{i+1,j} - \phi_{i-1,j}}{2h}\} - \frac{2M}{C}]$$

$$g_{i,j} = -C^2 [f_2 + f_5 \{\frac{\phi_{i+1,j} - \phi_{i-1,j}}{2h}\}$$

$$+ f_7 \{\frac{\phi_{i+1,j} - 2\phi_{i,j} + \phi_{i-1,j}}{h^2}\}]$$

$$p_{i,j} = C^2 [(1-M^2)\{\frac{\phi_{i+1,j} - 2\phi_{i,j} + \phi_{i-1,j}}{h^2}\}$$

$$+ f_1 \{\frac{\phi_{i+1,j} - \phi_{i-1,j}}{2h}\}$$

$$+ f_3 \{\frac{\phi_{i+1,j} - \phi_{i-1,j}}{2h}\}\{\frac{\phi_{i+1,j} - 2\phi_{i,j} + \phi_{i-1,j}}{h^2}\}$$

$$+ f_4 \{\frac{\phi_{i+1,j} - \phi_{i-1,j}}{2h}\}^2$$

$$+ f_8 \{\frac{\phi_{i+1,j} - \phi_{i-1,j}}{2h}\}^2 \{\frac{\phi_{i+1,j} - 2\phi_{i,j} + \phi_{i-1,j}}{h^2}\}$$

$$+ f_9 \{\frac{\phi_{i+1,j} - \phi_{i-1,j}}{2h}\}^3]$$

The resulting system of equations is a tridiagonal one in the unknowns $\phi_{i,j+1}$ at the j+1 level. The above system of algebraic equations can be solved using the Thomas algorithm.

The implicit scheme adopted here assumes unconditional stability. Convergence can be established by a suitable choice of the mesh ratio R = k/h.

Discussion and Conclusion:

A one-dimensional non-linear partial differential equation for the acoustic velocity potential in the Eulerian coordinate system is solved using an implicit finite difference algorithm. Figure (F.1) shows the solution of the linear equation with no flow using the present technique, the exact solution and the fourth-order Runge-Kutta method; the agreement for dimensionless time preiods 1 and 4 seem to be excellent for the three months. This provides a bases to extend the technique to the non-linear equation. For low Mach number flows the non-linear effect can be neglected as shown in Figures (F.3) and (F.4) where the finite difference linear and non-linear solutions are compared at time intervlas 2 and 4 for the no flow and 0.5 Mach number cases.

Increasing the Mach number to 0.8 results in a non-linear attenuation as shown in Figure (F.5). For higher Mach numbers, the trend is not obvious due to instabilities in the numerical solution. Frequency changes do not seem to have a significant effect on wave attenuation as can be seen from Figures (F.2) and (F.3) for dimensionless frequencies of 2 and 5. Note that the non-linear solution is very sensitive to amplitude changes, and shock waves can easily be formed when enough time is elapsed and/or higher sinusoidal amplitudes are imposed.

In conclusion, non-linear effects can be safely neglected for low Mach number flows but must be accounted for when high Mach number flows are encountered.

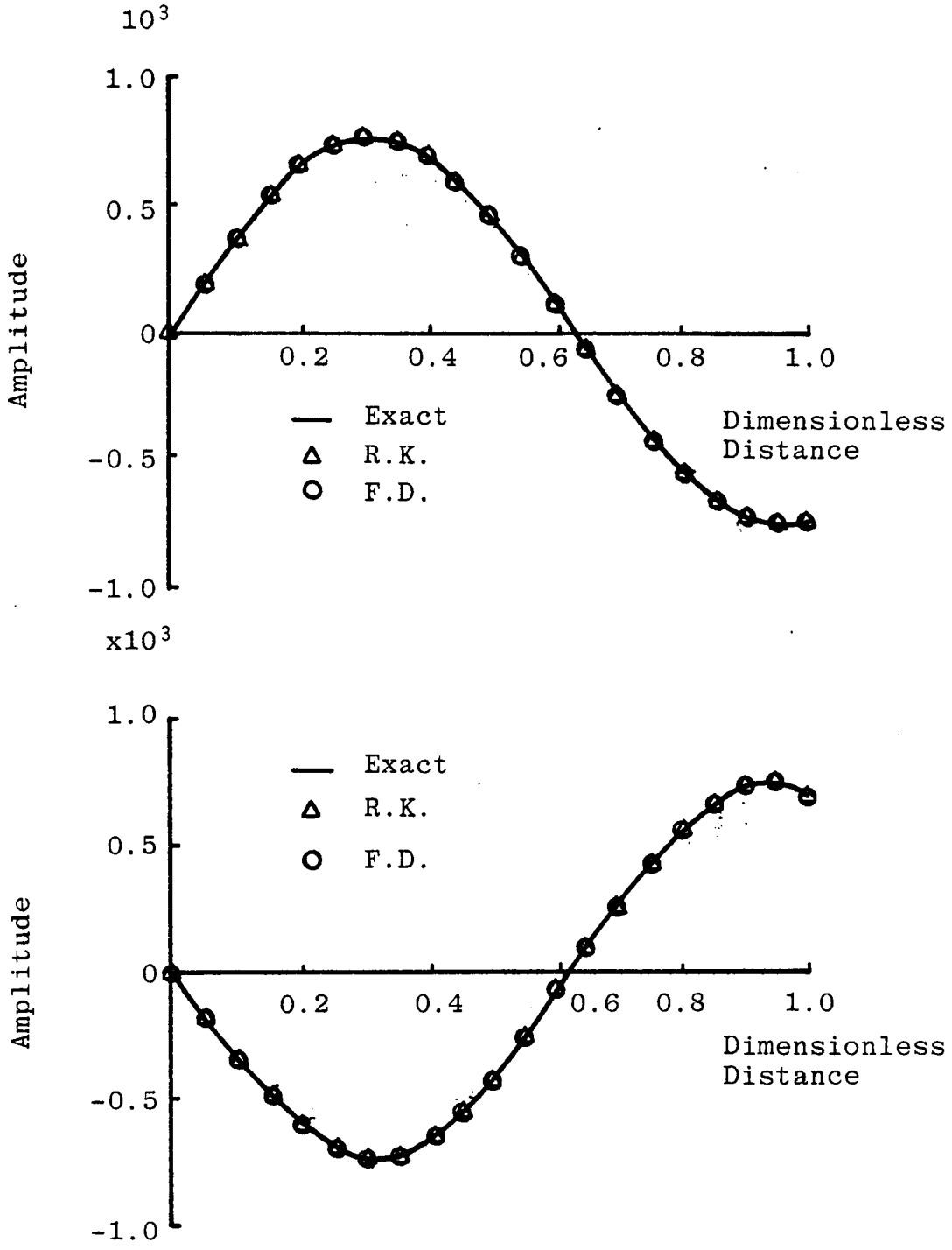


Figure F.1 Exact, Runge-Kutta and Finite Difference Solution (Frequency = 5.0)

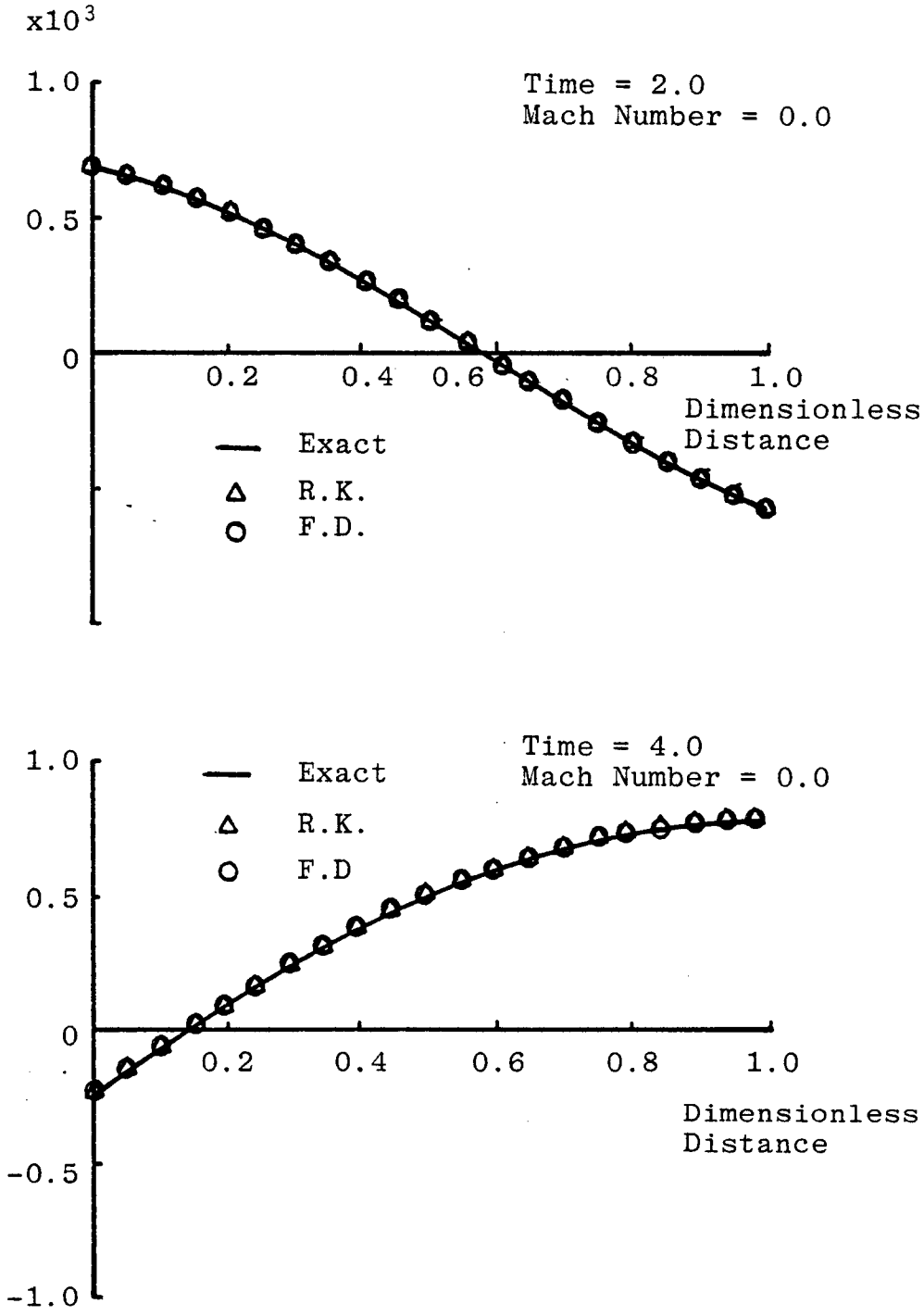


Figure F.2 Exact, Runge-Kutta and Finite Difference Solutions (Frequency = 2.0)

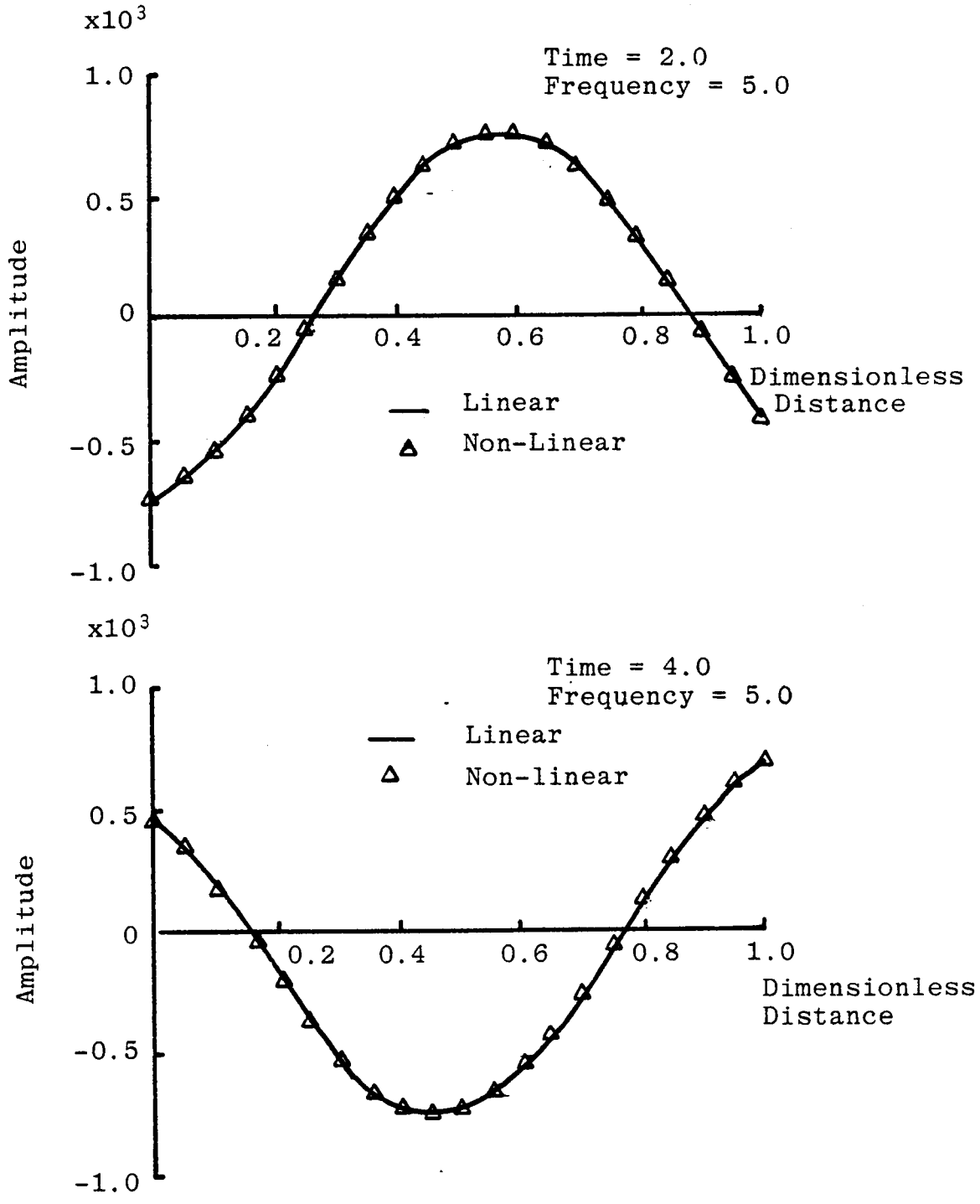


Figure F.3 Linear and Non-Linear Solutions
(M = 0.0)

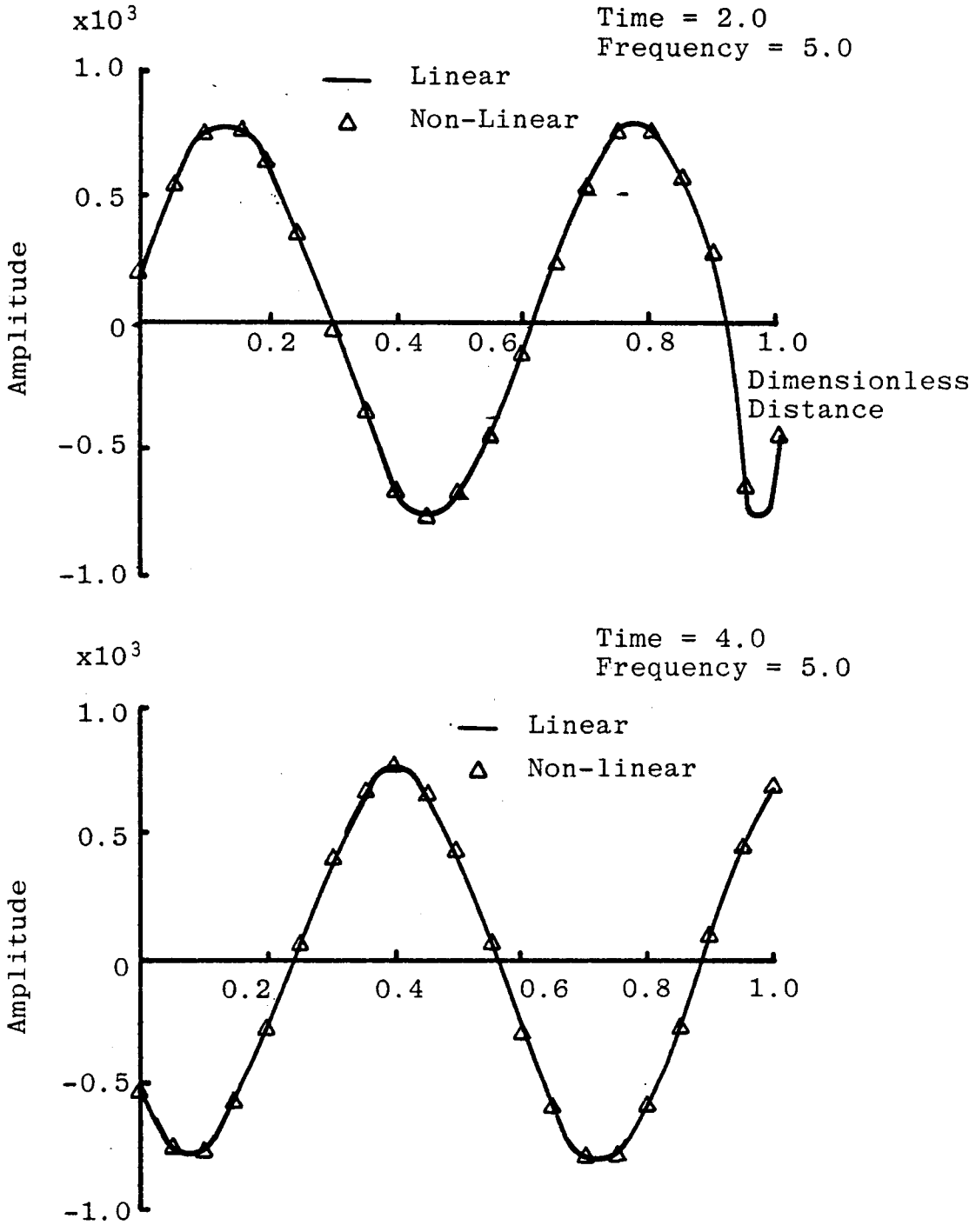


Figure F.4 Linear and Non-Linear Solutions
(M = 0.5)

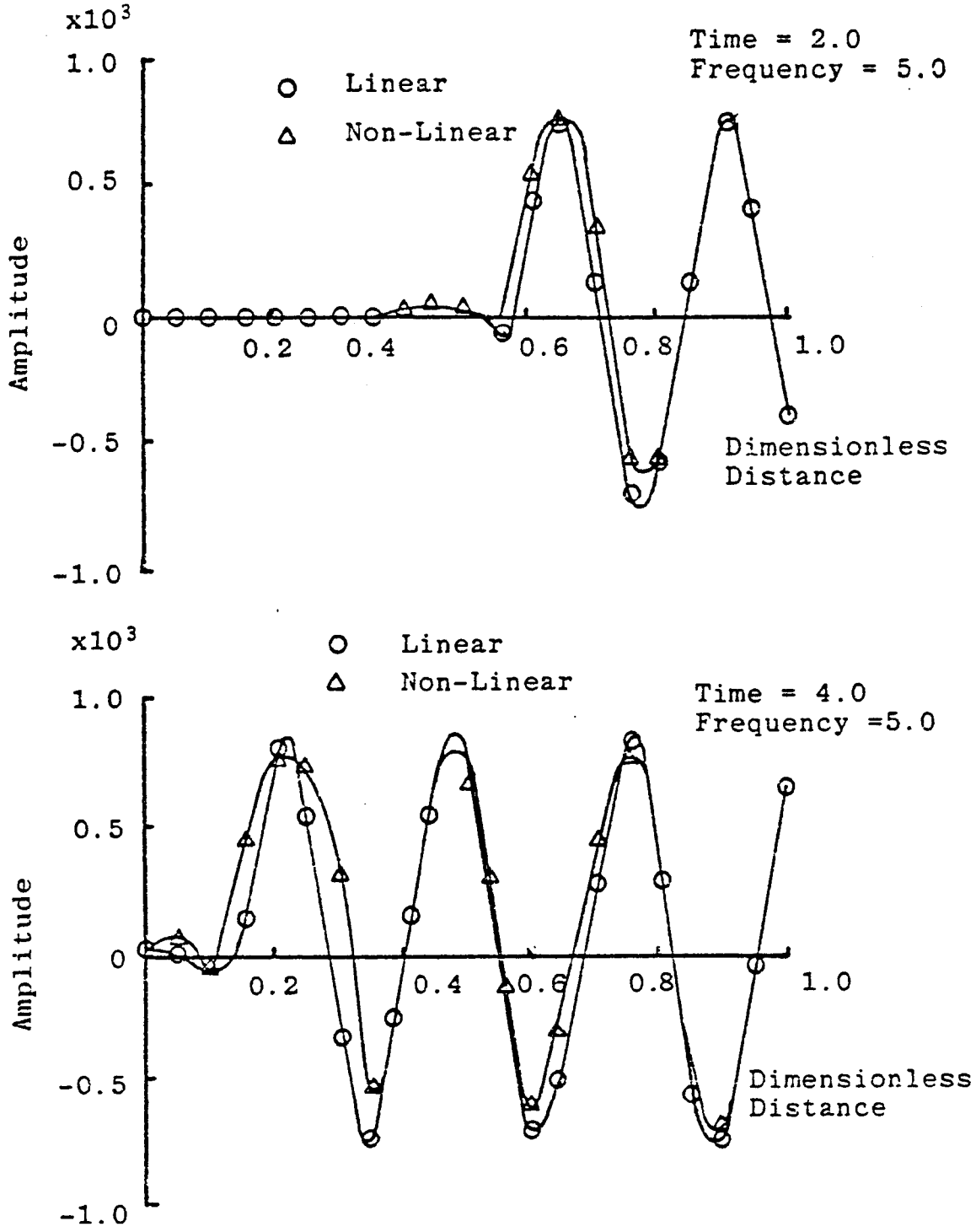


Figure F.5 Linear and Non-Linear Solutions
(M = 0.8)

VITA

Ismail A. Tag was born on October 6, 1947 in Cairo, Egypt. He received the Bachelor of Science degree with honor in Mechanical Engineering from Cairo University in 1968. After graduation, he was appointed as a demonstrator in the Mechanical Engineering Department at Cairo University until he came to the United States and entered the graduate school at South Dakota State University in August 1972. He received the Master of Science degree in Mechanical Engineering in June 1974.

In the fall of 1973 he enrolled in the Doctor of Philosophy program in the Mechanical and Aerospace Engineering Department at the University of Tennessee and received this degree in June 1978.

The author is a member of Phi Kappa Phi, American Institute of Aeronautics and Astronautics, American Association of University Professors and other professional societies.

Presently, the author is a visiting assistant professor at New Mexico State University.